LBL-34091
UC-401

Lawrence Berkeley Laboratory
UNIVERSITY OF CALIFORNIA

CHEMICAL SCIENCES DIVISION

Chemical Dynamics in Time and Energy Space

J.D. Myers
(Ph.D. Thesis)

April 1993

REFERENCE COPY
Does Not
Circulate
Bldg. 50 Library.
LBL-34091
Copy 1

Prepared for the U.S. Department of Energy under Contract Number DE-AC03-76SF00098

DISCLAIMER

This document was prepared as an account of work sponsored by the United States Government. While this document is believed to contain correct information, neither the United States Government nor any agency thereof, nor the Regents of the University of California, nor any of their employees, makes any warranty, express or implied, or assumes any legal responsibility for the accuracy, completeness, or usefulness of any information, apparatus, product, or process disclosed, or represents that its use would not infringe privately owned rights. Reference herein to any specific commercial product, process, or service by its trade name, trademark, manufacturer, or otherwise, does not necessarily constitute or imply its endorsement, recommendation, or favoring by the United States Government or any agency thereof, or the Regents of the University of California. The views and opinions of authors expressed herein do not necessarily state or reflect those of the United States Government or any agency thereof or the Regents of the University of California.

LBL-34091
UC-401

CHEMICAL DYNAMICS IN TIME AND ENERGY SPACE

James Douglas Myers

Chemical Sciences Division
Lawrence Berkeley Laboratory,

and

Department of Chemistry
University of California
Berkeley, California 94720, USA

April 1993

This work was supported by the Director, Office of Energy Research, Office of Basic Energy Sciences, Chemical Sciences Division, of the U.S. Department of Energy under Contract No. DE-AC03-76SF00098.

to my mother, father, sister and brother

Table of Contents

Preface xi

Acknowledgements xiii

Chapter I: The Design and Construction of a Picosecond UV/VUV Temporal Spectrometer 1

Introduction 1

The "Grand" Signal Calculation 4

The Picosecond Laser System 8

The Photon Sources 13

The Nd:YAG Amplifier Chain 16

The Dye Amplifiers 25

UV Generation 28

VUV Generation 29

System Specifications 31

Visible Wavelengths 31

UV Wavelengths 32

VUV Wavelengths 33

Cross Correlation / Temporal Resolution 35

Noise 40

CH_3I: An Experiment 41

Conclusion 46

References 48

Figure Captions 50

Chapter II: 193 nm Photodissociation of Cyclopentadiene 58

Introduction 58

Experimental 61

Analysis and Results 65

H Atom Elimination 67

$:CH_2$ Elimination 75

C_2H_2 Elimination 77

Slow Acetylene 78

Fast Acetylene 80

Branching Ratio 81

Multi-Photon Effects 85

Discussion 90

H Atom Elimination 90

$:CH_2$ Elimination 97

C_2H_2 Elimination 104

Branching Ratio 114

Multi-Photon Effects 123

Conclusions 128

References 135

Figure Captions 139

Chapter III: 193 nm Photodissociation of Thiophene 165

Introduction 165

Experimental 169

Analysis and Results 170

Hydrogen (H_2) Elimination/ Dimer Dissociation 172

Acetylene Elimination 174

Sulfur Atom Elimination 175

SH Elimination 176

C_3H_3 Elimination 178

C_3H_4 Elimination 178

Branching Ratio 180

Discussion 184

Hydrogen (H_2) Elimination/ Dimer Dissociation 184

Acetylene Elimination 186

Sulfur Atom Elimination 192

SH Elimination 194

C_3H_3 Elimination 195

C_3H_4 Elimination 197

Branching Ratio / Comparison with Cyclopentadiene 198

Conclusion 203

References 210

Figure Captions 212

List of Figures

Fig. 1-1. Schematic of the Picosecond Laser System: Commercial Pump Lasers and Nd:YAG Amplifier Chain. 53

Fig. 1-2. Schematic of the Picosecond Laser System: Dye Amplifiers. 54

Fig. 1-3. Autocorrelation of the 1 mJ, 710 nm Output of the Dye Amplifier. 55

Fig. 1-4. Typical Cross-correlation of the 1 mJ 594 nm and 1 mJ 710 nm Amplified Dye Laser Pulses. 56

Fig. 1-5. UV/VUV Cross-correlation / Instrument Temporal Response. 57

Fig. 2-1. Simplified Schematic of the Rotating Source Machine. 146

Fig. 2-2. H Atom Loss Power Dependence. 147

Fig. 2-3. Newton Diagram. 148

Fig. 2-4. m/e 65 Time-of-Flight Spectra. 149

Fig. 2-5. m/e 1 Time-of-Flight Spectra. 150

Fig. 2-6. H + C_5H_5 Translational Energy Distribution ($P(E_T)$). 151

Fig. 2-7. H + C_5H_5 Translational Energy Distribution with Theoretical Fits. 152

Fig. 2-8. C_4H_4 Time-of-Flight Spectra, 10°. 153

Fig. 2-9. CH_2 + C_4H_4 Translational Energy Distribution ($P(E_T)$). 154

Fig. 2-10. m/e 13 Time-of-Flight Spectrum, 10°. 155

Fig. 2-11. C_3H_4 Time-of-Flight Spectra, 20°, m/e 40 and m/e 39. 156

Fig. 2-12. C_3H_4 Time-of-Flight Spectra, 20°, m/e 27 and m/e 26. 157

Fig. 2-13. 'Slow' C_2H_2 + C_3H_4 Translational Energy Distribution ($P(E_T)$). . . . 158

Fig. 2-14. 'Fast' C_2H_2 + C_3H_4 Translational Energy Distribution ($P(E_T)$). . . . 159

Fig. 2-15. High Laser Power Time-of-Flight Spectra, m/e 65-60, 10°. 160

Fig. 2-16. High Laser Power m/e 2 Time-of-Flight Spectrum, 90°. 161

Fig. 2-17. High Laser Power Time-of-Flight Spectra, m/e 51,50,39,26, 15°. . 162

Fig. 2-18. Energy Level Diagram for Cyclopentadiene. 163

Fig. 3-1. m/e 51 Power Dependence. 218

Fig. 3-2. H_2 Loss/ Dimer Dissociation Time-of-Flight Spectra. 219

Fig. 3-3. H_2 + C_4H_2S Translational Energy Distribution ($P(E_T)$). 220

Fig. 3-4. C_2H_2S + C_2H_2 Time-of-Flight Spectra. 221

Fig. 3-5. C_2H_2S + C_2H_2 Translational Energy Distribution ($P(E_T)$). 222

Fig. 3-6. m/e 52 and m/e 32 Time-of-Flight Spectra. 223

Fig. 3-7. C_4H_4 + S Translational Energy Distribution ($P(E_T)$). 224

Fig. 3-8. m/e 51 Time-of-Flight Spectrum. 225

Fig. 3-9. m/e 33 Time-of-Flight Spectrum. 226

Fig. 3-10. C_4H_3 + SH Translational Energy Distribution ($P(E_T)$). 227

Fig. 3-11. m/e 45 Time-of-Flight Spectrum. 228

Fig. 3-12. 'HCS + C_3H_3' Translational Energy Distribution ($P(E_T)$). 229

Fig. 3-13. m/e 39 Time-of-Flight Spectrum. 230

Fig. 3-14. m/e 44 and m/e 40 Time-of-Flight Spectra. 231

Fig. 3-15. CS + C_3H_4 Translational Energy Distribution ($P(E_T)$). 232

List of Tables

Table 2-1. Heat of Reaction and Maximum Translational Energy Release for some Thermodynamically Accessible Photodissociation Pathways of Cyclopentadiene at 193 nm. 131

Table 2-2. Vibrational Frequencies used in RRKM calculations. 132

Table 2-3. Calculated Arhenius parameters for Cyclopentadiene Dissociation. . . 133

Table 3-1. Dissociative Flux as a Function of Mass-to-Charge Ratio. 208

Table 3-2. Product Branching Ratios. 209

Table 3-3. Relative Yields, ΔH_{rxn}, and Estimated Barrier Heights for the Thiophene Dissociation Channels. 210

Preface

Several years ago, I joined a project to implement what was known in the Lee group as "The Grand Plan": design and build an amplified tunable picosecond UV/VUV laser system and use it to probe the photodissociation of the chloroethyl radical (from a photolytic radical source, also to be built) excited to the fourth overtone of its C-H stretch vibration. The appearance of chlorine and hydrogen atoms from the dissociation was to be detected by a 1+1 resonantly enhanced multi-photon ionization scheme with an overall temporal resolution of roughly two picoseconds. I wish I could report here how "The Grand Plan" was accomplished. I cannot. I will report the development of the UV/VUV laser system and describe the chemical experiments that were attempted using the VUV light as a probe. These experiments point out the limits of using ion detection with ultrafast, high intensity lasers. Concluding this part, I will reassess "The Grand Plan" in light of what has been learned from these experiments.

In the second part, and with more emphasis on chemistry, I will describe some of my Photofragment Translational Spectroscopy (PTS) experiments. These studies were motivated by combustion chemistry; Cyclopentadiene, and the cyclopentadienyl radical, are important intermediates in the combustion of aromatic hydrocarbons. Thiophene, a five member sulfur containing ring that is isoelectronic with cyclopentadiene, is an important species in the combustion of fuel sulfur.

Thus, the title of my thesis: my personal attempt to directly measure the

dissociation lifetimes of molecules has been transformed into measurements of the energy disposal in chemical reactions. Of course, the temporal experiments were designed to give information on the movement of energy through the molecule and all the PTS data was taken in the time domain. Perhaps I am just trying to be confusing, or I'm striving too hard for a unifying theme, but in a very serious sense, I think that looking at chemical dynamics from both time and energy perspectives has been invaluable to my understanding of these processes. Considering chemical dynamics in terms of normal modes and local modes, with couplings that lead to intramolecular vibrational energy transfer, and then in terms of eigenstates and the dephasing of wavepackets is something I highly recommend.

ACKNOWLEDGEMENTS

I find it slightly difficult to finally write these acknowledgements because over the years I have written them hundreds of times in my head. Every kindness that has been extended to me over the years, when I was often too stressed to return the favor, was written in grand and glorious style in my internal, thousand-page acknowledgements. Any appreciation I can convey here is a shadow of what I truly feel and I assure you that the names and deeds left out here have not been forgotten. My time in graduate shool has been filled with greater joys and greater sorrows than I had previously known. Fortunately I have had friends and associates who have helped me celebrate the good times and to endure and overcome the bad.

I wish also to acknowledge those who have shared the absurd with me. When the slings and arrows of outrageous laser failure made me contemplate the merits of alternative career paths, I could always count on my friends to speculate on the adventures of Jim Myers, Fast Food Professional, Potato Specialist.

Berkeley has at times seemed very far from upstate New York. Nowhere else in the world is there such a juxtaposition of professors who walk around in a world of their own, seeking to understand the universe, and homeless people who walk around in a world of their own, claiming they already do. I must confess though, that I think I will miss the full vibrant spectrum of humanity that parades daily through Sproul Plaza.

Yuan Lee's research group at first seemed somewhat foreign to me as well.

From the first time I toured the laboratory, with it's huge vacuum chambers and flashing lasers, to the first group meeting I attended, where the senior students were testing to see if they could wiggle their tongues at the 10 Hz Nd:YAG laser repetition rate, the Lee group struck me as different.

I don't want my humorous tone to be taken as a sign of disrespect. The stories here are what make the Lee Group's members the individuals I know, but I cannot stress enough the brilliance and dedication common to all. Their enthusiasm and prowess and hard work have been both amazing and inspirational.

In this the group reflects Yuan Lee himself. I have never met anyone who works harder or more selflessly than Yuan. In my early days in the group, the best time to talk with Yuan without interuption was after midnight when his phone had stopped ringing and he had time to stop in each lab, or at a softball game between innings, if you brought your data. These days, the telephone and fax machine must sometimes be used because the rest of the world has learned to value Yuan's advice as well, but you can still find him in lab after everyone else has gone home. I am constantly impressed with Yuan's knowledge and skill, but even more so by his kindness and his commitment to science as a resource to be shared by all mankind. I have benefitted greatly from his guidance and I am grateful.

The Picolab has been the center of my life for many years here, and I owe great thanks to the PicoPeople who have toiled there with me. Andy Kung taught me much of the laser theory I know. Marion Helfand was my senior co-worker and taught me much about how to run equipment in the lab. Peter Weber gave me an

introduction to Photo-Electron Spectroscopy. James Chesko and Matt Côté are two people I wish to thank for much more than their work in taking the picosecond laser system from a jumble of optics to a jumble of optics that produces picosecond vacuum ultraviolet pulses. They are true friends and have helped me through more frustrations than I care to recount. James is unique. We have run a half marathon, discussed the implications of quantum mechanics for religious philosophy on road trips to laser conferences, and battled for photons together. I will not forget the bachelor party he organized that included meditation at a buddhist temple, golf, and San Francisco nightlife, nor the 5 bucks I made betting that he could out-argue all challengers at a molecular beams conference. Matt brought much needed post-doctoral insight to the lab. Through all the laser failures he kept us convinced that tomorrow was another day. Like many of Matt's greatest insights, this one requires the proper frame of mind for contemplation. Seriously though, Matt's curiosity about chaos, coherence, and the interpretation of quantum mechanics made me remember the excitement of science that can sometimes be lost during laser alignments.

My first experiments in the Lee group were done on the ion spectroscopy machine with Mitchio Okumura and Lisa Yeh. They both took time out to be helpful to a naive firstyear while working furiously toward their degrees. Ralph Page, who knew the size of every bolt on his machine (something very impressive to a firstyear), has been a source of cynical wisdom over the years.

John Price was my successor on the ion spectroscopy machine. Our friendship was forged in our early stressful years here. He and Matt helped to convince me that

'grease and poison' were essential in the pursuit of knowledge. John also convinced me that worthwhile things are often not done simply because no one attempts to do them. (You'll notice that the thought pattern is definitely similar to Matt's.) I look forward to working with John on such projects in the future.

Pam Chu and Xinsheng Zhao are students who entered the Lee group when I did. Pam and I struggled on different machines attempting difficult experiments. Her tales of life after graduation have been very inspirational. Xinsheng is the author of the original CMLAB programs and he deserves thanks from everyone doing photofragment translational spectroscopy.

Peter McAnally and Tom Tuttle also came to Berkeley the year I started. They made the apartment we rented a somewhat odd but pleasant place. Poolside barbeques with Pete, Tom, and their friends were not to be missed.

Many other people have had an impact on my Lee Group experience. Arthur Suits and Albert Stolow have talked computers, philosophy, and science with me. Bob Continetti, Gil Nathanson "Smart Person", and The Floyd were amazing resources and nice people too. Evan Cromwell shared his optics and patriotically defended the 'Black Flag'. Doo Wan Boo has tried very hard to 'enlighten' James and me. Simon North and Cheryl Longfellow helped me to become a photofragmentalist and helped me to take the H and H_2 spectra in this thesis. Jingsong Zhang (Dr. Z.) has helped me test new software and shared the wonders of thesis writing with me. Tsong Tzong Miau has been my software purchasing advisor and AutoCad wizard. Hong Tao Hou has my admiration for his inspiring battles with the A machine -- may he emerge the

victor. Cindy Berrie and Dave Blank, both of whom probably have many more vented detectors in their futures, have my best wishes.

I would also like to thank my friends in "the real world". I won't tell their stories here, but my thanks to them are just as great. From my long time friends Kyle, Kevin, Ellen, and Bob and my family, to my advisors Paul Houston and Don Chernoff, to my newer friends Andrea, Cherise, and Jay, they all have my appreciation.

Ann Lawhead, Kim Prather, and Laura Smoliar deserve special thanks for helping me through the roughest times. Ann and Tom have also asked the innocent question, "So have we finished our thesis yet?" enough to finally get a "Yes, we have.". Kim and Laura and I have had a lot of good times, and I would tell embarrassing stories here, but Kim and Laura can be the most ~~vicious~~ ~~intimidating~~ persuasive people I know (so you'll have to ask me in person).

A final thanks goes to Barbara Balko. She has changed my life in many ways, probably more than she knows. I don't think I can express more clearly what I think of her than to point out both that she is referenced in this thesis and that I once asked her to marry me. I wish her the very best.

Abstract

Chemical Dynamics in Time and Energy Space

by

James Douglas Myers

Doctor of Philosophy in Chemistry

University of California at Berkeley

Professor Yuan T. Lee, Chair

The development of a versatile picosecond ultraviolet/vacuum ultraviolet temporal spectrometer is described in detail. Its intended use -- measuring internal energy redistribution in isolated molecules -- is also discussed. A detailed description of the double-pass Nd:YAG amplifier and the dye amplifiers is given with the pulse energies achieved in the visible (1 mJ), ultraviolet (50-150 μJ), and vacuum ultraviolet (10^{10} photons). The amplified visible pulses are shown to be of sub-picosecond duration and near transform limited. The instrument's temporal response (≤10 ps) is derived from an instrument limited measurement of the dissociation lifetime of methyl iodide at 266 nm. The methyl iodide experiment is used to discuss the various sources of noise and background signals that are intrinsic to this type of experiment.

In the second part, non time-resolved experiments measuring the branching ratio and kinetic energy distributions of products from the 193 nm photodissociation of cyclopentadiene and thiophene are presented. These studies were done using the

molecular beam Photofragment Translational Spectroscopy (PTS) technique.

The results from the cyclopentadiene experiment confirm that H atom elimination to yield the cyclopentadienyl radical is the dominant dissociation channel (>96%). A barrier of ≥ 5 kcal/mol can be understood in terms of the delocalization of the radical electron of the cyclopentadienyl fragment. A concerted elimination yielding cyclopropene and acetylene was also observed and is proposed to occur via a bicyclo-[2.1.0]pent-2-ene intermediate. Two other channels, yielding acetylene plus the CH_2CHCH triplet carbene, and CH_2 plus 1-buten-3-yne, are postulated to occur via ring opening. The implications of the experimental results for bulk thermal oxidation and pyrolysis models are discussed.

The thiophene experiment shows six competing dissociation channels, including elimination of thiirene (c-C_2H_2S) and acetylene from a bicyclic intermediate. Atomic sulfur is produced, but not via the path equivalent to CH_2 loss in cyclopentadiene. SH and C_4H_3 are also observed as they were in bulk studies, confirming the primary nature of these products. CS plus C_3H_4, HCS plus propargyl radical, and H_2 elimination are also seen. The postulated intermediates for the various thiophene dissociation channels include bicyclo, ring opened, and possibly ring contracted forms.

Chapter I: The Design and Construction of a Picosecond UV/VUV Temporal Spectrometer

Introduction

The instrument to be described in this chapter was originally designed as part of "The Grand Plan", an experiment that would directly measure the timescale for energy transfer from a well localized vibrational 'mode' into another mode - the dissociation reaction coordinate. Since the laser system design specifications are largely based on the requirements of "The Grand Plan", the experiment itself will be described first. The plan is "grand" for several reasons. First is the nature of the excitation - absorption to a local mode of a C-H stretch. With the energy initially well localized in the C-H stretch and bends, the experimental results could then be compared to expectations from a very classical picture of energy transfer from one bond to another[1]. Second is the size and nature of the molecule - a seven atom radical, $\circ CH_2CH_2Cl$. While the weak C-Cl bond (~20 kcal/mol) in this radical is essential for the experiment, this does not detract from the inherent interest in studying

radical species. The chloroethyl radical would be prepared in a rather 'grand' fashion as well: a high density, cold, clean radical beam would be prepared by UV photolysis of a precursor immediately prior to expansion. Such a source would be of obvious utility in many experiments. Some early development work on a photolytic radical source was done in connection with this project, but it was terminated with the hope that other efforts within this research group would be fruitful and could provide a working source design before the laser system was operational[2]. A third "grand" attribute was the flexibility of the proposed laser system. It was designed to provide two amplified light pulses, 1 picosecond in duration, for pump and probe excitations, each independently tuneable from the infrared to the vacuum ultraviolet (VUV). In the visible range, the peak power output was to be 1 gigawatt (GW), with experiments possible at power densities in excess of 1 terawatt/cm^2. Such a laser system would allow studies of a wide variety of chemical systems and would allow experiments measuring lifetimes as a function of pump wavelength and probe wavelength. The detection scheme -- laser ionization, resonantly enhanced or direct, followed by time-of-flight mass spectrometry -- was to provide another independent variable, either to confirm the identity of the product and separate it from any background ions, or to allow simultaneous monitoring of multiple species. While "The Grand Plan" is perhaps a pretentious moniker for an experiment, it is less so than the label "perfect" that has been applied to others, and it truly is an amazing proposal, especially considering that it was envisioned before 1985.

Before I go any further, I wish to emphasize that, while it at times felt like a

personal burden, "The Grand Plan" was conceived and worked on by a large number of people. The early "Picosecond Group" consisted of Yuan Lee, Andy Kung, Tim Minton, Gil Nathanson, Howard Nathel, Marion Helfand, Natasha Chestnoy, and myself. This group did the early feasibility calculations and decided on such things as the ionization scheme and the basic choice of a double pass Nd:YAG based amplifier for the laser system. By the time money was available for construction, the group had shrunk to Yuan, Andy, Marion, and myself. Marion concentrated on the design of a radical source and testing the chosen 1+1 VUV+UV ionization scheme for Cl atoms. Some of this work is detailed in her thesis[3]. Andy Kung has functioned as a consultant throughout the lifetime of the project and was heavily involved in the initial design and construction phase. Yuan has funded and guided the project, and has been most involved in selecting interesting chemical systems for study. James Chesko, a graduate student, and Matt Côté, a post-doc, spent a substantial part of their lives helping to make the system operational. Peter Weber, and later Albert Stolow and Laurent Nahon, spent their post-doctoral stays designing and building photoelectron spectrometers for the system. The system is now primarily in the hands of James Chesko, with Yuan and Andy continuing to advise.

In this chapter, I would like to describe the signal calculations that led to the specifications for the picosecond laser system. This will be followed by a description of the laser system that was built. Data on the performance of the system is also given. The VUV output of this system, while powerful, is somewhat short of the design estimate. Some of the factors contributing to the discrepancy will be discussed.

Finally, "The Grand Plan" will be reevaluated, with emphasis on new options for achieving many of the original goals.

The "Grand" Signal Calculation:

While "The Grand Plan" has been described previously, this thesis was cited as providing details[3]. Hence, although I will not attempt to give full derivations for the estimates in this section, I will try to provide a reasonable amount of detail.

The estimate for the achievable radical density at the interaction region was based on assuming a 1% seed ratio of a precursor, CH_2ICH_2Cl, in argon. Radicals were to be generated by photolysis at 266 nm using the fourth harmonic of a Q-switched (~10 nanosecond) Nd:YAG laser. An estimate of 10% was used for the conversion efficiency of precursors to stable chloroethyl radicals. One concern was that secondary dissociation of the chlorine atom would occur. Yuan suggested that ethylene added to the beam could scavenge any free chlorine atoms and thereby regenerate the chloroethyl radical. It was assumed that conditions could be found where efficient cooling of the radicals would occur without excessive recombination or polymerization. Using an estimate of 10^{-4} torr as an obtainable pressure in the interaction region, and an interaction volume of 1 mm^3, these numbers led to an estimate of ~3 x 10^9 radicals/cm^3 and 3 x 10^6 radicals available for the experiment.

The absorption cross section for photo-exciting the radicals was based on a guess of 10^{-18} cm^2 for the fundamental C-H stretch transition and a factor of 10

decrease for each overtone. With an estimate for the C-Cl bond dissociation energy of 20 kcal/mol[4], excitation would have to be to the second (v=0 to v=3) or third (v=0 to v=4) overtone. To observe the competition of the Cl loss channel with the ~ 30 kcal/mol H atom loss channel, and to move higher in energy where the C-H stretch local mode character would be more fully developed, the third and fourth (v=0 to v=5) overtones were chosen as the target transitions. These were crudely estimated to lie near 11,000 cm^{-1} and 14,000 cm^{-1}, respectively. A proposed 1 mJ of light at these two photon energies would correspond to ~4.6 x 10^{15} and 3.6 x 10^{15} photons respectively. Given the .01 cm^2 interaction area and absorption cross sections of 10^{-21} and 10^{-22} cm^2 and a quantum yield of 1 for Cl atom production, these photon fluxes yield 1.4 x 10^3 and 1.1 x 10^2 Cl atoms produced per pulse.

(Did I mention that obtaining the absorption spectrum of the chloroethyl radical was part of the plan? It was hoped that this task could be done using a high energy, easily tuneable nanosecond Nd:YAG pumped dye laser pulse for the absorption step, followed at long times by a picosecond probe of the atomic dissociation products. This 'coincidence' absorption spectroscopy scheme is very similar to that used in our lab to measure the infrared absorption spectra of cluster ions[5]. The combination of lasers would have a larger signal than the available all nanosecond (Quanta-Ray DCR-1 Nd:YAG laser and PDL dye laser) or all picosecond setups. (The high power, narrowband laser system developed elsewhere in the group would be the best choice[6].))

Two detection schemes were proposed. Both relied on the high peak power of

the proposed picosecond pulses to greatly enhance nonlinear processes. In one scheme, the nonlinear process would be a two photon absorption of the Cl atom which would ionize by absorbing an additional photon (2+1 Resonantly Enhanced Multi-Photon Ionization). In the second, nonlinear mixing in a noble gas would yield photons at the 5th or 6th harmonic of the visible light, at 118.9 nm. A one photon absorption in the Cl atom at the VUV wavelength, with additional absorption of a UV photon (the second harmonic of the visible) would again yield Cl^+ ions (1+1 REMPI).

The 2+1 REMPI scheme was estimated using a value of ~ 10 μJ of 234 nm for the available UV energy in a 1 ps pulse. The original calculation of the expected ion yield incorrectly treated the absorption process as a three photon nonresonant transition (estimated $\sigma_3 = 10^{-74}$ cm^6s^2 based on results for cesium dimers[7]), rather than a two photon transition resonant with a real intermediate state with an additional one photon absorption step. Using these numbers, estimates of ~ .02 and .002 ions/laser shot for the third and fourth overtone excitations were derived. Using the correct cross section ($\sigma_2 \approx 10^{-34}$ cm^4 [8]), the ionization efficiency should be 100%, yielding 1.4 x 10^3 and 1.1 x 10^2 ions/ shot. It should be noted though, that the nonresonant calculation should apply to ionization of the unexcited radical as well as precursor molecules in the beam, as a *lower* limit. Due to the much greater density of these species, there could be ≥40 radical ions and ≥400 precursor ions per shot. While the mass spectrometer would separate the Cl^+ ions from these species, if the radical or precursor molecules dissociatively ionized (at 15.9 eV total energy = 3 x 234 nm) to Cl^+ ions, they would interfere with the signal.

For this reason, as well as the calculational error, attention turned to a 1+1 scheme where no high power < ~250 nm laser beams would irradiate the sample. The original calculation for the 1+1 VUV scheme was more promising. Using the strong Cl $^2D \leftarrow {}^2P$ absorption at 188.9 nm (oscillator strength f= 0.068[9]), it was estimated that ~10^{10} VUV photons would be required to saturate the transition across the .01 cm^2 interaction area. The residual UV left from producing the VUV photons would be sufficient to also saturate the second step. Starting with 1 mJ of visible light, it was estimated that a 20% conversion to the UV could be achieved using a nonlinear doubling crystal. The conversion from UV and visible to VUV was hypothesized to have a conversion efficiency of > 0.1% [10]. This yielded an estimate of 0.2 μJ of VUV light, corresponding to >10^{11} photons and giving a comfortable margin. The advantage of the VUV scheme relative to the 2+1 ionization scheme is in the wavelength of the required UV light. Two proposals were made, one for doubling of 713.4 nm light to 356.7 nm, followed by tripling of the UV in Xe gas, and the other for doubling 594.5 nm light to 297.25 nm and then mixing 2 UV photons with one visible photon, again in Xe gas. Both would produce VUV at 118.9 nm. In either case, the UV photon that would complete the ionization step is much less energetic than the 234 nm photons that would be present in the 2+1 scheme. (The total UV pulse energy, ~100 μJ, would be roughly 10 times greater at the longer wavelengths than at 234 nm since the longer wavelength UV can be produced directly by doubling the output of a 532 nm pumped dye amplifier.) It was hoped that the longer wavelength photons would not be so readily absorbed by the other species in the beam, so that confounding chemistry could

be kept to a minimum. Further, the three photon absorption would provide less energy than in the 2+1 case, thereby reducing the likelihood of dissociative ionization.

Thus signals of > 100 ions per shot could be obtained at long times (when all of the dissociation has occurred), which would be a comfortable margin for observations at shorter times given the near unity detection efficiency for ions. It was hoped that at least one of the three detection schemes would provide a sufficiently low background of Cl^+ ions, with the likeliest candidates being the two 1+1 VUV schemes. Thus work was begun to develop a > 3 x $10^9/cm^3$ chloroethyl radical source, a dual beam 1 mJ tuneable picosecond laser system capable of producing ~ 10^{11} VUV photons/pulse, and a single atom sensitivity Cl detection scheme. To date, we have only had success with the laser system.

The Picosecond Laser System:

The picosecond laser system described here has often been described as the 'Fourier transform' of the narrowband laser system built downstairs from it by Cromwell, Trickl, Lee and Kung[11]. The laser systems share the common ideal of achieving transform-limited laser pulses, pulses whose frequency bandwidth is at the minimum possible for a given pulse duration. (At this limit, the pulses would be smooth Gaussians in both time and frequency space.) The two systems differ in that they are designed to produce very narrow pulses in complementary domains. Given the similarity in their goals, and the fact that Andy Kung devised the initial designs

for both systems, it is not surprising that they share a common architecture. Both use pulse amplification of a commercial, near transform-limited source followed by nonlinear mixing in crystals and rare gases to achieve their high power, high energy UV and VUV outputs. Evan Cromwell has given a very detailed description of the narrowband laser system that would be very useful for understanding the workings of many of the elements common to both systems, such as Faraday Rotators, spatial filters, prism dye cells, and nonlinear media[6].

Schematics for the picosecond laser system, through the amplified visible light stage, are shown in Figures 1 and 2. The rough breakdown between them is that Figure 1 contains the commercial light source and the Nd:YAG amplifier chain, while Figure 2 shows the dual dye amplifier system. Before going into the details of the optical chain, I'd like to describe some of the early design choices that were made and the reasoning behind them.

As for the nanosecond laser system, flexibility was to be a main ingredient of the picosecond laser system. While it had to be capable of performing in "The Grand Plan", thought was given to providing as much tunability as possible for future experiments. Unlike for the narrowband system, a "proven (and reliable) commercial" [6] choice for the heart of the system and for the pump of the dye amplifiers was not available. The only commercial choice for picosecond light pulses were based on a mode-locked Nd:YAG pump laser and synch-pumped dye lasers (I'll describe their operation briefly later in the chapter). To achieve one picosecond light pulses from such a combination, either the output of the Nd:YAG laser had to be compressed to ~ 5

ps before pumping the dye laser, or a saturable absorber jet had to be added to the dye laser cavity. We eventually chose a system based on the latter technology because of the specifications claiming slightly shorter light pulses.

Several options were considered for a dye amplifier pump. One option that was rejected early was a copper vapor laser running at several kilohertz. While this system had an advantage of ~5 to 50 over a 10 Hz Nd:YAG based system in average power, it would have provided much less energy per pulse and hence less peak power, which would decimate the yields from the nonlinear conversion steps. This, and the copper vapor laser's finicky nature, narrowed the choices to Nd:YAG based systems. Two broad choices were available: one could use a commercial Q-switched Nd:YAG laser (~10 ns output) to pump the dye cells, or one could amplify a pulse selected from the mode-locked Nd:YAG laser (< 100 ps output). Estimating 10% conversion in the dye amplifiers, ~ 10 mJ at 532 nm would be required for each of the two 1 mJ dye pulses. A ~ 50% doubling efficiency from the Nd:YAG fundamental to the green leads to a specification of >40 mJ at 1064 nm. This is true for the short pulse case. For the 10 nanosecond pulse, the energy requirement is several times higher due to the short energy storage time of the standard dyes.

The energy specification would be easily met by commercial nanosecond Q-switched Nd:YAG lasers. Two factors weighed against them. The first is that the long pump pulse length would allow a large amount of time for amplified spontaneous emission (ASE) to build up. This basically means that it is easy for the amplifier to function as a single-pass laser without any input seed pulse from the picosecond dye

laser. The ASE pulse would be very long and very broad and would deplete the gain that is needed for amplifying the seed pulse. Techniques to reduce the ASE, such as spatial filtering and the use of saturable absorbers placed between amplifier cells, do exist, but they would complicate the optical chain[12]. The ASE problem should be much reduced with a short pump pulse since the seed pulse can be sent through the amplifier as soon as gain is established, before the initially weaker (starting from 1 noise photon) ASE can build up.

The second factor was flexibility. The shorter pump pulse would not only simplify the dye amplifier, it would provide all of the Nd:YAG harmonic frequencies at peak powers near that of the amplified dye laser beam. These harmonics could be used in a variety of nonlinear mixing schemes to provide new wavelengths. Because the Q-switched pulses are more than 100 times longer than the mode-locked pulse, the peak power of the Q-switched pulse is more than a factor of 10 below that of the proposed amplified mode-locked pulse, and any mixing process would suffer lower output by at least this factor using the longer pulses. (It is the difference in the length of the two mixing pulses that is important. Mixing two long, lower peak power pulses can be made efficient by using a long mixing crystal, but such a crystal will lengthen a short pulse.) One proposed mixing scheme was doubling of the dye laser followed by sum frequency generation with the Nd:YAG fundamental to produce tunable UV at and below 266 nm. Such a versatile pump source for future experiments could not be resisted.

Finally, there were two options for producing an amplified mode-locked pulse:

linear and regenerative amplification. The first, with the variant of double pass amplification, is the conceptually simpler of the two. The mode-locked pulse is sent through a gain medium, in this case just a flashlamp pumped Nd:YAG rod. There are no 'active' components and the pulse follows a preset optical path. In this case, since the mode-locked Nd:YAG laser runs at a repetition rate of 76 MHz while the amplifier runs at 10 Hz, a single mode-locked pulse must be selected from the high rep rate train. This can be accomplished through the use of a fast optical switch called a Pockels cell. This device is only used as a fast shutter here, blocking all but one of the pulses from entering the amplifier chain.

A regenerative amplifier differs in that the optical path for the pulse is determined by active components. In a regen, Pockels cells are used as switches, sending the pulse in one of two directions. The regen concept is then to make a simple laser cavity, with a gain medium surrounded by two end mirrors, and use one Pockels cell to switch a pulse into the cavity, and a second one to switch it out after it has made several passes through the gain medium and has thereby been amplified. The number of passes through the gain medium is not set - it is a function of the delay between the firing of the two Pockels cells. This delay is theoretically user controlled. The inherent jitter in a Pockels cell circa 1985 was one of the big drawbacks of this type of system. If the second Pockels cell does not fire on time, the pulse can be trapped within the cavity and build to a high enough energy to damage the Nd:YAG rod, the Pockels cells, the polarizers, and the mirrors. The one Pockels cell assembly that had been tested (Quantel PF 302) was based on a krytron high

voltage switch and was known to have both a ± 10 ns jitter and a long term drift. This did not compare well with the inter-pulse spacing of 13 ns from the mode-locked Nd:YAG laser, nor with a reasonable round trip time in the regenerative amplifier (a function of the cavity length). While a regen does have the advantage that the single round trip gain can be made relatively low and that the Pockels cells act as cavity beam blocks when they are off, thereby limiting ASE, the jittery nature of the then current generation of Pockels cells was considered a fatal flaw.

The ASE problem of a multiple stage linear amplifier was thought to be easily manageable, so this design was eventually chosen. In contrast to the schematic in Figure 1, the original design called for a single Pockels cell, followed by one Nd:YAG head (Nd:YAG rod and flashlamps) in a double pass configuration followed by two heads in single pass geometry. ASE was to be controlled by a saturable absorber cell attached to the end mirror of the double passed head, and a spatial filter if necessary. This was hoped to give > 40 mJ in a single pulse. As can be seen from the schematics, the system ended up being much more complex. The increased complexity did pay off though -- the amplifier can produce more than 3 times the initial design pulse energy.

The Photon Sources:

Based on the considerations above, a commercial mode-locked Nd:YAG/ synch pumped dye system was purchased. The original system used a Quantronix 416

Nd:YAG laser, which, during its year in the lab had a Mean Time Between Failure about 1/2 as long as the Mean Time Between Failure and Repair. After a year, the Quantronix laser was replaced with Coherent's Antares 76-S mode-locked Nd:YAG laser. Specifications of 18 W of 1064 nm light and 2 W of the second harmonic (532 nm) at a 76 MHz pulse repetition rate were easily met. However, the KTP doubling crystal had a very short lifetime before sustaining optical damage at the 2 W limit. Running with ~1.6 W of green light, split equally to pump two dye lasers proved to be an acceptable solution.

The dye lasers are Coherent 702-1 synch-pumped dye lasers with model 7220 cavity dumpers. These lasers must have their optical cavity length tuned to exactly match that of the pump laser. This allows the dye pulse to return to the gain dye jet every time a new 532 nm pump pulse arrives. Because the dye pulse can quickly deplete the gain accumulated in the gain jet during the 532 nm pulse, it is much shorter than the 532 nm pulse. Thus, the dye pulse is ~ 5 ps long vs. ~ 70 ps for the green pulse. By adding a saturable absorber jet, which removes the front edge of the dye pulse on every pass, shortening and sharpening the pulse, tuneable pulses less than 1 ps long can be obtained. Cavity dumping, diffracting the pulse out of the cavity using an acousto-optic crystal, allows extraction of most of the intra-cavity pulse energy. Thus ~ 10 nJ/pulse may be extracted from the cavity compared to the ~ 1 nJ that can be obtained by using a partially reflecting end mirror for the cavity.

Tuning of the pulse wavelength is accomplished by rotating an intra-cavity birefringent filter. Unfortunately, any change in the wavelength of the pulse changes

the optical length of the cavity due to the change in the index of refraction of the cavity components (dye jets, acousto-optic crystal, air) with wavelength. This necessitates a compensatory change in the cavity length to maintain a short pulse. Although creating a computer controlled servo loop to adjust the cavity length while scanning the wavelength was contemplated, it was never brought to fruition. Another similar problem with tuning is that the required saturable absorber concentration is a function of wavelength. These two factors led to most of the development efforts being performed with the dye lasers near 594 nm and 710 nm, the original wavelengths for "The Grand Plan".

The Antares laser has ports for simultaneous output of the 532 nm and 1064 nm light. The 532 nm light was all used to pump the dye lasers. The 1064 nm light was sent to our 'homebuilt' Nd:YAG amplifier. The Antares 1064 nm output was non-ideal as a seed beam in several ways (besides being invisible!). The beam pointing, divergence, spatial mode, and polarization all changed slowly as the flashlamps and the KTP doubling crystal aged. These were substantial effects which could reduce the maximum possible amplifier output by a factor of three over the 400 hour flashlamp lifetime and the ~100 hour lifetime of a given spot on the crystal. The pointing and focussing changes were presumed to occur due to changes in the thermal focussing in the Nd:YAG rod as the lamps aged and darkened and more energetic flashes were required to maintain the laser output. The polarization and spatial mode effects occurred in the doubling crystal. The polarization of the 1064 nm beam could be changed while maintaining 532 nm power by rotating the crystal about two axes.

The spatial mode change occurred as the crystal was slowly damaged by self absorption of the 532 nm light (a problem that has been lessened/eliminated in newer models). The mode could be restored by moving to a new spot on the crystal. Similarly, the other changes could all be compensated by adjustments 'under the hood' of the Antares. We also placed $\lambda/4$ and $\lambda/2$ waveplates in the 1064 nm beam path to allow compensation of polarization changes outside the laser housing.

The Nd:YAG Amplifier Chain:

The 18 W of 1064 nm light from the Antares implies an individual pulse energy of ~ 240 nJ. This corresponds to a ~ 100 nJ spatially clean, linearly polarized input pulse for the amplifier chain (details follow). The design goal then represents amplification by a factor of ~ 10^6. Measurements on the individual Nd:YAG heads showed small signal gains of 10-30 depending on the head. Thus, a four pass system, in which the pulse would certainly not be in the small signal regime in the fourth pass and would therefore experience even less gain than the estimates above, was unlikely to be sufficient. Tests on a four pass design confirmed this.

A five pass design was developed. This optical chain has a small signal gain in excess of 5×10^6. Many of the features of the final system are designed to combat ASE and lasing within the amplifier. With the extremely high gain of this system, anti-reflection (AR) coated optics (R = 0.25%) make perfectly good end mirrors for a laser cavity. Similarly, a photon can experience a gain of 10^{10} in a single round trip

of the cavity, a process requiring only one 'end mirror'.

A final design consideration for the amplifier chain is the necessary degree of suppression of unwanted seed pulses from the Antares laser. Originally, one Pockels cell was going to be used to select one pulse (at 10 Hz) from the 76 MHz train of pulses from the Antares. The extent to which a Pockels cell can transmit one pulse and reject others is primarily a function of the polarizers used outside of the cell. When no voltage is applied to the electro-optic crystal of the Pockels cell, it simply transmits light. If it is surrounded by crossed polarizers, the light will be attenuated, by a factor equal to the polarization ratio of the polarizing optics. For commercial Glan-Laser prism polarizers around a Pockels cell, a polarization ratio of ~1000 can be obtained. When the Pockels cell has the correct 'half wave' voltage applied to the crystal, it will rotate the polarization of the transmitted light by 90 degrees, allowing it to pass through the second polarizer without attenuation. Thus a suppression ration of 1000 can be obtained in one stage.

A rough calculation can be done to estimate the required suppression. Assuming a 100 μsec flashlamp pulse for the Nd:YAG amplifier heads and further assuming the gain in the heads is constant over that time yields 7600 as the number of pulses that will be amplified per pulse. If there is no saturation and all pulses are amplified by the same factor, the selected pulse, with 1000 times the initial energy of a single 'suppressed' pulse, will maintain its advantage in pulse energy. However, with 7600 of the 'suppressed' pulses being amplified, the selected pulse has only ~10% of the total energy of the amplified pulse train. Clearly this is not desirable. Further, the

ability of the 'suppressed' pulses, coming every 13 nanoseconds, to reduce the gain seen by the selected pulse has not been included. Thus, to attain maximum energy in the selected pulse, without a long accompanying train of >100 μJ pulses, a total pulse suppression of >>10,000 is required. The easiest way to accomplish this is with a second Pockels cell. The suppression from the cells is multiplicative, so that two cells should provide a suppression/rejection factor of 10^6.

All of these criteria, and more, are met by the final amplifier design shown in Figure 1. After the 1064 nm beam leaves the Antares, it is sent through a "nm Laser" model 200FNC 10 Hz shutter. This shutter lets through a ~ 5 ms slice of the pulse train at 10 Hz. Its main function is to reduce the energy incident on the later optics by roughly a factor of 20. This proved crucial in attaining good performance from the Pockels cells: with ~ 20 W of incident power, the electro-optic crystals were subject to enough thermal stress to cause a slight rotation of the transmitted laser beam's polarization, lowering the suppression ratio to less than 100:1. With <1 W incident light, the Pockels cells achieved suppression better than 1000:1. This shutter also helped to reduce the laser beam energy during alignment.

After the shutter, the beam passed through a $\lambda/4$ and a $\lambda/2$ waveplate (only the $\lambda/2$ waveplate is shown in the figure). As stated above, these were adjusted to optimize the beam transmission through the rest of the system. Since the next optic is the input polarizer of the first Pockels cell, the optimum rotation of the plates is the one providing the most vertically polarized light. The two Pockels cells and the driver are from Medox Electro-Optics. (Incidentally, the technology of these cells is a vast

improvement over the krytron based cell described above - no drift and ~ 2 ns jitter - making a regenerative amplifier a serious alternative to the system as built. They were not available when construction of the system was begun.) The input and exit polarizers for the first cell are Glan-Laser prism polarizers. The second serves double duty as it is also the input polarizer for the second cell. The output polarizer for the second stage is actually a couple feet further along the beam path, in the Faraday rotator assembly. This setup produced a suppression ratio of 300:1 for the second stage, which is still sufficient, and it eliminated the need for another separate polarizer.

After two turning mirrors, the beam was sent through a spatial filter assembly consisting of a +100 mm lens, a 50 μm diamond wire die pinhole, and a + 50 mm lens. This yielded a clean Airy pattern beam with an approximately 2 mm width. The transmission of the pinhole was ~50%. (See Evan Cromwell's thesis for details.) It was discovered during testing (ASE measurements) that one face of the pinhole was much more reflective than the other, and the more reflective side was subsequently oriented toward the input lens and away from the high gain amplifier.

The beam from the spatial filter was left with a slight divergence (equivalent to that from a ~ -1 meter lens) to help compensate for thermal lensing in the amplifier rods. The beam then entered a Faraday isolator, Electro-Optics Technology model 1845I-5. This device uses two thin film polarizers (TFPs) at its input, and two more at a 45° relative polarization angle at the output. The intervening material rotates the light from the input direction + 45° so that it suffers no transmission losses while rotating light going in the opposite direction by - 45° causing it to be completely

(~300:1) blocked by the input polarizer (again see Evan's thesis). The purpose of this isolator was not so much to protect the seed laser as it was in the narrowband laser system, but to 'protect' the amplifier from any reflective surfaces in the beam path. As stated above, even AR coated surfaces that are aligned well will cause huge amounts of ASE in the amplifier chain. In this system, both the face of the spatial filter, and the Pockels cell crystals (which have to be well aligned to provide maximum suppression) could produce double pass ASE. With the Faraday isolator in place, the ASE could be reduced to < 5 mJ/pulse (<5% of the output energy).

The light is then passed through another $\lambda/2$ waveplate to restore its polarization to vertical (the isolator keeps the linear polarization, but the output is 45° from vertical). The light pulse passes through a thin film polarizer (TFP) oriented to transmit vertically polarized light and is then reflected from a second TFP oriented to pass horizontal polarizations. The angles of the second TFP are adjusted to reflect the light pulse down the axis of the Nd:YAG amplifier chain.

The principle of the double pass section of the amplifier is relatively simple. The incoming pulse, with a vertical polarization, passes through a $\lambda/4$ waveplate and becomes circularly polarized. It then passes through the amplifier heads, bounces off the end mirror, and passes again through the $\lambda/4$ plate, which changes its polarization from circular to horizontal. When the pulse reaches the TFP which originally injected it into the amplifier, it passes through unhindered because of the overall 90° polarization rotation it received in the double pass of the $\lambda/4$ plate.

The Nd:YAG heads used were Quantel models 408-07 and 410-07, built in

1982, that were available from an earlier laser system. The 408-07 head was originally designed to hold a 93 x 7 mm Nd:YAG rod cut at Brewster's angle for use in an oscillator. This rod was replaced with a Nd:YAG rod cut with a 2°/2° wedge as is used in the other heads. (The wedge prevents lasing within the rod itself.) The other head used a 115 x 7 mm rod.

These two heads have two flashlamps each, one above and one below the rod. This geometry introduces some thermal birefringence in the Nd:YAG rod, leading to distortions in the polarization of the beamfront. After passage through polarizers, this leads to distortions in the beam profile (most noticeably, to an elliptical beam). This effect could be minimized (but not eliminated) by mounting one of the two heads on its side so that the birefringence of the two rods tended to cancel each other.

The thermal load on the rods was also manifested as a thermal lensing effect as was mentioned above. The magnitude of this effect was measured to be large enough to make each head act as an ~ 6 meter convex lens. To compensate for this, the input beam was made somewhat diverging. The end mirror of the double pass section had a 3 meter radius of curvature (a diverging mirror) to further compensate. With these optics, the output beam from the double pass section was roughly collimated and ~ 3 mm in diameter.

The small beam diameter relative to the size of the rods was required for two reasons. The first is that the housing of the formerly Brewster angle head would clip a beam bigger than ~ 5 mm. The second was for ease (relative ease) of alignment. Because of the thermal focusing, it was not possible to fully align the beam without

running the amplifier heads. The single amplified seed pulse was still too weak after single passing the two heads to be visible with an IR viewer (Find-R-Scope). The alignment procedure thus consisted of roughly aligning the pulse train through the quiescent heads, viewing it after each head, and then running the amplifier and observing the pulse after the double pass section. It was found to be difficult to align the beam through the double pass section with only this diagnostic if the beam was near the 5 mm limit. Aligning a 3 mm beam was a reasonable possibility. While such a small beam probably caused some loss of gain due to the smaller extraction volume, this was not a major problem. (At least larger diameter beams were never observed to yield more power, while diffraction rings would start to appear.) The output of the double pass section was usually several mJ and sometimes as much as 20 mJ, though the latter required very fresh flashlamps and a tailwind.

Saturation of the last amplifier with such a small beam would be more of a concern. Consequently, our design includes a non-focussing telescope to expand the beam by a factor of 2 in diameter. Again, the beam was made slightly divergent going into the amplifier. The last amplifier was a 115 x 9 mm Nd:YAG rod pumped by four flashlamps (Quantel model 410-09). Output from this stage in excess of 200 mJ has been observed, although damage to the Nd:YAG rod was also coincidentally observed at about the same time. It is not clear that the two are causally related: it is easy to misalign the beam and cause hot diffraction rings which would damage the rod. Thus 200 mJ/pulse may be a sustainable energy output, however, the pulse energy is usually run at the 120-150 mJ/pulse level, with a ~ 6 mm diameter beam, to

avoid testing this hypothesis.

The one feature of the amplifier that has so far been skipped are several optics designed for suppressing ASE. This includes the extra TFP before the injection TFP and the TFP after the injection TFP. These two optics increase the polarization purity of the beam. This is important to stop the following type of process. If light from the double pass section were to be vertically polarized and reflect out of the amplifier toward the Antares, it could reflect off a surface such as the pinhole (with an attenuation of 300 from the isolator), and return to the amplifier. After one trip through the amplifier, it should be horizontally polarized and should leave the double pass section headed toward the last amplifier stage. However, the injection TFP does reflect a few percent of the horizontal light back toward the Antares again. This would set up a cavity with a net gain and cause a rapid buildup of unwanted photons. By inserting an extra TFP the losses for this type of path can be increased enough to stop the process described.

Another method used to reduce ASE was the placement of irises along the beam path. It was particularly important to have an iris directly after the Faraday isolator to hide its reflective 5 mm diameter housing from the amplifier and another between the two double pass heads. The latter iris helped to limit the ASE to the small volume of the rods used by the seed beam. This stops ASE that might gain strength near the edge of the rod and then diffract into the central portion and extract gain there.

A third method was used to reduce reflections from downstream optics. A 9

mm Faraday isolator was placed after the last telescope. This reduced any back reflections from downstream optics by a factor of ~300. Unfortunately, it was very easy to damage this optic, and it was eventually removed.

It was also realized that the expansion telescope before the last head was also contributing back reflections, even if the lenses were slightly skewed. To stop this, a $\lambda/4$ waveplate was placed before the telescope. Any reflection from the telescope then returned toward the double pass section with a 90° rotation of its polarization and was consequently rejected by the TFPs. A compensating $\lambda/4$ plate was required after the last amplifier to restore linear polarization before the beam entered the doubling crystal. (These optics are not shown in the schematic.)

Despite its complexity, once this design was settled upon, it could be made to work. Misalignments did not cause damage to optics, just a reversible decrease in the output pulse power due to a rise in the ASE. (It was quite surprising to find that adjusting the angle of a crystal used to mix the 1064 nm light with the dye amplifier light, 2 meters past the end of the amplifier, could cause a 50% reduction in output pulse power due to increased ASE.) Its major drawback is probably the sensitivity to the fluctuations in the seed beam from the Antares noted above. Alignment is not trivial, and any change in the seed beam requires starting over at the beginning of the optical chain. In this incarnation, the amplifier suffered from the age of the Nd:YAG heads and electronics which passed their tenth birthday before retirement. A semi-commercial regenerative amplifier is now being built to replace this design[13].

The Dye Amplifiers:

The dye amplifier chains are structurally quite similar to those of the narrowband laser system, sharing the same prism dye cells[14], with the overall design adapted from that of R. Falcone[12]. Although it was originally part of the design to double pass the second cell as in the narrowband system, it was found not to be necessary. The main differences in the design stem from the short pump pulse. This pulse, 532 nm light from doubling the Nd:YAG amplifier output in a KDP or BBO crystal, is roughly 70 ps long. (Typical energies were 15-20 mJ per dye amplifier chain (30-40 mJ total).) To maximize the gain seen by the dye seed pulse, and to minimize ASE, the pump pulse had to irradiate the dye ~0-150 ps before the seed pulse arrived. This number is only approximate, and must obviously represent an 'average' value given the side-pumped geometry. Since the length of the last amplifier cell corresponds to 200 ps, the arrival time of the pump beam relative to the seed beam has a 200 ps spread over the length of the cell with the shortest delays at the cell entrance. (The pump beam is shaped to fill the amplifier cell with two cylindrical lenses in the same way as for the narrowband system.) The optical delay lines in each of the dye beam paths allowed tuning the delay of each beam to maximize gain. The pump beam did not have individual delays for the six dye cells: it was found that individually delaying the pump to each cell (by physically moving the pump turning mirrors) did not have much of an effect, which is perhaps not surprising given the averaging inherent in the geometry.

The second effect of the short pump beam was a greatly reduced ASE problem. The dye amplifier could actually be run with no ASE suppressing devices and have the seed pulse completely deplete the ASE. This could be dramatically seen by running the amplifier with no seed beam and observing the very broad spectrum of the ~ 0.5 mJ ASE pulse by dispersing it off of a grating and then allowing a seed pulse to enter the amplifier. The broad spectrum would collapse to that of the dye laser, with an estimate of <1% of the energy remaining in the ASE pulse. (this technique also helped when trying to set the seed pulse delay.) In actual operation, we did employ a large, ~200 μm, pinhole at the focus of a + 50 mm/+ 150 mm expanding telescope between the first and second cells. While this pinhole transmitted the entire seed pulse, its insertion would drop the free running ASE to <100 μJ, which again was further depleted when a seed pulse was present.

The last major design difference between the narrowband and picosecond dye amplifiers is the use of 'relay imaging' in the latter. While the narrowband system used spatial filters and underfilling of the gain volume to achieve a smooth, near-Gaussian beam profile without diffraction rings caused by clipping at the dye cell walls, the picosecond system uses relay imaging to accomplish a similar effect. The concept of relay imaging is to use telescopes to relay the image of an initial hard aperture to the location of the three dye cells. Since the beam at these locations then looks like a hard edged disk, it can nearly fill the cell without any intensity at the cell walls and therefore traverse the cell without being clipped and diffracted by the cell walls. While the beam profile contains diffraction rings from the initial aperture, the

uniform disk shape can be recreated at any location, such as at a nonlinear crystal, by use of the proper telescope. In practice, a 2.8 mm aperture is relayed by a ÷3 reducing telescope to the first 1 mm diameter cell, and then by x3 and x2 enlarging telescopes to the 3 mm and 6 mm diameter cells.

With an input dye pulse of ~5-10 nJ, these amplifiers provided 1 mJ output pulses. This level, assuming no broadening of the input pulse, represents peak power densities of ~ 5 GW/cm^2 (1 ps autocorrelation width, 6 mm diameter beam). This was estimated to be near the maximum that could be achieved without significant perturbations of the pulse by nonlinear optical effects in the dye solution. Higher energies, up to 3-5 mJ, were obtained when using correspondingly longer seed pulses (3-5 ps).

In addition, this power density limit cannot be exceeded in the first two cells, which limits their output to ~ 30 μJ and ~ 250 μJ respectively. This translates to a limit on the first cell's gain factor of 3000. It was found that up to 10,000 times gain could be achieved in this cell, but it was purposefully reduced to ~ 500-1000 by decreasing the dye concentration. Similarly, the second cell gain was then limited to ~ 50 to keep the energy of the pulse below 250 μJ (this was less difficult).

At these power densities, one should be concerned with changes to the pulse's temporal profile due to gain saturation. It was somewhat surprising to see how well the autocorrelation trace of the amplified light pulse matched that of the seed pulse (the autocorrelation width of the pulses is discussed more quantitatively later). Specifically, if the seed pulse was sharp with no 'wings', the output pulse showed no

wings, and if the seed pulse had more of a 'Prussian helmet' shape with a central spike and large wings, the ratio of these two features was maintained in the output. Perhaps in retrospect this can be rationalized considering that the synch-pumped dye laser pulse is already the product of saturation effects and in fact owes some of its short length to depletion of the gain in the dye jet by the front edge of the pulse and consequent differential amplification of the leading edge of the pulse.

UV Generation:

For various experiments, both of the visible picosecond pulses from the dye amplifiers had to be converted into the ultraviolet. To reach wavelengths from ~355 nm to ~ 290 nm, simple doubling in 1 cm x 1 cm x 3 mm KDP crystals was used. Conversions efficiencies of ~ 15-20% were achieved, yielding 150- 200 μJ of UV light. For shorter wavelengths, specifically ~266 nm, an additional nonlinear stage was required. In this setup, the unconverted 1064 nm light from the Nd:YAG amplifier was separate from its second harmonic by a dichroic mirror and was sent through an optical delay line and combined with the doubled 710 nm light (i.e. 355 nm) from the dye amplifier using a second dichroic mirror. The 355 nm generation stage was changed slightly by the addition of a double Fresnel Rhomb $\lambda/2$ polarization rotator and a ÷3 reducing telescope placed before the doubling crystal. The rotator change the visible pulse's polarization to horizontal (from vertical), producing vertically polarized 355 nm light. The telescope both reduced the beam size to ~ 2 mm diameter

and served to re-image the visible pulse at the doubling crystal. The IR and UV beams were overlapped temporally as well as spatially and sent through a BBO crystal to yield 266 nm light. The wavelengths were then separated using a Pellin-Broca prism. The 266 nm pulse was estimated at 40 μJ. Our results for pulse energy are very similar to those reported by Roberts et. al at 248 nm using essentially the same technique (coincidentally, their results were published the day we made 266 nm light)[15]. Their results also show that no pulse broadening (actually a slight compression) occurs in their dye amplifier, which runs at essentially the same peak power density as ours.

Incidental to producing the 266 nm light, we also produced ~237 nm light by mixing the dye light with its second harmonic, and ~425 nm light by mixing the dye fundamental with the 1064 nm light from the Nd:YAG amplifier. These capabilities were not seriously pursued, but they do point out the versatility inherent in the system.

VUV Generation:

Several increasingly sophisticated designs for producing VUV were implemented in our laboratory. From the first design with a simple cell containing xenon and a lithium fluoride (LiF) window into the chamber, all have produced detectable VUV signals. Using a windowless design, with a quartz capillary tube from the xenon cell to the chamber[16], we made VUV light at ~99 nm for use in detecting H_2 via 1+1 REMPI. We then switched to a series of tests requiring separation of the

VUV photons from the residual (and much more numerous) UV photons. The design for these experiments consisted of a Xe cell with an LiF window followed by an LiF prism. A pump beam could be combined with the VUV in the LiF prism and sent collinearly into the chamber. The last design is that described in Evan Cromwell's thesis, employing a Xe pulsed molecular beam for tripling, and a vacuum monochrometer for separating the VUV from the UV and visible light. Not only the design, but the actual equipment, including the jet, monochrometer, vacuum chamber, ion optics, and detector, were taken from the narrowband system when its focus drifted away from VUV production.

Two changes were required to 'optimize' the VUV output from the picosecond process. The first was to reduce the Xe pressure at the nonlinear mixing region. Whereas the nanosecond VUV output increased monotonically as the laser beam focus was moved closer to the Xe pulsed valve, the maximum ps VUV output occurred when the beam focus was ~ 2 mm from the Xe orifice. For the picosecond pulse, there was always a visible spark at the focal region, suggesting that at higher Xe densities, attenuation of the VUV occurred due to an increase in absorption by the plasma. The other change was to use a phase matched mixture of xenon and argon in the jet[17]. Matt Côté calculated a phase matched ratio for our 1189 Å wavelength of ~ 14:1 {Ar}:{Xe}. Experiment showed a maximum in the conversion efficiency at a ratio of ~ 12 with an increase in VUV output by a factor of 3 over pure Xe.

System Specifications:

Several of the power specifications have already been mentioned in the discussion above. They could all be obtained simply by reading a number off of a power meter. Other specifications, such as the pulse lengths, frequency bandwidths, VUV power, and overall temporal resolution of the instrument, are not so easily obtained. Their derivation is described here.

Visible Wavelengths:

The visible wavelength pulse energy, 1 mJ, was mentioned above. A typical autocorrelation width, measured on a homebuilt autocorrelator, is shown in Figure 3. for a 710 nm pulse. The full width at half maximum (FWHM) is 1.0 ps. This is the same width as the unamplified pulse measured on the same equipment. (It is actually shorter than the autocorrelation of the unamplified pulse as measured on a Spectra Physics model 409 rotating quartz block autocorrelator (~1.2 ps). This commercial autocorrelator is the one used to adjust the cavity lengths of the dye lasers to minimize the pulse widths.) For the $sech^2$ pulse shape expected from this system, this implies a pulse width of 650 fs.

The frequency spectrum of the amplified pulse was not quantitatively measured. However, both the unamplified and amplified pulses were dispersed using a diffraction grating and were observed by eye to have the same bandwidth within

30%. Experiments using "self-stabilization" (also called "coherent seeding") of the synch-pumped dye laser[18] showed that the normal frequency bandwidth of the laser could be reduced by roughly a factor of 1.5. This simple and elegant technique, which 'seeds' the dye laser with a tiny (as low as 10^{-10}) portion of its own output just slightly ahead (in time) of the main pulse, has been shown to produce pulses with a $\Delta t \Delta \nu$ product below that expected for a $sech^2$ pulse shape in a cavity dumped Coherent 700 series laser[19]. Our narrower bandwidth when using this technique could largely be maintained in the amplifier, suggesting that this system normally achieves roughly the same 1.4 times the $sech^2$ limit reported by Roberts et. al.[15] and with the "self stabilization" technique can perhaps do better.

UV Wavelengths:

No attempt was made to directly measure the length of the UV pulses. As stated above, ~ 20% conversion to ~ 200 μJ could be achieved in the doubling process, with an overall 5% conversion to ~ 266 nm in the two stage doubling and mixing process. (The conversion from doubled dye light to 266 nm is ~25% due to the stronger 1064 nm mixing beam. The latter has roughly the peak power of the visible light, i.e. 5 times that of the doubled dye light.)

VUV Wavelengths:

The attainable VUV energy has not yet been stated. The best estimate come from measurements of the number of ions that could be produced by nonresonantly ionizing gas in a molecular beam. The most recent measurements, using the amplifier designs above, involve CH_3I ionization. Measurements on some earlier configurations used NO gas for ionization, however this measurement has not yet been done for VUV from the Xe jet/monochrometer combination. For the CH_3I measurement, it is estimated that the number density in the pulsed molecular beam at the interaction region was ~ $3x10^{12}$ CH_3I/cm^3 (~10^{-3} torr with a 10% seed ratio). Using VUV light at 118.9 nm, an estimated 500 CH_3I^+ were observed. Using an estimated molecular beam width of ~ 2 mm, this corresponds to a 1.2 x 10^{-9} ionization efficiency for a 1 cm^2 beam (this arbitrary laser beam area cancels out in the calculation of the total number of photons). With an assumed ionization cross section of 10^{-18} cm^2, this yields ~10^9 photons/cm^2 and thus a total of 10^9 photons. With an estimate of 10% for the grating efficiency at this wavelength, the total VUV photon yield is 10^{10}/pulse. (This measurement is cruder than I would like, but laser power supply failures and other circumstances made it impossible to make a more accurate measurement before the scheduled installation of the new regenerative amplifier. Since the new system should produce essentially the same visible light pulse, the VUV output should also be the same. Hence, measurements on the new system should be able to refine the estimate above for VUV power from the present design.)

This photon flux is an order of magnitude less than was hoped for. The present conversion efficiency seems to be limited by breakdown in the xenon gas.

This breakdown, a very visible spark in the gas, was not anticipated as a limiting factor in the design calculations. Since this problem can be reduced with a softer focus in the Xe jet, the VUV generation may not be fully optimized. However, the ability to saturate the ionization of Cl atoms for "The Grand Plan" is no longer certain.

A frequency bandwidth limit for some VUV light produced from a 3-4 ps visible pulse can be inferred from our work on H_2 1+1 REMPI detection. The visible pulse energy for this work was 3-4 mJ, yielding the same peak power densities as for the shorter 1 ps, 1 mJ pulses above. Using the same $C^1\Pi_u$ intermediate state as used for some of the H_2 work done with the narrowband laser system, we tripled ~297 nm light in argon to yield ~99 nm photons and observed H_2^+ by resonant ionization through the $C^1\Pi_u$ state. We were able to observe H_2 initially in the J=0,1, and 2 rotational states. All three were clearly resolved. From the J=0, J=1 transition separation (100868.1 cm^{-1} - 100804.2 cm^{-1} = 63.9 cm^{-1}) and the width of the observed ionization peaks relative to this separation (~1/3), an estimate of < 20 cm^{-1} bandwidth in the VUV can be made. Since the duration of this pulse is unknown, this number cannot be used to calculate how close to the transform limit the pulse is. A 4 ps pulse would have a transform limited bandwidth ($sech^2$ shape) of ~4 cm^{-1}. If the VUV pulse is getting shorter in the nonlinear steps as the square root of the order of the process as one would expect for Gaussian pulses with no saturation effects, it would be $4 \div \sqrt{6} = 1.6$ ps long, corresponding to a transform limited bandwidth of 10 cm^{-1}. This would imply our VUV pulse is roughly twice the transform limit.

No measurements of this nature have been made for VUV at the 5th or 6th

harmonics of the 1 ps starting visible pulses. While the peak power density in the shorter visible pulse is the same as in the pulse measured, which suggests that the factors tending to lengthen and broaden the pulse should be similar for the two pulses, there are some factors that could cause differences. For the shorter pulses, we now use a phase-matched mixture of Ar and Xe to get slightly more power (3x). However, Mahon et. al. have shown that phase-matching in the 118.9 nm region should only occur over a < 1 Å bandwidth, raising the question of the effect of the Ar/Xe gas mixture on the pulse shape[20]. A more minor effect present for the 5th harmonic case, which requires mixing of the UV and visible light in the Xe jet, is the ~200 fs offset of the two pulses due to the different delays the two wavelength experience in traversing the quartz window of the vacuum chamber. The only measurement to date that can address these questions at all is the VUV/UV cross correlation described below, and this measurement can only place a rather long upper limit on the pulse length.

Cross Correlation/ Temporal Resolution:

A cross correlation of the amplified visible pulses was obtained by sending the unfocused pulses from the two dye amplifiers through a 3 mm long KDP crystal at a ~ 10 degree angle with respect to each other. The crystal was adjusted to the correct angle to yield the sum frequency UV light at ~323 nm. The central 1 mm region was passed through a slit and monitored with a photodiode. One of the two pulses was delayed using a computer controlled delay stage. The diode signal as a function of

this delay is shown in Figure 4. The FWHM of the peak is roughly 4 ps. This is much longer than expected simply from the pulse lengths, which would yield a cross correlation width equal to the autocorrelation widths, i.e. 1 ps. The extra width is likely to come from jitter between the two synch-pumped dye lasers. Although both are pumped by the same doubled Nd:YAG pulse, which synchronizes them to within the Nd:YAG pulse width, there is still some timing jitter within the pulse width. This comes mainly from the different responses of the two dye lasers to amplitude variations in the pump pulse. Each dye laser's pulse occurs when the integrated gain from the pump pulse exceeds the cavity losses. If this does not occur at exactly the same point on the pump pulse in the two lasers, changing the amplitude of the pump pulse will change not only the time required to build up the necessary gain in each laser, but also the relative timing of this event in the two lasers.

This inter-laser jitter is the important quantity for a pump-probe experiment and is the factor that adds width to the cross correlation. This jitter will depend on the timescale over which it is measured since it will depend not only on high frequency noise in the pump pulse, but longer term 'drift' in the pump power as well. The cross correlation shown in the figure was taken over a two minute interval. Shifts of the position of the cross correlation peak of 3-5 ps were observed over 10 minute intervals. Adjusting the dye lasers' length and end mirror angles to minimize their pulse widths and maximize their power, which changes their losses and hence the timing of the dye pulse relative to the start of the pump pulse, could shift the position of the peak by > 15 ps. Thus, temporal resolution for a visible/visible pump-probe

experiment using this laser system would be < 3-4 ps as long as the scanning took less than 2 minutes, or if the relative timing of the two pulses were recalibrated on this timescale. Without such measures, 5-8 ps resolution would be expected. The temporal resolution could be increased to ~ 1 ps, limited by the pulse widths, if part of the pulses were sent to a single shot cross correlator. This would allow monitoring the exact pump-probe delay for each shot and the data points could then be binned as a function of this delay. (This idea led to the concept of removing the delay stage entirely and banging on the laser table to cause a large enough jitter to cover the required time range. Implementation of this concept was not pursued.)

A cross correlation of the UV and VUV pulses was also obtained. The nonlinear medium used was a molecular beam of CH_3I. In essence, a pump-probe experiment to measure the dissociation lifetime of CH_3I excited at 266 nm was performed. However, the lifetime of CH_3I is known to be < 70 fs at this excitation energy, which is much less than our instrument resolution. Hence, the observed signal risetime is the instrument response and can also be viewed as the integral of the UV/VUV cross correlation.

This is the most complex measurement ever made with the picosecond system and is as close as one can get to measuring chemical dynamics without completing an experiment. It is possible that replacing methyl iodide with bromobenzene, which might have a measurable lifetime, would be the only required change to obtain chemical dynamics data. (Power supply problems have prevented any quick attempts at this goal.) The CH_3I data does represent more than just a cross correlation

measurement however, and will be discussed in terms of an experiment in the next section. For the purpose of this section, only the fact that an instrument response limited signal can be obtained is important.

Two such signals are actually observed. The first derives from methyl iodide absorbing a 266 nm photon and dissociating with the methyl fragment that is produced being ionized by the VUV light:

$$CH_3I \xrightarrow{266\ nm} CH_3I^{*} \xrightarrow{70\ fs} CH_3 + I \xrightarrow{118.9\ nm} CH_3^+$$

Thus, monitoring the rise of CH_3^+ yields the instrument response. Another process occurs which shows a drop as a function of time delay between the 266 nm and 118.9 nm light:

$$CH_3I \xrightarrow{118.9\ nm} CH_3I^+ \xrightarrow{266\ nm} CH_3I^{+*} \longrightarrow I^+$$

This process occurs only if the VUV pulse arrives at the sample before the UV pulse. The drop in I^+ signal again shows the instrument's temporal resolution.

Unfortunately, the competing processes shown below also occur:

$$CH_3I \xrightarrow{266\ nm} CH_3I^{*} \xrightarrow{70\ fs} CH_3 + I \longrightarrow I^+$$

$$CH_3I \xrightarrow{118.9\ nm} CH_3I^+ \xrightarrow{266\ nm} CH_3I^{+*} \longrightarrow CH_3^+$$

They differ from the above processes only in that they produce ions of the complementary fragments. They should rise and fall, respectively, with the instrument response time, and tend to cancel the signal from the first two channels. The

measurement here shows that the first two channels are dominant. Thus, a change of opposite sign is seen when observing the CH_3^+ and I^+ ion peaks in the time-of-flight mass spectrum, though the magnitude of the change is decreased by the latter processes and there is no region where the fragment ion signals go to zero. This leads to very poor signal to noise ratios.

The subtraction of the two partially power normalized (see below) spectra (CH_3^+-I^+), rescaled to go from 0 to 1, is shown in Figure 5. The calculated fit is to the integral of a 10 ps FWHM Gaussian. While the signal itself is clear, the risetime is definitely difficult to determine given the low signal to noise ratio. The 10 ps cross correlation width should probably be considered as 10 ± 5 ps.

This is possibly somewhat longer and definitely less precise than the visible cross correlation width. The data acquisition time for the UV/VUV cross correlation was roughly 10 minutes, several times longer than for the visible measurement. Because of this, the source of any real difference between the two cross correlation widths is ambiguous. While it could represent broadening of the UV and/or VUV pulses, it could also represent the larger range for jitter over longer timescales. From the estimates for temporal jitter/drift over 10 minutes from the visible measurement, it can be seen that no broadening of pulses is required to account for the UV/VUV signal risetime.

Noise:

While the nonlinear doubling and mixing processes used in this laser system provide the wavelengths necessary to do experiments, they also make such experiments difficult because they amplify the fluctuations present in the fundamental beams. With so many nonlinear steps, this laser system produces UV and VUV pulses with large fluctuations even though the pump laser fluctuations are relatively small. Specifically, starting from the mode-locked Nd;YAG laser with a specification of 2% noise (1064 nm), we observe fluctuations in the pump-probe ion signal, which combines the fluctuation of both the UV and VUV beams, of ~100%.

This is roughly what one would expect simply from the fluctuations in the commercial lasers assuming no saturation at any of the amplification or mixing stages. The final value should be proportional to the square of the pump-dye laser fluctuations times the fifth power of the probe dye laser fluctuations. In addition to the noise in the Nd:YAG pump laser, there is additional noise in the synch-pumped dye lasers due to such things as vibrations from the dye circulators used to run the dye jets. Our Nd:YAG amplifier chain certainly adds noise to the system as well.

Given this fluctuation, it is clear that shot-to-shot power normalization can greatly enhance the overall signal to noise ratio of an experiment. So far we have not directly measured the VUV energy each shot which could be done using the platinum photodiode created for use on the narrowband system. We have attempted to measure VUV fluctuations by monitoring an ion, such as CH_3I^+ in the case above, that should only depend on the VUV photon flux. Unfortunately, the dynamic range of our detector is insufficient to simultaneously monitor the abundant CH_3I^+ and the fragment

ions without saturating the parent signal to some extent. Seeding a small impurity in the beam, yielding an ion signal at a noninterfering mass, should allow improved normalization attempts. Similarly, monitoring the UV pump beam is also possible so that complete power normalization is theoretically possible. The experimentally achievable signal to noise ratio after full power normalization is not yet known.

CH_3I: An Experiment:

In addition to yielding an estimate for the laser system's temporal resolution, the measurement of the CH_3I dissociation lifetime described above also represents a full experiment: it has the same degree of difficulty as a measurement on a longer lived molecule. As such, calculations regarding the observed amounts of signal and background should be widely applicable to similar experiments on longer lived molecules. In particular, the factors contributing to the low signal-to-noise ratio here must be addressed in any proposed experiment, including "The Grand Plan".

Starting with a stable molecule and using a pulsed beam helps to give about three orders of magnitude more starting material in the CH_3I experiment relative to "The Grand Plan". Similarly, the cross-section for ultraviolet absorption in methyl iodide is 3-4 orders of magnitude greater than the overtone cross-sections for the chloroethyl radical (~10^{-18} cm^2 for CH_3I absorption). This factor is partially offset by the fact that we can only generate ~ $1/50^{th}$ as many photons at 266 nm as we can in the visible (1 mJ vs. 40 μJ). Overall, there should be roughly $2x10^4$ to $2x10^5$ times more dissociative CH_3I molecules than there would be chloroethyl radicals. This yields an

estimate of 1.6 x10^7 dissociating CH_3I molecules (assuming a 1 mm interaction length).

To maximize the detection of the CH_3 and I fragments relative to CH_3I, it is necessary to produce them in as small a volume as possible. This is true because of the inefficiency of nonresonant detection: as long as neither the pump nor probe steps are saturated, reducing the interaction volume increases the two laser signal.

It is important to note that, for single photon excitation and single photon detection, with equal excitation and detection volumes, the fragment ion signal is inversely proportional to the interaction area. This is in contrast to the one (VUV) photon signal yielding CH_3I^+ which is independent of the spot size. Decreasing the spot size, thereby maximizing the fragment ion (specifically I^+) signal relative to the parent ion signal, was important for this experiment because monitoring the I^+ ion became difficult as the CH_3I^+ signal became large. With the mass resolution of our detector, these two ions could not be completely resolved when the CH_3I^+ signal was >1000 times larger than the I^+ signal.

The inverse linear dependence of the pump-probe ion signal on spot size is also in contrast to the inverse quadratic dependence expected for *coherent* two photon processes. Coherent processes can only occur when the absorbed photons are overlapped in time as well as space. Our lower limit on laser spot size was dictated not by focussing ability, but by the appearance of ions from coherent multiphoton processes involving only the 266 nm light. These ions, both CH_3I^+ and fragment ions, became abundant enough to obscure the two laser signal as the spot size was

decreased below an estimated diameter of 200 μm. At this limit, these ions were probably being produced mainly in hot spots in the beam, and in any case represented a small fraction of the excited molecules. At ~ 200 μm, the excitation efficiency is ~17 %. Given the 10^9 VUV photon estimate above, the ionization efficiency is ~ $3x10^{-6}$, assuming a 10^{-18} cm^2 VUV cross section. Thus, a multiphoton 266 nm process, with an efficiency only ~10^{-5} times that of single photon excitation, would yield a background roughly as large as the expected signal.

These considerations of the dependence of the 'signal' ions and the various 'background' ions as a function of laser spot size imply an optimum spot size. If the spot is too large, the signal becomes small, and small compared to background from one (VUV) photon ionization. If the spot is too small, the one (266 nm) laser background overwhelms the two laser signal. In all cases, a match of the 266 nm and VUV spot sizes is the best choice. Using the experimentally determined 200 μm optimum spot size, the figures above yield predicted CH_3^+ and I^+ signals of ~ 50 ions per shot. This is roughly an order of magnitude larger than observed. The estimated cross-sections above, as well as the estimate for the spot size, could be off by enough to account for the difference.

Even with the lower observed signal of a few ions per shot, and with the difficulty of aligning two 200 μm laser beams (both invisible, one unable to propagate in air) to cross within the molecular beam, and with the fluctuations in laser power, this signal level would be 'easily' observable if there were no background. Even a reasonably small (roughly as big as the signal) constant background that depends on

only one of the two laser beams can be dealt with by a two laser signal minus one laser signal subtraction scheme. However, as described in the section above, in addition to two laser ionization of the fragments, two laser fragmentation of the ions can occur. These two types of processes occur for pump-probe and probe-pump temporal ordering of the two laser pulses. Thus they tend to cancel each other's signal change as the pulses are scanned through zero relative delay. For CH_3I under our conditions, CH_3^+ is produced mainly by fragmentation followed by ionization, but the ionization/fragmentation channel yield is nearly 90% as large. For I^+, the fragmentation/ionization channel has only half the yield of the ionization/fragmentation route, yielding an I^+ signal that decreases as one delays the probe laser.

These interfering processes are the most disturbing of the experimental difficulties. Since both pathways involve the same photons, changing the laser powers or the spot size will not change their relative contributions. The relative yields are properties of the molecule itself. Further, while for CH_3I the temporal profiles for the fragmentation/ionization and ionization/fragmentation pathways are mirror images of each other about time zero, in a molecule with a measurable dissociation lifetime this is no longer true. The fragmentation/ionization pathway will grow in over the dissociation timescale. The ionization/fragmentation pathway is still instrument limited however, because the ionization step is 'instantaneous' and the dissociation occurs *after* the second laser pulse and does not influence the observed dynamics. Thus the combined signal will no longer have a simple shape.

In the CH_3I case, the interfering pathways become a problem because of the

nonresonant detection scheme. If the CH_3I molecule were studied using resonant ionization of the I atom with high efficiency, not only would the signal be larger, but there would be no corresponding resonant enhancement of the interfering pathway. Certainly "The Grand Plan" has this detection advantage (ignoring the fact that we have not yet been able to detect a Cl REMPI signal with this system). However, it also has a very inefficient excitation step. Thus, normally neglected multi-photon processes, acting on the large unexcited radical, or even precursor, populations might produce unexpected, interfering signals. As noted in the signal calculation of "The Grand Plan" above, three photon nonresonant processes can produce nearly the same number of ions (at the precursor mass) as were expected for the Cl^+ signal. Any resonances would increase these signals. If the lower VUV power actually obtained, the VUV's non transform limited bandwidth, and the different time profiles of the UV and VUV combine to reduce the Cl ionization efficiency, the interference of nonresonant and/or resonant channels may become very significant. If "The Grand Plan" ever achieves the signal level calculated here, it may still be doomed by these unanticipated multiphoton background signals.

One could avoid the problem above by distinguishing between the two ionization pathways. While both pathways produce the same ions, the energetics of the electron from the ionization step should be different and characteristic of the ionizing species. Thus photo-electron spectroscopy (PES), the direction planned for the immediate future of the picosecond system, should allow observation of the fragmentation/ionization pathway in isolation.

Additionally, since PES can distinguish internal states of the ionizing species, it allows measurement of not only dissociation lifetimes, but of internal conversion and inter-system crossing timescales and even intramolecular energy redistribution. Thus, photo-electron spectroscopy may allow many of "The Grand Plan's" goals to be achieved, without requiring radicals or resonant detection, and without the problems of ion detection described above.

Conclusion:

In some sense, this must be considered a very preliminary report although VUV light has been produced in our lab for several years now. The picosecond system is still undergoing evolution for a variety of reasons, not the least of which is the temperamental nature of the aging equipment. Despite our best efforts to date, the system has so far remained too volatile to allow optimization of the detection scheme or for more than a cursory study of molecular dynamics. At various stages of this project, we have investigated iodobenzene, bromobenzene, and NO_3 with the intent to measure their as yet unknown dissociation lifetimes. Unfortunately, exploding power supplies and the like always seemed to appear at the least opportune moments.

Yet, in another sense, vast progress has been made. Starting from a bare lab, three tables full of lasers and optics have been aligned (!) and used to observe molecular dissociation with a time resolution of a few picoseconds. Useable amount of a variety of VUV and UV wavelengths have been produced. Hopefully (as always)

the replacement of the 11 year old laser equipment in the Nd:YAG amplifier with a new semi-commercial regenerative amplifier, and a switch to photoelectron detection, will push the project 'over the edge' into a working temporal spectrometer. And as always, the very 'cool' "Grand Plan", and its as yet un-named descendants (are you working on this James?), remain just another technical accomplishment or two away.

References

(1) Sewell, T. D.; Schranz, H. W.; Thompson, D. L.; Raff, L. M. *J. Chem. Phys.* **1991**, *95,* 8089-8107.

(2) Hintsa, E. J., Ph. D. Thesis, University of California, Berkeley, **1989**.

(3) Helfand, M. S., Ph.D. Thesis, University of California, Berkeley, **1989**.

(4) Mintin, T. K.; Felder, P.; Brudzynski, R.; Lee, Y. T. *J. Cehm. Phys.* **1984**, *81,* 1759.

(5) Okumura, M.; Yeh, L. I.; Myers, J. D.; Lee, Y. T. *J. Phys. Chem.* **1990**, *94,* 3416-3427.

(6) Cromwell, E. F., Ph. D. Thesis, University of California, Berkeley, **1991**.

(7) Normand, D.; Morellec, J. *J. Phys. B.: Atom. Molec. Phys.* **1980**, *13,* 1551-1561.

(8) Arepalli, S.; Presser, N.; Robie, D.; Gordon, R. J. *Chem. Phys. Let.* **1985**, *118,* 88-92.

(9) Schwab, J. J.; Anderson, J. G. *J. Quant. Spectrosc. Radiat. Transfer* **1982**, *27,* 445-457.

(10) Kung, A. H.; Young, J. F.; Harris, S. E. *Appl. Phys. Lett.* **1973**, *22,* 301-302.

(11) Cromwell, E.; Trickl, T.; Lee, Y. T.; Kung, A. H. *Rev. Sci. Inst.* **1989**, *60,* 2888.

(12) Falcone, R., private communication.

(13) Chesko, J. D., Ph. D. Thesis, University of California, Berkeley

(14) Bethune, D. S. *App. Opt.* **1981**, *20,* 1897.

(15) Roberts, J. P.; Harper, S. E.; Gosnell, T. R.; Taylor, A. J. *Opt. Comm.* **1991**, *83,* 231-234.

(16) Tonkyn, R. G.; White, M. G. *Rev. Sci. Instrum.* **1989**, *60,* 1245-1251.

(17) Hilbig, R.; Wallenstein, R. *IEEE J. Quant. Elect.* **1981**, *QE-17,* 1566-1573.

(18) Beaud, P.; Bi, J. Q.; Shutz, J.; Hodel, W.; Weber, H. P. in Ultrafast Phenomena VII; Harris, C. B.; Ippen, E. P.; Mourou, G. A. Zewail, A. H.; Springer, Berlin, 1990; pp 23.

(19) Cotter, D. *Opt. Comm.* **1991**, *83,* 76-80.

(20) Mahon, R.; McIlrath, T. J.; Myerscough, V. P.; Koopman, D. W. *IEEE J. Quant. Elect.* **1979**, *QE-15,* 444-451.

Figure Captions

Fig. 1-1.

Schematic of the Picosecond Laser System: Commercial Pump Lasers and Nd:YAG Amplifier Chain. The optical components are shown in roughly their correct positions on a 4 x 8 foot laser table. All of the components except mirrors are labelled in the drawing. Not shown are a $\lambda/4$ waveplate after the 10 Hz shutter, two more $\lambda/4$ waveplates surrounding the -60 mm/+100 mm telescope, and irises after the 5 mm Faraday Isolator, between the first two Nd:YAG heads, and before the telescope mentioned above. See the text for a more detailed description of the components.

Fig. 1-2.

Schematic of the Picosecond Laser System: Dye Amplifiers. The optical chain is shown very approximately on a 4 x 8 ft. laser table. The optical delay lines were adjustable with micrometer driven translation stages. The optics for the dye laser beams are labelled for the 594 nm chain (the left chain) in the diagram. The optics are identical for the other chain. The three dye cells in each chain (shown as rectangles at the end of the 'fans' of 532 nm light) are 1 mmϕ x 20 mm, 3 mmϕ x 30 mm, and 6 mmϕ x 60 mm. The 532 nm light from the Nd:YAG amplifier is separated from the 1064 nm light by a dichroic mirror and then split into equal portions to pump the two dye cell chains. The partial reflectors further split the green to pump the three cells with 4%, 15%, and 81% of the light respectively. Cylindrical lenses are used to shape the 6

mm circular 532 nm beam to fill the input area of the three dye cells (i.e. forming a 4 mm x 20 mm beam for the first cell. See Evan Cromwell's thesis for details.). Not shown are two autocorrelators and the second harmonic and mixing optics used to produce ultraviolet light (297 nm and 266 nm for the CH_3I experiment discussed in the text.).

Fig. 1-3.

Autocorrelation of the 1 mJ, 710 nm output of the dye amplifier. This trace was recorded using the 'homebuilt' autocorrelator described in the text. The FWHM of the peak is 1.0 ps. This is equal to the autocorrelation width of the unamplified output of the dye laser using the same autocorrelator.

Fig. 1-4.

Typical cross-correlation of the 1 mJ 594 nm and 1 mJ 710 nm amplified dye laser pulses. This trace was recorded with the optical setup described in the text over a roughly 2 minute interval. The FWHM is < 4 ps and is typical for a two minute interval. Over longer intervals, the peak position shifts by several ps. The peak width is much longer than expected from the pulse widths of the amplified pulses (~1 ps). Both the width and the jitter are caused by changes in the relative timing of the two dye lasers pulses.

Fig. 1-5.

UV/VUV Cross-correlation / Instrument Temporal Response. The signal shown here has a complex origin which is explained in the text. Experimentally, it is the difference of the power normalized CH_3^+ and I^+ ion

signals from a CH_3I precursor in a molecular beam irradiated at 266 nm and 118.9 nm. The signal is plotted as a function of the relative delay of these two pulses. Positive time is defined as the 266 nm light arriving first. The smooth trace is the integral of a 10 ps FWHM Gaussian centered at the estimated time zero. The risetime of the signal is estimated as 10 ± 5 ps from comparison of the two traces. Since the relevant molecular processes (dissociation, ionization) occur much faster than this risetime (< 70 fs), it represents the overall instrument response time of the picosecond spectrometer.

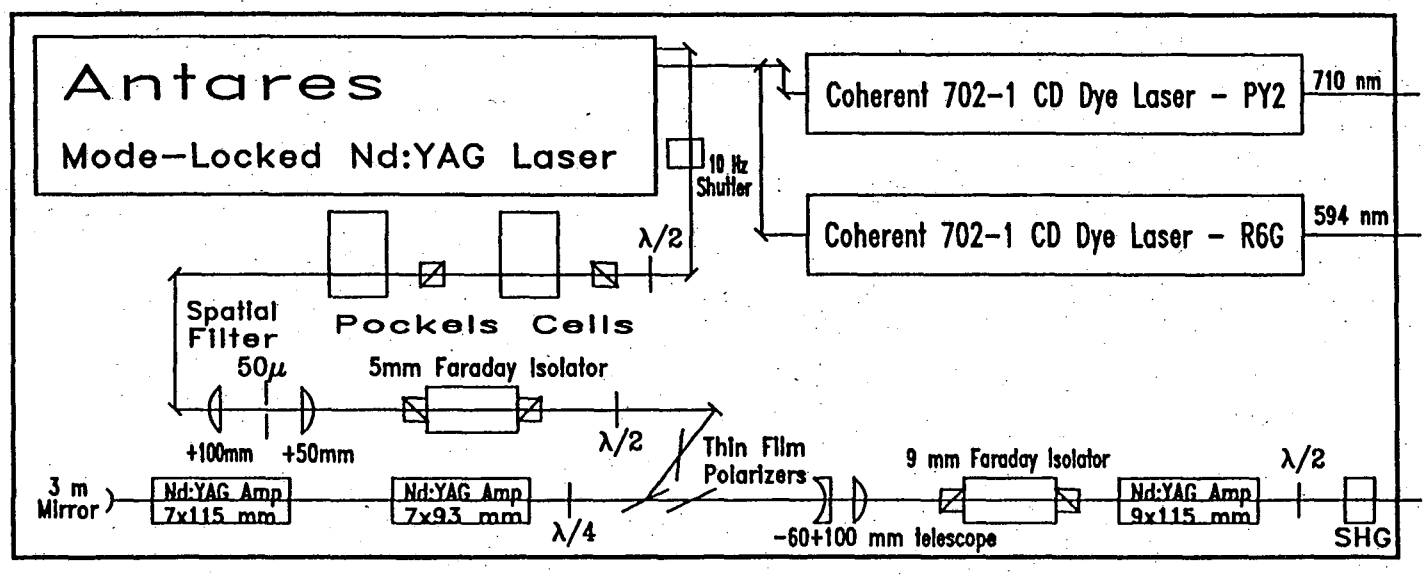
Antares
Mode-Locked Nd:YAG Laser
10 Hz Shutter
Coherent 702-1 CD Dye Laser - PY2
710 nm
Coherent 702-1 CD Dye Laser - R6G
594 nm
λ/2
Pockels Cells
Spatial Filter
50μ
5mm Faraday Isolator
+100mm
+50mm
λ/2
Thin Film Polarizers
9 mm Faraday Isolator
λ/2
3 m Mirror
Nd:YAG Amp 7x115 mm
Nd:YAG Amp 7x93 mm
λ/4
-60+100 mm telescope
Nd:YAG Amp 9x115 mm
SHG

Figure 1.

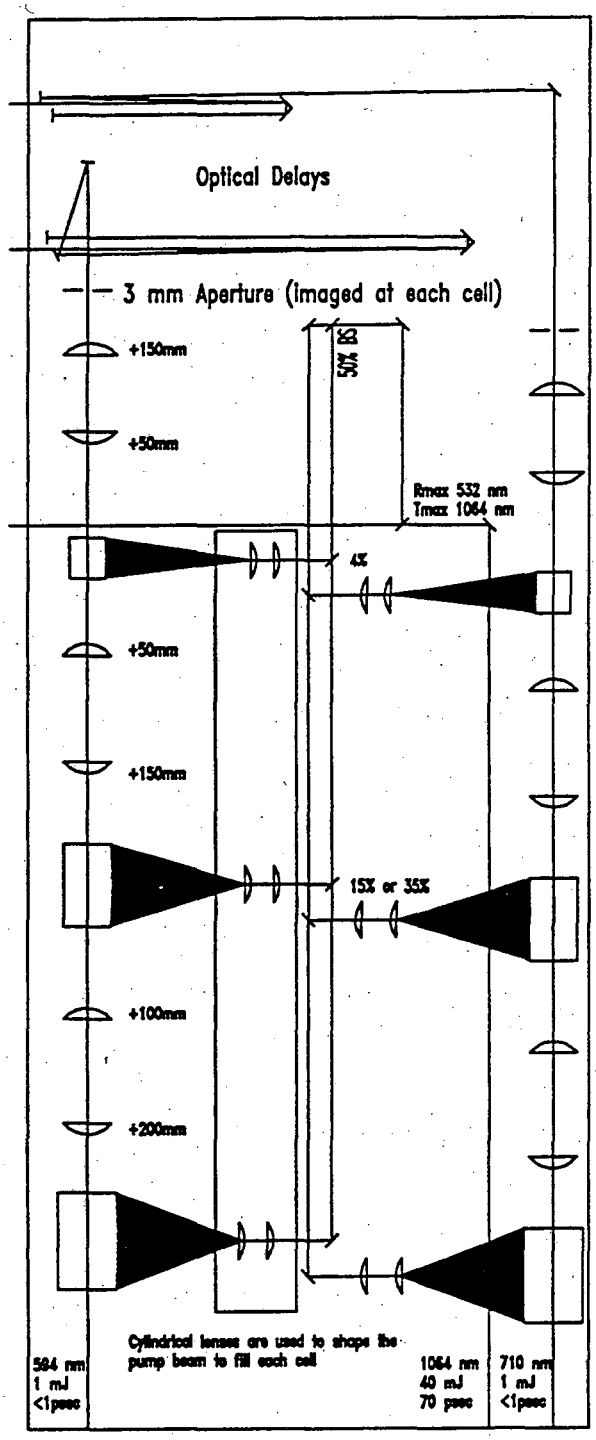
Optical Delays
3 mm Aperture (imaged at each cell)
+150mm
+50mm
50% BS
Rmax 532 nm
Tmax 1064 nm
4%
+50mm
+150mm
15% or 35%
+100mm
+200mm
Cylindrical lenses are used to shape the pump beam to fill each cell
584 nm
1 mJ
<1psec
1064 nm
40 mJ
70 psec
710 nm
1 mJ
<1psec

Figure 2.

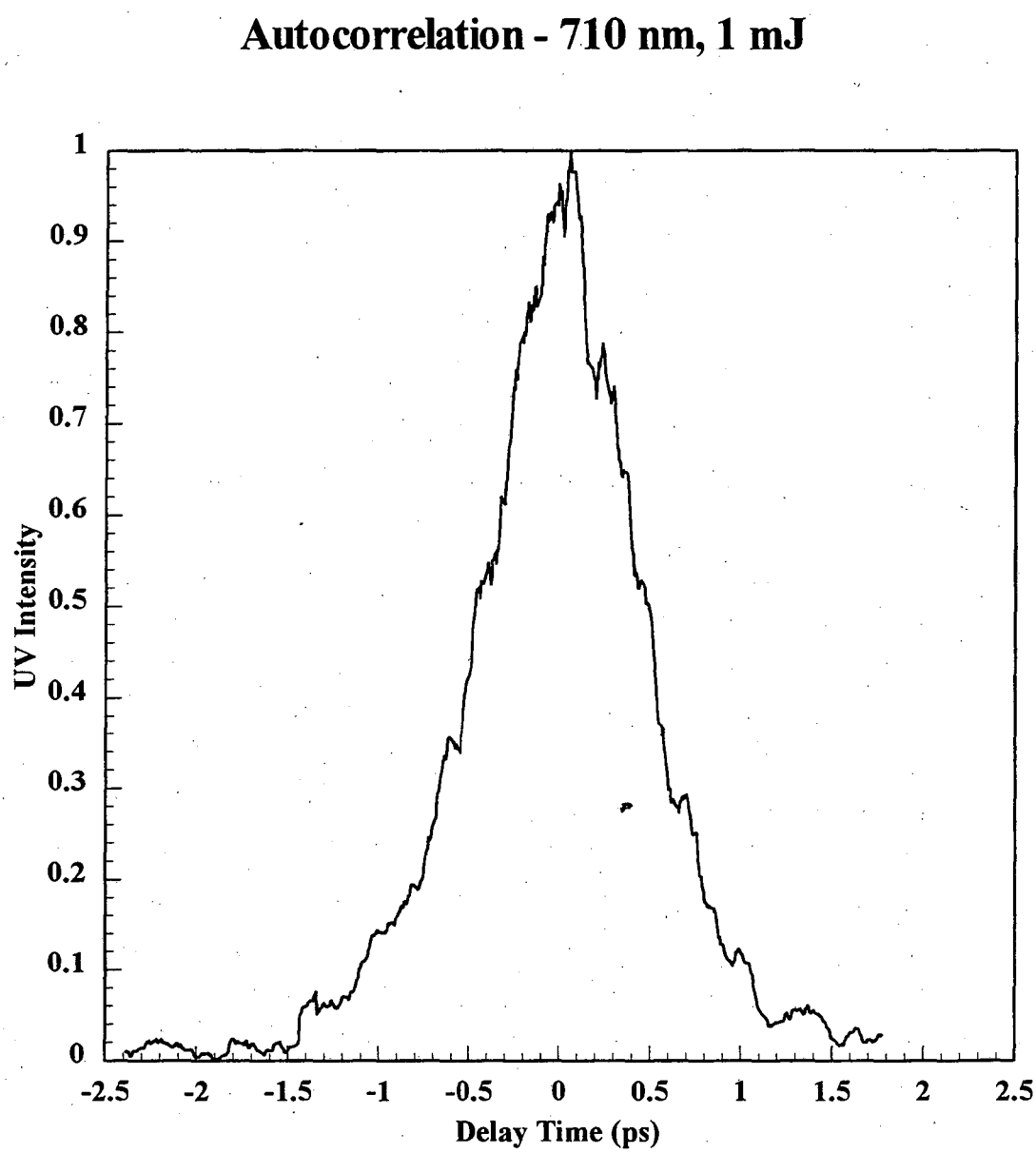
Autocorrelation - 710 nm, 1 mJ
UV Intensity
1
0.9
0.8
0.7
0.6
0.5
0.4
0.3
0.2
0.1
0
-2.5
-2
-1.5
-1
-0.5
0
0.5
1
1.5
2
2.5
Delay Time (ps)

Figure 3.

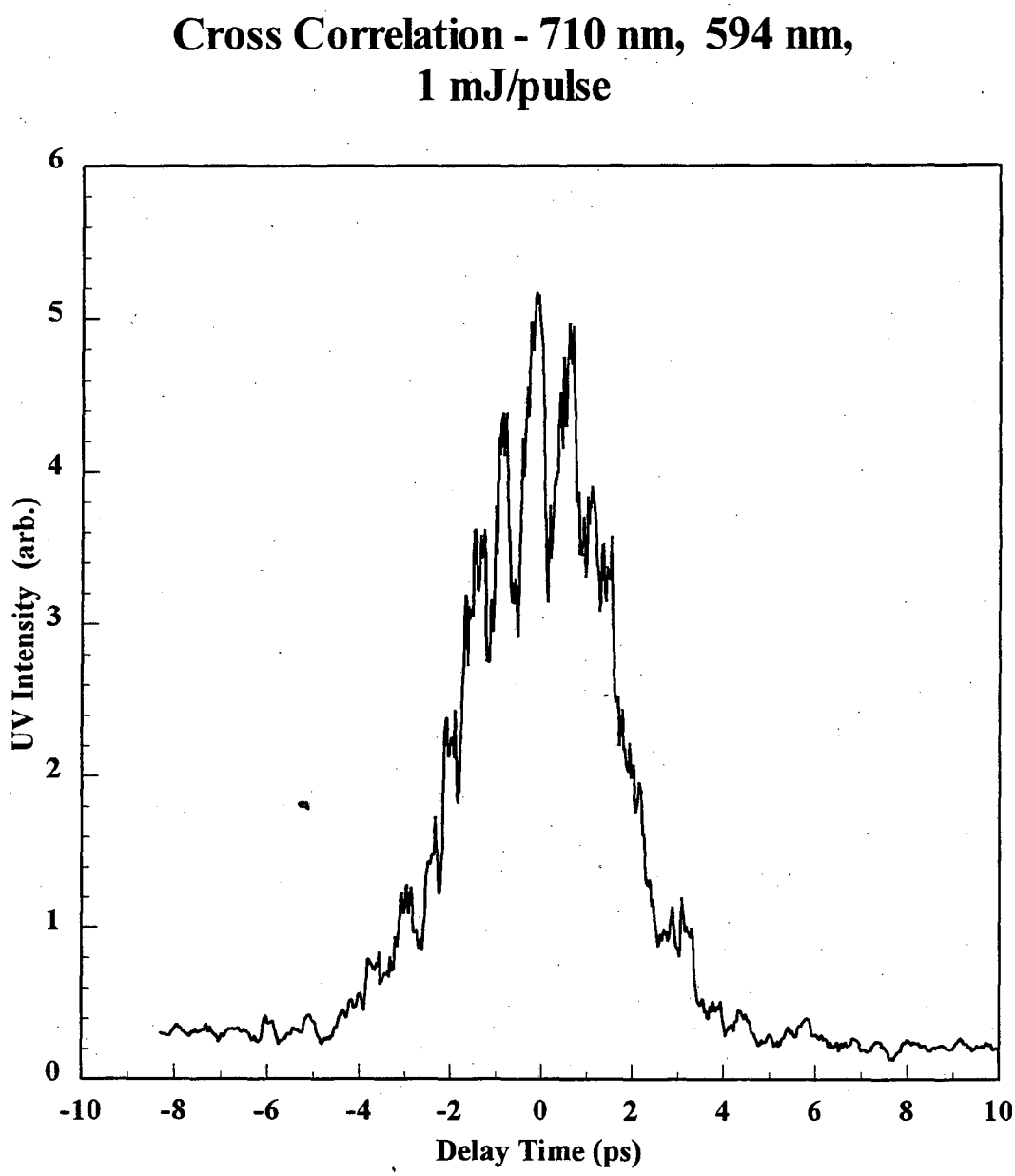
Cross Correlation - 710 nm, 594 nm,
1 mJ/pulse
UV Intensity (arb.)
0
1
2
3
4
5
6
-10
-8
-6
-4
-2
0
2
4
6
8
10
Delay Time (ps)

Figure 4.

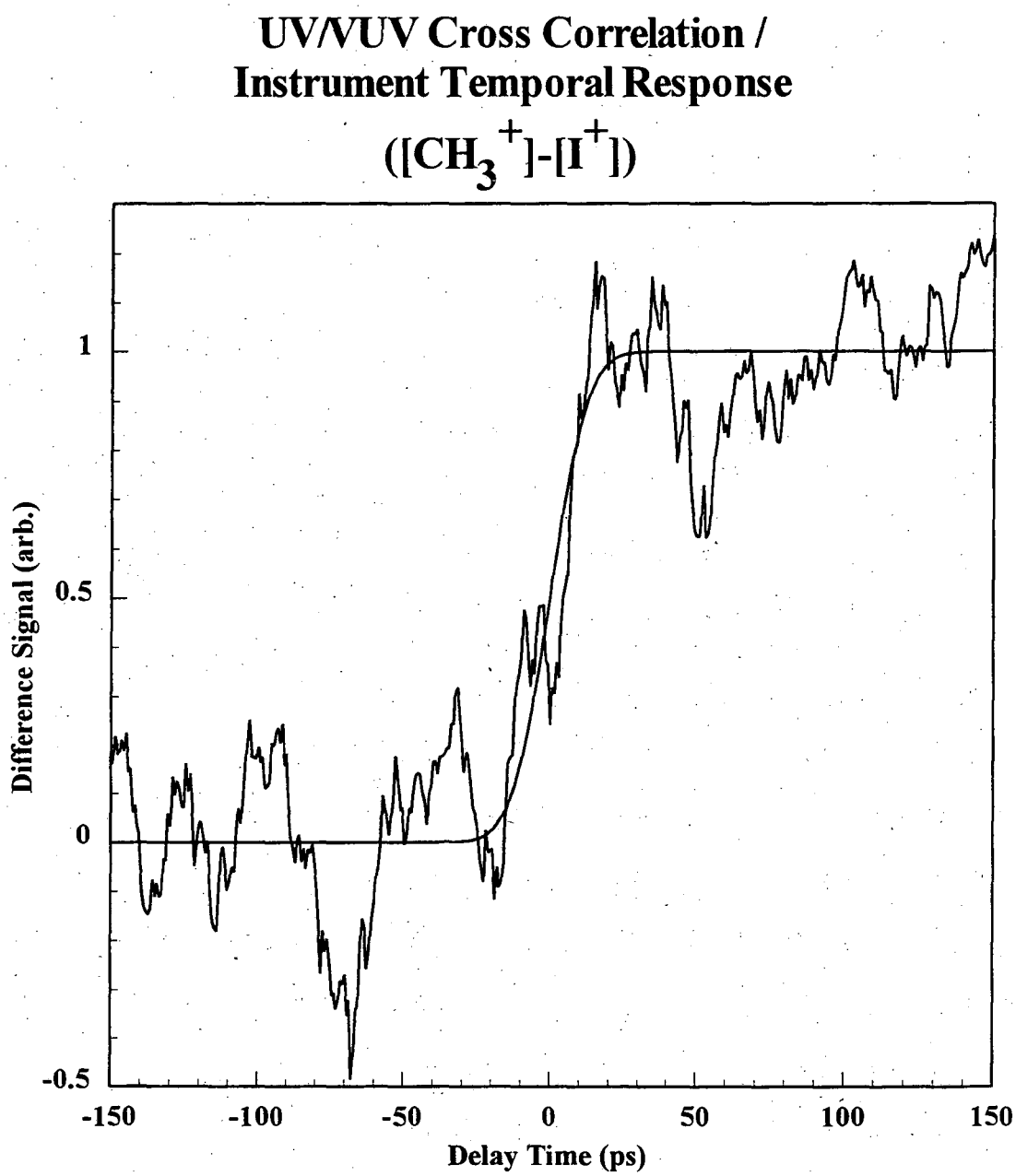
UV/VUV Cross Correlation /
Instrument Temporal Response
([CH3+]-[I+])
Difference Signal (arb.)
1
0.5
0
-0.5
-150
-100
-50
0
50
100
150
Delay Time (ps)

Figure 5.

Chapter II: 193 nm Photodissociation of Cyclopentadiene

Introduction:

The dissociation of cyclopentadiene (C_5H_6) to an H atom and the cyclopentadienyl radical(C_5H_5) requires only 78 kcal/mol. This low value is due to resonance stabilization of the radical electron in the cyclopentadienyl ring. However, the most thermodynamically stable dissociation pathway is not H atom loss but opening of the ring and formation of methyl acetylene (propyne) and acetylene (66.1 kcal/mol). The activation energy for this channel is not known, but a simple calculation based on group additivity (described in a later section) yields a barrier of ~87 kcal/mol to ring opening and a second very high barrier (>118 kcal/mol relative to C_5H_6) for hydrogen migration. A variety of other channels are thermodynamically accessible with 193 nm excitation. They are listed in Table 1.

Interest in the unimolecular dissociation of cyclopentadiene has arisen in several systems in combustion chemistry. The phenoxy radical has been found to undergo unimolecular decomposition to CO and cyclopentadienyl radical in thermal decomposition studies above 1000 K[1,2,3]. This reaction has also been observed in infrared multiphoton dissociation studies using the molecular beam photofragment

translational spectroscopy technique[4]. Butler et. al. have suggested that this reaction is part of a common reaction pathway of aromatic hydrocarbons[5]. Their work on the oxidation of alkylated aromatics shows that side chains oxidize before the aromatic ring, leaving benzene or phenyl radical[6,7,8,9]. The phenyl radical is then oxidized to phenoxy which then dissociates to cyclopentadienyl radical. In Butler et. al.'s turbulent flow reactor study cited above, the oxidation of cyclopentadiene itself was studied to extend knowledge of this pathway[5]. It was found that cyclopentadiene exhibits production of CO_2 with a concentration vs. time profile unique from that of other hydrocarbons, suggesting an unusual reaction mechanism. Specifically, the CO_2 was produced early, before the peak of CO production, it occurred without a measurable temperature rise, and it increased relative to CO concentrations at higher fuel to oxygen ratios. These anomalies could not be fully explained, but mechanisms which postulated cyclopentadiene dissociation to $:CH_2$ or acetylene which would then react to produce CO_2 were described. Another mechanism relying on a large H atom population due to the weak C-H bond in cyclopentadiene was also investigated.

Cyclopentadiene has also been shown to be important in the buildup of hydrocarbons from smaller precursors. Dean[10] has shown that cyclopentadiene is largely responsible for the autocatalytic effect in the production of ethane and larger hydrocarbons during methane pyrolysis. He describes how cyclopentadiene, once formed, catalyzes the dissociation of methane into methyl and H radicals. The weak C-H bond in cyclopentadiene allows a cycle of dissociation to cyclopentadienyl radical and subsequent abstraction of hydrogen from methane to occur very rapidly. Dean's

analysis did not require the existence of other unimolecular dissociation reactions of cyclopentadiene, although if they existed they would limit the catalytic cycle above.

These studies suggested that investigating the unimolecular dissociation pathways of cyclopentadiene with a technique that is sensitive to minor channels could be of use in understanding combustion reactions. Fundamental questions about the competition between ring opening, H atom loss, H_2 loss, and isomerization to bicyclic structures could also be answered. The present study uses 193 nm excitation followed by analysis of the photofragment translational energies. Cyclopentadiene's absorption bands near 193 nm have been assigned to several 3p-Rydberg <-- X transitions[11]. The non-bonding character of the excited electronic state and the large size of the cyclopentadiene make it reasonable to expect that internal conversion to the ground electronic state should be faster than dissociation. Thus, a photolysis experiment can be expected to probe the same potential surface as the thermal experiments, although with a much higher average energy ('temperature' >3600K). It turns out that 193 nm photolysis probes an energy that is near the most probable energy for dissociating molecules at 1000 K, making this experiment very relevant to the thermal work. There has been one previous study of the unimolecular dissociation of cyclopentadiene in the gas phase by 193 nm laser excitation. This study by Yi et. al.[12] used laser induced fluorescence (LIF) to measure the translational energy of the H atom product. The quantum yield for H atom was found to be .85±.07 with a Maxwell velocity distribution described by a temperature of 3690 K. The identification of other channels could not be accomplished with the LIF technique, but H_2 elimination was

proposed as the only other channel.

Experimental:

Our study was done using the molecular beam Photofragment Translational Spectroscopy (PTS) technique. The main apparatus used for this study has been described previously[13]. It consists principly of a vacuum chamber with a differentially pumped rotatable molecular beam source that can be crossed by a laser beam at right angles, and a mass-resolved time-of-flight spectrometer. The spectrometer consists of a 20.7 cm flight path, electron bombardment ionizer, quadrupole filter, and a Daly ion counter[14]. A schematic is shown in Figure 1. Signal was recorded using a multichannel scaler triggered by the laser. Photofragments were detected as a function of mass, lab velocity, and the angle between the molecular beam and the fragment's lab velocity. Data was analyzed to yield the branching ratio between the various dissociation channels and the center-of-mass translational energy distribution, $P(E_T)$, for products from each channel using standard techniques[15]. This involves attempts to fit all time-of-flight spectra with a single set of molecular dissociation parameters (fragments masses, $P(E_T)$s, and the branching ratio of the dissociation channels, etc.). A new interactive version of the program CMLAB2 is used to perform the required iterative convolution of the molecular parameters with the instrument response function[16]. The program also computes all coordinate transformations neccesary to yield laboratory frame time-of-flight spectra from the given center-of-mass

distributions. The original CMLAB2 program, developed by X. Zhao, is described in his thesis along with the mathematical formalism of the calculation[15].

Cyclopentadiene was prepared by cracking dicyclopentadiene as described in a standard organic chemistry lab text[17]. The dicyclopentadiene was obtained from Aldrich Chemical Co. Helium at a pressure of 760 torr was bubbled through the cyclopentadiene at a temperature of -16 C to yield a mixture of 7% cyclopentadiene in helium. This mixture was metered through a needle valve and then expanded through a .3 mm nozzle into the chamber. Pressure behind the nozzle was kept around 95 torr, limited by the pumping speed of the chamber. The nozzle was heated to 100 C to eliminate significant dimer formation (dimers were observed as a laser dependent off-axis signal at the parent cyclopentadiene mass, m/e 66) . The molecular beam was collimated by two 1 mm diameter skimmers. Pressure in the source region was $3x10^{-4}$ torr. The beam/laser interaction region was maintained at 10^{-7} torr.

The beam was characterized by recording time-of-flight spectra of the beam at 0 degrees. A detector aperture of .13 mm was used to reduce the particle flux into the detector. Spectra were recorded at several masses and were used to determine the ion flight constant, beam velocity, and the velocity spread of the beam[18]. (The program KELVIN.EXE was used[16].) Data were also taken at 1, 2, and 3 degrees when it became obvious from the analysis that the beam must have some variation across its width.

Lambda Physic EMG 103 MSC and EMG 202 MSC excimer lasers, lasing on the 193.3 nm ArF transition were used as the photolysis source. The spot size at the

interaction region varied from 1x3 mm to 2x6 mm and pulse energy varied from 25 to .1 mJ at the interaction region. The majority of data was taken at less than 10 mJ/cm^2. The experiments were run between 70 and 200 Hz, depending on the laser's capability at the time.

The apparatus described above was used to take time-of-flight spectra of masses from 66 to 12. H and H_2 could not easily be detected on this apparatus due to high backgrounds and low signals (H and H_2 are much less massive than their conjugate fragments. For a given energy release, conservation of linear momentum makes H and H_2 the fastest fragments by far. Since a large recoil velocity disperses fragments into a large volume before detection, and because the detection efficiency is inversely proportional to velocity, the signal is much lower for hydrogen than for more massive fragments. The ionization efficiency for H and H_2 is also much smaller than that for heavier fragments.) Experiments to directly measure H and H_2 products were performed, but on a second apparatus using a pulsed molecular beam. The standard configuration for machines of this type has also been detailed previously[19]. Normally used for crossed molecular beam experiments, this machine was modified to allow very high sensitivity photodissociation experiments. A similar setup has been used on another machine in our group to measure photolytic H and D atoms from several molecules[20]. A pulsed molecular beam valve[21] with a 1 mm diameter orifice was mounted vertically in the source chamber. It was backed by 760 torr of 10% cyclopentadiene seeded in helium which was prepared as before. The laser beam crossed the molecular beam 5 mm above the valve, in the source region.

Photofragments were allowed to enter the main chamber through two large (2-3 mm) skimmers and were detected by placing the mass spectrometer along the skimmer axis, at 90 degrees relative to the molecular beam.

Thus, in this geometry, the molecular beam, laser beam, and detector were mutually perpendicular and only photofragments with laboratory recoil velocities perpendicular to the molecular beam could be detected. This meant that only fragments with a center of mass velocity greater than the beam velocity could reach the detector. For H_2 detection and a beam velocity of 10^5 cm/second, this corresponds to a low energy cutoff of 1 kcal/mol which is better than could be achieved for the cyclopentadienyl fragment in the rotating detector setup (where we were limited to a minimum laboratory angle of ~8 degrees due to the background from cracking in the ionizer of parent molecules near the beam axis). The setup on this machine was estimated to provide roughly 3000 times as much signal as the first setup due to the reduction in the nozzle to interaction region distance and to the use of a pulsed instead of continuous source. An exact calibration was not performed. Spectra were taken at various pulsed valve to laser time delays in order to maximize the signal and to determine if there were any effects on the product velocity distributions due to secondary collisions in the molecular beam. The only variation of the spectra was in the slow, time dependent background due to the pulsed valve alone.

Analysis and Results:

The largest mass for which signal was detected was m/e 65, $C_5H_5^+$, as expected. This corresponds to H atom loss from cyclopentadiene. Experimental conditions for investigating dissociations from single photon absorption were determined by a power dependence study at m/e 65 and m/e 64. (Studies over a narrower range of laser fluence were done at all masses to confirm that single photon events were the source of photofragments.) Figure 2 shows the results of this study. The data were taken with two different laser beam spot sizes, with two different methods of measuring the laser power. This is probably the major source of scatter in the data. Also plotted in the figure is a line representing linear power dependence. As can be seen in the inset, the data deviates from this line above 5 mJ/cm^2. The other curve on the figure represents the data of Yi et.al. on H atom fluorescence vs. laser fluence. The matching of the data above to Yi's is subject to an arbitrary scaling of the Y axis. I have chosen to put Yi et. al.'s lowest point (~ 7 mJ/cm^2) at .9 of linear dependence. This fits their data within the uncertainty of mine, but is otherwise arbitrary. This would imply that nearly all of Yi et. al.'s data are somewhat saturated. This would cause their estimate for the quantum yield of H atoms to be systematically low. Since absolute fluence measurements are harder to make than relative ones, it might be reasonable to assume a systematic error in the laser fluence values for my data or Yi et. al.'s and to adjust the relative scaling of the fluence axis between the data sets. Our spot size measurements are done by measuring the extent of a burn

pattern on photographic paper made by multiple laser shots. An error of 50% in estimating the laser spot size by this method would not be impossible. This would mean that the linear region extends to roughly 10 mJ/cm^2 and that the lowest fluence portion of Yi et. al.'s data would also be linear. However, it does not appear reasonable to include the data from 15 to 25 mJ/cm^2 in this region as Yi et. al. do. It is clear from the additional data in the present experiment that what Yi et. al. took to be scatter about a linear power dependence is a real saturation effect. (This also becomes more apparent if one requires the point 0,0 to be part of Yi et. al.'s data set.) Thus, the caution about saturation during the quantum yield measurement could still apply as the measurement, according to their paper, was done at "<25 mJ/cm^2 " which includes fluence levels that partially saturate the transition.

Another point to note from this study is that both m/e 65 and m/e 64 exhibit the same saturation effect. The time profile of the photofragments at these two masses are identical as well. This suggests that both signals arise from cyclopentadienyl fragments, which sometimes lose a second hydrogen during ionization in the detector. Since the saturation at both masses persists to fluences well above that at which Yi et. al. see a multiphoton effect in the H atom signal, a two photon process involving absorption by cyclopentadienyl radical leading to the loss of a second H atom cannot explain both data sets. Indeed, the difference between the H atom data and the m/e 65 data shows an approximately cubic power dependence, suggesting that at least three photons are involved in producing the additional H atom signal. This point will be discussed further in conjunction with the results from my high fluence data later in

this section.

Based on this power dependence study, only data at fluences less than 3 mJ/cm^2 were used to determine the branching ratios and translational energy distributions ($P(E_T)$s) for single photon dissociation of cyclopentadiene. The dissociation channels discovered will be discussed in order of increasing symmetry of conjugate fragment masses (decreasing mass of the heavier fragment). A Newton (velocity space) diagram that shows the extremal laboratory velocities and angles for various possible reaction channels based on thermodynamic limits is provided in Figure 3. Results obtained at higher fluences will be discussed at the end of the section.

H ATOM ELIMINATION:

As stated above, signal was observed at m/e 65, corresponding to H atom loss from cyclopentadiene. Signal with the same time-of-flight profile was observed at all m/e ratios corresponding to possible fragments of the cyclopentadienyl radical as well as at m/e 32 - 30. The latter are probably doubly charged ions with masses from 64-60. They have been previously observed in the mass spectrum of cyclopentadiene[22]. The highest signal was recorded at m/e 39 with roughly three times more signal than m/e 65. Other prominent masses (>4% of the total) were m/e 64-61,38, and 37. The H atom elimination channel is so dominant that it accounted for at least 25% of the ions formed at every m/e except 52, even at mass-to-charge

ratios that had less than .05% of the total H atom loss signal.

Time-of-flight(TOF) spectra at m/e 65 for laboratory angles of 7, 10, and 14 degrees are shown in Figure 4. Shown in Figure 5 is the TOF spectrum for H atom taken with the pulsed valve setup. The lines through the data points are the fit to the spectrum from CMLAB2.EXE using the $P(E_T)$ shown in Figure 6.

Before describing the $P(E_T)$ in detail, I think it is worthwhile to discuss the unique analysis difficulties presented by the H atom elimination channel. They stem primarily from the very unequal distribution of translational energy between the cyclopentadienyl and H atom photofragments due to the conservation of linear momentum during the dissociation. The H atom receives 98.5% of the kinetic energy, 65 times as much as the cyclopentadienyl fragment. As can be seen in the Newton diagram (Figure 3) even the fastest cyclopentadienyl fragments will only reach a laboratory angle of 16.5 degrees. Their maximum center of mass velocity is roughly one quarter of the beam velocity. As it turns out, more than 90% of the signal has less than 20% of the thermodynamically allowed maximum translational energy, and correspondingly, less than 30% of the maximum possible velocity. This presents two major problems. One is that for accurate determination of the $P(E_T)$ with a resolution of 2 kcal/mol, one must measure the laboratory velocity and angular distributions of the products to precisions better than the velocity (~9%) and angular spread (~2°) of the molecular beam. At this level of resolution, the representation of the molecular beam as a cone with separable velocity and angular distributions as well as the choice of a 'supersonic' functional form for the beam velocity introduces errors into the calculated

fit of the data. (The beam actually has a small, low velocity tail that is not fit by the 'supersonic' functional form. It was also noticed that the velocity spread is somewhat larger (~12% FWHM) at the edges of the beam than in the center (~9% FWHM).) These errors make it impossible to fit data taken at different angles with the same $P(E_T)$ using the measured beam parameters. The use of 'effective' beam parameters, boosting the velocity spread to ~ 11% in the simulation, allows the construction of a single $P(E_T)$ to fit data from all lab angles, but may introduce small distortions to the true $P(E_T)$.

The second problem stems from the fact that the background from cracking of parent cyclopentadiene in the detector overwhelms the cyclopentadienyl radical signal within 7 degrees of the beam. This means that cyclopentadienyl fragments from dissociations with less than roughly 13 kcal/mol of translational energy cannot be seen. The $P(E_T)$ below this cutoff, down to roughly 3 kcal/mol, can be obtained by looking at the H atom directly at a 90 degree lab angle. However, the H atom data is not sensitive to the high energy portion of the $P(E_T)$ because the detector is inherently less sensitive to faster fragments and because each microsecond of time represents many more velocities at high translational energies. Thus, for high energy H atoms, the signal is small (and noisy) and the $P(E_T)$ is not uniquely determined by data with a 1 microsecond time resolution because many high energy points on the $P(E_T)$ contribute to very few time bins. This makes the synthesis of the H atom results, which determine the low energy portion of the $P(E_T)$, and the cyclopentadienyl results, which determine the high energy portion of the $P(E_T)$, somewhat arbitrary with regard to

scaling. The two data sets do overlap for about a 6 kcal/mol region, but the beam effects noted above could easily introduce a 10% error in the height of the $P(E_T)$ at low energies relative to that at high energies. Note that this error only affects the slope of the $P(E_T)$ between 13 and 19 kcal/mol and the relative scaling of the regions on either side of this range, i.e. it does not affect the shape of the $P(E_T)$ within the low and high energy regions. (This sort of error in the $P(E_T)$ will affect calculated yields for the reaction channels. Since the sizes of the other channels are determined relative to the H atom loss channel using data at 10 degrees or greater, they are really being compared only to the high energy portion of the H atom signal. Calculating the true branching ratio requires estimating the amount of signal for each channel that is not seen from their $P(E_T)$s. Fortunately, due to the dominance of the H atom channel, the quantum yield of H atom product would be changed only 0.6 % by the possible 10% error in the $P(E_T)$ above.)

To some extent, the scaling problem also exists when trying to fit the cyclopentadienyl data at the various angles, since each angle is most sensitive to a different portion of the $P(E_T)$ with only a few kcal/mol of useful overlap. However, in this case, the fact that the beam conditions were the same for the cyclopentadienyl data at the three different angles introduces a useful constraint: one can require that the calculated to experimental signal ratio remain constant over the data sets. This ratio is a measure of the total reactive flux required to produce a given experimental signal. It is the factor required to scale the calculated signal, resulting from a total reactive flux of one (arbitrary unit), to the experimental data. All Jacobian factors in

the transformation of a given center-of-mass distribution to the laboratory frame at a given angle are taken into account. Holding this ratio constant between data sets taken at different laboratory angles is equivalent to requiring that all of the data represent the same physical event, namely a given number of dissociating molecules.

This procedure was used to construct a $P(E_T)$ from the cyclopentadienyl data. An 'effective' molecular beam was used in the fitting. The root mean squared velocity was maintained at the measured value (13.3×10^4 cm/s), but the speed ratio was lowered from measured value of 11.4 at the beam center to an effective value of 9. The cyclopentadienyl data files represent 20-40,000 laser shots. The constant background is subtracted and the data are smoothed by 7 point averaging for analysis.

The H atom data was processed differently because it has much more laser induced noise. No smoothing was attempted because the H atom time-of-flight data has much higher frequency components than the m/e 65 data. The molecular beam was arbitrarily assigned a velocity of 15×10^4 cm/s with a speed ratio of 10. (Because of the kinematics, changing the beam velocity by even a factor of 3 does not appreciably affect the calculated spectrum.) The noise in this data, a severe version of the high frequency ringing common in all of the data, has been postulated to involve modulation of the transmission of the quadrupole mass spectrometer by the RF emissions of the excimer laser [23]. It is proportional to total count rate. The H atom signal is only 1-3% of the background level and occurs very close in time to the triggering of the laser. Both of these factors make the H atom data very noisy (20-50% modulation at high frequencies, even after 200K to 400K laser shots). To

reduce this effect, the trace shown (Figure 5) is the subtraction of data taken at 8 mJ/cm^2 from data taken at 25 mJ/cm^2 fluence. From the discussion of Yi et.a al.'s power dependence data above, one can conclude that the 25 mJ/cm^2 data should show some saturation, but should not include much of a contribution from multiphoton processes. This, and the fact that the two data sets do not appear to differ in overall shape suggests that the procedure is not introducing spurious signal. The main benefit of this procedure, other than improved aesthetics, is an improvement in the fit to the higher energy H atom signal. This portion of the $P(E_T)$ is already well defined by the m/e 65 data. In the individual data sets, there is a large negative spike of laser noise in the high velocity portion of the spectrum and it was not clear whether the $P(E_T)$ derived from the m/e 65 data was consistent with the H atom data. After the subtraction, it is clear that the two data sets are consistent. It should also be noted that this subtraction does not affect the shape of the data in the low H atom velocity region. Both spectra have the same shape in this region.

There are certainly many places that small errors can be introduced into the characterization of the H atom elimination channel as described above. Yet, even with these caveats, there is a lot of useful information in the derived $P(E_T)$ (Figure 6). The most obvious feature of the $P(E_T)$ is the peak at ~ 5 kcal/mol. One could question whether this is an experimental artifact since it is determined solely from the H atom time-of-flight. Such an artifact would arise if slow H atoms were depleted by some mechanism. However, n-propyne was studied using the same experimental setup and was observed to have no barrier to H atom loss, corresponding to a $P(E_T)$ that peaks at

zero translational energy[24]. The time-of-flight spectra for the two molecules are quite different. Thus, if the peak is artificial, there must be a chemically specific mechanism that depletes slow H atom signal, which I consider unlikely. It should be noted that the point at 0 kcal/mol is not well determined by the data and is therefore somewhat arbitrary. However, the point at ~2 kcal/mol is well determined and must be lower than the next two points to fit the data.

Conversion of the 5 kcal/mol peak into a limit on the barrier to H atom loss can be accomplished as follows. Assume an RRKM type $P(E_T)$ at the transition state and consider the changes in the product distribution to occur as the products descend the barrier. If all of the potential energy is converted to translational energy, the minimum observed translational energy, which would also be the maximum of the $P(E_T)$ distribution, would be the height of the barrier. If some of the potential energy of the barrier becomes internal energy, lower translational energies would be observed and the maximum of the $P(E_T)$ could also be shifted to an energy below the actual barrier. Thus, 5 kcal/mol is a lower limit to the barrier height to H atom loss in cyclopentadiene.

Shown in Figure 7 are some limiting cases for the H loss $P(E_T)$ from Figure 6. The first is an RRKM type $P(E_T)$. This was calculated using *ab-initio* frequencies for cyclopentadiene and the cyclopentadienyl radical [25]. The cyclopentadiene H loss transition state was assumed to have the frequencies of the cyclopentadienyl radical with two additional low frequency bending modes. I assigned frequencies to these modes based on results for CH_3 loss from ethane. In the ethane transition state, bend

frequencies are roughly 20% of their value in the ground state molecule[26]. Thus I assigned these modes frequencies of 310 cm^{-1}, roughly 20% of a normal C-H bend at 1500 cm^{-1}. (Using cyclopentadiene frequencies for the transition state and lowering two of the bends and removing one stretch (the reaction coordinate) produces an almost identical $P(E_T)$ and none of the observations below would be changed.)

Obviously the RRKM $P(E_T)$ differs from the best fit $P(E_T)$ because it peaks at zero kinetic energy. A second, less obvious difference occurs in the high energy tail of the distribution. The best fit $P(E_T)$ is roughly 10 times larger than the RRKM $P(E_T)$ in the 30 kcal/mol region. At higher energies, the mismatch becomes several orders of magnitude (~4). This is further evidence for a barrier in the H atom loss channel. A much better fit to the high energy data can be obtained by creating an RRKM $P(E_T)$ with only 65 kcal/mol available to translation (vs. 70 kcal/mol without a barrier) and then shifting it 5 kcal/mol.

Thus, the entire best fit $P(E_T)$ would be consistent with an RRKM picture where energy was completely randomized in the transition state and some additional translational energy was imparted to the fragments by repulsive forces as the products descended a barrier somewhat greater than 5 kcal/mol.

Yi et. al. claimed that the H atom translational energy distribution could be fit by a 3690 K Maxwell-Boltzmann (M-B) distribution. This curve, as well as one for 2500 K is shown in Figure 7. Our $P(E_T)$ actually peaks at higher energy than the 3690 K curve, but it also falls off faster at higher energies. Both have a half width much larger than the RRKM $P(E_T)$ and it is easy to believe that our $P(E_T)$ would yield

a temperature near 3690 K if it were converted to a M-B distribution based on the half width alone (as Yi et. al. did).

As can be seen from the figure, our $P(E_T)$ cannot really be fit by a M-B distribution. However, above roughly 12 kcal/mol, it is fit surprisingly well by the 2500 K M-B curve. I consider this merely a coincidence since below 12 kcal/mol, the two curves are very different. In the discussion section I will argue that an interpretation of the $P(E_T)$ in terms of a temperature is not useful.

:CH_2 ELIMINATION:

A second channel appears at m/e 52. On the assumption that this is the unfragmented dissociation product, this channel is identified as methylene loss. As shown in Figure 8, fragments from this channel have a much higher velocity, by roughly a factor of 2, than those from the H atom loss channel. Ions from this channel are concentrated in the m/e 52-49 region. The $P(E_T)$ for this channel is shown in Figure 9. It is a smoothly decreasing curve with a maximum translational energy of 17 kcal/mol. This corresponds well with the thermodynamic limit for dissociation to ground state methylene and 1-buten-3-yne (max E_T=17.0 kcal/mol).

It is interesting to note that the maximum energy release here is only one quarter of that in the H loss channel, but the fastest mass 52 product is still much faster than the fastest mass 65 product. This makes analysis of the methylene channel much less sensitive to the molecular beam characteristics. It also moves the signal

farther from the beam axis, reducing the background and allowing detection of much smaller fluxes, as well as allowing determination of the $P(E_T)$ to much lower energies.

Even so, there are still some difficulties to be faced when interpreting the data. The points below ~2 kcal/mol produce fragments with the same velocities as the fragments from the H loss channel. This makes the $P(E_T)$ somewhat arbitrary in this range. Since the fragmentation pattern of the mass 65 and 52 species are unknown, changing the height of the first three methylene $P(E_T)$ points and changing the linear combination of the two channels will reproduce the fit to the time-of-flight spectrum. Specifically, a peak away from zero, up to 2 kcal/mol, would be consistent with the data. The choice for these points as shown in Figure 9 is based on arbitrarily continuing the pseudo-exponential curve that fits the higher velocity products. (This pseudo-exponential is an exponential curve modified to have a definite cutoff value. The program FUNC.EXE was used[16].) This type of curve is typically a good initial guess for a $P(E_T)$ form and in this case no modification was required to fit the data other than changing the exponential factor. Whether such a form for the $P(E_T)$ is consistant with the expected kinetics will be discussed in a later section.

Often, one could look at the lighter conjugate fragment, in this case methylene at m/e 14-12, to get information on the lower energy portion of the $P(E_T)$. Unfortunately, the channels described below completely cover the region of the time-of-flight spectrum where methylene would appear and make a determination of its distribution difficult if not impossible. (I chose impossible.) As shown in Figure 10, a methylene contribution with the proposed $P(E_T)$ is consistent with the data.

C_2H_2 ELIMINATION:

The spectra at masses down to m/e 40 can be explained by the two channels above. At mass 40, a new faster signal appears. At a lab angle of 10 degrees, it is almost lost in the noise. However, at 20 degrees, it can be seen at m/e 40 and m/e 39 as shown in Figure 11. It is especially clear at m/e 39 that the signal contains two components: a fast spike, and a slower blob. Both are faster than signals from the previously described channels. Another point to notice is that the relative ratio of the two components is different at the two ion mass ratios.

It is tempting, given the noise at m/e 40, to try to fit this signal as a spike with a slow tail at mass 40 (C_3H_4 + C_2H_2) with a new slower channel at mass 39 (C_3H_3 + C_2H_3). There are several reasons that I believe this is not the correct scheme . The first concerns the shape of the required mass 40 channel $P(E_T)$. The data at m/e 39 require a peak in the $P(E_T)$ at 20 kcal/mol. The good signal to noise ratio and the fact that the peak in the TOF spectrum is well separated make this a secure result. To fit the m/e 40 data with only this $P(E_T)$ and the two higher mass channels requires that a 'kink' be put in the $P(E_T)$. The $P(E_T)$ down to ~15 kcal/mol is defined by the m/e 39 data. To fit the m/e 40 data, the $P(E_T)$ must have a flat portion from 15 kcal/mol down to ~8 kcal/mol. The mass 52 channel can provide signal at times longer than that corresponding to 8 kcal/mol. Such a $P(E_T)$, with a plateau and then a peak seems highly unlikely. Thus it appears that a second channel at mass 40 is necessary to yield

reasonably smooth $P(E_T)$s. Another concern is that there does not appear to be any faster signal at m/e 27 that would correspond to the conjugate fragment of mass 39. In fact, m/e 27 can be fit very well by assuming a crack from the slower component at m/e 39, i.e. the m/e 27 spectrum has the same shape as the slower component at m/e 39 and 40. This is in contrast to the data at m/e 26, where the conjugate products of both the fast and slow m/e 39 and 40 components appear. Spectra for m/e 27 and 26 at 20 degrees are shown in Figure 12. In order to maintain the mass 39 channel hypothesis one must assume that all of the conjugate mass 27 product fragments in the ionizer. This seems unlikely.

Such interpretational contortions are not necessary if one assumes two mass 40 channels. In fact, by fitting the data at m/e 39 (good signal to noise) with two mass 40 channels, all of the data at m/e 40 to m/e 15 can be fit without any changes other than the relative ratios of the two products and their conjugate partners (to account for their different cracking patterns). The larger relative amount of slow channel products at m/e 40 vs. m/e 39 can be rationalized as being due to the greater propensity for internally vibrationally hot products, i.e. the slower channel, to dissociatively ionize. Thus, in the following sections, I will adopt the more aesthetic interpretation of the data as arising from two C_3H_4 + acetylene channels.

Slow Acetylene:

Determining an exact $P(E_T)$ for the slow acetylene channel is not possible. As

was true in trying to determine the methylene loss $P(E_T)$, cracking from a higher mass channel obscures the lower energy portion. In this case, any signal below ~6 kcal/mol could be replaced by fragments from the methylene channel. From the m/e 39 data, it appears that there is a problem in determining the higher energy side as well. The decomposition of the data in the m/e 39 spectrum into two channels as shown assigns some of the signal with only 8 kcal/mol to the tail of the fast channel. Such an assignment would obviously be arbitrary if based on this spectrum alone. In fact, two other constraints have been used. The first is to assume that the m/e 27 spectrum, which shows no fast peak, is the true shape of the slow channel. This is equivalent to requiring that the shape of a given channel's TOF spectrum does not change at the various m/e values it can crack to. This has been implicitly assumed in all of the fitting so far, except to explain the difference in the cracking pattern of the fast and slow acetylene channels. In that case, as I will argue later, it is likely that a difference in structure of the C_3H_4 product between the two channels is also involved in making the fast channel product less likely to crack; i.e. a difference in the heat of formation of the C_3H_4 products leaves the fast channel product even colder relative to the slow channel product than one would expect from the difference in translational energies. If you believe this, then there is no contradiction here. If you don't believe, then you would suspect that using the m/e 27 data to derive the slow channel $P(E_T)$ makes it slower than it should be. The effect cannot be too drastic since the m/e 40 and m/e 39 data do constrain the $P(E_T)$ as well. However, the high energy cutoff of the slow channel at ~35 kcal/mol could be too low.

The second constraint used to obtain a $P(E_T)$ for the slow channel is an assumption that it has a pseudo exponential form. As stated previously, this form is usually a good approximation for a statistical, simple bond rupture type dissociation. This form seems empirically justified here in that it fits the m/e 27 data fairly well. Other than that, it is somewhat arbitrary.

With these constraints, the $P(E_T)$ is found to be as shown in Figure 13. It peaks at zero energy and extends to 35 kcal/mol, with an average energy, $\langle E_{Trans} \rangle$, of 6.9 kcal/mol. A peak away from zero, but less than 6 kcal/mol would be consistent with the data. However, the only experimental suggestion for such a $P(E_T)$ is the fact that with a monotonically decreasing $P(E_T)$, all of the data with m/e ratios below 40 can be fit without any contribution from the methylene elimination channel. While this may be somewhat surprising in contrast to the H loss channel, which had visible signal at all m/e ratios, it is not incomprehensible. The methylene channel is less than 1% as large as the H atom loss channel, and because of the thermodynamics, produces much colder fragments. Also, it is known that internally cold C_4H_4 does not produce many fragments below m/e 49 [22]. Thus the experimental evidence is inconclusive on this question.

Fast Acetylene:

This channel is the easiest to analyze of all four. As mentioned above, its $P(E_T)$ has a peak at 20 kcal/mol. The portion above ~6 kcal/mol is fairly well

determined by the spectrum at m/e 26 due to a relatively small contribution of the slow mass 26 channel. The m/e 26 spectrum also has good signal to noise. The $P(E_T)$ for the fast acetylene loss channel is shown in Figure 14. The high energy tail is a pseudo exponential form extending to 60 kcal/mol. The middle range was fit point by point to the data and the lower portion was aesthetically dropped to zero. As with the H atom loss channel, the peak in the $P(E_T)$ implies a barrier to reaction. In this case, one can infer a barrier of at least 20 kcal/mol for acetylene loss.

BRANCHING RATIO

The branching ratio for the four channels described above was calculated from the TOF spectra at 10 and 20 degrees.The general procedure is as follows. The CMLAB2 program reports the weighting of the channels for a given spectrum. These weightings can be thought of as the branching ratio of the ions at this m/e ratio. This value should be independent of the laboratory angle because it has already been corrected for the kinematic effects (the mass ratio of the products and the shape of the $P(E_T)$) that determine how large a contribution a given yield of products from a channel will have at a given lab angle. (The number of signal counts expected from one unit of reactive flux in a given channel is reported as the INTEGRAL for each channel in CMLAB2.) The two additional factors that must be considered to arrive at the true branching ratio are the summation of ion signals from all m/e ratios and the ionization cross section for each product.

The first factor is easily handled using the new CMLAB2 program. A new output, the ratio of the calculated to experimental TOF spectrum, is used to determine the relative weighting of the different m/e data. This number is a measure of the number of dissociation events required to produce the observed signal. These numbers, normalized for the number of laser triggers and laser power for each TOF spectrum, can be summed over all m/e ratios to give a total relative yield. Dividing the calculated/experimental ratio for a given m/e TOF spectrum by the relative total yields the fraction of dissociation events appearing in that spectrum. The fraction of ion counts from a given product is then the sum of the weighting for that product at an m/e ratio multiplied by the fraction of events occurring at that m/e ratio, over all m/e ratios.

At this point, one has the branching ratio of the ions from each possible product. This can then be corrected by dividing by the relative ionization cross section for each product to yield the branching ratio of neutral products. Cross sections for the products in this experiment were calculated using the method of Fitch and Sauter [27]. This method is especially convenient since the only required input is atomic composition of the product - no details of structure or bonding are necessary. This point and a general discussion of calculating ionization cross sections can be found in the thesis of A.-M. Schmoltner[28]. Uncertainties in relative cross sections produced by different methods of 25% are reported therein. Uncertainties of this size must also be assumed for the data herein. (This reference also conveniently reproduces the formula and atomic values necessary for the calculation.)

The result of all of this calculation is the following ratio:

Product	Relative Yield
C_5H_5	650
C_4H_4	5.3
CH_2	0.85
C_3H_4(f)	12.8
C_2H_2(f)	13.2
C_3H_4(s)	7.5
C_2H_2(s)	6.4

The (f) and (s) stand for the 'fast' and 'slow' channels respectively. No value is reported for H atom since m/e 1 was not measured relative to the other m/e ratios. For the same reason, it has been necessary to hope that cracking to m/e 1, which was not measured, does not significantly change the results above. This is equivalent to assuming that the signal at m/e 1 from cracking is small and/or representative of the ratio above.

In a perfect world, the yields for the two products of a dissociation channel would be the same. This is probably true within the uncertainty for both acetylene loss channels. However, there is definitely a problem with the methylene loss channel. The methylene product can easily be increased by a factor of 4 by requiring that signal at m/e 14-12 be fit using the maximally reasonable amount of methylene contribution.

It turns out that the methylene signal looks very much like a combination of the slow 40 and 26 products together. Using a least squares fitting procedure, these two channels account for much of the signal at m/e 14-12. This could easily be an artifact; the replacement of one component (methylene) by two (slow 40 and 26) gives a better fit to noisy data simply because of the increase in degrees of freedom.

At the same time, the conjugate product of methylene, mass 52, is being over-represented. The number shown above, 5.3 is the average of values obtained from the 10 degree data (7.9) and the 20 degree data(2.6). The large disparity between these values stems from two effects. At 10 degrees, the dominant product is mass 65 from the H loss channel. Inspection of the least squares fit to the data shows that mass 52 is often increased beyond a reasonable value to fill in the fast side of the mass 65 peak. This is probably a manifestation of a slight increase in beam velocity which shifts the mass 65 peak to slightly higher velocities than calculated. This effect causes overestimation by a factor of 3 at a few masses. This effect does not occur at 20 degrees. However, an effect similar to the one that underestimates the methylene contribution is at work. Below m/e 40, any mass 52 contribution can be replaced by the slow mass 40 product. The size of this underestimation is difficult to calculate.

My answer to this is to average the values for mass 52 and 14 to arrive at a value for the methylene loss channel yield in hopes that the above problems largely cancel. The value, 3.1, seems reasonable to me. Similarly, I'll average the yield of the two products from a channel to estimate the yield of the channel for the acetylene channels as well. Doing this, and normalizing the total yield to 100% gives:

Channel:	65+1	52+14	fast 40+26	slow 40+26
% Yield:	96.6%	0.5 %	1.9 %	1.0 %

The sources of error in these ratios are numerous, but the overall conclusions are certainly valid. From considerations of the shape of the H loss $P(E_r)$ discussed above and ionization cross section uncertainties, the yield of that channel could be off by a couple percent. However, the roughly 1:4:2 relative ratio of the other three channels should be fairly secure. Even the uncertainties in ionization cross section and the other unknown described above are unlikely to change the relative ordering of the yields of these channels.

MULTI-PHOTON EFFECTS:

UV Photodissociation experiments don't demand much more from a laser than that it be a black (orange?) box with a power knob. In our group, it is often referred to as 'using a laser as a sledgehammer'. This section describes the application of a very large sledgehammer to cyclopentadiene. As one might expect, with all of the difficulties in analyzing and separating product channels described above, increasing the laser power and thereby adding another dimension of confusion, makes rigorous analysis impossible. However, several interesting qualitative results can be obtained.

The first set of results comes from a series of TOF spectra at ~200 mJ/cm^2 at m/e 65-m/e 60, shown in Figure 15. There are large jumps in the width of the TOF

spectra between m/e 64 and 63, m/e 62 and 61, and m/e 61 and 60. Slight increases occur at m/e 65-64 and m/e 63-62. Based on this data, as well as the m/e 2 TOF spectrum shown in Figure 16, I have fit this data using a sequence of four reactions:

Reaction:	$\langle E_{Trans} \rangle$ kcal/mol	$E_{T,Max}$ kcal/mol
$C_5H_6 \rightarrow C_5H_5 + H$	7.76	70
$C_5H_5 \rightarrow C_5H_3 + H_2$	4.62	34
$C_5H_3 \rightarrow C_5H + H_2$	12.68	68
$C_5H \rightarrow C_5 + H$	19.14	70

The secondary and higher reactions above were all modelled as secondary processes with pseudo-exponential $P(E_T)$ curves. The latter constraint is obviously wrong based on the m/e 2 spectrum as well as from the cracking pattern data. (The amount of fragmenting of the m/e 65 product should be the same as at low power. This will not be the case if the secondary processes produce as much low energy m/e 64-60 product as the pseudo exponential $P(E_T)$s suggest.) In the m/e 2 spectrum shown in Figure 16, a barrier of at least 4 kcal/mol for at least one of the two H_2 channels would improve the fit.

An alternative explanation with only sequential H atom loss channels cannot be ruled out. The pattern of large increase in width followed by small increase as one

goes down in m/e from 64 to 60 could be fit as a series of fast and slow H atom loss channels, perhaps due to variation in bond energies, or due to stimulated loss of an H atom followed by spontaneous loss of a second H atom for each absorption event. It is likely that H_2 forms in at least one of the steps due to the relatively large amount of m/e 2 signal at high power (see below regarding data at m/e <=52). A reaction mechanism with competing H and H_2 loss channels would still be consistent with all of the data.

No attempt was made to determine the photon order of the various products. A study of power dependence at each m/e could in principle determine this. However, the system is underdetermined in practice due to the large degree of overlap of the proposed channels.

The major conclusion from this data is that all six H atoms can be removed from cyclopentadiene. This conclusion relies only on the fact that six different peakwidths are observed in the m/e 65 - 60 TOF spectra.

TOF spectra for lower m/e values were taken at laser fluences between 35 and 70 mJ/cm^2 at a variety of angles. Again, this work should be considered more of a survey than an attempt to rigorously define the multi photon processes. Besides the channels described above, three new channels are required to explain the observed TOF spectra. Figure 17 shows the four spectra where new products appear.

The TOF spectrum at m/e 51 is markedly faster than at low power. The m/e 52 spectrum does not change, suggesting that the new product has mass 51. It is possible to fit this channel two ways. The first is to postulate H atom loss from the

primary mass 52 channel. This requires a pseudoexponential $P(E_T)$ with an $\langle E_{Trans} \rangle$ = 27 kcal/mol and a high energy tail past 150 kcal/mol. Such a high energy tail would require putting at least two 148 kcal/mol photons into the mass 52 product. The second alternative is to postulate decomposition of the cyclopentadienyl radical, with loss of CH_2 (or two photon dissociation of cyclopentadiene, producing for instance CH_3 and mass 51). Such a channel could be fit with a pseudo exponential $P(E_T)$ with $\langle E_{Trans} \rangle$ = 6.3 kcal/mol and $E_{T,Max}$ = 33 kcal/mol. The mass 51 signal is relatively intense compared to the mass 52 product, suggesting that if mass 52 is the precursor, this is a major decomposition pathway for mass 52. Conversely, if mass 65 is the parent, it would be a minor pathway involving at most a few percent yield.

The m/e 50 spectrum shows an even faster channel than the m/e 51 data. Data at a fluence of 14 mJ/cm^2 show that this new channel is of higher order than the mass 51 channel, i.e. at least three photon overall. This channel could be fit as a secondary product of the cyclopentadienyl radical using a $P(E_T)$ with a barrier of 18 kcal/mol, extending out to 85 kcal/mol. Dissociation of any of the C_5H_n would require a similar $P(E_T)$. Dissociation from mass 52 or 51 seems unlikely since translational energies > 200 kcal/mol would have to be invoked. At 45 mJ/cm^2, the mass 50 channel is larger than either the 52 or 51 channels, but still only a few percent of the C_5H_n channels.

The last identifiable channel appears at m/e 39. It appears as a broadening (toward faster time) of the fast 40-26 primary channel. There is no broadening on the slow side of the peak. One can fit this as a secondary H loss channel from the fast mass 40 product. However, the lack of broadening toward the slow side would then

imply a substantial barrier to H atom loss (> 15 kcal/mol), yielding a fast forward peak, and a slow backward peak that would be slow enough to be under the broad slow mass 40 channel. If this possibility is rejected, the remaining options involve dissociation of a C_4 or C_5 species. Either of these would require a substantial barrier, on the order of 30 kcal/mol, to reproduce the TOF spectrum. As shown in Figure 17, the m/e 26 spectrum also shows a new fast component. A dissociation of mass 65 to 39 and 26 can fit both the m/e 39 and 26 spectra. While this does not rule out a channel such as mass 52 yielding 39 and 13, a mechanism to give a 30 kcal/mol barrier for this reaction eludes me. Further, inspection of m/e 14 - 12 show no signal faster than the proposed mass 26 channel that is clearly above the noise level.

The 39-26 channel was used to yield the fits shown in Figure 17. The $P(E_T)$ used is exactly the same shape as the $P(E_T)$ for the fast mass 40-26 channel (shown in Figure 13), but with a maximum energy of 96 kcal/mol. (The increment per point in the $P(E_T)$ was raised from 2.6 to 4 kcal/mol.) The overall yield of this channel is still relatively small. In fact, the secondary channels involving two hydrocarbon fragments (i.e. channels that break the carbon framework in two) are of the same order of magnitude as the primary hydrocarbon channels. The point here is that since the primary hydrocarbon channels represent less than 5% of the yield, it is likely that the secondary hydrocarbon channels are also minor channels. I would estimate that they represent less than 30% of the secondary products, but this is definitely crude given all of the overlap of various channels, etc. This means that H and H_2 loss from C_5 species are the predominant secondary and higher processes.

Discussion:

H ATOM ELIMINATION:

H atom loss is normally well described as a simple bond rupture. The reaction coordinate is simply(!) the C-H bond length. As the bond lengthens, the attraction between the atoms smoothly decreases and the electrons in the bond become non-bonding radical electrons localized on the C and H atoms. The translational energy distribution in such a dissociation, peaking near zero and decreasing smoothly, can be described well by variational RRKM theory.

The translational energy distribution for H atom loss from cyclopentadiene derived from Yi et. al.'s work and in more detail from this experiment does not fit this picture. It peaks several kcal/mol away from zero energy and the high energy tail is much larger than RRKM theory would predict. With the data in hand, it is fairly easy to understand why the cyclopentadiene dissociation does not follow the pattern: the radical electron left with the cyclopentadienyl fragment does not remain localized on the carbon atom - it delocalizes around the ring to all five carbon atoms. This is the same phenomena responsible for the extraordinary stability of the cyclopentadienyl radical and for the weakness of the cyclopentadiene C-H bond. In propane, the C-H bonds of the methylene group are roughly 99 kcal/mol. In cyclopentadiene, this is lowered to 78 kcal/mol, a drop of 21 kcal/mol.

Delocalization of the radical electron changes the forces between the nuclei. It

can cause a repulsion of the H atom, leading to increased translational energy. It can also cause vibrational excitation of the cyclopentadienyl radical. From the experimental translational energy distribution, one can infer a barrier of at least 5 kcal/mol. The limiting value assumes that all of the energy released by the electronic rearrangement can appear as translation, which seems unlikely in this case. The reaction coordinate is not simply the C-H internuclear distance. The motion is a combination of this C-H bond lengthening with a bend of the methylene hydrogens to bring the remaining H atom into the plane of the ring and with a rearrangement of the carbon-carbon bond lengths from a pattern of long and short (single and double bonds) to five equal bonds (neglecting Jahn-Teller distortion[29]). For the entire barrier to appear as translation, these other motions would have to be possible without vibrationally exciting the cyclopentadienyl radical. An accurate estimate of the amount of vibrational excitation in the cyclopentadienyl fragment is difficult, but it is not unreasonable to expect several kcal/mol, yielding an estimated barrier of 8 kcal/mol or greater.

While such a barrier would be surprising for a simple bond rupture, the complexity of motion in this dissociation is perhaps more aptly described as 'concerted'. This term is often reserved for a reaction in which more than one bond is broken, but perhaps a better definition requires only that more than one bond changes its bond order. A barrier occurs in the 'standard' concerted reaction as electronic rearrangement creates two stable closed shell molecules at very small separations. These molecules gain kinetic energy from their mutual repulsion as they descend the

reaction barrier. They also become vibrationally excited as the electrons from the breaking bonds either create new bonds or strengthen existing ones in the product molecules. H loss from cyclopentadiene shares many of these features. Although only a single bond is broken, the bond order changes in several bonds. Additionally, although the products in this case are not stable molecules, the delocalization of the cyclopentadienyl radical electron away from the breaking bond causes repulsion between the fragments and vibrational excitation of the cyclopentadienyl fragment.

It should be pointed out that Yi et. al. do not believe that a barrier exists in this reaction. The difference seems to be largely one of interpretation rather than a conflict between our respective experimental results. The translational energy distribution obtained in this work and the one inferred by Yi et. al. are both shown in Figure 7. As was mentioned above, the curves are quite different except perhaps in their prediction of the halfwidth of a doppler peak for the H atoms. Since the choice of a Maxwell-Boltzmann distribution by Yi et. al. was based on theoretical arguments rather than their experimental findings, and since their published spectrum is definitely non-Gaussian (a M-B distribution would yield a Gaussian line shape) it is not clear whether the two sets of experimental results differ. An earlier work on methylsubstituted benzenes from the same laboratory by Park et. al. noted that distributions with a barrier produce doppler profiles with noticeably flat tops[30]. It should be obvious that the Maxwell Boltzmann $P(E_T)$s shown in Figure 7 could be considered indicative of a barrier and that it is not necessary for a distribution to peak at zero to yield a peaked doppler profile. The important parameter is how fast a $P(E_T)$

distribution goes to zero. (Our $P(E_T)$ is shown having a nonzero value at 0 kcal/mol. This is physically impossible. The contradiction arises because the 0 kcal/mol point represents contributions between 0 and ~2 kcal/mol in our discrete $P(E_T)$.) It is easy to see that a distribution that goes to zero more slowly than a M-B distribution will produce a sharper doppler profile. Thus a barrier that produces no slow products because it funnels its energy exclusively into translation, the case for which Park et. al.'s argument is true, is not consistent with either Yi et. al.'s nor our data. From some crude calculations, it appears that an appropriate choice for the form of the $P(E_T)$ from this work between 0 and 2 kcal/mol would put the two experiments in agreement except for the high velocity tail. It was noted above that Yi et. al. may have used a laser fluence high enough to have significant amounts of multiphoton processes occurring. If so, one would expect that this multiphoton signal could increase their measured linewidth, perhaps giving rise to the broad base in their spectrum.

The Maxwell-Boltzmann distribution was chosen by Yi et. al. based on a theory that the vibrational temperature of the molecule after photon absorption should equal the translational temperature of the H atom after dissociation. This theoretical model is argued to be a consequence of the H atom's low mass. The experimentally measured H atom velocity distributions for several molecules are claimed to be in agreement with this theory and at odds with an explanation in terms of a potential barrier[30,12]. However, such a general theory of H atom loss from large molecules obviously violates the conservation of energy as the dissociation energy approaches the photon energy: if the bond energy in the present case were 148 kcal/mol, the H atom

could not have any translational energy while the theory predicts a distribution with a temperature of >3500 K, the same as for the molecule with the true bond energy of 78 kcal/mol.

Given this flaw, it is tempting to dismiss this line of thought completely. I will pursue it slightly further to point out that the arguments based on the low relative mass of the hydrogen atom cannot lead to a peaked $P(E_T)$ without a barrier, a fact independent of whether or not the entire distribution conserves energy. This leads to the conclusion that the essential ingredient of a barrierless model for peaked translational energy distributions is really an exotic multidimensional transition state.

The starting point for Yi et. al.'s picture of the dissociation is a Born-Oppenheimer like approximation that the H atom is decoupled from the motions of the cyclopentadiene skeleton. The reaction is then to be considered as a series of nonadiabatic transitions to excited 'hydronic' states of the cyclopentadienyl radical, and eventually to a continuum 'hydronic' state where the H atom is free. The terminology above is mine. Yi et. al. describe their theory as the "adiabatic motion hypothesis" in which the H atom equilibrates to the vibrational temperature of the excited molecule and then passes through the transition state, keeping its 'temperature', before the carbon skeleton can 'relax'. (The fact that nonadiabatic transitions must occur for the initial equilibration points out the limited validity of the approximation.)

The description above is meant to emphasize the analogy with the electronic process of ionization. (Yi et. al.'s theory is equivalent to claiming that because the electron is so light, it can maintain its original thermal kinetic energy distribution

while leaving the molecule, regardless of the ionization potential.) The intuitive picture of the H atom leaving the cyclopentadienyl radical before it can 'relax' is, in this language, clearly equivalent to the electronic process of vertical ionization in which the vertical ionization potential is larger than the value obtained by removing the electron sufficiently slowly to keep the ionic core in its ground state. This makes it clear that the decoupling of the H atom from the slower carbon motions implies a barrier to dissociation. Further, this type of barrier would be invisible in the translational energy distribution because it only excites the cyclopentadienyl radical, just as vertical ionization results in excitation of the ionic core rather than increased translational energy of the electron.

The experimental fact that the H atom translational energy distribution is peaked away from zero implies one of two things. The first would be an incomplete separation of the timescales for motion of the H atom and the carbon skeleton (non-Frank-Condon transitions between the hydronic states!). The cyclopentadienyl radical is then able to vibrationally 'relax' by kicking the H atom before they separate. The second possibility is that there is an electronic 'kick'. Unlike the ionization case, the H atom, equivalent to the ionizing electron, is not the fastest particle in the system. While the H atom may decouple from the carbon motions, the electrons are still faster than the H atom. Thus, as the electrons rearrange, the force on the H atom may become repulsive, yielding a barrier visible in the translational energy distribution. The first possibility represents a breakdown of Yi et. al.'s assumption while the latter is independent of it, but both represent barriers in the potential. (These are the same

effects I invoke elsewhere to explain the existance of a barrier.)

In order for the H atom to end up with a translational energy distribution with a 'temperature' through a barrierless, RRKM type process as Yi et. al. suggest, one must invoke a three dimensional reaction coordinate, i.e. one in which not only the stretch, but the bending coordinates as well, are unbound and contribute to the final translational energy. A one dimensional transition state with no barrier yields a $P(E_T)$ peaked at zero (as is a one dimensional Maxwell-Boltzmann velocity distribution), not the type shown in Figure 7, and would not yield a Maxwell-Boltzmann distribution of speeds. This point is independent of any effects due to the H atom being much lighter and faster than the carbon skeleton.

The concept of a multidimensional transition state is not difficult to comprehend. Consider a diatomic molecule. It is equally easy to dissociate the molecule in the x,y, or z directions. Thus, by symmetry, the transition state is multidimensional, and one should expect a translational energy peaked away from zero. Normally, this problem is thought about in different coordinates, namely the bond stretch and two rotations. In this coordinate system, the transition state is nominally one dimensional and one invokes a non-physical centripetal barrier to include the coupling of some rotational energy into translation. This pseudopotential barrier again causes the translational energy peak away from zero. (In this sense, all transition states are multidimensional, which explains why all $P(E_T)$s must peak slightly away from zero.)

In Yi et. al.'s theory, the C-H bends would also have to contribute almost all of

their energy to the H atom translational energy. To reach the limit of a 3-D Maxwell Boltzmann $P(E_T)$ without a potential barrier requires that these bends be free internal rotations at the transition state. This is not the case for simple bond ruptures, e.g. H atom loss from methane[31]. Further, if the bends become free rotors due to a very loose transition state, much of their energy will result in fragment rotation, rather than translation, due to angular momentum constraints. A transition state that can *efficiently* couple three degrees of freedom into translation is very hard to imagine.

This discussion points out that one cannot use the low mass of the H atom to explain the peaked translational energy distributions observed in cyclopentadiene, indene, methyl substituted benzenes, or methyl substituted pyrazines[12,30]. Further, it does not seem reasonable to posit that all of these molecules shared an exotic, tight, 3-dimensional transition state. This implies that the observed translational energy distributions for all of these molecules should be reinterpreted as arising from potential energy barriers. All of the species noted above should have a partially delocalized radical electron on the molecular fragment which coould give rise to potential barriers for the reasons discussed above for cyclopentadiene.

:CH_2 ELIMINATION:

The CH_2 loss channel seems almost mundane by comparison. The translational energy distribution peaks at zero and extends out to the thermodynamic limit for the production of the most thermodynamically favored products, ground state triplet $^3CH_2$

and 1-buten-3-yne. The smooth nature of the curve near 10 kcal/mol suggests that butatriene is not being formed as methylene's partner (max E_T=9.6 kcal/mol). This is the only other thermodynamically accessible C_4H_4 species.

Similarly, production of singlet $^1CH_2$, which is thermodynamically possible in concert with 1-buten-3-yne (max. E_T = 8 kcal/mol), would not seem to be indicated by the $P(E_T)$. However, this point bears further consideration. To fit the $P(E_T)$ as shown (Figure 9), the $^3CH_2$ channel would have to be barrierless. This might be somewhat surprising given that a barrier of ~ 4 kcal/mol is observed for $^3CH_2$ elimination from ketene[32]. Further, studies of ketene dissociation have shown that singlet methylene elimination quickly (within 125 cm^{-1} of the threshold, and without a barrier) becomes the dominant channel as the dissociation energy increases[32,33,34]. This suggests that the observed methylene loss $P(E_T)$ for cyclopentadiene may represent a barrierless $^1CH_2$ elimination channel, peaked at zero energy and extending to ~ 8 kcal/mol, and a $^3CH_2$ elimination channel, peaked away from zero and extending to the thermodynamic limit of ~ 17 kcal/mol[35]. However, the electronic states of the C_5H_6 diradical may be different enough from those of ketene to invalidate the comparison. As was mentioned above, the $P(E_T)$ for methylene loss is not well determined below ~ 2 kcal/mol in this experiment due to overlapping signal from the H atom elimination channel and could actually peak at 2-3 kcal/mol and represent $^3CH_2$ product. However, if the $P(E_T)$ does peak at zero, roughly 80 % of the product flux would have < 8 kcal/mol and could therefore represent $^1CH_2$ product. Given the uncertainty, the singlet/triplet methylene branching ratio cannot be determined from the $P(E_T)$.

However, consideration of the large overall yield of CH_2, and the evidence from ketene, would suggest a prominent role for the $^1CH_2$ or a barrierless $^3CH_2$ channel. This point will be discussed further below.

The presence of CH_2 fragments implies that ring opening occurs. Dissociation from the ring to yield cyclobutene is not thermodynamically allowed. Similarly, a hydrogen migration can also be inferred. Ring opening would produce the $\circ CH_2CHCHCHCH\circ$ diradical. Direct dissociation of this diradical would yield CH_2 and two acetylene molecules. Again, this process requires more energy than is available.

Two hydrogen migration pathways can lead to a viable dissociation geometry. These would be a 4,2 shift yielding $\circ CH_2CH_2CHCCH\circ$, or a 3,5 shift yielding the symmetric $\circ CH_2CHCCHCH_2\circ$. Both would yield CH_2 and CH_2CCHCH (1-buten-3-yne) as dissociation products.

To differentiate between these two pathways, and to prove the feasibility of this mechanism requires an estimate of the reaction barriers along the way. The heat of formation of the intermediate radicals can be crudely estimated in the following way. The ΔH_f of the stable molecule that differs from the desired radical by the addition of a hydrogen atom at each radical site is estimated via Benson's group additivity rules[36]. Then, an assumption is made that the two radical sites will not interact in the final diradical. The energy to form the diradical is then calculated from estimates of the CH bond strengths at the radical sites and the ΔH_f of the hydrogen atoms. Bond strengths are estimated by comparing the starting molecule with similar but smaller

molecules whose bond strengths are known. Such a calculation for the three radicals described above is shown below:

C_5H_6 Ring Opening:

Diradical: $\circ CH_2\text{-}CH{=}CH\text{-}CH{=}CH\circ$

	ΔH_f (kcal/mol)
$CH_3\text{-}CH{=}CH\text{-}CH{=}CH_2$ by Benson's rules	18
H from CH_3, bond energy $\cong$ 85 from $CH_2{=}CH\text{-}CH_3$	85
H from CH_2 , B.E. $\cong$ 114 from $CH_2{=}CH\text{-}CH{=}CH_2$	114
$2\ H \rightarrow H_2$	-104
	113
$\therefore$ for c-$C_5H_6 \rightarrow \circ CH_2\text{-}CH{=}CH\text{-}CH{=}CH\circ$	-32
$\Delta H_{rxn} = 113 - 32 =$	81 kcal/mol

CH_2 Loss:

Diradical: $\circ CH_2\text{-}CH{=}C{=}CH\text{-}CH_2\circ$

	ΔH_f (kcal/mol)
$CH_3\text{-}CH{=}CH\text{-}CH{=}CH_2$ by Benson's rules (same as above)	18
H from CH_3, bond energy $\cong$ 85 from $CH_2{=}CH\text{-}CH_3$	85
H from CH B.E. $\cong$ 102 from $CH_2{=}CH\text{-}CH{=}CH_2$	102
$2\ H \rightarrow H_2$	-104
	101
$\therefore$ for c-$C_5H_6 \rightarrow \circ CH_2\text{-}CH{=}C{=}CH\text{-}CH_2\circ$	-32
ΔH_{rxn} = 101 - 32 =	69 kcal/mol

CH_2 Loss:

Diradical: $\circ CH_2\text{-}CH_2\text{-}CH{=}C{=}CH\circ \leftrightarrow \circ CH_2\text{-}CH_2\text{-}CH\circ\text{-}C{\equiv}CH$

	ΔH_f (kcal/mol)
$CH_3\text{-}CH_2\text{-}CH_2\text{-}C{\equiv}CH$ by Benson's rules (same as above)	34
H from CH_3, bond energy $\cong$ 103 from $CH_3\text{-}CH_2\text{-}CH_3$	103
H from CH B.E. $\cong$ 89 from $CH_3\text{-}C{\equiv}CH$	89
$2\ H \rightarrow H_2$	-104
	122
$\therefore$ for c-$C_5H_6 \rightarrow \circ CH_2\text{-}CH_2\text{-}CH{=}C{=}CH\circ$	-32
ΔH_{rxn} = 122 - 32 =	90 kcal/mol

This method is certainly unrealistic. The most obvious example is for the symmetric radical where both radical electrons should have some resonance stabilization. The calculation above assumes that one electron is localized while the other is stabilized by an allyl type resonance. While the average resonance energy for the electrons may not be as great as in $\circ C_3H_5$, the total is probably greater leading to the conclusion that the energy for the diradical should be lower than 69 kcal/mol above cyclopentadiene. Beyond this alteration, the heat of formation for all three radicals must be considered to have error bars of many kcal/mol.

To estimate the barrier to ring opening, one needs to know whether the resonance stabilization of the CH_2 group is fully developed in the strained cyclic geometry. Given that the cyclopentadienyl radical develops 21 kcal/mol stabilization for delocalization over 5 carbons in this geometry, it may not be a bad assumption that the CH_2 radical electron is able to delocalize well. This leaves only the ~6 kcal/mol strain energy to contribute to the reaction barrier. Thus a value of ~87 kcal/mol should be a reasonable estimate.

Given the likely errors already and the difference in stability of the two radicals resulting from H atom migration, no attempt will be made to be precise about the barriers to H atom migration. Instead, I will assume a value of ~10 kcal/mol. Both processes are transfers across two carbon atoms, with the 3,5 transfer having the energetic advantage that the hydrogen is transferring to a radical site. I will further assume that the full barrier applies above the ΔH_f of the least stable of the reactant and product diradicals. This assumption should overestimate the barrier since the stability

of the more stable form may still be felt at the transition state. Thus a barrier of 100 kcal/mol relative to the cyclopentadiene ground state is the estimate for the 2,4 migration, while a barrier of 91 kcal/mol applies for the 3,5 migration to the symmetric diradical. All of the energies discussed above, as well as those pertaining to the other channels are displayed in Figure 18.

Even at this crude level, it is obvious that the symmetric diradical is the more important intermediate in CH_2 formation. It is also clear that the rate limiting step in the dissociation will be the final loss of CH_2 with a barrier of $\geq$ 131 kcal/mol, due mainly to the thermodynamic (in)stability of the products. As noted before, overlap with cyclopentadienyl ion fragments from the H loss channel in the TOF spectra would make a $P(E_T)$ with a peak at 2 kcal/mol consistent with the data.

The entire proposed sequence of events leading to CH_2 is then photon absorption and fast conversion to the ground state, ring opening to a diradical, H atom migration yielding a very stable symmetric diradical, and finally bond rupture of this radical to yield CH_2 and 1-buten-3-yne.

The only experimental observation regarding the CH_2 channel which may be surprising is the estimate that it accounts for 0.5% of the dissociation products. With a barrier more than 45 kcal/mol above the H atom channel, this channel might be expected to be unobservably small. As will be described below, a very crude harmonic RRKM calculation of Arhenius A factors and activation energies supports this intuition: an A factor more than 4 orders of magnitude larger than that of the H atom loss channel is required to account for the amount of product from this channel.

The experimental errors in estimating the branching ratio and $P(E_T)$, etc. which would affect the A factor should not be able to lower its value by more than an order of magnitude, implying that the 'overabundance' of CH_2 is real. After discussing the other channels, I will return to consideration of the CH_2 yield and argue that the reaction path developed above is consistent with the experimental branching ratio.

C_2H_2 ELIMINATION:

Acetylene produced in the dissociation of cyclopentadiene seems to be formed through two distinct mechanisms. One pathway shows evidence of a large barrier, ≥ 20 kcal/mol, that results in a large translational energy release. The translational energy release extends out to a maximum of ~60 kcal/mol. The other pathway leads to very little translational energy ($\langle E_{Trans} \rangle$ = 7 kcal/mol). The translational energy release is estimated to extend to roughly 35 kcal/mol for this channel, with the exact value obscured by the other channel. These channels have only a slightly higher yield than the CH_2 channel; twice as large in the case of the slow channel and roughly a factor of 4 for the fast channel.

The thermodynamics for acetylene production from cyclopentadiene dissociation are much different from those for CH_2 production. There are three possibilities for forming pairs of stable molecules for which the ΔH_{rxn} is far below the 148 kcal/mol supplied by the photon. Dissociation to acetylene and allene or methyl acetylene actually requires less energy than the H atom loss. These product pairs, more

stable than the H atom and cyclopentadienyl radical pair by 10 and 12 kcal/mol respectively, are the most stable dissociation products. The third possibility, forming acetylene in concert with cyclopropene requires 10 kcal/mol more than H atom loss. Various excited state products are also possible and will be discussed more later.

Based on thermodynamics alone, these channels have the possibility to be the major dissociation products. However, it is obvious that the possible mechanisms for forming these products all have barriers which will make them kinetically less favored. One obvious route for acetylene production would be through ring opening, with its barrier of ≥ 87 kcal/mol. This is not likely to be the rate limiting step however since an H atom migration is also required for formation of acetylene with allene or methyl acetylene. Other channels, which lead to less stable products would also be expected to have barriers higher than the ring opening step.

Rather than following the methods of the last section to compute barriers, I will make use of information available for the methyl acetylene-allene isomerization. The argument for the relevance is that the diradical from ring opening, $C_5H_6(RO)$, can be considered as a C_3H_4 diradical with one of the electrons stabilized by reaction with acetylene. The various barriers for the present system can then be estimated by using the values from C_3H_4 and an estimate as to whether the stabilization energy provided by the addition of acetylene applies in the transition states.

The stability of the C_3H_4 diradical relative to $C_5H_6(RO)$ can be estimated by noting that adding acetylene to it results in the formation of one carbon-carbon single bond and a reduction in strength of the acetylene triple bond to that of a double bond.

Taking 100 kcal/mol as an average value for a C-C single bond, and 70 kcal/mol for the breaking of one π bond of a triple bond suggests that the C_3H_4 diradical is stabilized by roughly 30 kcal/mol upon reaction with acetylene to yield C_5H_6(RO).

C_5H_6(RO) was estimated above to lie 81 kcal/mol above cyclopentadiene. Thus, this line of reasoning yields an energy of 111 kcal/mol for C_3H_4 diradical and acetylene relative to cyclopentadiene vs. 88 for cyclopropene and acetylene, and therefore a C_3H_4 diradical energy 23 kcal/mol above cyclopropene. This later energy has been calculated to be 24.8 kcal/mol for the most stable form of the C_3H_4 diradical[37]. This suggests that there is perhaps some additional stabilization beyond the 30 kcal/mol expected. This could be due to some resonance stabilization (~ 2 kcal/mol) of the second electron by the addition of acetylene. However, the agreement is probably well within the overall error. The calculated structure for this diradical shows it to be a triplet carbene. Both results support the present reasoning based on independent radical electrons.

I'll note briefly here that the energetics for the production of acetylene and the C_3H_4 carbene just described make it a potential reaction channel. Although these products are much less stable than the others described so far, they are only 113 kcal/mol unstable relative to cyclopentadiene. Further, the dissociation to such a radical might be expected to occur without a barrier. To determine the probability for reaction via this channel, one must then consider whether the barrier for H atom migration to the more stable products will be above or below this value.

With these points in mind, I'll turn to a discussion of the allene-methyl

acetylene system in detail before exploring the consequences for $C_5H_6(RO)$ dissociation. To convert allene to methyl acetylene nominally requires a 1,3 hydrogen shift. However, the barrier for a direct transfer has been calculated to be 94.9 kcal/mol by Honjou et. al.[38,39]. The most energetically favored pathway involves a multistep process with a cyclopropene intermediate. This process can be described as a sequence of H atom migrations; a 1,2 shift, a 1,3 shift and finally a 2,1 shift to the methyl acetylene product. The diradical after the 1,2 shift is stabilized by ring closure to cyclopropene. Honjou et. al. calculated two large barriers on this pathway; 68.4 kcal/mol for the initial 1,2 shift and a 63.4 kcal/mol barrier for 1,3 migration. Both values are relative to allene. The final 2,1 shift would be expected to be much lower in energy. The 2,1 shift required to isomerize from vinylidene to acetylene has a barrier of ~ 3 kcal/mol[40]. It is not clear whether this value is relevant in the present case, since vinylidene has a singlet ground state and the CH_3CHC: diradical has a triplet ground state (the singlet state is unstable by 11.8 kcal/mol[37]). Perhaps a better value might be Benson's suggestion of 11 kcal/mol for 2,1 H atom shift in a 1,3 diradical[36]. This yields an estimate for 2,1 shift to produce methyl acetylene between 48 and 56 kcal/mol relative to allene.

One might question whether ring closure of the transition state is essential to this scheme. The energy of the diradical has been calculated to be only 45 kcal/mol (triplet carbene) and 57 kcal/mol (singlet carbene) above allene (using a value of 20 kcal/mol for the stability of cyclopropene relative to allene)[37]. These energies are still below the H atom shift barriers. Further, the geometry of the transition states for

these H atom transfers have been calculated[39,41]. The 1,2 transition state has a <CCC bond angle of 170 degrees and the 1,3 transition state has a <CCC bond angle of almost 90 degrees. Both of these suggest that there is not significant stabilization of the diradical by ring closure at the transition states.

The last notes on the C_3H_4 system concern the involvement of the radical electrons in the transition state. For the initial 1,2 shift, a π bond is broken and the diradical is formed. The reverse of this process, which is relevant to this discussion, involves radical electrons on carbons 1 and 2 forming a π bond during the shift. Both radical electrons are involved.

This is in contrast to the subsequent 1,3 shift which creates the $:CCHCH_3$ carbene from the $\circ CH{=}CH{-}CH_2\circ \leftrightarrow :CH{-}CH{=}CH_2$ diradical. Here, one of the electrons is more of a spectator. If the electron that remains on carbon 1 were involved in another bond, the energy of the transition state might merely shift by the stability of the new bond.

The last transition state to examine is the 2,1 shift in the $:CCHCH_3$ carbene. While this barrier is well below the other two, like the first 1,2 shift, the transition involves both radical electrons. In both of these cases, one might then expect that if one of the radical electrons were involved in additional bonding, the bond must be broken, and that energy cost incurred, before the H atom shift can occur.

With this information, I'll return to consideration of the $C_5H_6(RO)$ diradical. Dissociation of this radical to allene and acetylene requires a 2,3 hydrogen shift, analogous to the reverse of the first step in allene isomerization. Arguing that this

transition requires the localization of both radical electrons in the future allene moiety implies that the 30 kcal/mol stabilization of $C_5H_6(RO)$ relative to CH_2=CH-CH: will not result in a concomitant change of barrier height for this H atom shift. This leads to an estimated barrier height 68.4 kcal/mol above the products. This converts to a barrier 136.4 kcal/mol above cyclopentadiene.

For methyl acetylene and acetylene products, the barrier would not be as high. Here, the reaction pathway involves two barriers equivalent to the 1,3 shift and 2,1 shift in the allene isomerization. The first transition, transferring an H atom from the central carbon to the CH_2 group, might be expected to be stabilized by the stabilization of the 'spectator' electron. Thus, while the barrier is 63.4 kcal/mol above allene for the three carbon system, the barrier is only 33.4 kcal/mol relative to allene plus acetylene in the five carbon system. This barrier is only 101.4 kcal/mol relative to cyclopentadiene, and is below the barrier to dissociation to the CH_2CHCH: carbene and acetylene.

The second barrier along this path to methyl acetylene, which is not rate limiting in the C_3H_4 case, becomes important here. Like the shift required to produce allene, this shift involves both radical electrons. Hence, as before, the transition state is not likely to be stabilized by a process that pulls the radical electron away from the C_3H_4 moiety. Thus the full barrier of 48-56 kcal/mol relative to allene should apply for cyclopentadiene dissociation to methyl acetylene plus acetylene. The barrier here is then 116-124 kcal/mol relative to cyclopentadiene, making this the rate limiting step for this pathway.

Thus, in the final analysis, the pathways for both acetylene plus allene and acetylene plus methyl acetylene have higher barriers than a simple dissociation to acetylene plus the CH_2CHCH diradical, which, assuming no barrier for the formation of the triplet ground state diradical, requires only 113 kcal/mol. This picture would suggest that photodissociation at 193 nm (148 kcal/mol) would yield mass 26 and 40 products with a monotonically decreasing translational energy distribution extending out to roughly 33 kcal/mol.

(The possible similarity between this channel and CH_2 elimination should be noted. Both channels involve ground state triplet carbenes. Hence, one might expect a small (~ 4 kcal/mol) barrier for triplet CH_2CHCH production. Further, one might expect the singlet diradical to be the dominant channel above its threshold. However, it is not clear what effect the substitution of a CH_2=CH- group for the methylene hydrogen will have on the chemistry of the diradical. Because of the uncertainties, this line of thought will not be continued through the discussion.)

Given the effort I have expended in developing the diradical loss picture, it is not surprising that this description fits one of the observed dissociation channels. The translational energy release of the 'slow' acetylene observed in the experiment was fit with a pseudoexponential function extending to 35 kcal/mol. (This was long before I knew about the excited states of C_3H_4.) The diradical mechanism would also help to explain the cracking pattern for this channel relative to the 'fast' channel. For the slow acetylene channel, all of the C_3H_4 product has at least 47 kcal/mol internal energy. The slowest fragments, with at least another ~17 kcal/mol of internal energy could

overcome the isomerization barriers and yield vibrationally hot C_3H_4, while the remainder of the fragments must remain in the diradical geometry. Both the vibrational excitation and the weak CH bonds in the diradical (removing an H atom allows the formation of a CC π bond yielding a 'mono' radical) would be expected to enhance cracking of the C_3H_4 to $C_3H_3^+$ in the ionizer. This mechanism, where most of the energy not appearing in translation belongs to the C_3H_4, would predict more cracking of the C_3H_4 from this channel for a given translational energy release than for a different channel that divided the internal energy more equitably between the two fragments. In particular, the increase in cracking of the diradical due to its weak bonds is likely to be much larger than the normal increase as translational energy release decreases. This idea helps to justify the assumption used in obtaining separate $P(E_T)$s for the fast and slow acetylene channels that the $P(E_T)$ for a channel did not change as a function of which daughter ion was selected while the ratio of the $P(E_T)$s from the two channels could change.

The slow channel was estimated to account for 1% of the dissociation yield. Two comparisons should be made here. One is a comparison of the slow acetylene channel (113 kcal/mol barrier) with the CH_2 elimination channel (131 kcal/mol barrier). The large enhancement of the yield of CH_2 can clearly be seen when one considers that an increase in the barrier height of 18 kcal/mol only reduces the yield by a factor of two relative to slow acetylene.

The second comparison is with the fast acetylene channel. If the fast channel, which is a factor of two more prevalent than the slow channel, were produced via the

H migration channels discussed above, one would expect the higher barriers to reduce its yield below that of the slow channel. While the CH_2 yield suggests that this argument is not necessarily valid, it is hard to imagine a mechanism for enhancing the fast channel relative to the slow channel if they both are produced directly from the $C_5H_6(RO)$ diradical.

This logic would also apply for a cyclopropene channel going through the $C_5H_6(RO)$ diradical. Following the arguments used for the H migration barriers, one can compute a barrier of 130 kcal/mol relative to cyclopentadiene for the $C_5H_6(RO)$ diradical to close to a three membered ring and dissociate. As for the other transition states that involve participation of both electrons, this one is not assumed to be stabilized relative to that in the C_3H_4 system. Thus, it is unlikely that this mechanism can explain the observed yield of fast acetylene. The other features of the fast channel - a barrier of ≥20 kcal/mol and a maximum translational energy release near 60 kcal/mol - would be consistent with this mechanism.

There is another interesting possibility which seems to fit all of the available data. This pathway is a two step process involving isomerization of cyclopentadiene to a bicyclo[2.1.0]pent-2-ene and concerted elimination of cyclopropene and acetylene from the isomer.

Bicyclo[2.1.0]pent-2-ene is formed from cyclopentadiene by rearrangement of the π bonds to form one π bond and a sigma bond between the carbons adjacent to the CH_2 group. The transition is similar to the formation of cyclobutene from 1,3 butadiene, but the barrier is much higher because the cyclopentadiene reaction must

proceed via a symmetry forbidden disrotary transition state due to the constraining CH_2 group. From experimental and theoretical work, the bicyclo compound is estimated to lie 47 kcal/mol above cyclopentadiene with a barrier to formation of 74 kcal/mol, again relative to cyclopentadiene. This is the lowest barrier to geometry change among all of those discussed, suggesting that this isomerization is facile compared to H atom loss and ring opening.

The barrier from this isomer to products is more difficult to estimate. In the simplest picture, two single C-C bonds are broken, one single bond becomes a double bond, and a double bond becomes a triple bond. Using values of 100, 80, and 70 kcal/mol respectively for the individual bond energies, a difference in stability of 50 kcal/mol can be calculated. This suggests that roughly 50 kcal/mol of energy is required to weaken the single bonds before the electrons will rearrange. This leads to a barrier of 97 kcal/mol to reaction. If one accounts for the fact that the cyclopropene π bond is weaker than normal by roughly 10 kcal/mol due to ring strain, the barrier estimate would rise to 107 kcal/mol relative to cyclopentadiene.

This is wonderfully close to the experimentally deduced >= 108 kcal/mol barrier. The agreement is certainly a fortuitous coincidence. This simple picture ignores the release of the strain energy of the four carbon ring and does not fully account for the strain energy incurred by forming the π bond in the three carbon ring.

One way to show the limitation of this picture is to apply it to cycloaddition of ethylene to form cyclobutane. This process has an activation energy of 43.8 kcal/mol relative to two ethylenes with a ΔH_{rxn} of ~ 18 kcal/mol[42]. Thus the reverse barrier is ~62

kcal/mol. The loss of two 100 kcal/mol single bonds and formation of two 80 kcal/mol π bonds would yield an estimated barrier of 40 kcal/mol relative to cyclobutene, 22 kcal/mol below the experimental activation energy. If this error is due to strain energy in the transition state (Benson gives a value of 26.2 kcal/mol for the cyclobutane strain energy[36]), one might expect that the error in the bicyclo system may be much smaller because of the offsetting contributions from strain in the two rings. (Benson gives a cyclobutene strain energy of 29.8 kcal/mol and a change in strain upon going from cyclopropane to cyclopropene of 53.7 - 27.6 = 26.1 kcal/mol yielding a net release of 3.7 kcal/mol.)

This type of concerted dissociation would certainly result in a large repulsion between the fragments and a peaked translational energy distribution. The fact that this channel has a higher yield than the slow acetylene channel and the expectation that this transition state is likely to have higher vibrational frequencies than the linear diradical seem to imply that the total barrier is less than 113 kcal/mol. Thus a barrier to reaction slightly above 108 kcal/mol is suggested. These limits would yield a relatively high percentage of available energy appearing in translation, even for a concerted reaction. If the true barrier for dissociation is much above this estimate, the assignment of the fast acetylene product to this channel might be in jeopardy.

BRANCHING RATIO:

Given the above description of the dissociation pathways, the experimental

branching ratio makes qualitative sense. H atom loss, the lowest energy channel by 24 kcal/mol is dominant with 96.6% of the yield. The fast acetylene channel, with the next lowest barrier near 108 kcal/mol, accounts for 1.9%. The slow acetylene pathway, with a barrier around 113 kcal/mol, has a slightly lower yield of 1%, and the highest energy channel, CH_2 at 131 kcal/mol, accounts for the remaining 0.5%.

As one would expect, the highest energy barrier along the reaction path has a large effect on the product yield. Assuming a statistical distribution of energy at the transition state, this effect is just a reflection of the fact that the number of available dissociative states increases rapidly as a function of available energy (in this case photon energy - barrier height). Available energy is not the only factor that affects the number of dissociative states: the vibrational frequencies and moments of inertia of the transition state also affect the state count.

Such effects are definitely important in the cyclopentadiene system. The easiest way to see this is to look at the theoretical branching ratio of four H atom loss channels, all with the same transition geometry and forces, but with different barriers, corresponding to those above. The frequencies for cyclopentadiene and the H atom loss transition state used for this calculation were discussed in the results section. The calculated ratio is $1 : 8\times10^{-4} : 1\times10^{-4} : 3\times10^{-8}$ for the equivalents of the H, fast C_2H_2, slow C_2H_2, and CH_2 channels respectively. While the barriers to reaction may be slightly different than those I've estimated, it is clear that the discrepancy between this distribution and the experimental ratio cannot be accounted for by energy considerations alone.

Obviously, the vibrational frequencies of the various transition states must be quite different. In particular, one might expect that the highly constrained ring geometry of the H loss channel would cause it to have higher frequencies than for the 'linear' diradicals and hence to have a lower relative contribution than expected from barrier heights. The bicyclo transition state might also be favored relative to the H loss channel as the various bending modes of the 'acetylene' with respect to the 'cyclopropene' drop in frequency due to the increase in distance between the two 'fragments'.

The CH_2 channel seems to be favored not only with respect to the H atom loss channel but also with respect to the two acetylene channels. The floppiness of the diradicals relative to the cyclic transition state for H atom loss can explain some of the CH_2 channel's enhancement relative to H loss, but it's enhancement relative to the 'slow' acetylene channel requires an additional factor since the 'slow' channel also proceeds via a straight chain diradical

Such a factor is hard to imagine for a pathway with a barrier, as might be true for the $^3CH_2$ elimination pathway. However, for a barrierless pathway relatively close to threshold, one would expect a very loose transition state and therefore an enhanced rate. This is the limiting case for which Phase Space Theory applies[43]. The loose transition state can be understood if one realizes that for a barrierless transition near threshold, the minimum state density, i.e. the 'bottleneck' one would call the transition state, occurs at the top of the centripetal barrier. This 'pseudo' barrier (see the H atom loss discussion) is located at much larger inter-fragment separation than would be

expected for a true potential barrier. At these large distances, the fragments are nearly free rotors, which greatly enhances the state count at the 'bottleneck'. It should be noted that, as the excess energy is increased (e.g. for the possible singlet CH_2CHCH plus acetylene channel), the transition state shifts to shorter inter-fragment distances and the enhancement relative to a channel with a true barrier is reduced.

Another factor which could enhance the other pathways relative to H atom loss would be evolution on an electronic excited surface. For instance, if the ring opened diradical were formed on an electronic excited surface and conversion then occured to the ground state, the transition state for H atom elimination would be the ring closure barrier. This is because the ring closure barrier is higher than the barrier for H atom loss from the cyclopentadiene geometry. Thus, the CH_2 to H atom branching would be determined by how well CH_2 loss competed with ring closure. This would enhance the yield of CH_2 compared to its value when starting on the electronic ground state in the cyclopentadiene geometry. A rigorous calculation of the branching ratio expected between the H and CH_2 loss channels, starting from the cyclopentadiene geometry, could be compared with the experimental value to infer the importance of excited electronic states in this reaction.

Such a calculation is not possible with the limited knowledge I have of the barrier heights and transition state frequencies. I have, however, gone in the reverse direction and attempted to deduce the general 'frequency pattern' from the experimental data to allow some comparison of the results of this experiment with the bulk thermal work mentioned at the start of the chapter and to answer the question of how large the

yield of the minor channels might be expected to be at 1000 K. The concept of this calculation is that even if the frequencies picked for the transition state are not right, as long as they correctly predict the reaction rate, and, for barrierless reactions, the $P(E_T)$ of the products as well, they can be used to derive approximate Arhenius A factors and activation energies[44]. These factors then allow calculation of the thermal reaction rates. While the calculation here will be quite qualitative, it does show that the photodissociation data obtained in this experiment can be applied to yield information useful for thermal combustion studies. The limitations here are in the crudeness of the calculation, not the data: the data are sufficiently precise that they should constrain more quantitative calculations as well.

Because of the multiple wells and the possible excited state dynamics, etc. one cannot really expect the thermal behavior to be fit by an Arhenius model. One should certainly question the validity of using such numbers to model the thermal branching ratio. However, at the 1000 K temperature of interest here, the most probable dissociation energies fortuitously turn out to be slightly below the 148 kcal/mol energy used in this experiment. Thus, the A factors that will be calculated here are used mainly as a way to smoothly extrapolated the observed branching ratio and implied dissociation rates (based on an estimate for the H atom loss rate) to zero at the estimated barrier heights. Since this experiment yields the branching ratio near the most probable dissociation energies at 1000 K, the exact choice for the extrapolating function is not critical and the errors from assuming Arhenius behavior should be small. At higher temperatures, the most probable dissociation energy will be much

higher than 148 kcal/mol. The extrapolation of our 148 kcal/mol data to higher energies based on the Arhenius parameters derived here could then introduce serious errors. Thus, either higher energy photodissociation data or a better (non-Arhenius) model are required to estimate thermal rates above 1000 K.

In the first step of the calculation, the rate of H atom loss is calculated for a 148 kcal/mol excitation using RRKM theory. The barrier for H atom loss was set at 84 kcal/mol, just above the lower experimental limit. A harmonic state density was calculated for the cyclopentadiene molecule using the known normal mode frequencies. As described in the results section, the frequencies for the H atom loss transition state were estimated as those of the cyclopentadienyl radical with two additional 310 cm^{-1} bending modes. The sum of states was also done in the harmonic approximation. The calculations were performed using a variant of the RRKM program written by Hase and Bunker (Quantum Chemistry Program Exchange #234). The result is a dissociation rate of $4x10^8$ per second. This is approximately 40 times above the experimental lower limit of 10^7 per second determined by Yi et. al.

This value was then used to set the rates for the other channels based on the branching ratio and the degeneracies for each channel (2 for H atom and CH_2 loss, 1 for the acetylene channels). Barriers for each channel were estimated from the available theoretical and experimental data as discussed above. These values are 131 kcal/mol for CH_2 loss, 113 kcal/mol for slow acetylene, and 108 kcal/mol (the lower limit) for fast acetylene. (The possibility that the methylene channel is composed of $^3CH_2$ and $^1CH_2$ channels is ignored here. The conclusions drawn below are not greatly

affected by such an omission.) The same density of states for the cyclopentadiene molecule was used. Initial frequencies for the three transition states were estimated by assuming the transition state bonding to be exactly halfway between reactant and products. Thus, the bond between CH_2 and the 1-buten-3-yne fragment was treated as a one electron bond, while the forming triple bond was estimated as order 2.5. Frequencies were then assigned to each degree of freedom based on average values tabulated by Benson [36]. (Note that the $C \circ CH_2$ bond mentioned above is the reaction coordinate and was not assigned a frequency, but the methylene rock frequencies were affected.) No attempt was made to calculate normal mode frequencies.

RRKM rates were then calculated. For the 'barrierless' CH_2 and slow acetylene channels, the translational energy distribution of the products was also calculated. The estimated frequencies were adjusted to produce agreement with the rates estimated via the H atom loss rate and the branching ratio and with the experimental translational energy distributions. To fit the observed rates, the frequencies of the lowest frequency modes had to be greatly reduced from the initial values described above. The final frequencies are listed in Table 2.

These parameters were then used to calculate the dissociation rates for a wide range of energies. The harmonic state density of the cyclopentadiene molecule was also calculated over a wide energy range. This state density was weighted by the Boltzmann factor $e^{-E/kT}$ yielding the thermal population of these states for temperatures of 500 to 4000 K. Then, the dissociation rate for each channel was determined for each temperature by multiplying the normalized populations as a function of energy by

the corresponding reaction rate for states at that energy. An Arhenius plot of the natural logarithm of the rate vs. 1/T was used to extract A factors and activation energies (from the intercept and slope respectively).

The results are shown in Table 3. The most striking feature is an estimated A factor of nearly 10^{20} for the CH_2 loss channel. All four A factors are fairly large. They could all be lower by roughly a factor of 40 assuming the rate of H atom loss is near the experimental lower limit determined by Yi et. al. A lower rate for H atom loss would be reasonable, considering that a calculation including anharmonicity would predict a lower rate. The harmonic approximation is undoubtedly a poor one in this case since the state density obviously cannot be harmonic in all degrees except the reaction coordinate if there are multiple dissociation pathways. This factor is perhaps sufficient to bring the acetylene A factors into a reasonable range, but the CH_2 channel continues to stand out.

As discussed above, the 'high' yield for the CH_2 channel can be understood in terms of an expected loose transition state, and perhaps excited state dynamics. The extreme A factor calculated here is an artifact of neglecting these mechanisms. Neither of these mechanisms will cause as large a dependence of the dissociation rate on energy as would the fixed loose transition state model implied by the calculation. For instance, the loose transition state expected for a barrierless channel becomes tighter as the energy increases. If an A factor were calculated using data from higher energy experiments, it would not be so large. Thus, as discussed above, the dissociation rates are not really fit by an Arhenius model. While the large yield of

methylene is real, the derived A factor should not be overinterpreted.

The thermal branching ratio calculated for 1000 K from the parameters in Table 3 is

$$1 \quad : \quad 8.2\text{x}10^{-6} \quad : \quad 1.5\text{x}10^{-4} \quad : \quad 3.4\text{x}10^{-5}$$

for H, fast C_2H_2, slow C_2H_2, and CH_2 respectively. It is clear from these numbers that the H loss channel is very dominant near 1000 K. It would seem unlikely that such small yields could explain the qualitative difference between Butler et. al.'s oxidation study of cyclopentadiene and the similar studies of aromatic fuels. Similarly, it would seem unlikely that the catalytic cleavage of methane by cyclopentadiene discovered by Dean could be affected much by such minor channels. The numbers presented here should allow the calculations necessary to confirm these impressions.

While the minor channels are therefore likely to be unimportant, the models in both studies will certainly be affected by the new value for the barrier height for H atom loss which is at least 5 kcal/mol larger than the previously estimated value. Similarly, the estimate from this work that there is a diradical form of C_5H_6 accessible by a relatively low H migration barrier (~91 kcal/mol relative to cyclopentadiene) that is likely to be the most probable form of C_5H_6 at 148 kcal/mol above cyclopentadiene could also have a large impact on the models. The reactivity of such a diradical would be much different than that of the cyclopentadiene form of C_5H_6. Such a diradical might therefore account for some of the anomalies in the oxidation studies. Lastly, while the acetylene elimination channels may be slow compared to H atom

loss, the reverse reactions provide mechanisms to form cyclopentadiene directly from stable molecules without intermediate monoradicals. It is again unclear without further calculation whether these reactions can compete with monoradical pathways under the conditions present during methane pyrolysis or in other sooting environments.

MULTI-PHOTON EFFECTS:

The original purpose of the high power survey was to investigate the chemistry of the cyclopentadienyl radical. However, in the course of analysis, it has become less clear that this is actually what was studied. From the crude RRKM calculation above, the dissociation rate of cyclopentadiene was estimated as $< 4x10^8$ per second. It is likely that the real value is at least somewhat below this, but above the 10^7 per second limit set by Yi. et. al. This suggests that the cyclopentadiene molecule may not dissociate during the laser pulse and that some of our two photon signals are due to direct dissociation of cyclopentadiene molecules with 296 kcal/mol of internal energy. Higher order events almost certainly involve photon absorption by the fragments since the highly excited cyclopentadiene cannot be expected to linger.

An argument against this picture comes from the fact that the m/e 65 spectrum is not broadened at high laser power. One would expect that if two photon excited cyclopentadiene dissociated to H atom and cyclopentadienyl radical, the translational energy release would be larger than for the one photon process and hence the

time-of-flight spectrum should broaden with increased laser power. That this is not observed suggests that the cyclopentadiene single photon dissociation is rapid, and/or that the cyclopentadienyl fragment's absorption cross-section is much larger than that of the excited cyclopentadiene molecule, and/or that two photon excited cyclopentadiene dissociates mainly to polyatomic fragments. The latter two factors could explain the data without requiring a fast primary dissociation to cyclopentadienyl radical.

A determination of the precursor for the polyatomic fragments is possible in principle: find the two momentum matched fragments and add their masses together to yield the precursor mass. This information would distinguish between the two processes above. A mass 66 precursor implies direct two photon dissociation while a mass 65 precursor implies a cyclopentadienyl intermediate. The latter case appears to be true for the new channel detected at m/e 39 and m/e 26. Unfortunately, the problem of dissociative ionization makes this determination suspect. Even the primary 'slow' acetylene channel shows a large amount of fragmentation of the mass 40 product to m/e 39. A two photon process, leaving the fragments with even more internal energy, might appear only at m/e 39 with virtually all of the hypothetical mass 40 product cracking in the ionizer. Thus, a determination of the precursor is not possible from the experimental data.

One can still make some interesting observations about the dissociation. Two of the three polyatomic channels, appearing at m/e 50 and m/e 39 - m/e 26 (conjugate fragments), show peaked translational energy distributions, implying barriers to

dissociation >18 kcal/mol and >30 kcal/mol respectively. These barriers represent only 1/4 to 1/3 of the available energy as estimated by the high energy tail. (One might argue that the tail is from the dissociation of very highly internally excited intermediates and not from the same population of intermediates that accounts for the peak in the translational energy distribution. However, at least for a cyclopentadienyl radical intermediate, the average internal excitation is only ~ 8 kcal/mol less than the maximum possible (based on the translational energy distribution for H atom loss). Thus, the high energy tail is unlikely to be more than 8 kcal/mol above the one expected from a homogeneous intermediate population.) These barriers suggest concerted transition states where the translational energy release is governed mainly by repulsion of the forming products. For the m/e 39 - m/e 26 product pair, one might propose a mechanism similar to the primary 'fast' acetylene channel with dissociation occurring from a bicyclic structure. Dissociation of CH_2 from the bicyclic intermediate would also be energetically allowed in a multi-photon dissociation.

These channels are in contrast to the m/e 51 channel which has a maximum translational energy release of only 33 kcal/mol (assuming loss of carbon in the final step). This channel overlaps with the primary CH_2 loss channel making it difficult to determine if there is any peak away from zero in the translational energy distribution. The low energy release argues against a concerted loss and also against a CH_3 + mass 51 channel, with the latter based on thermodynamic stability of the products (~115 to 135 kcal/mol relative to cyclopentadiene, depending on the form of C_4H_3). This suggests that multiple dissociations occur -- either H followed by CH_2 or vice versa.

A secondary loss of H would be argued against by the >150 kcal/mol translational energy that would be required in this step to fit the data. It is difficult to reconcile such a large energy release with estimates of the thermodynamic stability of the products assuming two photon absorption. The best explanation seems to require a cyclopentadienyl intermediate. If true, the goal of observing radical dissociation has been achieved; cyclopentadienyl radical excited to an average internal energy of ~210 kcal/mol (148 kcal/mol + ~64 kcal/mol from the primary step) yields CH_2 as a product.

The last observation I'd like to discuss is the branching between hydrogen loss and C-C bond cleavage at very high powers. The time-of-flight spectra clearly show that the majority of multi-photon products are in the C_5H_n series. They also show that bare C_5 is a product. C_5 must have survived through at least four dissociation events that eliminated all six hydrogens. This is a remarkable tribute to the π bonding ability of carbon. (Forgive me - it's been a long chapter.) After an initial H atom loss, all of the C-C bonds in cyclopentadiene acquire at least a partial multiple bond character. This means that the remaining C-H bonds will always be the weakest bonds in the molecule. In this light, it is not so surprising to observe C_5 products.

If C_5 forms in the molecular beam, it may also exist in outer space. Many other highly unsaturated molecules and radicals based on carbon chains, including C_3 (linear and cyclic) and C_5H have been observed in interstellar and/or circumstellar clouds[45,46]. The question does remain as to the nature of the product in our study. The above description implies that the C_5 product should be cyclic assuming that the initial H loss yields the cyclopentadienyl radical. However, work by Raghavachari

and Binkley indicates that a linear C_5 structure is more stable than a cyclic one[47]. Formation of cyclic C_5 in this reaction would then be thermodynamically disfavored but it might still be the most kinetically favored path starting from cyclopentadiene. If this is true, the observation of C_5 in this experiment may not have direct application to estimating the likelihood of C_5 existing in interstellar clouds. The formation of C_5 in outer space is thought to proceed via carbon insertion reactions leading to linear C_5H[48]. The important information would then be the probability of H atom loss from linear C_5H relative to C-C bond rupture.

Due to the averaging in our experiment, especially for the higher order processes, it is impossible to estimate the thermochemistry of the intermediates and the final C_5 species. It may be possible to assess whether ring opening occurs after a primary H loss from studying the cyclopentadienyl radical directly. A comparison of the experimentally derived thermodynamic stability of a C_5H_3 product with theoretical results for cyclic and linear structures could answer the question. (I am not aware of theoretical work on these species.) The experimental number is technically deriveable from the present experiment. It is ~180 kcal/mol ($E_{photon} + E_{Int,\ primary} - E_{T,max}$). I regard this number as too speculative to warrant analysis due to the following concerns. First, it is derived by assuming that the dissociating radicals have an average internal energy of 210 kcal/mol (max E_{Int} = 218 kcal/mol), based on the assumption that only one photon is absorbed by the radical. It further assumes the existence of a conjugate H_2 product, which is not unequivocally observed, in order to determine the translational energy release from the TOF spectrum. (The observed H_2 may be from

other reactions and the dissociation under discussion may occur via two H atom eliminations). These problems could both be addressed by a direct study of the cyclopentadienyl radical. Assuming an H_2 loss process yields a maximum observed translational energy of ~34 kcal/mol. If this value is not representative of the thermochemistry, i.e. if the fragments are always vibrationally excited, then a direct study of the cyclopentadienyl radical will not yield an improved estimate.

Conclusions

This photodissociation study of cyclopentadiene has yielded a wealth of information. The most basic result is confirmation that H atom loss yielding the cyclopentadienyl radical is the major channel. The quantum yield calculated from our results, 96.6 %, is significantly larger than the previous estimate of 85±7% by Yi et. al. This result, and our H atom loss translational energy distribution suggest that the previous work suffers from saturation and multi-photon processes. The peak away from zero in the translational energy distribution, found qualitatively in both studies, has been shown to be 5 kcal/mol. It has been interpreted in this work as evidence of a potential barrier as large as 8-10 kcal/mol in the H loss channel due to repulsive forces between the fragments caused by delocalization of the cyclopentadienyl radical electron into the ring.

Three other primary channels were identified for the first time. They are, in order of decreasing yield, acetylene and cyclopropene (1.9%), acetylene and the C_3H_4

triplet carbene (1%), and CH_2 and 1-buten-3-yne (0.5%). The acetylene plus cyclopropene reaction coordinate is shown to include a barrier > 108 kcal/mol above cyclopentadiene based on its $P(E_T)$. The latter two channels appear to be barrierless. The translational energy distribution for the acetylene plus C_3H_4 carbene channel gives support for the theoretical calculated energy for this radical (~ 25 kcal/mol above cyclopropene). The surprisingly high yield of CH_2 is suggested to be due to a very loose transition state for CH_2 elimination, though the relative importance of $^1CH_2$ and $^3CH_2$ cannot be obtained. Loss of H_2, suggested by Yi et. al., was not observed.

The four observed channels span a surprisingly wide variety of transition state geometries. While H atom loss occurs directly from the ring, acetylene and cyclopropene appear to form in a concerted reaction from a bicyclic geometry. The second acetylene loss channel proceeds via ring opening followed directly by dissociation to the C_3H_4 carbene. CH_2 production requires H migration after ring opening. The resulting symmetric diradical, $CH_2CHCCHCH_2$, is suggested to be the most probable form of C_5H_6 at 148 kcal/mol above cyclopentadiene. Estimates of the various barriers encountered on these reaction paths seem to be in accord with simple group additivity estimates. Further refinement of these values from the present data will require a model calculation that accounts for the multiple well nature of the potential energy surface.

Attempts were made to relate the results above to thermal studies of methane pyrolysis and cyclopentadiene oxidation. Based on admittedly crude calculations, the minor channels are estimated to account for less than .02% of the unimolecular

dissociation products at 1000 K. The estimated thermal branching ratio should help constrain kinetics models in these two systems. Several other results from this study are perhaps more interesting with regard to the thermal studies above. The most relevant is probably the conclusion that there is a barrier to H atom loss. Another is the estimate that a very stable diradical form of C_5H_6 is accessible from cyclopentadiene via a barrier only a few kcal/mol (~ 5) above the new value for the H atom loss barrier. The existence of the acetylene loss channels may also prove interesting. Run in reverse, these channels represent pathways to form cyclopentadiene with barriers relative to cyclopropene and acetylene of only 20-45 kcal/mol.

The higher laser power studies also provide a few tantalizing results that suggest the dissociation channels of the cyclopentadienyl radical. In a pessimistic sense (if you have just done this experiment), the uncertainties in the analysis of the multi-photon results point out the need for a good source of cold radicals for photodissociation experiments. In a more balanced sense, these results, though uncertain, are the first information available on the cyclopentadienyl dissociation channels. The dominant channel seems to be H_2 loss, though the nature of the C_5H_3 fragment cannot be determined. H atom loss cannot be ruled out, but no positive evidence was found for its occurrence. Other channels include CH_2 loss and possibly a concerted split into acetylene and mass 39. The acetylene plus mass 39 channel could be a misassignment of the dissociation of two photon excited cyclopentadiene yielding acetylene plus cyclopropene. The highest power results showed evidence for

C_5H and C_5 species, with unknown geometries. These results suggest that bare C_5 should be present in interstellar clouds.

Product 1	Product 2	ΔH_{rxn}	$E_{T,Max}$
c-C_5H_5	H	78	70
c-C_5H_4	H_2	~88	~60
1-buten-3-yne	CH_2	131	17
butatriene	CH_2	138	10
H_2CCCCH	CH_3	114	34
HCCHCCH	CH_3	133	15
allene	acetylene	68	80
propyne	acetylene	66	82
cyclopropene	acetylene	88	60
C_3H_3	C_2H_3	113	35

Table 1. Heat of Reaction and Maximum Translational Energy Release for some Thermodynamically Accessible Photodissociation Pathways of Cyclopentadiene at 193 nm.

Cyclopentadiene

3105.0	3091.0	3075.0	3043.0	2900.0	2886.0	1580.0	1500.0	1378.0	1365.0
1292.0	1239.0	1106.0	1100.0	1090.0	994.0	959.0	941.0	925.0	915.0
891.0	805.0	802.0	700.0	664.0	516.0	350.0			

H Loss Transition State

3061.0	3048.0	3039.0	3029.0	3024.0	1404.0	1364.0	1337.0	1275.0	1201.0
1080.0	982.0	955.0	917.0	903.0	894.0	834.0	805.0	767.0	710.0
702.0	652.0	497.0	484.0	310.0	310.0				

CH_2 Loss Transition State

3100.0	3100.0	3100.0	3100.0	3100.0	3100.0	1950.0	1650.0	1450.0	1150.0
1150.0	1150.0	1150.0	1150.0	1150.0	1000.0	600.0	600.0	600.0	600.0
600.0	85.0	20.0	20.0	20.0	20.0				

Fast C_2H_2 Loss Transition State

3100.0	3100.0	3100.0	3100.0	3100.0	3100.0	1950.0	1450.0	1300.0	1150.0
1150.0	1150.0	1150.0	1150.0	1150.0	1000.0	1000.0	700.0	700.0	700.0
700.0	382.0	275.0	120.0	120.0	50.0				

Slow C_2H_2 Loss Transition State

3100.0	3100.0	3100.0	3100.0	3100.0	3100.0	1950.0	1950.0	1150.0	1150.0
1150.0	1150.0	1150.0	1150.0	1150.0	1150.0	1150.0	1000.0	700.0	700.0
700.0	500.0	400.0	300.0	40.0	10.0				

Table 2. Vibrational Frequencies used in RRKM calculations. Frequencies are in cm^{-1}.

Channel	H Loss	CH_2 Loss	Slow C_2H_2 Loss	Fast C_2H_2 Loss
A Factor (per second)	4.3×10^{15}	9.5×10^{19}	8.7×10^{16}	8.7×10^{16}
Activation Energy (kcal/mol)	87.7	133.4	115	111.4

Table 3. Calculated Arhenius parameters for Cyclopentadiene Dissociation. Values based on experimental translational energy distributions and branching ratio at a 148 kcal/mol excitation energy. The calculation was done using simple (single well) RRKM theory under the harmonic approximation with best fit frequencies.

References

(1) Lin, C.-Y.; Lin, M. C. *J. Phys. Chem.* **1986**, *90,* 425-431.

(2) Harrison, A. G.; Honnen, R. L.; Dauben, H. J.; Lossing, F. P. *J. Am. Chem. Soc.* **1960**, *82,* 5593.

(3) Colussi, A. J.; Zabel, F.; Benson, S. W. *Int. J. Chem. Kinet.* **1977**, *9,* 161.

(4) Schmoltner, A.-M.; Anex, D. S.; Lee, Y. T. *J. Phys. Chem.* **1992**, *96,* 1236-1240.

(5) Butler, R. G.; Brezinsky, K.; Glassman, I.; The Eastern States Section Meeting of The Combustion Institute, **1990**.

(6) Emdee, J. L.; Brezinsky, K.; Glassman, I. *J. Phys. Chem.* **1991**, *95,* 1626-35.

(7) Brezinsky, K. *Prog. Energy Combust. Sci.* **1986**, *12,* 1.

(8) Brezinsky, K.; Linteris, G. T.; Litzinger, T. A.; Glassman, I.; *Twenty-first Symposium on Combustion,* **1986**, 833.

(9) Lovell, A. B.; Brezinsky, K.; I., G. *Twenty-second Symposium on Combustion,* **1988**, 1063.

(10) Dean, A. M. *J. Phys.Chem.* **1990**, *94,* 1432-1439.

(11) Sabljic, A.; McDiarmid, R.; Gedanken, A. *J. Phys. Chem.* **1992**, *96,* 2442-2448.

(12) Yi, W.; Chattopadhyay, A.; Bersohn, R. *J. Chem. Phys.* **1991**, *94,* 5994-5998.

(13) Wodke, A. M.; Lee, Y. T. *J. Phys. Chem.* **1985**, *89,* 4744.

(14) Daly, R. N. *Rev. Sci. Instrum.* **1960**, *31,* 264.

(15) Zhao, X., Ph.D. Thesis, University of California, Berkeley, **1988**.

(16) Several programs related to the analysis of Photofragment Translational Spectroscopy (PTS) experiments are available from Yuan Lee's laboratory. The main

analysis program is CMLAB2. KELVIN analyzes beam time-of-flight measurements to yield the beam parameters for CMLAB2. Alternatively, T2V creates a velocity point form for the beam from the beam time-of-flight measurements that can be used by CMLAB2. FUNC yields a 'pseudo-exponential' distribution useable as an initial $P(E_T)$ in CMLAB. All of the programs have some documentation that provides more information on the analysis procedure than is given here. Versions running on uVAX (obsolete), IBM PC, and IBM RS6000 computers exist.

(17) Adams, R.; Johnson, J. R.; Wilcox, C. F. J. Laboratory Experiments in Organic Chemistry, Macmillin Publishing Co., Inc.: New York, NY, **1979**; pp 538 .

(18) Wodke, A., Ph.D. Thesis, University of California, Berkeley, **1986**.

(19) Lee, Y. T.; McDonald, J. D.; LeBreton, P. R.; Herschbach, D. R. *Rev. Sci. Instrum.* **1969**, *40,* 1402.

(20) Continetti, R. E.; Balko, B. A.; Lee, Y. T. *Chem. Phys. Let.* **1991**, *182,* 400-405.

(21) Proch, D.; Trickl, T. *Rev. Sci. Instr.* **1989**, *60,* 713.

(22) Stenhagen, E.; Abrahamsson, S.; McLafferty, F. W., Atlas of Mass Spectral Data; **1969**.

(23) Lee, Y. T. private communication.

(24) Chiang, S.-Y., private communication.

(25) Karni, M.; Oref, I.; Burcat, A. *J. Phys. Chem. Ref. Data* **1991**, *20,* 665-683.

(26) Hase, W. L. in Dynamics of Molecular Collisions, Part B; Miller, W. H.; Plenum Press, **1976**.

(27) Fitch, W. L.; Sauter, A. D. *Anal. Chem.* **1983**, *55,* 832.

(28) Schmoltner, A.-M., Ph.D. Thesis, University of California, Berkeley, Appendix 1 **1989**.

(29) Yu, L.; Foster, S. C.; Williamson, J. M.; Heaven, M. C.; Miller, T. A. *J. Phys. Chem.* **1988**, *92,* 4263-4266.

(30) Parke, J.; Bersohn, R.; Oref, I. *J. Chem. Phys.* **1990**, *93,* 5700.

(31) Hu, X.; Hase, W. L. *J. Chem. Phys.* **1991**, *95,* 8073.

(32) Chen, I.-C.; Green, W. H. J.; Moore, C. B. *J. Chem. Phys.* **1988**, *89,* 314.

(33) Nesbitt, D. J.; Petek, H.; Foltz, M. F.; Filseth, S. V.; Bamford, D. J.; Moore, C. B. *J. Chem. Phys.* **1985**, *83,* 223.

(34) Hayden, C. C.; Neumark, D. M.; Shobatake, K.; Sparks, R.; Lee, Y. T. *J. Chem. Phys.* **1982**, *76,* 3607.

(35) Moore, C. B., private communication.

(36) Benson, S. W. Thermochemical Kinetics; John Wiley and Sons, Inc.: New York, **1968**.

(37) Davis, J. H.; Goddard, W. A. I.; Bergman, R. G. *J. Am. Chem. Soc.* **1976**, *98,* 4015-4017.

(38) Honjou, N.; Pacansky, J.; Yoshimine, M. *J. Am. Chem. Soc.* **1984**, *106,* 5361.

(39) Honjou, N.; Pacansky, J.; Yoshimine, M. *J. Am. Chem. Soc.* **1985**, *107,* 5332.

(40) Gallo, M. M.; Hamilton, T. P.; Schaefer, H. F. I. *J. Am. Chem. Soc.* **1990**, *112,* 8714-8719.

(41) Karni, M.; Oref, I.; Barzilai-Gilboa, S.; Lifshitz, A. *J. Phys. Chem.* **1988**, *92,* 6924-6929.

(42) Quick, L.; Knecht, D.; Back, M. *Int. J. Chem. Kinetics* **1972**, *4,* 61.

(43) Klippenstein, S. J.; Marcus, R. A. *J. Chem. Phys.* **1989**, *91,* 2280-2292.

(44) Robinson, P. J.; Holbrook, K. A., Unimolecular Reactions; Wiley: New York, **1972**.

(45) Turner, B. L. *Space Science Reviews* **1989**, *51,* 235-337.

(46) Guelin, M.; Cernicharo, J. *Angewandte Chemie* **1990**, *29,* 595-608.

(47) Raghavachari, K.; Binkley, J. S. *J. Cehm. Phys.* **1987**, *87,* 2191-2197.

(48) Herbst, E. *Astron. and Atrophys.* **1991**, *244,* L21-L24.

Figure Captions

Fig. 2-1.

Simplified Schematic of the Rotating Source Machine. (1) - Molecular Beam Source, (2)(3)(4) - Vacuum regions at 10^{-4},10^{-6}, and 10^{-7} torr respectively, (5) - Interaction Region where the laser beam, perpendicular to the plane of the page, crosses the molecular beam, (6) - Electron Bombardment Ionizer, (7) - Quadrupole Mass Spectrometer, (8) Daly type Ion Detector and Photomultiplier Tube, (Θ) - Laboratory angle between molecular beam and fragment recoil direction.

Fig. 2-2.

H Atom Loss Power Dependence. Signal counts at m/e 65 and m/e 64 are plotted vs. laser fluence. Assuming no secondary H atom process, both should reflect the amount of primary H atoms produced. The data from Yi et. al. is for H atom LIF signal vs. laser fluence. The vertical scaling of this data relative to the data from this work is arbitrary and was adjusted to yield the best fit between the two data sets at lower powers. Both data sets show a saturation affect while Yi et. al.'s data show the onset of a higher order H atom producing process as well (which would not show up in our m/e 65 data). The inset shows the lowest laser fluence region in greater detail.

Fig. 2-3.

Newton Diagram. This diagram shows the maximum laboratory angle and velocity thermodynamically possible for the four proposed primary channels.

The channels and their maximum center of mass translational energies are: C_5H_5 + H - 70 kcal/mol (the H atom limit is off scale), C_4H_4 + CH_2 - 17 kcal/mol, cyclic C_3H_4 + C_2H_2 - 60 kcal/mol, C_3H_4 + C_2H_2 - 80 kcal/mol. The last value represents the total available for the methyl acetylene form of C_3H_4, not the triplet carbene (~35 kcal/mol max. E_{Trans}).

Fig. 2-4.

m/e 65 Time-of-Flight Spectra. Data (circles) are shown at laboratory angles of 7, 10, and 14 degrees. All three spectra were fit (solid lines) using the H + C_5H_5 $P(E_T)$ (Fig. 6.) and an 'effective' beam velocity as described in the text.

Fig. 2-5.

m/e 1 Time-of-Flight Spectra. Data (circles) taken at a laboratory angle of 90 degrees using the pulsed valve beam source and the alternative reaction geometry described in the text. The data represents a subtraction of two data files at different powers. This was done to reduce noise from RF modulation of the very large background signal. The fit (solid line) uses the same H + C_5H_5 $P(E_T)$ (Fig. 6.) used to fit the m/e 65 data. Signal at times longer than 90 μsec can be due to cracking of 'fast' acetylene in the ionizer to yield m/e 1.

Fig. 2-6.

H + C_5H_5 Translational Energy Distribution ($P(E_T)$). The curve represents the normalized product flux as a function of total center-of-mass translational energy for the H + C_5H_5 dissociation channel. 70 kcal/mol is the maximum thermodynamically possible translational energy.

Fig. 2-7.

$H + C_5H_5$ Translational Energy Distribution with theoretical fits. Squares show the experimentally derived $P(E_T)$ as shown in Fig. 6. Also shown are an RRKM fit (dashed line) created using parameters described in the text. The solid and gray lines show Maxwell Boltzmann distributions at 2500 K and 3690 K respectively. The latter was suggested as the appropriate theoretical form by Yi et. al. The 2500 K curve is shown because it fits the high energy tail (30-70 kcal/mol, not shown) of the experimentally derived curve surprisingly well.

Fig. 2-8.

C_4H_4 Time-of-Flight Spectra, 10°. Shown are data (circles) taken at m/e 52 and m/e 51 that show contributions from the C_4H_4 product. The data was fit using two contributions: mass 52 product from the $C_4H_4 + CH_2$ channel with the $P(E_T)$ shown in Figure 9 (the faster signal) and mass 65 from the $C_5H_5 + H$ channel with the $P(E_T)$ from Fig. 6. Both are seen to dissociatively ionize to m/e 51.

Fig. 2-9.

$CH_2 + C_4H_4$ Translational Energy Distribution ($P(E_T)$). The curve represents the normalized product flux as a function of total center-of-mass translational energy for the $CH_2 + C_4H_4$ dissociation channel. 17 kcal/mol is the maximum thermodynamically possible translational energy for ground state $^3CH_2$ production.

Fig. 2-10.

m/e 13 Time-of-Flight Spectrum, 10°. The data (circles) at m/e 13 are shown with a fit (heavy black line) composed of four contributions : (from fastest to slowest) mass 26 and mass 40 from the 'Fast' acetylene channel, mass 14 from the CH_2 + C_4H_4 channel, and mass 40 from the 'Slow' acetylene channel. This shows that the data are consistent with the proposed CH_2 + C_4H_4 channel. However, the dissociative ionization of the mass 26 product from the 'Slow' acetylene channel would produce a contribution (not shown) almost identical to that of the mass 14 product, making it impossible to determine the true source of the observed signal.

Fig. 2-11.

C_3H_4 Time-of-Flight Spectra, 20°. Data (circles) are shown at m/e 40 and m/e 39. The calculated fits (heavy black line) have two major contributions due to mass 40 from the 'Fast' (black line) and 'Slow' (gray line) acetylene channels. A minor contribution from cracking of mass 52 product appears at m/e 39. Note that both 'Fast' and 'Slow' acetylene channels produce mass 40 and 26 product pairs and might therefore be considered to be one channel. However, the large difference in the ionization behavior of the mass 40 products, as evidenced by the large change in branching ratio between the two channels at the two mass to charge ratios shown, suggests that the mass 40 products are structurally different and should be treated as arising from separate dissociation channels. The $P(E_T)$ distributions used to calculate the 'Fast' and 'Slow' mass

40 contributions are shown in Fig. 14 and Fig. 13 respectively.

Fig. 2-12.

C_3H_4 Time-of-Flight Spectra, 20°. Data (circles) are shown at m/e 27 and m/e 26. The calculated fits (heavy black line) shows four contributions that arise from the mass 26 and mass 40 products of the 'Fast' channel and the mass 26 and mass 40 products of the 'Slow' channel (in order from fastest to slowest (left to right in the graph)). Note that no contribution from the nominal mass 26 species are required to fit the data at m/e 27, suggesting that the assignment of the 'Slow' channel as a mass 40-26 split of cyclopentadiene is better than an assignment as a mass 39-27 combination.

Fig. 2-13.

'Slow' C_2H_2 + C_3H_4 Translational Energy Distribution ($P(E_T)$). The curve represents the normalized product flux as a function of total center-of-mass translational energy for the 'Slow' C_2H_2 + C_3H_4 dissociation channel. 35 kcal/mol is the maximum thermodynamically possible translational energy assuming acetylene and the ground state triplet carbene C_3H_4 as products. A maximum of 80 kcal/mol is thermodynamically possible for dissociation to acetylene and methyl acetylene, the most stable products.

Fig. 2-14.

'Fast' C_2H_2 + C_3H_4 Translational Energy Distribution ($P(E_T)$). The curve represents the normalized product flux as a function of total center-of-mass translational energy for the 'Fast' C_2H_2 + C_3H_4 dissociation channel. 60

kcal/mol is the maximum thermodynamically possible translational energy assuming acetylene and cyclopropene products. Again, a maximum of 80 kcal/mol is thermodynamically possible for dissociation to the most stable products. The $P(E_T)$ for this channel shows a peak at ~ 20 kcal/mol.

Fig. 2-15.

High Laser Power Time-of-Flight Spectra, m/e 65-60, 10°. Data (circles) are shown for m/e 65-60 at roughly 200 mJ/cm^2 laser fluence. The calculated fits (solid line) have up to four components based on the four step model described in the text. They are primary H loss (medium dash), secondary H_2 loss (long dash), tertiary H_2 loss (short dash), and quaternary H loss (dots). These components, listed in order from slowest to fastest, were all fit as secondary channels using CMLAB2. The assignment of these channels is based on the fact that the secondary channel first appears at m/e 63, the tertiary at m/e 61, and the quaternary at m/e 60.

Fig. 2-16.

High Laser Power m/e 2 Time-of-Flight Spectrum, 90°. Data (circles) taken at a laboratory angle of 90 degrees using the pulsed valve beam molecular source and the alternative reaction geometry described in the text. The calculated curve (heavy black line) is composed of contributions from the proposed secondary and tertiary (again fit as a secondary channel) H_2 loss channels with pseudoexponential $P(E_T)$ distributions as described in the text. No attempt was made to adjust the $P(E_T)$s to fit the m/e 2 data. Instead they were taken

directly from the fits to the m/e 65-60 data shown in Fig. 3-15. Note that a $P(E_T)$ with a peak away from zero would reduce the long tail in the calculated time-of-flight curve and would fit the data at m/e 2 better. This is consistent with findings from the m/e 65-60 data as described in the text.

Fig. 2-17.

High Laser Power Time-of-Flight Spectra, m/e 51,50,39,26, at 15°. Data (circles) are shown at the three mass to charge ratios that show new hydrocarbon fragmentation (non hydrogen loss) channels. Also shown is m/e 26 in which new signal appears, but all of which can be accounted for by dissociative ionization of the other multiphoton channels. The three new channels are described in the text and will be described here as secondary 51, tertiary 50, and secondary 39. The assignment of these channels is not clear and the names here are for identification purposes only. See the text for a discussion. The total calculated signal is shown as a heavy black line in each spectrum. The m/e 51 spectrum is composed of primary mass 52 from the C_4H_4 + CH_2 channel (gray line) and a faster signal from the secondary mass 51 channel (thin black line). The m/e 50 spectrum has the same two slower components plus a new faster signal from the tertiary 50 channel (thinnest black line). The m/e 39 spectrum show the primary 'Fast' and 'Slow' mass 40 signals (thick and thin black lines, respectively) and a fast signal from the secondary 39 channel (gray line). The m/e 26 spectrum is fit with five contributions which are, in order of fast to slow, 'secondary 39' mass 27,

primary 'Fast' mass 26, 'secondary 39' mass 39, primary 'Fast' mass 40, and primary 'Slow' mass 26. No new signals at m/e 26 are apparent above the noise.

Fig. 2-18.

Energy Level Diagram for cyclopentadiene and many of the thermodynamically allowed dissociation channels. The arrow shows the photon energy of 148 kcal/mol for the wavelength used in the dissociation (193 nm). The diagram is roughly to scale (~2 kcal/mol) for all species and barriers with the ΔH of each species relative to cyclopentadiene shown in kcal/mol. The products shown include the $^3CH_2$ loss channels with the two allowed C_4H_4 geometries (far left column), the intermediate symmetric diradical reached by ring opening and H atom migration (2nd column), acetylene plus three of the possible C_3H_4 geometries - triplet carbene, allene, and methyl acetylene (third column), the diradical reached by direct ring opening at the methylene group of cyclopentadiene (fourth column), cyclopentadiene itself (fifth column), cyclopentadienyl radical plus H atom (sixth column), bicyclo[2.1.0]pent-2-ene, and acetylene plus cyclopropene (far right). The barriers from cyclopentadiene are ~87 kcal/mol for ring opening, and 83-88 kcal/mol for H atom loss (dashed line = minimum consistent with the data, solid line = likely estimate). The ring opening can be followed by three H atom migrations with barriers near 124, 118, and 91 kcal/mol, or by dissociation to acetylene and the triplet carbene C_3H_4. The lowest barrier to H migration leads to the stable symmetric

diradical and to the CH_2 product. The barrier to isomerization to the bicyclo compound is 74 kcal/mol, with a further barrier >108 kcal/mol to dissociation to acetylene and cyclopropene. The origin of the numbers given here are described in the text.

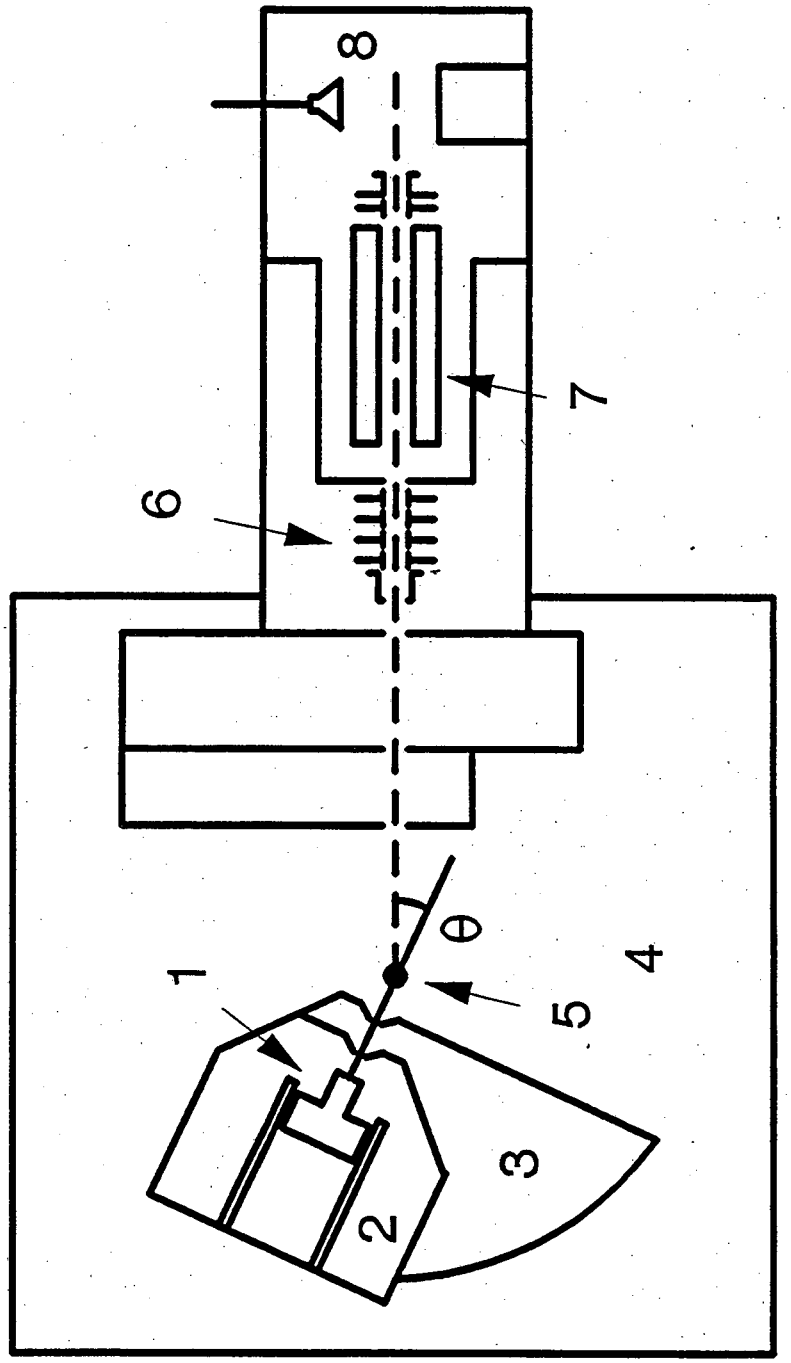

Figure 1.

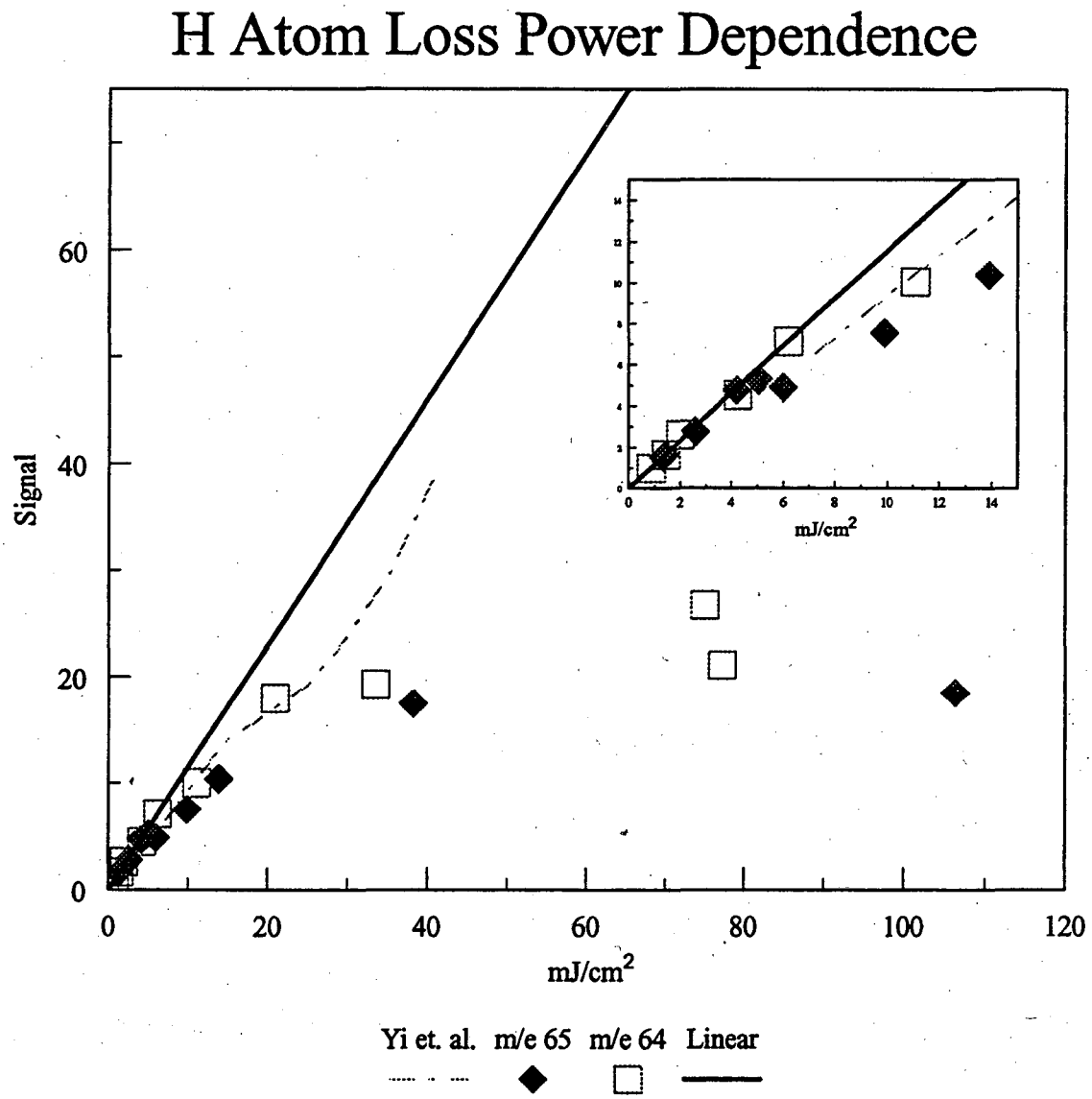
H Atom Loss Power Dependence
Signal
0
20
40
60
0
20
40
60
80
100
120
mJ/cm2
0
2
4
6
8
10
12
14
mJ/cm2
Yi et. al.
m/e 65
m/e 64
Linear

Figure 2.

Newton Diagram

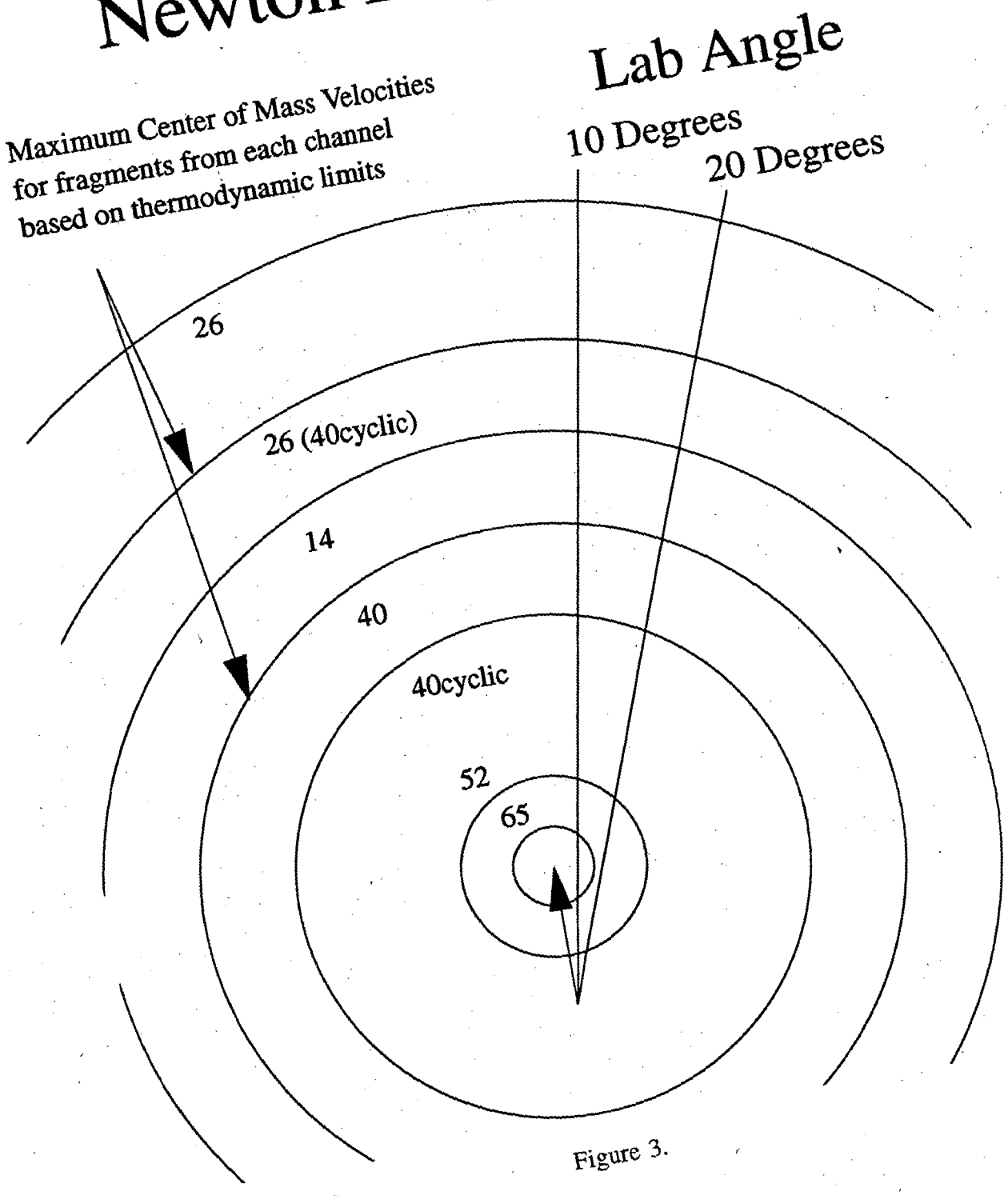

Figure 3.

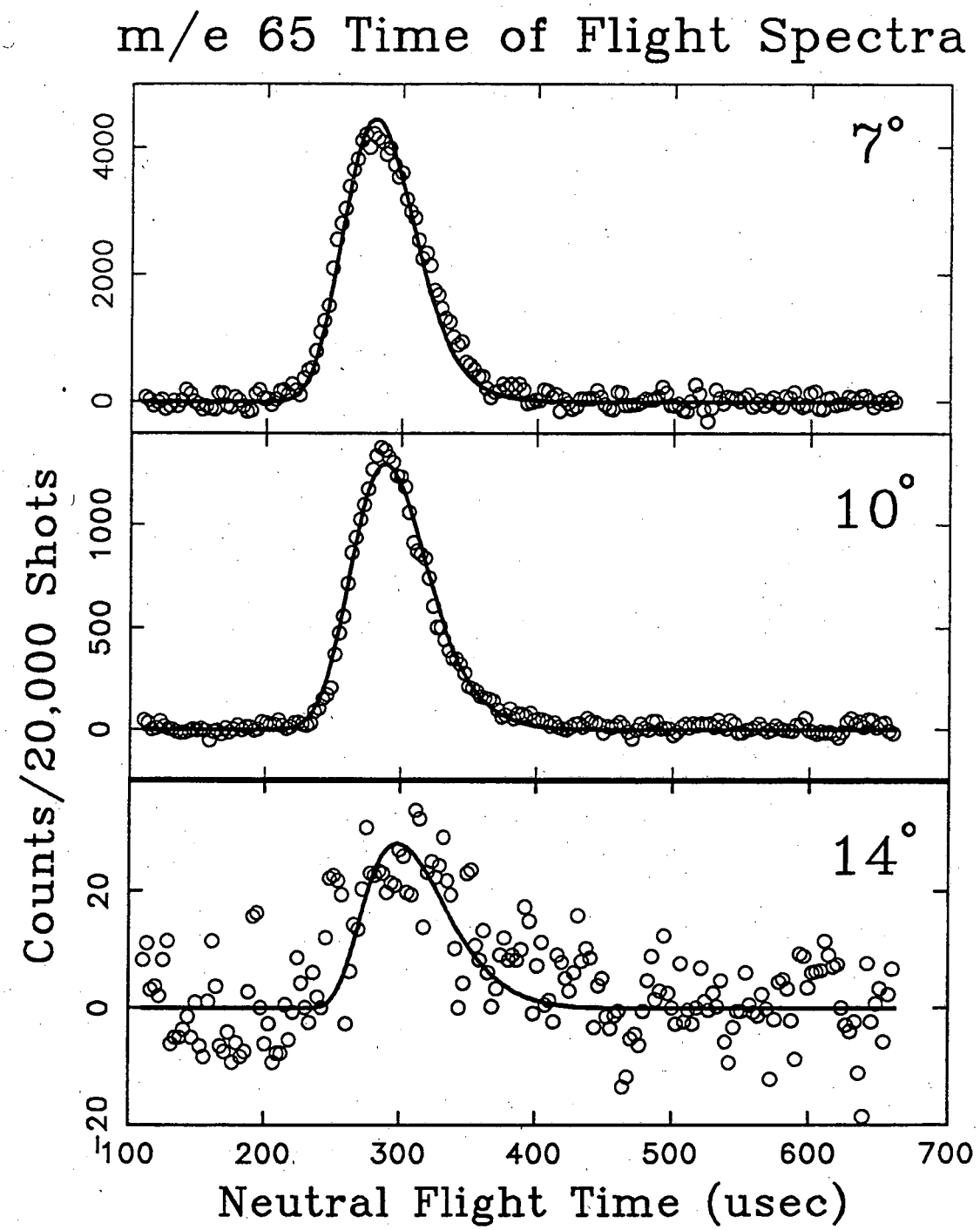
m/e 65 Time of Flight Spectra
7°
10°
14°
Counts/20,000 Shots
4000
2000
0
1000
500
0
20
0
-20
100
200
300
400
500
600
700
Neutral Flight Time (usec)

Figure 4.

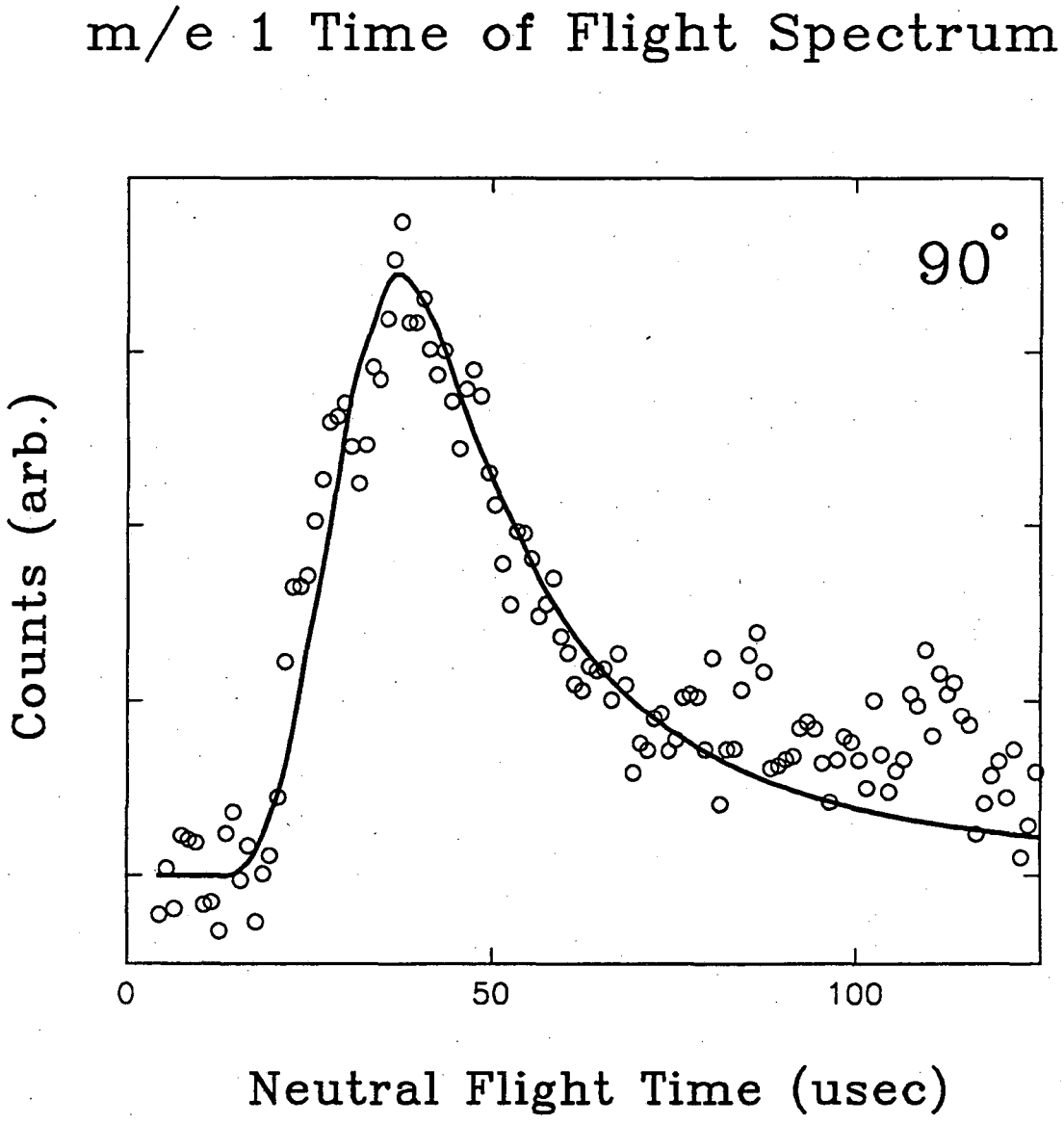
m/e 1 Time of Flight Spectrum
90°
Counts (arb.)
0
50
100
Neutral Flight Time (usec)

Figure 5.

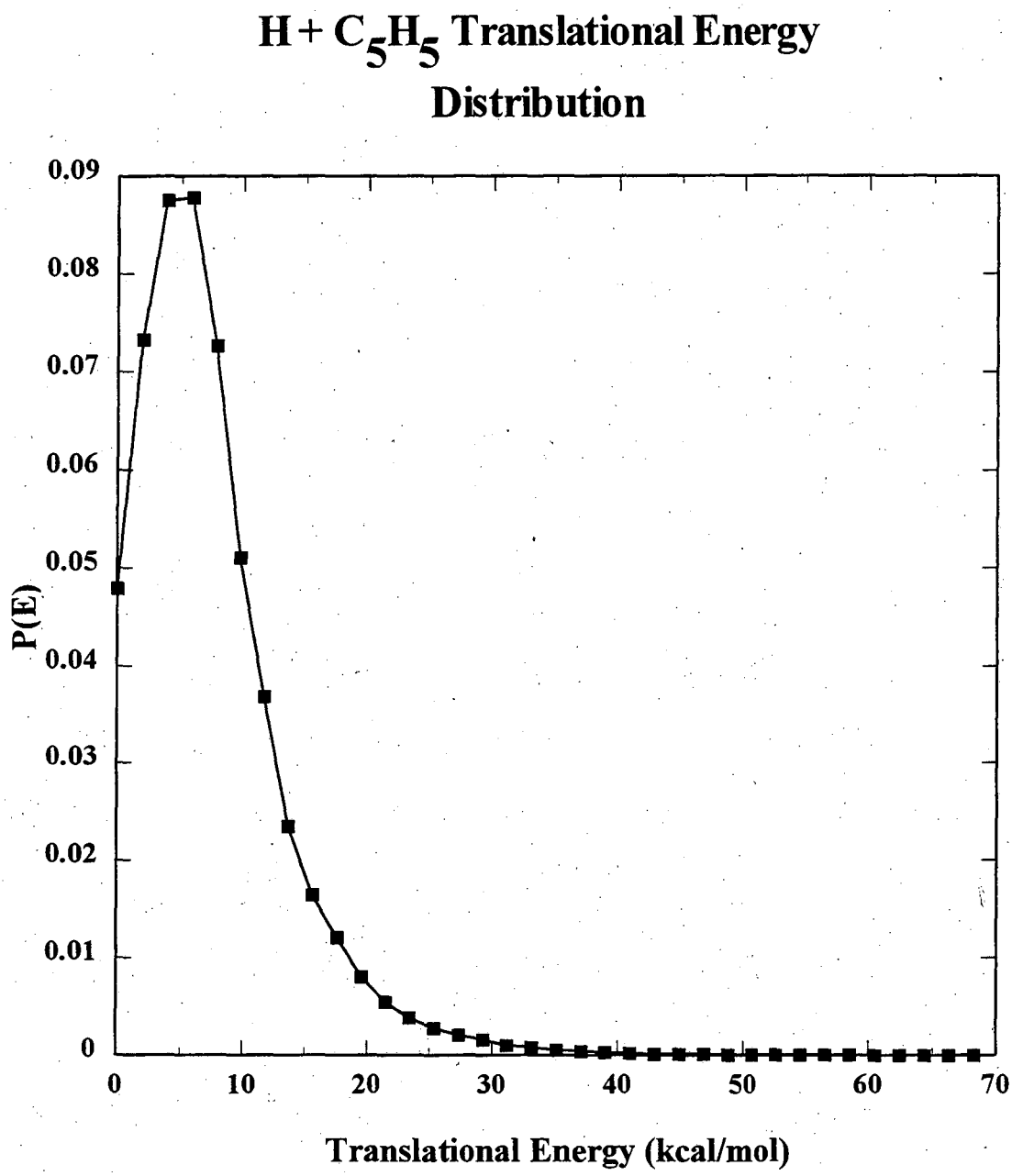
H + C5H5 Translational Energy Distribution
0.09
0.08
0.07
0.06
0.05
0.04
0.03
0.02
0.01
0
P(E)
0
10
20
30
40
50
60
70
Translational Energy (kcal/mol)

Figure 6.

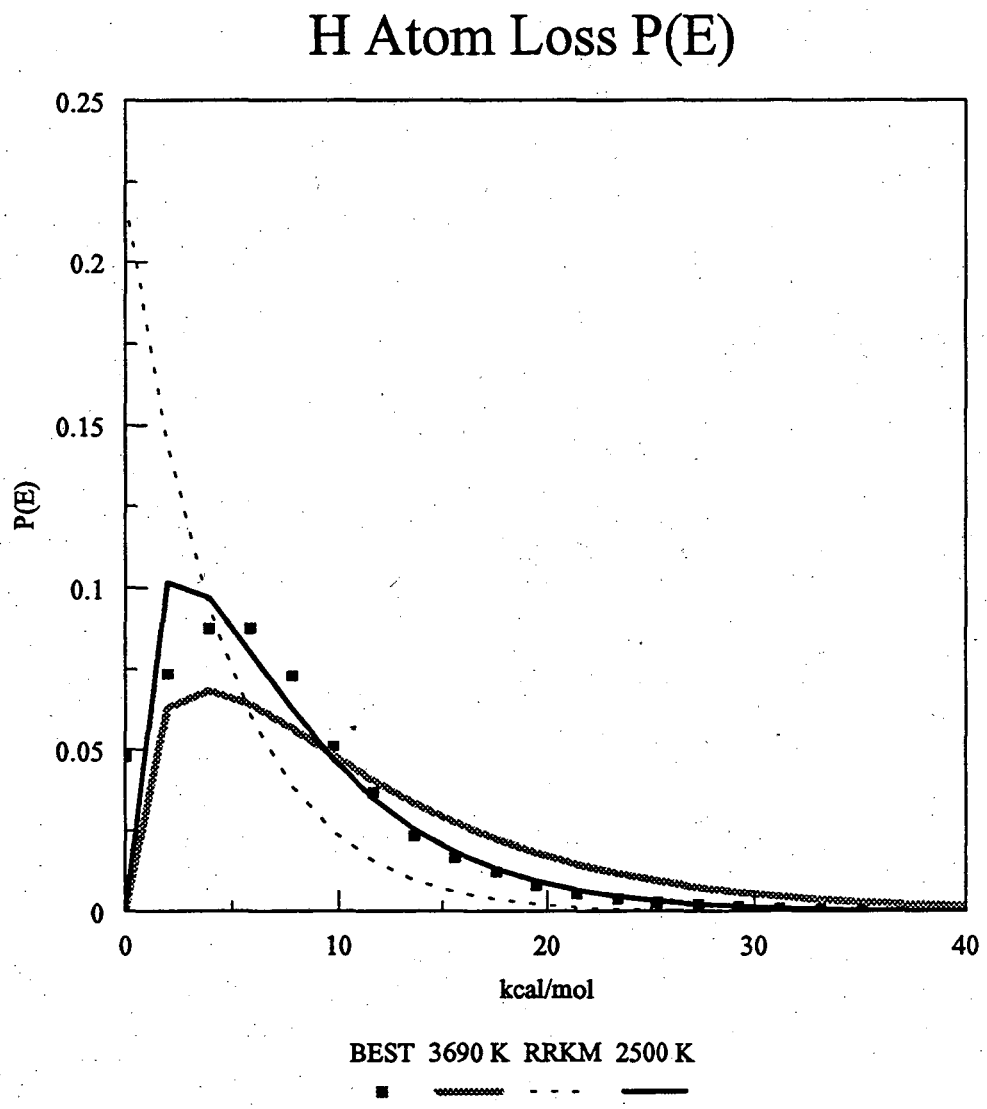
H Atom Loss P(E)
0.25
0.2
0.15
0.1
0.05
0
P(E)
0
10
20
30
40
kcal/mol
BEST 3690 K RRKM 2500 K

Figure 7.

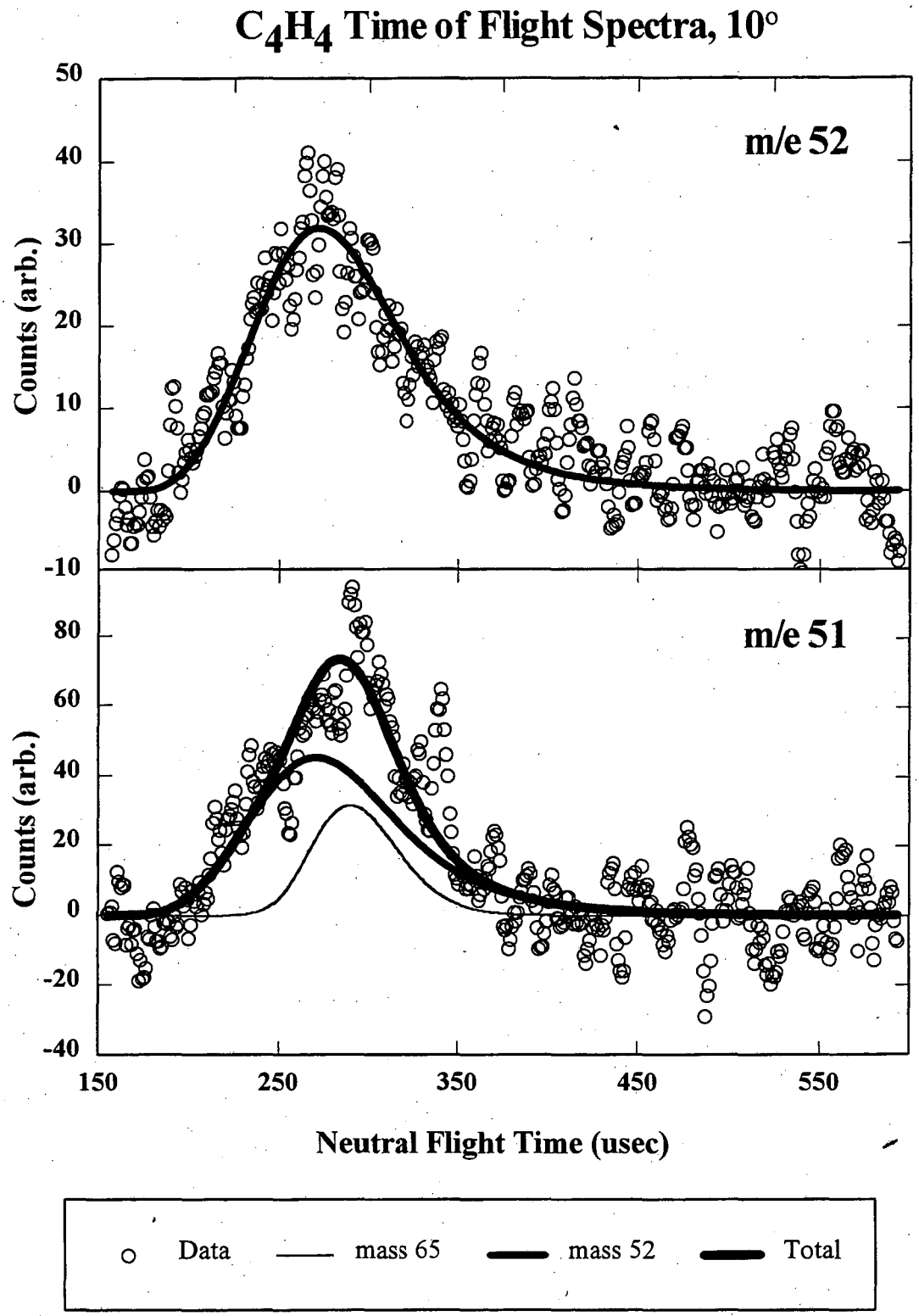
C4H4 Time of Flight Spectra, 10°
m/e 52
m/e 51
Counts (arb.)
Counts (arb.)
50
40
30
20
10
0
-10
80
60
40
20
0
-20
-40
150
250
350
450
550
Neutral Flight Time (usec)
Data
mass 65
mass 52
Total

Figure 8.

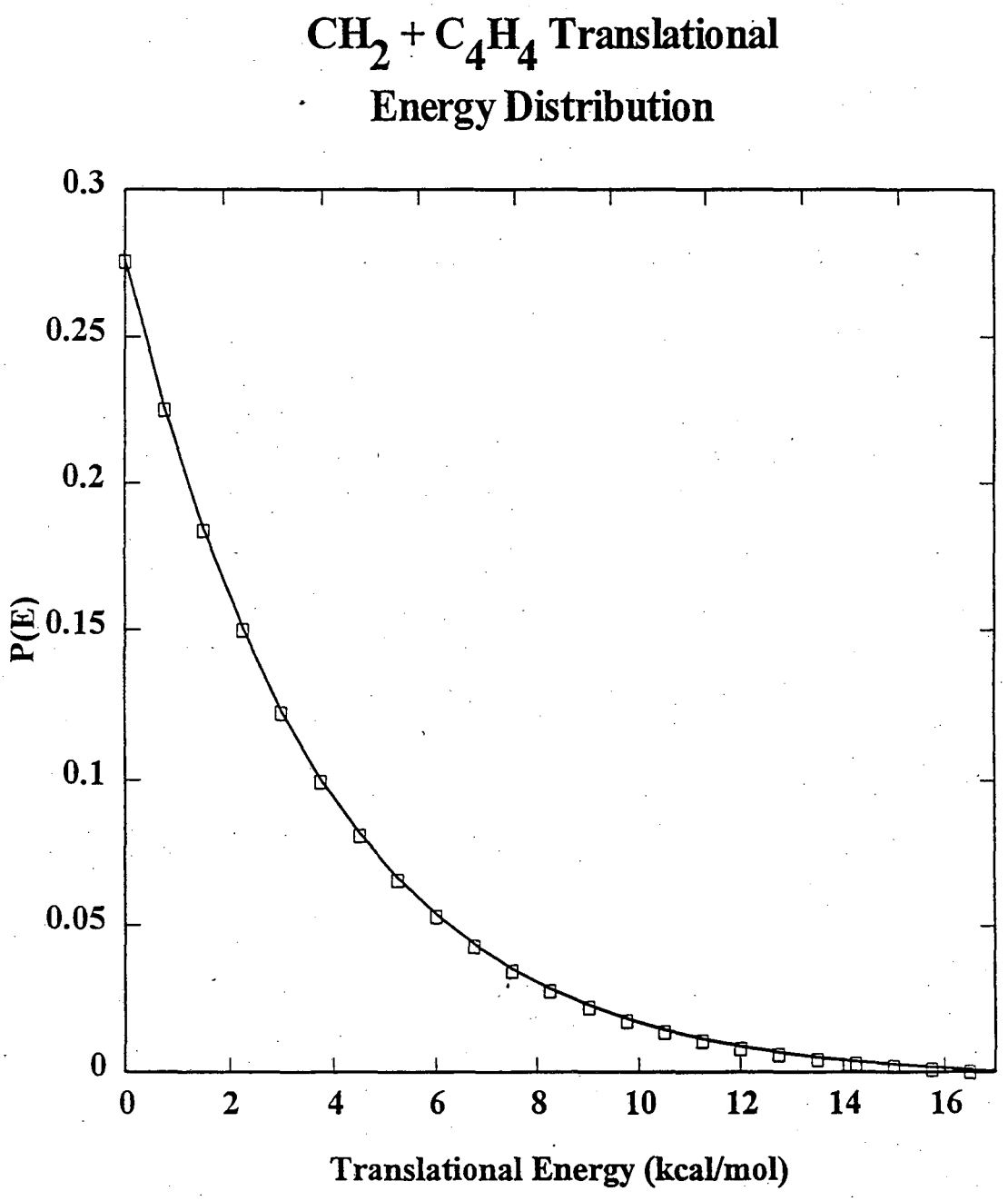
CH2 + C4H4 Translational
Energy Distribution
0.3
0.25
0.2
0.15
0.1
0.05
0
P(E)
0
2
4
6
8
10
12
14
16
Translational Energy (kcal/mol)

Figure 9.

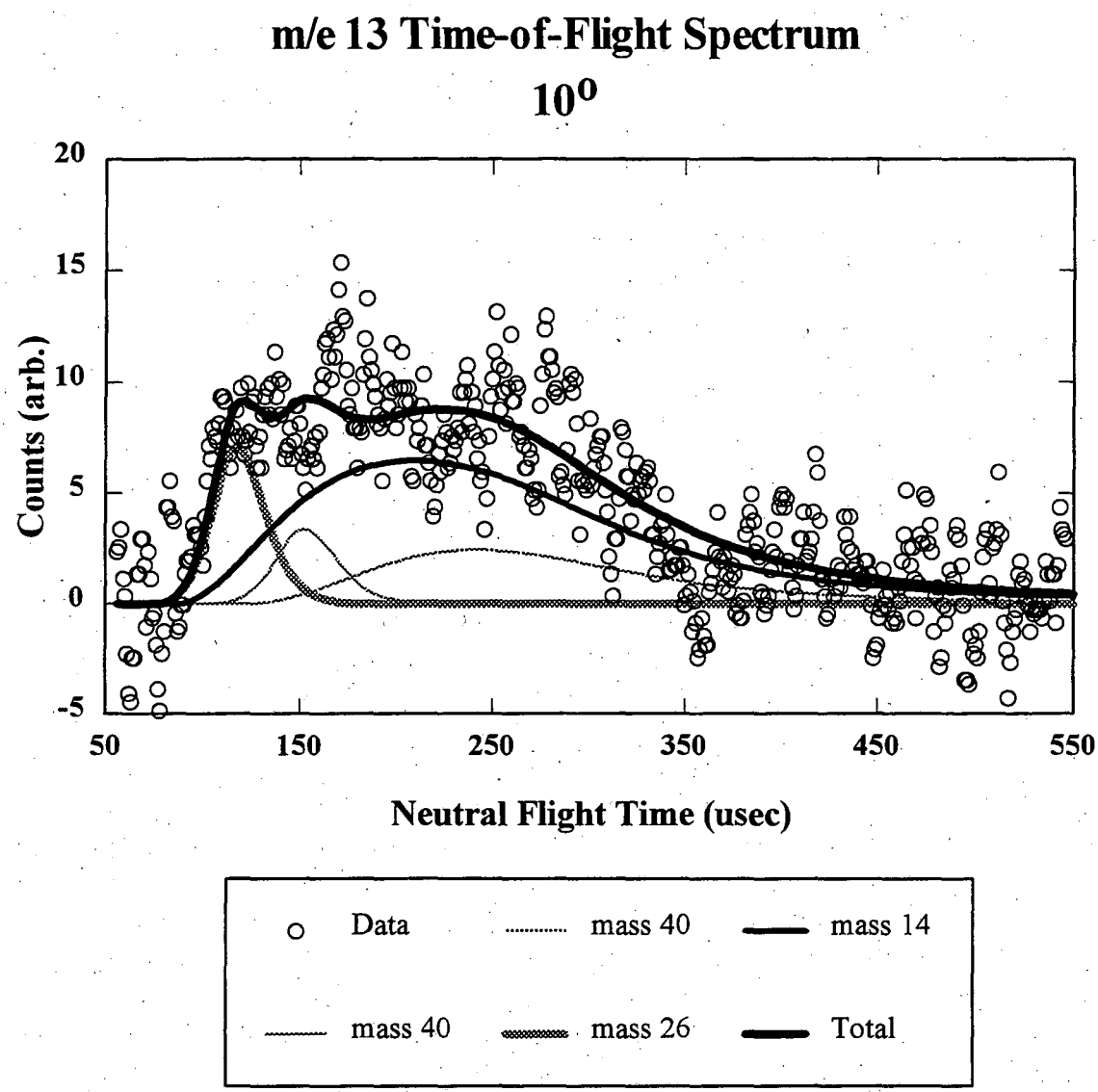
m/e 13 Time-of-Flight Spectrum
10⁰
Counts (arb.)
20
15
10
5
0
-5
50
150
250
350
450
550
Neutral Flight Time (usec)
Data
mass 40
mass 14
mass 40
mass 26
Total

Figure 10.

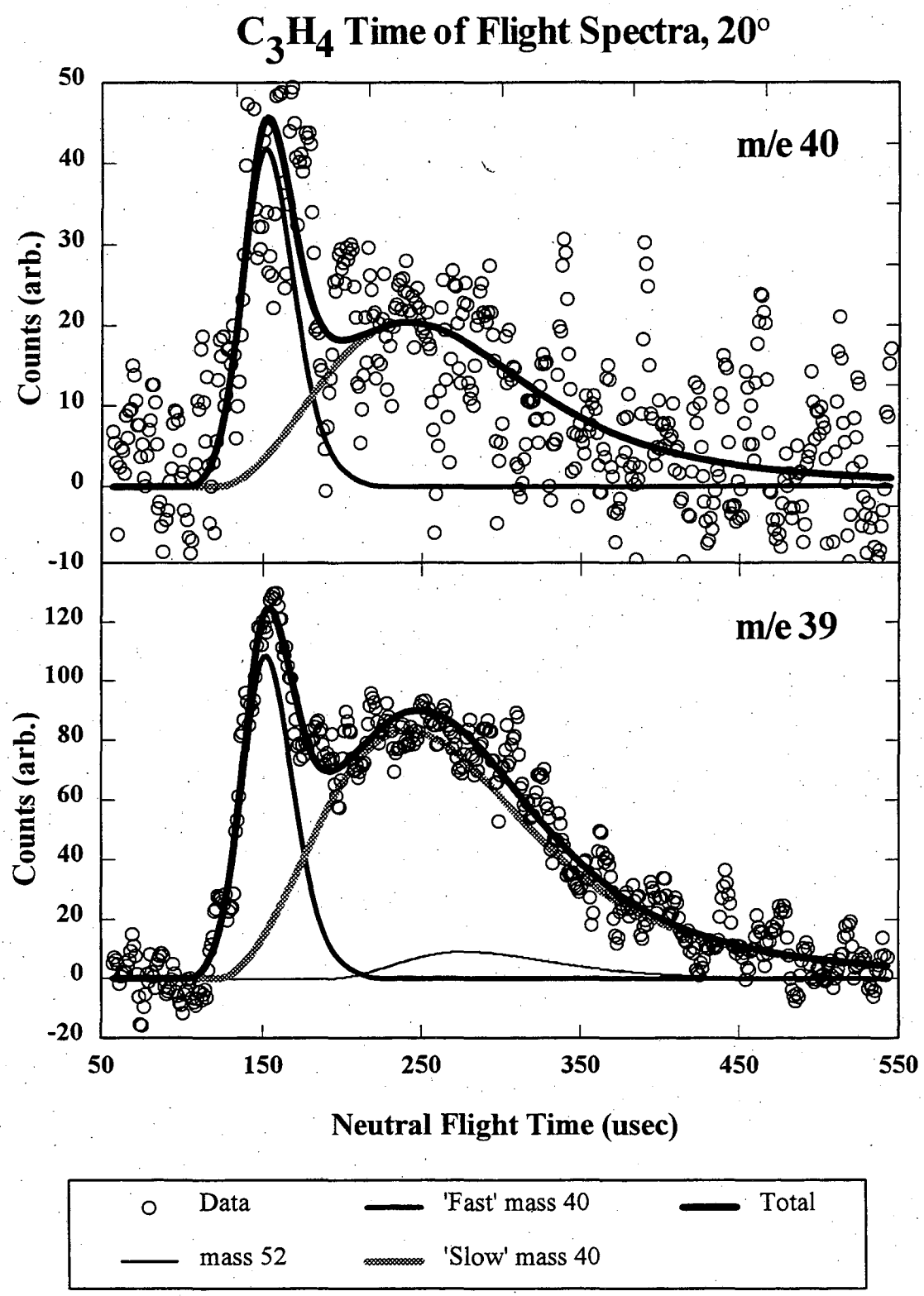
C_3H_4 Time of Flight Spectra, 20°
m/e 40
m/e 39
Counts (arb.)
Counts (arb.)
50
40
30
20
10
0
-10
120
100
80
60
40
20
0
-20
50
150
250
350
450
550
Neutral Flight Time (usec)
Data
'Fast' mass 40
Total
mass 52
'Slow' mass 40

Figure 11.

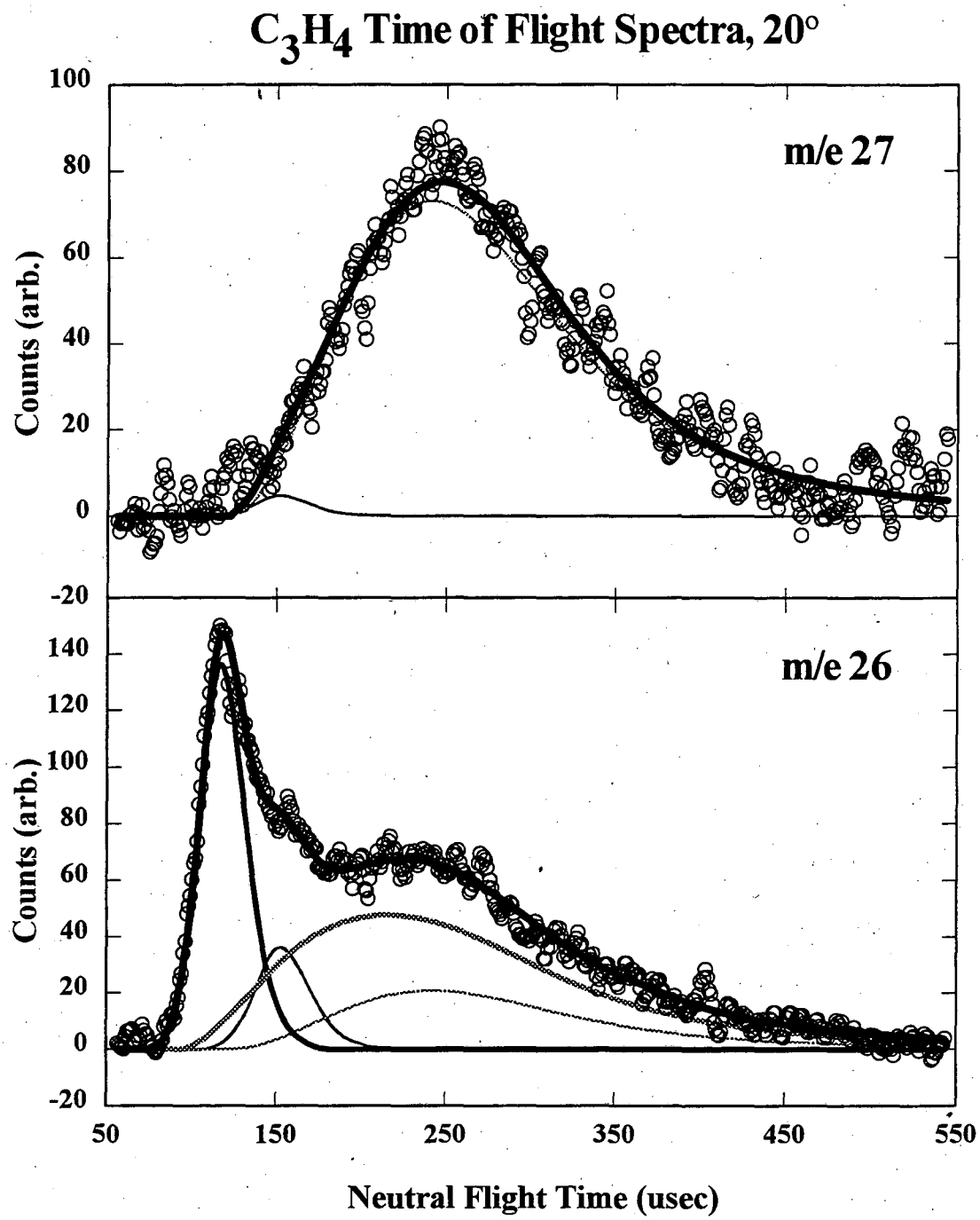

○ Data	'Slow' mass 40	'Slow' acetylene
'Fast' mass 40	'Fast' acetylene	Total

Figure 12.

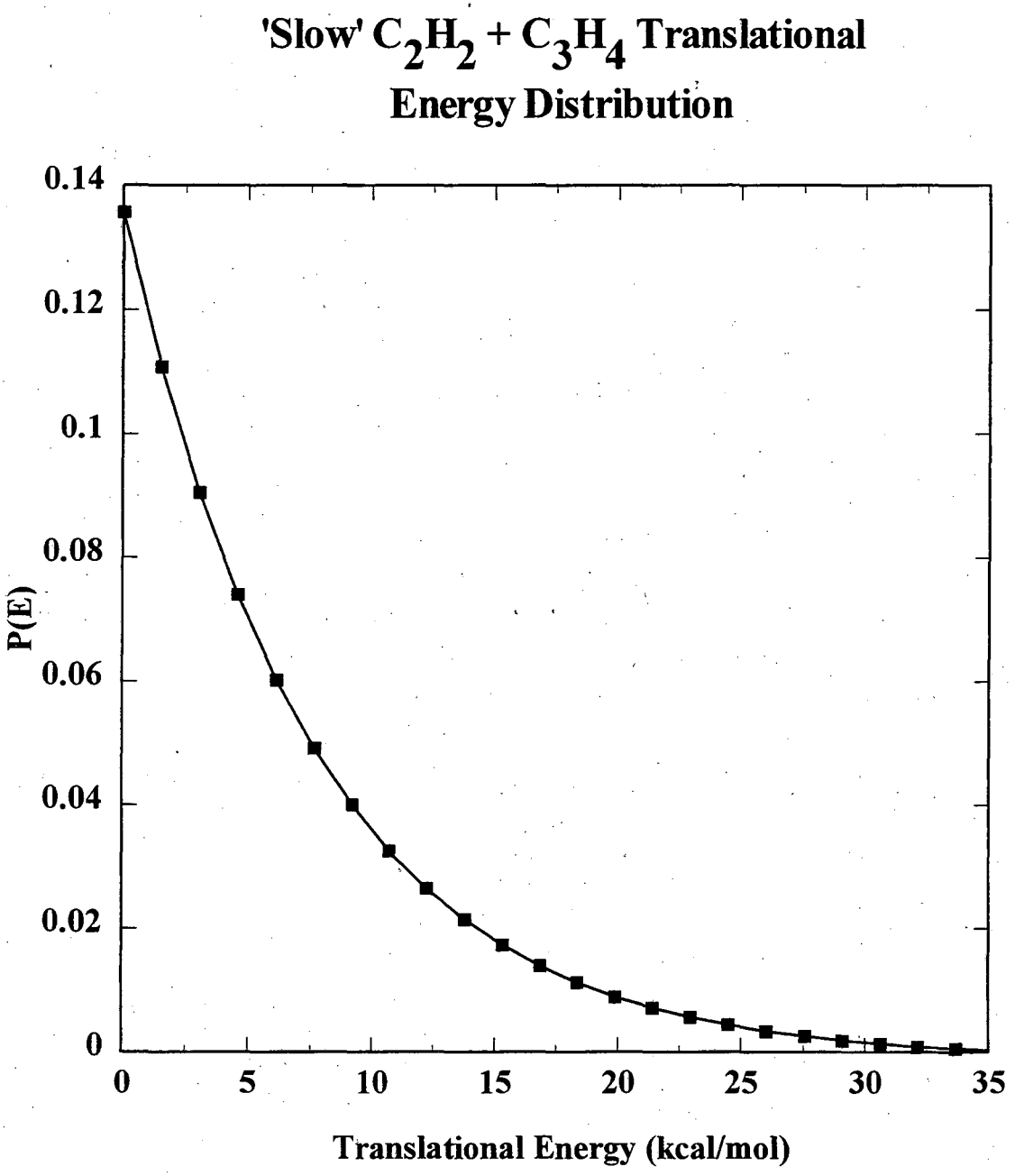
'Slow' $C_2H_2 + C_3H_4$ Translational Energy Distribution
0.14
0.12
0.1
0.08
0.06
0.04
0.02
0
P(E)
0
5
10
15
20
25
30
35
Translational Energy (kcal/mol)

Figure 13.

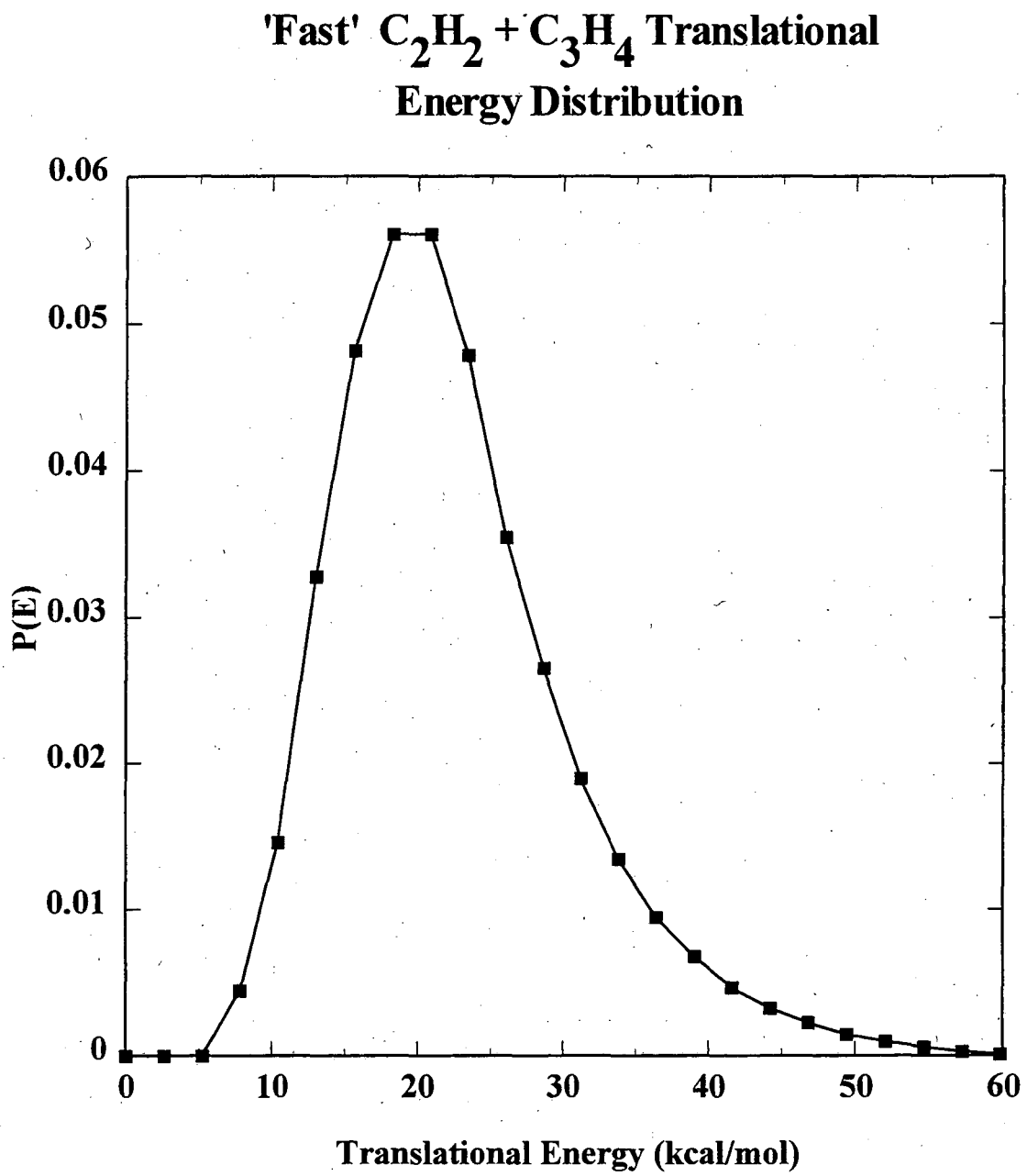
'Fast' $C_2H_2 + C_3H_4$ Translational Energy Distribution
0.06
0.05
0.04
0.03
0.02
0.01
0
P(E)
0
10
20
30
40
50
60
Translational Energy (kcal/mol)

Figure 14.

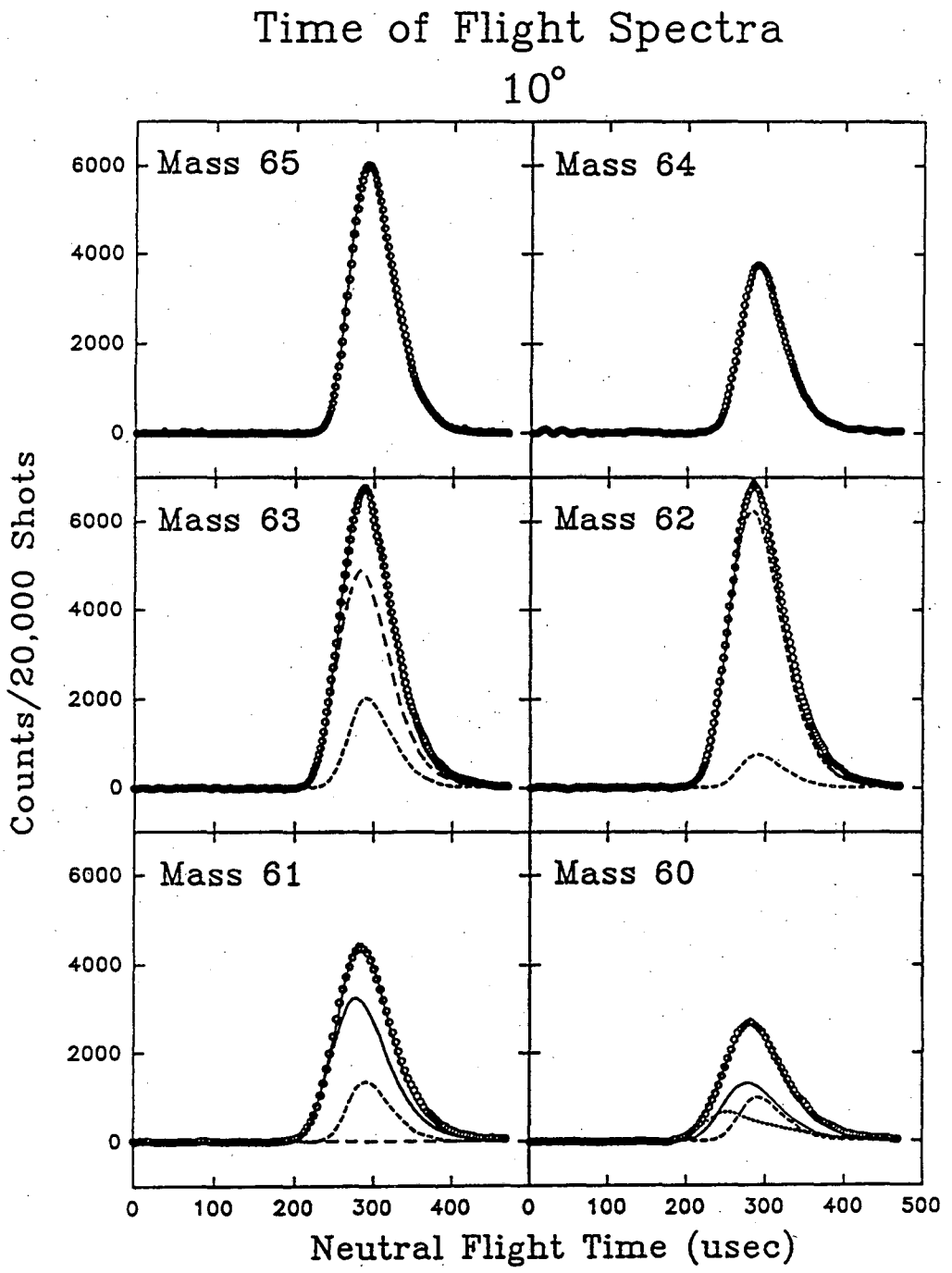
Time of Flight Spectra
10°
Mass 65
Mass 64
Mass 63
Mass 62
Mass 61
Mass 60
6000
4000
2000
0
Counts/20,000 Shots
0
100
200
300
400
500
Neutral Flight Time (usec)

Figure 15.

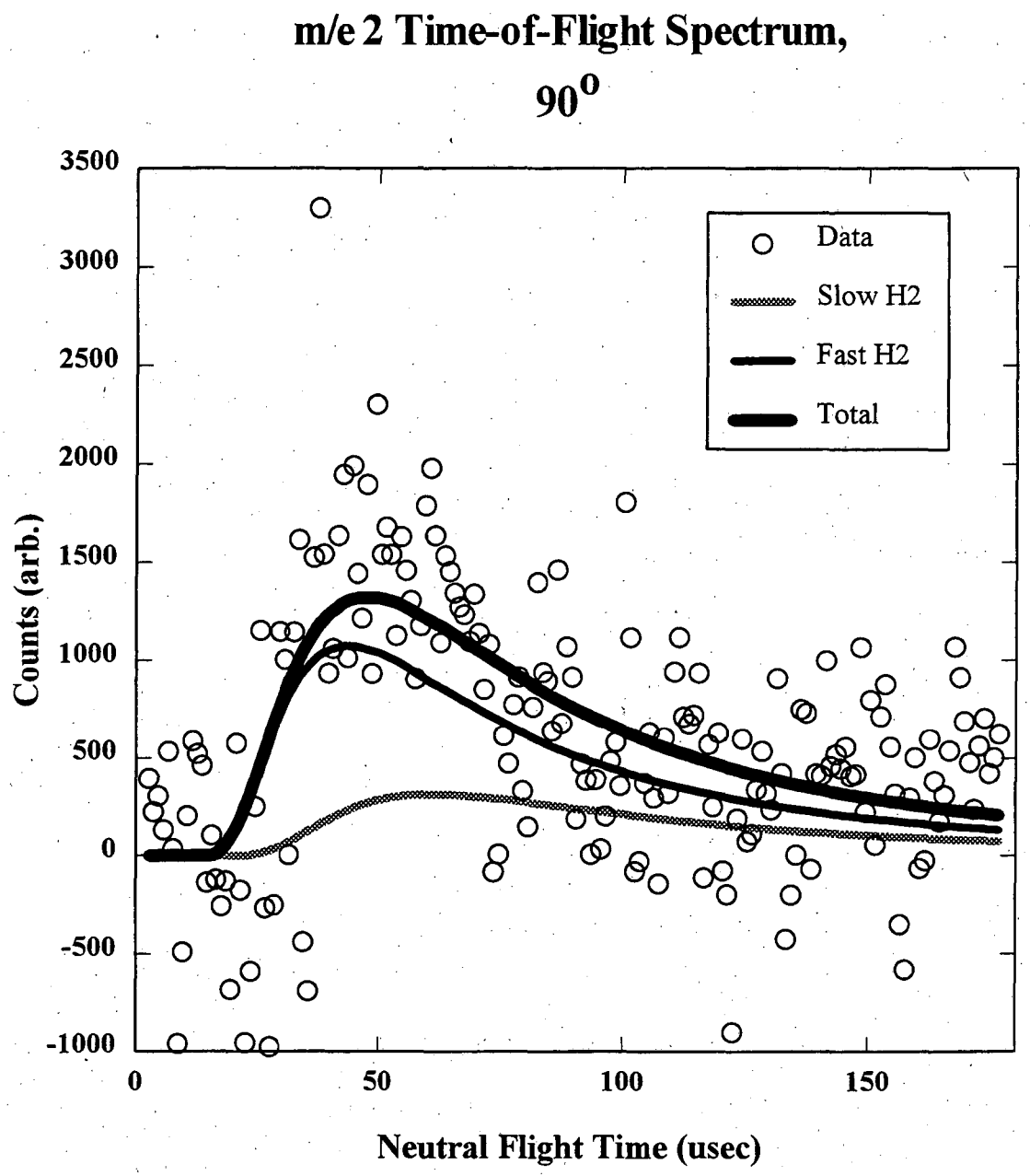
m/e 2 Time-of-Flight Spectrum,
90°
Data
Slow H2
Fast H2
Total
Counts (arb.)
3500
3000
2500
2000
1500
1000
500
0
-500
-1000
0
50
100
150
Neutral Flight Time (usec)

Figure 16.

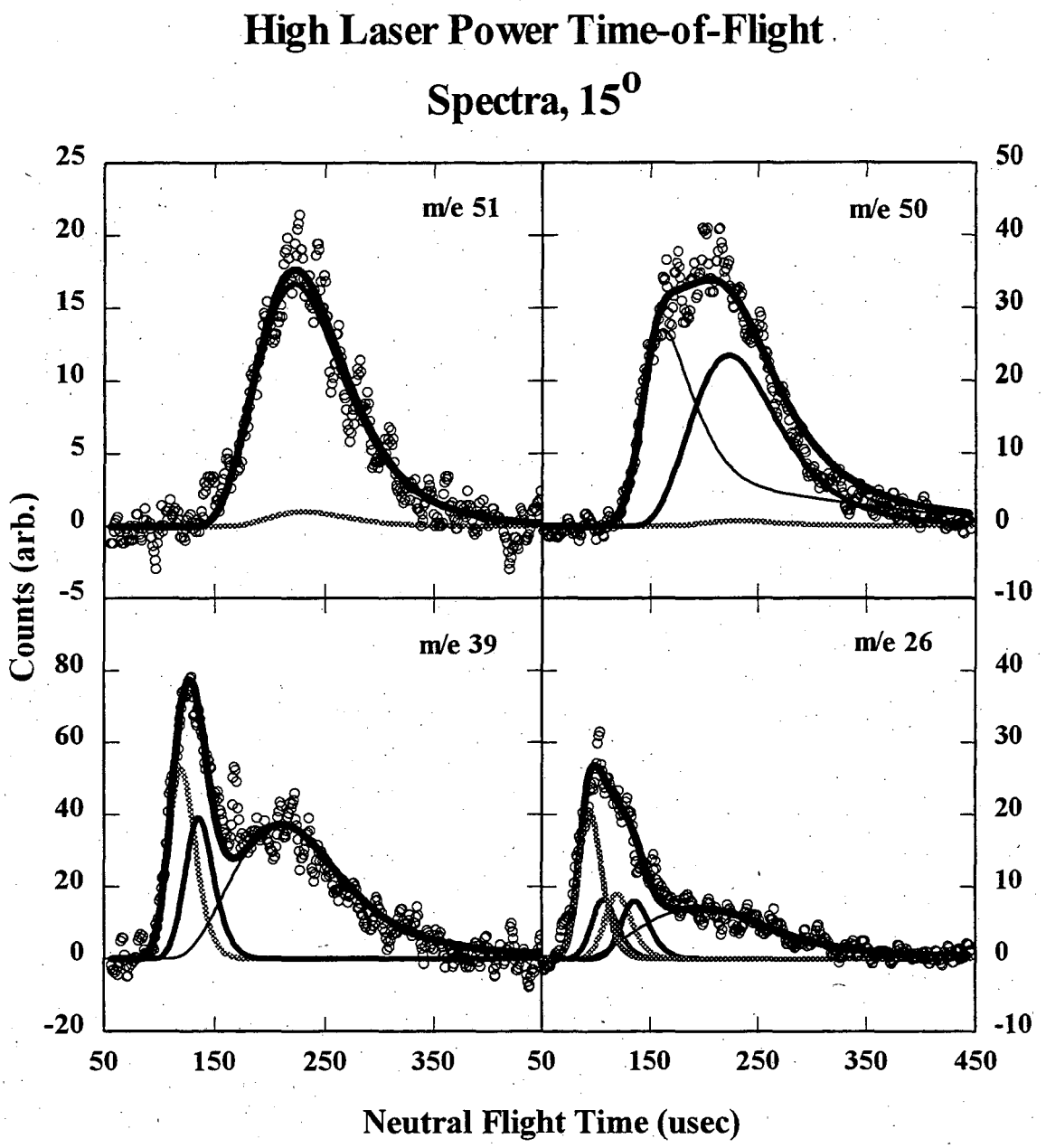
High Laser Power Time-of-Flight
Spectra, 15^0
m/e 51
m/e 50
m/e 39
m/e 26
Counts (arb.)
Neutral Flight Time (usec)
25
20
15
10
5
0
-5
50
40
30
20
10
0
-10
80
60
40
20
0
-20
50
150
250
350
450

Figure 17.

Energy Level Diagram

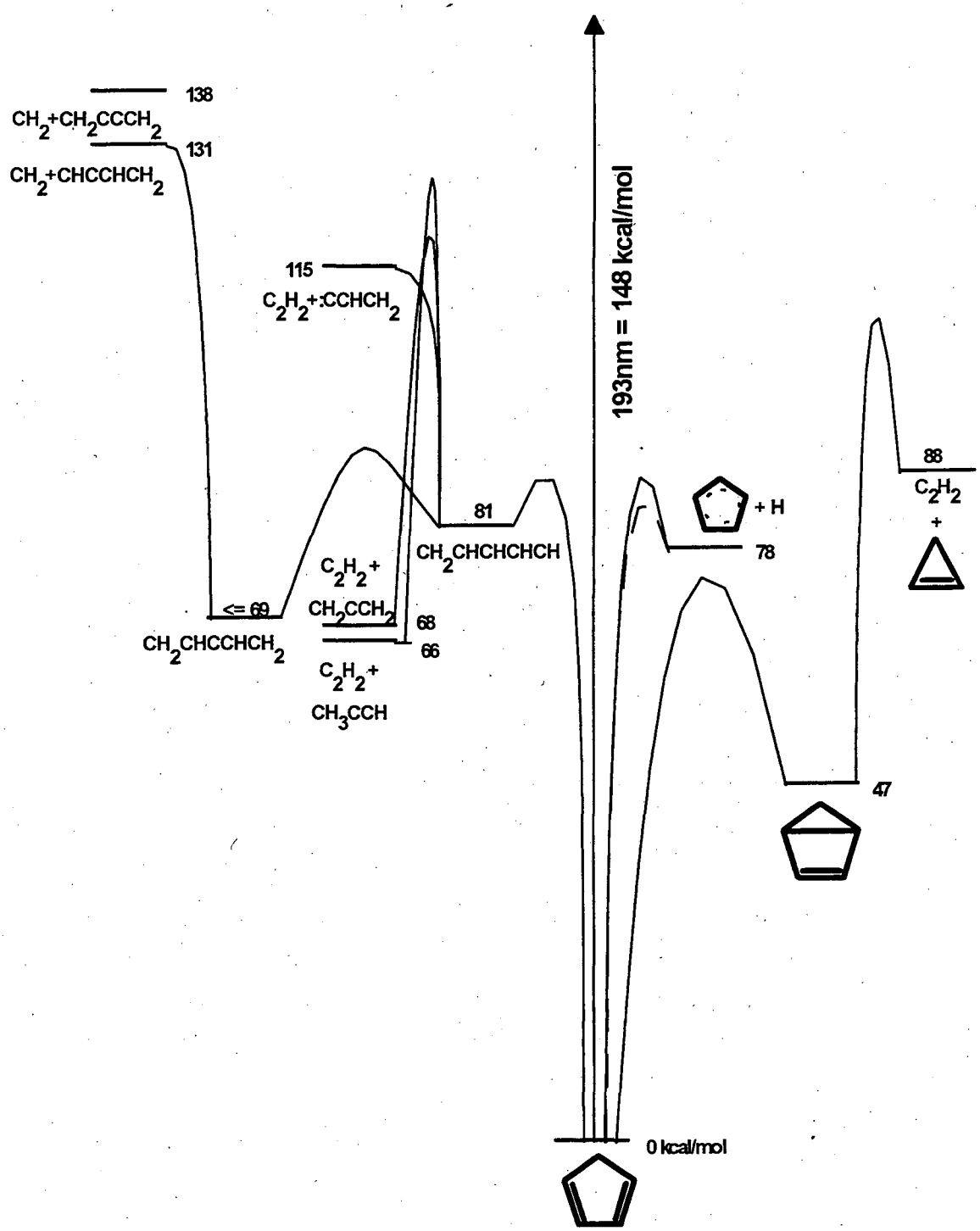

Figure 18.

Chapter III: 193 nm Photodissociation of Thiophene

Introduction:

Thiophene is a heterocyclic analog of cyclopentadiene, with a sulfur atom replacing the CH_2 group. Thiophene is a carrier of sulfur in fossil fuels and much research has been done exploring the chemistry of sulfur atom addition to C-C double and triple bonds that can lead to the formation of thiophene and substituted thiophenes[1]. Our study was additionally motivated by the possibility for comparison of thiophene dissociation with that of cyclopentadiene.

One might expect thiophene's chemistry to mirror that of cyclopentadiene except for phenomena based on the weak C-H bond of the methylene group, which would suggest that all of the minor dissociation channels of cyclopentadienewill be major dissociation pathways in thiophene. There is some evidence to support this view. The lowest electronic transitions for these molecules are very similar and are postulated to involve the π-π^* transition of the conjugated diene system[2]. The similarity of the spectra has been alternatively interpreted as proof that the sulfur atom does not significantly perturb the electronic structure of the diene system, and as proof that, since the sulfur electrons should be involved in homocyclic conjugation, that the

methylene group of cyclopentadiene also produces this effect via hyperconjugation. It seems likely that the 193 nm absorption in thiophene would also be similar to that of cyclopentadiene, involving the 3p-Rydberg <-- X transitions of the diene system[3]. Thiophene is also similar to cyclopentadiene in that it is suspected to have a bound bicyclic valence isomer, although this isomer has only been isolated in substituted thiophenes [4].

Thiophene and cyclopentadiene also undergo many similar photoisomerizations in solution. However there are differences[5,6]. While much of the photoisomerization chemistry of cyclopentadiene can be understood in terms of 1,3 sigmatropic walk rearrangements of the CH_2 group in the bicyclo[2.1.0]pent-2-ene isomer, and 1,5 substituent shifts[7], the chemistry of thiophene cannot. In addition to the rearrangements just mentioned, thiophene can undergo swapping of the carbons at the 2 and 3 positions. Several proposals have been made to explain these isomerizations including ring contraction to cyclopropene intermediates in equilibrium with the bicyclo isomer, tri-cyclic zwitterions involving the sulfur d orbitals, and multiple intermediates that have two of the five ring atoms twisted 90° out of the plane of the remaining three atoms[8]. All of this suggests that thiophene can explore an even wider range of geometries during photodissociation than cyclopentadiene.

Several gas phase photodissociation studies have been done on thiophene. Two studies involving flash photolysis of thiophene report observation of SH and C_4H_3 radicals[9,10]. The authors suggests that these are primary photoproducts, though the shortest time delay used was 5 μsec (.25 torr thiophene in 100 torr of argon). Other

studies have identified stable species from irradiation of thiophene and substituted thiophenes in the presence of various other gases and inferred the primary kinetic photodissociation products[11,12]. These studies were done at slightly lower excitation energies than the present study (213.9 nm, 228.8 nm, and 253.7 nm, the last via mercury sensitization, vs. 193 nm). Primary channels yielding acetylene and thiirene (the C_2H_2S episulfide), ring opening to the diradical (which is then consumed in bimolecular events), and CS and methyl acetylene, as well as an intermediate postulated to be the bicyclo isomer were proposed. The last species was assumed to yield allene and CS. The authors precluded the possibility of sulfur atom production based on a lack of the expected episulfides (thiiranes) and thiols upon addition of olefins to the gas mixture.

Another study, which analyzed the infrared multi-photon dissociation of thiophene should also be mentioned[13]. The thermodynamics cited in this work are at odds with accepted values, but should not affect their kinetics scheme. The authors propose that all of the thiophene undergoes ring opening to the diradical followed by fragmentation in one of three ways; acetylene and thioformylmethylene (CHCHS) diradical, SH and C_4H_3, and CS and formylmethylene ($CHCHCH_2$) diradical. These species then react bimolecularly to yield the products actually oberved.

The present study, observing the 193 nm photodissociation of isolated thiophene molecules via Photofragment Translational Spectroscopy, is the first to directly observe the photoproducts.

Experimental:

This study was done in essentially the same manner as the cyclopentadiene study in Chapter II. All data was taken using the molecular beam Photofragment Translational Spectroscopy (PTS) technique on the Rotating Source Machine described in that chapter.

Thiophene was obtained from Aldrich Chemical Co. Helium at a pressure of 320 torr was bubbled through the thiophene at a temperature of 0 C to yield a mixture of ~5% thiophene in helium. This mixture was metered through a needle valve to a pressure of ~90 torr and then expanded through a .3 mm nozzle into the chamber. The nozzle was heated to 65 C to eliminate significant dimer formation The molecular beam was collimated by two 1 mm diameter skimmers. Pressure in the source region was $3x10^{-4}$ torr. The beam/laser interaction region was maintained at 10^{-7} torr.

The major experimental problem in dealing with thiophene was its effect on mechanical pump oil. After running a molecular beam into the vacuum chamber for a 12 hour day, the mechanical pump on the source chamber would only pump down to 400 mtorr (vs. <100 mtorr normally). This occurred even with a nitrogen flow into the pump ballast, and the ultimate pressure did not improve with time. Changing the pump oil daily solved the problem, but also brought complaints from the people working on other experiments within ~50 yards due to the obnoxious odor. Similarly, wearing gloves during the procedure greatly improved one's social interactions during

the rest of the day.

The beam was characterized in the same manner as for cyclopentadiene. Time-of-flight spectra were recorded with the detector looking directly into the beam (0 degrees) for the 15 most prominent mass to charge ratios. The data were then used to yield the beam velocity and width as well as the ion flight constant.

Lambda Physic EMG 103 MSC and EMG 202 MSC excimer lasers, lasing at 193.3 nm were used as the photolysis source. The spot size at the interaction region was measured to be 1x4 mm. Pulse energy varied from 1.5 to .15 mJ at the interaction region. The majority of data was taken at laser fluences of 50 mJ/cm^2 and 20 mJ/cm^2. The experiments were run at 100 Hz. This experiment show much more laser induced noise in the time-of-flight spectra than did the cyclopentadiene experiment, a fact which I originally attributed to lower overall signals in the present case. However, failure of the excimer laser soon after completion of this experiment suggests that it may have been producing more RF noise than normal during the data acquisition.

Analysis and Results:

The analysis of this experiment proceeds as for cyclopentadiene. Time-of-flight mass spectra were recorded at mass to charge ratios from 84 to 12 at laboratory angles of 10° and 20°, with some spectra at 30° and 50°. A thorough power dependence study was done at m/e 51, a mass to charge ratio that shows reasonably

clean signals from two channels. The shape of the time-of-flight spectrum did not change with increased laser power, while the total signal counts varied as shown in Figure 1. Below 20 mJ/cm^2, there does not appear to be any deviation from linear behavior. Above that, multi-photon dissociation begins depleting the signal. The curvature is unlikely to be due to saturation, since the total ionization cross-section normalized ion signal for thiophene at 20 mJ/cm^2 is still at least 10 times less than that of cyclopentadiene at 3 mJ/cm^2. (The fluences are near the highest limit of the linear power region for the respective molecules, and the other conditions are approximately equal.) This implies that either thiophene has a large radiative decay channel that lowers the dissociation quantum yield, or that the curvature is due to multi-photon events that lower the ion signal at mass 51. There is certainly evidence for the latter process occurring in higher power time-of-flight spectra at lower m/e ratios. Lastly, it should be noted that the 193 nm region of the cyclopentadiene spectrum is highly structured and that a large difference in cross section between cyclopentadiene and thiophene at 193 nm would not be inconsistent with a similar assignment for the excited state in both molecules [14].

To avoid multi-photon signals in the time-of-flight spectra, the laser fluence was kept near 20 mJ/cm^2. The power dependence of signals detected in these spectra were checked by repeating the experiment at ~50 mJ/cm^2. The lower power results were sometimes quite noisy due to the lower overall signal level in this experiment relative to cyclopentadiene. At m/e ratios where there was no new signal in evidence at the higher fluence, the higher fluence spectra were used to improve the precision of

the derived translational energy distributions (P(E)s). The P(E)s were then checked to see that they fit the low fluence results within the noise.

There is one final complication in the analysis of the thiophene data which results from the natural isotope abundance ratio of sulfur. Sulfur exists naturally in the ratio 95% : .75% : 4.25% for mass 32 : 33 : 34 respectively. The carbon ratio of 98.9% : 1.1% for mass 12 : 13 should also be considered. Because of this, a product such as C_2H_2S should appear not only at mass 58, but also at 59 and 60 with intensities of roughly .95 : .0295 : .0425, respectively. Thus, a signal at m/e 60 with less signal at m/e 59 does not indicate a $C_2H_4S + C_2$ channel. This issue must also be faced, along with the confounding issue of dissociative ionization, when trying to determine the existence of S and SH products from the m/e 35-32 spectra. This will be discussed in detail later in the section.

As for cyclopentadiene, the dissociation channels will be discussed in order of increasingly equal mass partitioning between the fragments. The branching ratio between the channels is presented at the end of the section.

HYDROGEN (H_2) ELIMINATION/ DIMER DISSOCIATION:

The highest mass to charge ratio with visible signal is 82. The signal to noise for this m/e ratio is very poor, due to both a fairly large background count rate and a very small signal. The same time-of-flight profile appears in isolation at m/e 81, 80, and 70-68 with up to ten times the count rate of m/e 82. No evidence of signal at the

level of that at m/e 82 was seen at m/e 83, though it should be noted that the background at m/e 83 is ten times higher than at m/e 82. No signal was seen at mass 84 either. This ion would be expected from a dimer dissociaton. No attempt was made to detect an H_2 product directly as was done in the cyclopentadiene experiment due to the much lower signal in this case. I will interpret the spectrum here as an H_2 loss yielding C_4H_2S with a few notes about a dimer interpretation and then reconsider the possibilities in the discussion section.

The time-of-flight spectra, along with calculated fits assuming H_2 loss, are shown in Figure 2. for m/e 82 at 13°, as well as for m/e 68 at 10° and 20°. The derived $P(E_T)$, again assuming H_2 loss, is shown in Figure 3. This $P(E_T)$ is a pseudoexponential extending to ~84 kcal/mol, with an average translational energy release of 10.5 kcal/mol. The high energy tail is required to fit the spectra at 20°. This tail shows linear power dependence, with even faster products appearing at higher energy. Similarly, a spectrum at 6°, which is sensitive down to ~ 7 kcal/mol, shows no evidence of a barrier.

This channel is a very minor one. If it were from dimers, it would represent only a 1-2% dimer population in the beam (assuming no change in cross section or nondissociative decay rate for the monomer thiophene units). A $P(E_T)$ with only a few (< 5) kcal/mol would fit even the 'fast' mass 82 signal since the conjugate fragment would be another thiophene molecule.

ACETYLENE ELIMINATION:

A new channel appears at m/e 58 as shown in Figure 4. Also shown is the m/e 26 spectrum at 50° which shows a component momentum matched to the m/e 58 signal. No such signal is apparent at m/e 27. There is some signal buried in the noise at m/e 59 and m/e 60 that is sufficient to account for the expected isotopic components of a nominal mass 58 fragment. This channel is then assigned as dissociation to mass 58 and mass 26 ($C_2H_2S + C_2H_2$).

The only inconsistency in this assignment is the relative abundance of the two fragments: the mass 58 fragment appears to be less than half as abundant as its mass 26 counterpart. Some of this inequity may be due to incorrect estimates for the ionization cross section of the products, a factor that will be discussed more in the section on branching ratios. However, it seems that some other factor is required to explain the full magnitude of the discrepancy. One possibility is that the mass 58 fragment is being destroyed by secondary dissociation. Since the mass 26 and mass 58 peaks are easily fit by the same $P(E_T)$, it does not seem likely that a spontaneous secondary process that preferentially depletes internally hot mass 58 can explain the observations. Increasing the laser power from 20 to 70 mJ/cm^2 only increases the mass 58 signal by 66%, vs the 140% increase seen at m/e 51, suggesting that a stimulated secondary process is depleting the mass 58 signal. No attempt was made to analyze this multiphoton process due to the congestion at lower mass to charge ratios from the other primary channels. It is likely that the secondary fragments from this

channel have been misassigned to other primary channels. This does not affect the derived $P(E_T)$s for the other channels, since all of them can be determined at masses where the mass 58 secondary products cannot appear. However, it will affect the estimated branching ratios to some extent. This will be discussed more in the appropriate section.

As can be easily seen from the time-of-flight spectra, the $P(E_T)$ for this channel peaks away from zero. It is shown in Figure 5. The $P(E_T)$ extends to ~ 41 kcal/mol with a peak at 18.7 kcal/mol. The average is also near 18.7 kcal/mol. This $P(E_T)$ is reminiscent of that from the acetylene loss channel in cyclopentadiene. Aside from the difference in maximum translational energy, the two differ in that thiophene's acetylene loss $P(E_T)$ is more symmetric about the peak (vs. higher probability on the high energy side for the cyclopentadiene channel). I wish only to note here that the signal on the low energy side of the peak is real and is required, down to at least 5 kcal/mol, to fit the observed signal. (Below this, the H_2 loss channel can provide signal.)

SULFUR ATOM ELIMINATION:

Any signal that appears at m/e 52 cannot be accounted for by either of the other channels without invoking nuclear fission during dissociative ionization. Thus, the m/e 52 signal shown in Figure 6 must imply a new channel. Assignment of the m/e 52 signal to a new channel is also supported by fact that the recoil velocity

distributions of the fragment detected at m/e 52 and m/e 58 are distinctly different. This signal only appears in isolation at m/e 52. A conjugate fragment at mass 32 would be consistent with the signal at m/e 32 as shown in the lower half of Figure 6. The derived $P(E_T)$ for this channel is shown in Figure 7. It extends to 15.6 kcal/mol with a peak away from zero at about 2.6 kcal/mol. The average translational energy is 4.66 kcal/mol. Because of the fairly even mass distribution and the lack of interfering channels, the $P(E_T)$ is well determined to less than 0.65 kcal/mol (1 point in the $P(E_T)$ as shown).

SH ELIMINATION:

At first glance, the time-of-flight spectrum at m/e 51, shown in Figure 8 does not appear different from the m/e 52 spectrum. Closer inspection reveals that the rising edge is definitely slower. The upper graph of Figure 8 shows the spectrum fit only with the mass 52 + 32 channel. The lower graph shows a fit assuming a new channel. The exact shape of the new channel is very uncertain. Some additional information about the shape comes from a fit at m/e 33 where the conjugate fragment, SH, should appear. This is shown in Figure 9. At m/e 33, it is possible to have additional contributions from the mass 58 + 26, and 32 + 52 channels, and two other channels described below.

This channel is in some sense the exact opposite of the mass 52 channel in that there is absolutely no mass to charge ratio where it exists by itself. The shape of the

$P(E_T)$ is therefore difficult to ascertain. It must obviously have a lower maximum translational energy than the mass 52 channel in order to fit the slower rising edge of the m/e 51 spectrum. The low energy part of the distribution is also difficult to derive. Assuming that the H_2 channel is not a dimer channel would limit the contribution from dissociative ionization of the nominal mass 82 fragment to m/e 51 to roughly 4% of what appears at m/e 50 since mass 51 can then only be $^{13}C\ ^{12}C_3H_2$. Based on the relatively small contribution of the mass 82 fragment at m/e 50, it follows from this assumption that the m/e 51 spectrum only contains signal from the mass 52 and mass 51 products. Within noise limits, the contribution of the mass 52 product at m/e 51 can be fixed by fitting the fast edge of the time-of-flight spectrum. The mass 51 $P(E_T)$ must then account for all remaining signal. This procedure suggests that is peaked very near zero and extends past 8 kcal/mol. If there is off-beam-axis mass 84 signal from dimer dissociation, it may contribute to the m/e 51 spectrum, which would allow a small (1-2 kcal/mol) peak away from zero in the mass 51 channel. I have chosen a pseudoexponential $P(E_T)$, with a maximum energy of 12 kcal/mol and an average of 2.5 kcal/mol as a reasonable guess. This guess is consistent with the m/e 51-48 spectra, as well as being consistent with the less demanding constraint of the conjugate fragment's contribution fitting within the m/e 35-32 spectra. An encouraging sign is that the yields assigned to the mass 51 and mass 33 products by fitting all of the time-of-flight spectra with the channels and $P(E_T)$s discussed here are roughly equal (more precisely, they are in the same ratio as for the conjugate fragments of the other channels - see the branching ratio section for

a discussion).

C_3H_3 ELIMINATION:

Yet another channel appears at m/e 45 (HCS) and at m/e 47 in small amounts. Only sulfur containing fragments can yield ions in the m/e 47-44 range. Thus, contributions from the mass 82 and mass 58 fragments above could appear, but contributions from mass 52 and mass 51 fragments cannot. The latter point is particularly important since the time-of-flight spectrum at m/e 45 is very similar to the time-of-flight contribution of the mass 51 channel. The time-of-flight spectrum for m/e 45 is shown in Figure 10. The derived $P(E_T)$, a pseudoexponential, is shown in Figure 11. It has an $\langle E_T \rangle$ = 2.65 kcal/mol, with a maximum energy set at ~25 kcal/mol. The latter value is fairly uncertain due to the overlapping mass 58 contribution at the fastest part of the spectrum. I estimate that the maximum could be as low as ~13 kcal/mol without affecting the fit, as long as the curvature of the rest of the $P(E_T)$ remained the same.

C_3H_4 ELIMINATION:

The absolutely last channel required to fit the data is seen most prominently at m/e 39 as a fast shoulder on the mass 39 contribution from the channel above. This spectrum is shown in Figure 12. The only other channel to have a translational energy

distribution with a large peak away from zero that would fit the m/e 39 spectrum is that of mass 58. However, mass 58, C_2H_2S, cannot crack to m/e 39. Thus a new channel is required in the proposed schema.

The argument for assignment of this channel to a mass 44-40 split is a little more complex. Figure 13 shows spectra from m/e 44 and m/e 40. The m/e 44 spectrum shows a fast peak that will momentum match with the fast signal from m/e 39. The m/e 45 spectrum (Figure 10.) does not show such a feature above what one would expect for isotopes of a nominal mass 44 fragment. However, the mass 58 fragment can appear at m/e 44 (and m/e 45) and is almost fast enough to fit the m/e 44 signal. With a small amount of secondary dissociation ($C_2H_2S \rightarrow CS + CH_2$) the m/e 44 spectrum could probably be fit.

This would not explain the m/e 40 spectrum, which, although noisy, indicates the presence of a fast component. Unfortunately, this mass to charge ratio was not studied as much as now seems appropriate due to my mistaken belief during the data acquisition that this feature could be explained by the mass 58 channel (it can't). The signal at m/e 40 is roughly 15-20% of what appears at m/e 39 in the fast channel. This is larger than any expected isotope effect, and is a larger amount than is observed for the slower nominal mass 39 component. In other words, the fast component is enhanced relative to the slow component in the m/e 40 spectrum when compared to their abundances in the m/e 39 spectrum. An effect from $^{13}C^{12}C_2H_3$ should produce identical spectra at m/e 40 and 39. Such a change in relative ratio can only be explained by postulating that the fast signal is from mass 40 which undergoes efficient

dissociative ionization to m/e 39 in the detector.

Thus the simplest consistent picture is the assignment to mass 44 and mass 40. With this assignment, a $P(E_T)$ was derived. It is shown in Figure 14. It has a maximum translational energy of 30 kcal/mol and a peak at 8.75 kcal/mol. Both of these values are fairly well defined by the m/e 39 data. For energies less than 8 kcal/mol, the $P(E_T)$ is somewhat arbitrary and has been picked to drop smoothly to zero by ~ 2.5 kcal/mol. It is possible that the $P(E_T)$ should drop more slowly at energies less than that of the peak (more like the mass 58 + 26 $P(E_T)$ in Figure 5.) which would lower the $\langle E_T \rangle$ from the 12.34 kcal/mol for the $P(E_T)$ as shown. With the postulated $P(E_T)$, this channel also has a rough balance between mass 44 fragments, observed at m/e 44 and m/e 32, and mass 40 fragments observed at m/e 40-36, 27-24, and 14-12.

BRANCHING RATIO:

The calculation to derive the branching ratio for photodissociation from the time-of-flight data has been described in chapter II. The same procedure is used here with modification described below.

With so many dissociation channels, and with the overlap of their contributions due to dissociative ionization in the detector, incorrect assignment of signal to a product, which would affect the branching ratio, becomes a concern. Table 1 shows the percentage of the total ion yield as a function of mass to charge ratio. It shows

that the three most probable ions were m/e 26,39 and 32, all of which have multiple contributing channels. In fact, most of the signal occurs at mass to charge ratios where multiple channels contribute. The exact partitioning of signal counts to the various channels is uncertain to the extent that the signal from one channel has the same temporal shape as that of another or a combination of others. This does occur, especially at the lower mass to charge ratios such as 32 and 26 where almost all of the channels can contribute.

Since the cracking patterns of the various products, with internal energy distributions appropriate to this experiment, are not known, I've mainly relied on the least squares fitting routine of CMLAB2 to assign signal to the various product channels. I have made exceptions to this general principle to enforce isotopic ratios, i.e. the signal from the nominal mass 32 product is held at m/e 33 and m/e 34 to < ~10% of its contribution at m/e 32 (10% was chosen to allow for the possibility of some leakage of adjacent masses in the quadrupole spectrometer). Another exception was made in the case of very noisy spectra where fitting individual spectra with the least squares routine gave very different product abundances for spectra at the same m/e ratio but different angles, i.e. spectra which should have the same product abundances. In these cases, an aesthetic fit which agreed within the noise limits of all applicable spectra was created. Since the noisy spectra were usually the low signal spectra, this latter procedure probably does not introduce much error.

The branching ratio of the ions attained from this procedure is shown in Table 2. The neutral product ratio, assuming ionization cross sections derived by the method

of Fitch and Sauter are also shown in the table[15]. All five channels for which both fragments are visible (all but the H_2 channel) are deficient in the sulfur containing fragment. Excluding the mass 82 fragment, the remaining fragments have a ratio of about 62% : 32 % for the abundance of non-sulfur products vs. sulfur containing products.

This relative mismatch could have several explanations. The most horrifying would be that the experiment was done on a mixture of compounds that was only about 2/3 thiophene with the other third being pure hydrocarbons. An impurity of this magnitude seems highly improbable. Another, more believable, alternative is that the estimation of ionization cross sections is incorrect. Since Fitch and Sauter's method is based on the additivity of atomic cross sections, the discrepancy could be explained by an overly large value for the sulfur atom[15]. Their values for the atomic cross sections were obtained by linear regression analysis of the known cross sections of 179 molecules. However, only two of them contain sulfur and both were inorganic, making the value for the sulfur cross section questionable. If the value for sulfur is lowered from 3.8×10^{-16} cm^2 to 1.8×10^{-16} cm^2, the ratio of sulfur to non-sulfur containing products from this experiment would be one to one. (For comparison, the values for carbon and hydrogen and oxygen are 1.43, .73 and 1.1 (x 10^{-16} cm^2) respectively.) Fitch and Sauter's work also shows that the cross sections are smaller for atoms involved in π bonding (such effects are not included in the analysis leading to the numbers used here), suggesting that a reduction of the sulfur contribution is reasonable given the bonding in the products, e.g. CS. The last column in Table 2

reports the relative product yields assuming a 1.8 x 10^{-16} cm^2 cross section for sulfur.

The last factor I can think of that would affect the sulfur to non-sulfur ratio is misassignment of the products. If ion signals from a 1:1 yield of mass 44 and 40 products were misassigned as belonging to mass 58 and 26 fragments, it would appear that the ratio of neutrals is 1 : 2.56 in favor of the non-sulfur fragment (using Fitch and Sauter's original cross sections). It does not seem likely that the assignment of signal to various channels can be off enough to account for the entire effect seen. However, there could be some contribution from misassignment, which would reduce the change in the sulfur atom cross section from Fitch and Sauter's value required to balance the product yields.

Looking at the last column of Table 2 gives some encouraging results: balancing the total sulfur to non-sulfur product yield also balances that ratio independently for the 51+33, 45+39, and 44+40 channels. For calculating the branching ratio, I will assume that the mass 82+2 channel is also balanced, since the H_2 was not observed. This leaves the mass 58+26 and 52+32 channels. The first has 7.5% and 15.5% of the signal at mass 58 and 26 respectively, while the second has 10% and 19% at mass 52 and 32. The mass 58+26 channel is missing sulfur containing product while the mass 52+32 channel is sulfur rich. It was noted above that there may be some secondary dissociation of the mass 58 fragment which would lower its apparent yield. The other three products could also be dissociating, though there is not much evidence for this happening at the 20 mJ/cm^2 fluence level. It is probably more likely that misassignment of the products at m/e 32 and below are the

cause of the inequalities. Further, there does not seem to be a good way to determine where the errors lie, i.e. whether the more abundant mass should have its yield reduced, or the less abundant one have its yield increased. There are simply too many parameters to manually adjust. Given this, I will resort to summing the yields of the conjugate masses to give the total yield for the dissociation channel. One might consider the extremes of assuming one or the other of the conjugate product yields to be correct as an indicator of the size of the possible error, i.e. the mass 58+26 channel has a yield of 23±8%.

The estimate of the relative dissociation yields for the six channels is then:

82+ 2	:	58+26	:	52+32	:	51+33	:	45+39	:	44+40
5%	:	23%	:	29%	:	9%	:	20%	:	14%

The likely errors in these values are all relative to the size of the yield. Based on this and the estimates for the mass 58+26 and 52+32 channels, one can infer errors of ~±35% of the stated value for each channel.

Discussion:

HYDROGEN (H_2) ELIMINATION/DIMER DISSOCIATION:

To determine the best assignment for the signal that appears at m/e 82 and

lower mass to charge ratios requires consideration of the thermodynamic and kinetic implications of the assignment. A dimer dissociation is the easier option to consider. A dimer should only be bound by a very small amount and it would make sense for the $P(E_T)$ to peak at zero, as it would in a simple bond rupture, and for it to only extend for a few kcal/mol since most of the energy would likely remain as internal energy in the thiophene monomers, assuming an RRKM like process (for at least the photoexcited monomer). Thus a dimer dissociation seems feasible. This model's upper limit for the required dimer population of 1-2% of the molecules in the beam also seems to be within reason. The only inconsistency with this hypothesis is that there is, at m/e 84, less than 1/5 the signal expected assuming the known dissociative ionization pattern of thiophene[16]. Similarly, the dearth of signal at m/e 83 is at least a factor of 3.

The H_2 loss hypothesis seems to be consistent with at least thermodynamic arguments. For instance, H_2 loss from one of he double bonds in the ring should have a ΔH_{rxn} of ~ 46 kcal/mol assuming two 110 kcal/mol C-H bonds are broken, a 104 kcal/mol H-H bond is formed, and a 70 kcal/mol C-C π bond is formed. Any increase in ring strain would increase this value. Given the 148 kcal/mol of the exciting photon, a >80 kcal/mol maximum translational energy seems feasible. H_2 loss from a ring opened diradical could also yield a ΔH_{rxn} in the same range.

The problem for the H_2 hypothesis is one of kinetics and excess energy distribution. For this channel to be so minor compared to the others discussed below, it must have a barrier well above 100 kcal/mol, at least 40 kcal/mol above the

presumed products. It would be very surprising if H_2 loss, a concerted elimination with a large barrier, would show no evidence of a peak away from zero in the $P(E_T)$. For comparison, the $P(E_T)$ for loss of H_2 from ethylene shows a peak more than 20 kcal/mol away from zero [17].

This suggests very strongly that at least some of the signal is from dimers. If the H_2 channel also exists, with a reasonable $P(E_T)$ similar to that of H_2 loss from ethylene, it must contribute less than 1% of the total photodissociation yield, whereas a peak on the order of 7 kcal/mol would give an H_2 yield of 3-4% and be more consistent with the m/e 84, and m/e 83 data.

ACETYLENE ELIMINATION:

Breaking thiophene into a mass 58 (C_2H_2S) and a mass 26 (C_2H_2) fragment is the equivalent of breaking cyclopentadiene into mass 40 (C_3H_4) and mass 26 (C_2H_2). In cyclopentadiene, two different mechanisms produced the product combination, with different structures for the mass 40 fragment, and different $P(E_T)$s. One of these mechanisms yielded a C_3H_4 carbene and acetylene from the ring opened diradical,without a barrier to reaction, while the other produced cyclopropene and acetylene from the bicyclo valence isomer of cyclopentadiene with a barrier of more than 20 kcal/mol. The thiophene 58+26 channel would, on the basis of the $P(E_T)$ which indicates a barrier to reaction of > 19 kcal/mol, seem to proceed via a mechanism of the latter type. This mechanism, proceeding through the bicyclo

valence isomer of thiophene, would yield acetylene and thiirene (cyclic C_2H_2S). From an *ab initio* calculation yielding a $\Delta H_{rxn} \approx -60$ kcal/mol for $S(^1D_2)$ + HCCH $\rightarrow$ thiirene, and ΔH_f values for the reactants, 93.1 and 54.2 kcal/mol, respectively, the ΔH_f of thiirene is found to be ~87.3 kcal/mol[1]. Using a value of 27.66 for the ΔH_f of thiophene then yields 113.84 kcal/mol for the ΔH_{rxn} of thiophene dissociating to acetylene and thiirene. This yields a maximum possible translational energy of ~34 kcal/mol for photodissociation via this route with a 193 nm photon. The $P(E_T)$ derived from this experiment has a maximum of ~41 kcal/mol. It is possible to reduce this value by 3-4 kcal/mol before there is a noticeably worse fit to the data. This close of an agreement with the theoretical estimate lends credence to the proposed mechanism. Assuming this assignment is correct and working backward then yields an experimentally determined maximum ΔH_f for thiirene of ~84 kcal/mol.

The peak in the $P(E_T)$ would then imply a barrier of at least ~129 kcal/mol for dissociation via this channel. The barrier in thiophene would then be much higher than the > ~108 kcal/mol in cyclopentadiene, but the difference is almost exclusively due to the relative thermodynamic stability of the products in the two cases. One would expect that since the barrier is due to repulsive forces between the leaving acetylene and the two carbons in the three membered ring in both cases, that the barrier relative to the products would be the same in both cases. This appears to be the case.

It is interesting to investigate the energetics in the thiophene system of the other mechanism that occurs in cyclopentadiene, ring opening and dissociation to

acetylene and a diradical, and to consider the evidence for its occurrence. The relevant energies for this mechanism are the barrier for ring opening to the ∘SCHCHCHCH∘ diradical and the overall ΔH_{rxn}. The stability of the diradical above has been estimated at 99.7 kcal/mol above thiophene based on Benson's rules[13]. Given Benson's estimate for the ring strain in thiophene, 1.73 kcal/mol, one would expect the barrier to ring opening would then be less than 101.4 kcal/mol (the ring strain would only contribute to a barrier if the bond must be broken before the geometry can change enough to release the strain). As in cyclopentadiene, this is well below the overall heat of reaction and this barrier will not be important for the mechanism. The heat of reaction can be determined from the same set of *ab initio* calculations cited above which puts the lowest states of the ∘CHCHS∘ diradical 14 kcal/mol above thiirene. The thioketocarbene structure, :CHCHS, is found to lie 17 kcal/mol above the 1,3 diradical. The theoretically derived ΔH_{rxn} for thiophene yielding acetylene and the most stable C_2H_2S diradical is then 127.84 kcal/mol. If one assumes that the theoretical value of 14 kcal/mol for the relative energy of the diradical and thiirene is correct but uses the value for thiirene experimentally derived above, the ΔH_{rxn} becomes ~124.5 kcal/mol. This is below the estimate for the barrier in the concerted mechanism suggesting that this diradical channel could be competitive with the concerted process. Dissociation to the thioketocarbene would require 144.84 kcal/mol (theoretical values), and would certainly not be competitive with the other mechanism.

The maximum translational energies expected for the lowest energy diradical plus acetylene channel would then be ~23 kcal/mol. While there does not seem to be

an RRKM-like pseudoexponential channel at mass 58, it is not clear whether the low energy tail on the mass 58 $P(E_T)$ could indicate a small amount of a 'slow' channel. (One would then reassign some the slowest signal attributed to the mass 82 channel as mass 58 to raise the mass 58 $P(E_T)$ to a second low peak at zero energy.)

In cyclopentadiene, the assignment was confirmed by observing a change in the ratio of the 'fast' and 'slow' channels at different mass to charge ratios due to a difference in their ionization cracking patterns. In cyclopentadiene, the big change was between m/e 40 and m/e 39. Here there is not much difference between m/e 58 and m/e 57, but there is a large change at m/e 45, HCS^+. This change has so far been assigned as a new HCS + C_3H_3 channel with perhaps somewhat exaggerated maximum E_T of ~20-25 kcal/mol (above ~10-12 kcal/mol the signal could be assigned instead to the 'fast' mass 58 channel). It must be realized that the same m/e 45 time-of-flight contribution, when considered as a product of mass 58 recoiling off mass 26 instead of mass 45 off of mass 39, requires a $P(E_T)$ that extends well beyond 20 kcal/mol to about 40-48 kcal/mol (a factor of 1.93 times the old limit). Restricting the $P(E_T)$ to less than ~23 kcal/mol (mass 58+26) would not change the fit to the data since the 'fast' mass 58 channel can provide any required signal above this energy. Thus, there is evidence for a 'slow' acetylene loss channel in thiophene. Given the expected low barrier for the 'slow' 58 channel, it would actually be hard to understand its complete absence unless there is a barrier to dissociation of the diradical. Such a reassignment would have some 'ripple' effects, but none that would invalidate the assignment. For instance, signal previously assigned to the mass 39 partner of mass 45 appearing above

m/e 26 would have to be reassigned mostly to the mass 52 channel. The 9% yield of the mass 45 product would drop to about a 6% yield for the new 'slow' 58 product due to the change in the assumed ionization cross section. The ~45% of the old mass 39 signal appearing at m/e 26 and below would be sufficient, given the correct ionization cross sections, to roughly match the 6% yield of the new mass 58 fragment with another 8% for the mass 26 product. Thus the 'slow' mass 58+26 channel would account for ~12-14% of the total yield.

The old mass 39 signal reassigned to the mass 52 channel would raise the mass 52 yield from ~ 10% to ~15%, vs 19% for the S atom. This helps to remove the otherwise inexplicable deficit of mass 52, and would raise the overall yield of the S atom loss channel to ~34% from 29%. The other channels would only be minimally affected, with their branching percentage changed by only a percent or two.

A last note on mechanisms for producing mass 58 and 26 deals with a concerted mechanism proposed by Verkoczy et. al.[1]. It would produce the same products as the concerted process described above, thiirene and acetylene, but does not invoke a stable intermediate bicyclo structure, though it does involve a bicyclic transition state. A bond would form between the sulfur atom and carbon 3, while carbons 4 and 5 form the acetylene triple bond and break their bonds with the sulfur atom and carbon 3. While the mechanism as described is for the addition of thiirene to acetylene to yield thiophene, this type of mechanism seems to have been first proposed to explain the production of thiirene and N_2 in the photodissociation of five membered ring, cyclic SNNCHCH. While this mechanism thus seems to have

experimental support, it is not clear that it should be considered as concerted. A concerted reaction occurs when, if one bond is broken, the energy that would be gained by forming the new bonds is greater than the energy required to break the rest of the old bonds, causing the 'simultaneous' rearrangement of all the electrons. This is equivalent to saying that the intermediate diradical is not a minimum on the energy surface, or at least it is not below the energy of the final products.. For instance, in the 'fast' acetylene loss mechanism above, two C-C single bonds are broken and two π bonds are formed. If one C-C bond is broken, the energy gained by forming the π bonds (~150 kcal/mol) is greater than the energy required to break the remaining C-C bond (~100 kcal/mol), and the intermediate diradical will unstable with respect to the products. For the Verkoczy mechanism, if the C-S bond is broken, one can form a π bond in acetylene (~70 kcal/mol) and a new C-S bond to form the thiirene ring (~14 kcal/mol) while a C-C single bond (~100 kcal/mol) must be broken. The intermediate diradical is stable relative to the products by ~ 16 kcal/mol. In such a case, one would expect that the bonds would break in a sequential manner and the reaction is better thought of as a two step process of ring opening to the diradical followed by the dissociation step. If this is true, it does not seem likely that this mechanism would produce fragments with a highly peaked translational energy distribution as we observe. Similarly, though its products are more stable than the proposed 'slow' mechanism above, it should have a barrier relative to the 'slow' mechanism due to the expected barrier to forming the thiirene ring (see the cyclopentadiene chapter for a more detailed description). Thus, I believe that the concerted dissociation from the

bicyclo isomer and dissociation to the diradical from the ring opened isomer of thiophene remain the best mechanisms to explain the observed dissociation yield.

SULFUR ATOM ELIMINATION:

Sulfur atom elimination appears to be the major elimination channel for thiophene photodissociated at 193 nm. In cyclopentadiene, the equivalent channel, CH_2 loss appeared to occur via ring opening and H atom migration to yield the 1-buten-3-yne form of C_4H_4 with a maximum translational energy of ~ 17 kcal/mol. In thiophene, the equivalent channel would be much lower in energy due to the increased stability of the sulfur atom relative to CH_2. The ΔH_{rxn} would be only 108 kcal/mol, allowing a maximum translational energy of 40 kcal/mol. The observed translational energy release in this dissociation has a discernable maximum of only 16 kcal/mol suggesting either electronically excited $S(^1D_2)$ atoms (yielding a maximum E_T of 13.6 kcal/mol) or a less stable form of C_4H_4 is produced.. Three other less stable forms of C_4H_4 are energetically possible in the thiophene reaction: butatriene (ΔH_{rxn}=114 kcal/mol, max E_T = 33.6 kcal/mol), 3-methylene cyclopropene (ΔH_{rxn}=134.7 kcal/mol, max E_T = 13.3 kcal/mol), and cyclobutadiene (ΔH_{rxn}=137.6 kcal/mol, max E_T = 10.4 kcal/mol)[18]. Direct triple dissociation to two acetylenes and a sulfur atom requires 147.26 kcal/mol.

The closest match for the maximum E_T would be for the 3-methylene cyclopropene form, though the theoretical ΔH_f would have to be lowered ~ 2 kcal/mol

to 93.5 kcal/mol in order to explain the whole observed distribution. One would expect a barrier somewhere along the reaction coordinate for this mechanism since H atom transfer to yield the CH_2 group attached to the ring must occur. This mechanism would be consistent with the expectation that the ring contracted form of thiophene can be formed by photoexcitation as proposed in the Van Tamelen-Whitesides mechanism[6].

This mechanism would argue against the importance of the ring opened diradical pathway. If the ring opened radical were formed, one might expect a barrier similar to that in the cyclopentadiene for 3,5 H atom migration (estimated at ~10 kcal/mol) to allow dissociation to the stable 1-buten-3-yne isomer. While the ring opened diradical here is ~19 kcal/mol higher relative to the starting material, the total estimated barrier would only be ~ 110 kcal/mol. It is unclear why such a channel is not observed. The estimate for the barrier could be much too low, preventing this channel from competing with the possible 'slow' 58+26 channel above, or the ring opened diradical may not be an important intermediate due to more stable ring contracted forms. A third possibility is that the triplet ground state S atom is not produced and only the excited $S(^1D_2)$ form is allowed. The triplet/singlet question here is analogous to that of $^1CH_2$ vs. $^3CH_2$ production in CPD. However, unlike the expected barrierless transition state for $^1CH_2$, a singlet sulfur channel would have to have a barrier based on the observed $P(E_T)$.

Finally, it should be noted that while S atom production is a major channel here, it has been ruled out in other photodissociation experiments[11]. This does not

imply a contradiction though. These studies were done at longer wavelengths than the present one, and the maximum photon energy was ~133.7 kcal/mol (213.9 nm), with an estimate of another 8-11 kcal/mol of thermal energy available (T = 305 C). From the ~2.6 kcal/mol peak in our $P(E_T)$ one can infer a barrier of at least 135 kcal/mol to dissociation to S atoms. This would make S atom loss much less likely in the longer wavelength study, and impossible for all but the shortest wavelength and highest temperature conditions used.

SH ELIMINATION:

The SH channel does not appear by itself at any mass to charge ratio and its derived $P(E_T)$ is therefore somewhat arbitrary. However, the two limits that it must peak at or near (~2 kcal/mol) zero energy and that it cannot extend beyond the mass 52+32 $P(E_T)$ limit of ~16 kcal/mol are not in question. The derived $P(E_T)$ with a maximum E_T of 12 kcal/mol suggests a ΔH_{rxn} of~136 kcal/mol. With the known values for the ΔH_f of SH (34.1 kcal/mol) and thiophene (27.82 kcal/mol) this leads to estimate of 129.7 kcal/mol for the ΔH_f of the C_4H_3 radical formed as the conjugate fragment. This is in excellent agreement with theoretical predictions for the HCCHCCH radical; cis form ΔH_f = 129.92 kcal/mol, trans form ΔH_f = 130.22 kcal/mol[18]. This assignment would also be in agreement with the structure proposed by Krishnamachari and Venkitachalam for the structure of the transient C_4H_3 radical they observed in the flash photolysis of thiophene[9]. There is a lower energy structure,

H_2CCCH, predicted to lie at 111.34 kcal/mol, which would allow a maximum translational energy of ~ 30 kcal/mol for SH loss from thiophene. This pathway would have a barrier due to the required H atom migration (in addition to the H atom transfer to the sulfur atom) which probably explains its apparent unimportance relative to the HCCHCCH pathway.

C_3H_3 ELIMINATION:

The m/e 45 and m/e 39 signals have been discussed above in terms of the m/e 45 signal being caused by dissociative ionization of a mass 58 product. Here, these signals will be considered as conjugate mass 45 and 39 products, and the derived energetics will be compared with the known thermochemistry. The question of the correct assignment for these signals can then be reexamined.

The ΔH_f of HCS, the conjugate fragment of C_3H_3, can be derived from the known ΔH_f of H_2CS (~24 kcal/mol) and a theoretical estimate for the dissociation energy to HCS and H atom of 85.2 kcal/mol[19]. With the H atom ΔH_f of 52.095, this yields ΔH_f (HCS) = 57.1 kcal/mol. An earlier approximate experimental value for the H_2CS bond dissociation energy would put the ΔH_f (HCS) at 63.3 kcal/mol.

The C_3H_3 radical ΔH_f has also been calculated. The lowest energy propargyl structure, $H_2C\circ$-CCH, is estimated at 80.7 kcal/mol[19]. The cyclopropen-1-yl radical is estimated by Collin et. al. to lie ~ 52 kcal/mol above the propargyl form, which using the propargyl ΔH_f above yields a ΔH_f of 132.7 kcal/mol[20]. However, using estimates

for the C1-H (110 kcal/mol) and C3-H (101 kcal/mol) bond energies in cyclopropene and its ΔH_f of 66 kcal/mol, yields a cyclopropen-1-yl ΔH_f of ~124 kcal/mol and a cyclopropen-3-yl ΔH_f of ~115 kcal/mol.

Thus the ΔH_{rxn} for thiophene dissociating to HCS and the three C_3H_3 radical forms above are: (propargyl) ~110 kcal/mol, (cyclopropen-3-yl) ~144 kcal/mol, and (cyclopropen-1-yl) ~153 kcal/mol. The propargyl radical would be the only possible form of C_3H_3 and would yield a maximum translational energy of ~38 kcal/mol. The $P(E_T)$ determined from the proposed C_3H_3 channel in this experiment only extends to ~ <25 kcal/mol and possibly only to 15 kcal/mol. The latter value would imply that the C_3H_3 radical must form with at least 23 kcal/mol internal energy all of the time. This would be a somewhat surprising result, but would be consistent with the results from the photodissociation of allene at 193 nm (using the same technique as used here, on the same machine), where Jackson et. al. found that the C_3H_3 radical formed by H loss from allene had to form with ~ >26 kcal/mol internal energy to explain the time-of-flight spectra[21]. They conclude that excess vibrational energy is the most reasonable explanation.

The only question not addressed so far is the height of the barrier for the required 4,5 H atom migration to reach an S=CH---CH=C=CH_2 intermediate. In allene, the barrier to forming cyclopropene, which is largely the barrier to H atom migration, is ~69 kcal/mol[22]. Assuming a similar barrier in the 'SCH substituted allene' shown above, which presumably lies more than 69 kcal/mol below the separated HCS and C_3H_3 products (i.e. the SCH----C_3H_3 bond is greater than 69 kcal/mol), would

imply that the H atom barrier is below the overall ΔH_{rxn}.

Thus, the assignment of the m/e 45 signal to an HCS plus propargyl C_3H_3 radical channel seems reasonable. It would seem that there is roughly equal evidence pointing to the two possible m/e 45 assignments ('slow' 58+26, or the present 45+39 channel). The other photodissociation experiments cited above do not seem to favor one mechanism either. The existence of the diradical C_2H_2S has been proposed by Nayak et. al., but their evidence against the thiirene form seems to rely on a grossly inaccurate value for the thiirene CS bond energy (56.3 kcal/mol vs the 14 kcal/mol value cited above and the ~ 25 kcal/mol value for the C-C bond in cyclopropene)[13]. HCS and the C_3H_3 radical have not been proposed as primary products before, but it is unclear whether they would appear kinetically different from a CS + C_3H_4 channel in an experiment measuring only end products.

C_3H_4 ELIMINATION:

The C_3H_4 + CS channel is the second channel for thiophene dissociation that appears to have a substantial barrier (58 +26 is the other one). The $P(E_T)$ shows a peak at 8.75 kcal/mol and extends to 30 kcal/mol. Using a CS heat of formation of 60 kcal/mol, one can infer that the C_3H_4 species formed in this study has a ΔH_f <= 85.8 kcal/mol[23]. This is well above that for allene or methylacetylene (~46 and 44 kcal/mol) and cyclopropene (~66 kcal/mol). It is below the ΔH_f of the CH_2CHCH carbene (~91 kcal/mol). The allene and methylacetylene possibilities would both require multiple H

atom transfers, perhaps sharing the intermediate proposed for the HCS loss mechanism. With a fairly low barrier estimated above for the first H atom transfer, the transition state would then involve the transfer of the second H atom. The cyclopropene form could be created with a single H atom transfer from the ring contracted form of thiophene. Given the questions over the true geometry and bonding nature of this structure, it does not seem feasible to estimate the H atom transfer barrier from a theoretical viewpoint. The peak in the $P(E_T)$ would imply a barrier greater than 127 kcal/mol relative to thiophene, but without further insight into the possible transition state geometries this fact does not help differentiate between the possible products.

BRANCHING RATIO / COMPARISON WITH CYCLOPENTADIENE:

The branching ratio for the channels described above is juxtaposed in Table 3 with the derived ΔH_{rxn} values and the estimated barrier heights relative to thiophene for the transition states on the various reaction coordinates. The easiest thing to note is that all of the likely barriers are within about 10-12 kcal/mol (except perhaps for H_2 loss) and the yields vary by less than an order of magnitude. Even without a calculation, it would seem that only a couple of orders of magnitude difference between the 'A factors' of the channels would explain the observed yields. This is in stark contrast to the cyclopentadiene case where an 'A factor' of $\sim 10^{20}$ was needed to explain the CH_2 yield while the other channels had 'A factors' in the $\sim 10^{15}$ range.

Given the limitations to the RRKM calculation done in the cyclopentadiene chapter, and the increased ambiguities in the transition state geometries for thiophene, it does not seem worthwhile to repeat that effort here. However, qualitative comparisons based on the ideas discussed in the cyclopentadiene chapter can still be made.

The channel producing thiirene and acetylene is the one with the closest correspondence to a cyclopentadiene (CPD) channel. Just like the cyclopropene plus acetylene in CPD, it has a bicyclic transition state and has roughly the same exit barrier. The main difference comes from the relative instability of the thiirene product which puts this channel's barrier at > 129 kcal/mol above thiophene. Its yield is about 23% here though, simply because there is no equivalent of the very low barrier H loss channel of CPD.

The energetics of the ring opening step remain about the same as in CPD, relative to the barrier for the bicyclo transition state: in both cases the barrier for ring opening is ~27 kcal/mol below the bicyclo barrier. The equivalent of the 'slow' acetylene channel in CPD is shifted lower by about 11 kcal/mol in thiophene. This actually puts its barrier lower than the 'fast' channel. However, depending on the assignment of the m/e 45 data, the relative yield of the 'slow' acetylene channel is either equal to (~ 1/2 of the 'fast' acetylene yield) or much less than that in CPD. This would seem to argue for either a barrier to 'slow' acetylene plus thioformylmethylene formation, or simply for the reduced importance of the ring opened diradical and associated dissociation channels. One might expect the latter since the diradical's

importance in CPD depends on its lower frequencies offsetting its ~81 kcal/mol instability vs. the CPD ground state. Shifting all of the channels higher in energy by ~20 kcal/mol in thiophene would reduce the relative importance of the geometries with the lowest frequencies because their relative state densities would drop more than that of the geometries with deeper wells and higher frequencies. These arguments apply to the transition states as well as the diradical intermediate.

The S atom channel, nominally equivalent to the CH_2 loss channel in CPD, does not seem to proceed via the same mechanism. If it did, its yield might be expected to increase significantly due to the stability of the S atom relative to CH_2 (~26 kcal/mol). The energy for its transition state, at ~108-111 kcal/mol, would be the lowest of any channel, significantly below the 131 kcal/mol required in CPD. The energy of the transition states for the other channels are all elevated relative their values in the CPD system. The S atom channel would have the same advantage as CH_2 loss in CPD of low frequencies from a straight chain (non-cyclic) transition state. Thus, one would expect and increase from the roughly 1:4 ratio seen for the CH_2: fast acetylene channels in CPD.

An increase is indeed seen: S atom loss seems to be the major channel by a factor of 1.2 to 1.5 over the fast acetylene/thiirene channel. However, both the $P(E_T)$ and the other photodissociation studies cited above suggest that the products formed must have a much higher energy relative to thiophene than the 108-11 kcal/mol for the above mechanism. It was proposed earlier in the section that the C_4H_4 isomer with a cyclopropene ring would be the closest match energetically to the derived value. From

the high yield for this channel and the fact that its barrier, at 135 kcal/mol, is one of the highest among the observed dissociation pathways, it would seem that the transition state should be very loose. It is unclear that the isomer with a 3 membered ring would meet this requirement., since it should not have many low frequencies to boost the yield.

The possibility exists that the S atom does dissociate from the linear diradical but only to excited products. The excess energy in the products would be ~ 24 kcal/mol. This could mean excited $S(^1D_2)$ atoms, or vibrationally excited C_4H_4. The loose linear diradical transition state could help explain the high yield of S atoms even with the high observed ΔH_{rxn}.

The three channels above are the only ones with possible equivalents observed in cyclopentadiene. The new channels that appear in thiophene are ones that have their barriers lowered in thiophene relative to the channels above. The SH + C_4H_3 channel has almost exactly the same total ΔH_f as the equivalent CH_3 + C_4H_3 channel in CPD. Due to the ~ 4 kcal/mol lower ΔH_f of thiophene relative to CPD, its ΔH_{rxn} is shifted upward by 4 kcal/mol to 136 kcal/mol. Its ~9% yield, the lowest of the 5 main channels, would be consistent with it having the highest barrier. Similarly, since it has a barrier (~132 kcal/mol) higher than any of the observed channels in CPD, its absence in that system is understandable. An additional possibility is that the H atom transfer to the leaving methyl group may have a higher barrier than the equivalent transfer to the sulfur atom, further increasing the difference expected for this pathway in the two systems.

The CS, and possible HCS channels are actually shifted downward from their equivalents in CPD, due to the stability of the sulfur containing equivalents of vinylidene and the vinyl radical. CS, ΔH_f = ~60 kcal/mol, is 34 kcal/mol more stable than the equivalent vinylidene[24]. Similarly, with a ΔH_f = ~57 kcal/mol, HCS is more stable than C_2H_3 by ~14 kcal/mol[17]. Thus channels lying at 144 kcal/mol (with a ≥153 kcal/mol barrier) and 120 kcal/mol (with an ~143 kcal/mol barrier) shift to 114 kcal/mol (~123 kcal/mol barrier) and 110 kcal/mol (barrier of 133 kcal/mol) and become competitive.

The relatively low yield of the CS channel, ~ 14 %, despite its low barrier relative to the other channels, is consistent with its concerted nature. Similarly, a yield of 21% for HCS is not unreasonable for a channel with a ~ 133 kcal/mol barrier if it has a fairly loose intermediate such as the linear diradical.

The only channel yet to be discussed is the possible H_2 elimination channel. The yield for this channel does not appear to be greater than 5% even though its barrier cannot possibly be as high as those for the other channels. Similarly, H atom loss does not seem to occur even though it is energetically feasible. For comparison, benzene dissociation at 193 nm yields 80% H loss and 16% H_2 loss[25]. The only substantial difference between the two systems that could influence the yield of these products is the 'floppy' nature of the thiophene ring. If the thiophene ring quickly distorts, to a bi- or tri-cyclic isomer, or the ring contracted isomer, or the open chain diradical, at least several of which have barriers below the hydrogen dissociation barriers, hydrogen loss may be suppressed.

Conclusion:

Thiophene certainly fulfills the expectation that a five membered cyclic diene system will have many competing channels if there is not a weak C-H bond as in cyclopentadiene: all six identified channels in thiophene have yields within roughly a factor of 6 of each other.

All of the observed channels, except for H_2 loss, have barriers in excess of 125 kcal/mol. The low yield of H_2 would then have to be explained in terms of a distorted excited state of thiophene. A 'reasonable' picture of the excited state may be that of five balls in a bag, where bicyclo, tri-cyclo, ring contracted, and ring opened forms of the thiophene skeleton are all more likely than the pentagonal geometry we usually think of.

The largest channel is sulfur atom loss, with nearly 1/3 of the yield. The form of the C_4H_4 species left behind is not clear: the best choice from the derived thermodynamics is 3-methylene cyclopropene but the rapid rise of this channel between 213.8 nm and 193 nm dissociations required to fit all of the relevant experimental data suggests a very floppy transition state which would perhaps suggest a vibrationally excited linear C_4H_4 instead.

The next largest channel, producing thiirene and acetylene, is a concerted dissociation from the bicyclo form of thiophene. This is the same mechanism that was seen to produce cyclopropene and acetylene from cyclopentadiene. The barriers in the

two systems are nearly identical suggesting that they arise from repulsion of the acetylene and the -C=C- part of the respective rings as one would expect for concerted eliminations.

The other acetylene loss channel in cyclopentadiene, assigned to dissociation from the ring opened diradical, is not clearly in evidence in thiophene, though the signal at m/e 45 can be interpreted as thioformylmethylene produced via this mechanism. Regardless of the decision on this, the yield for this channel is still lower relative to that for the thiirene form of mass 58 than one would expect based on the yields of the equivalent channels in cyclopentadiene and the fact that the relative barriers have shifted 10 kcal/mol in favor of this channel in thiophene. However, the lower yield is understandable in light of the fact that the ring opened diradical of thiophene is ~ 20 kcal/mol less stable in thiophene than in cyclopentadiene and the importance of this intermediate geometry and the transition state (in terms of number of states) is thereby reduced in thiophene.

Several additional channels appear in thiophene that are not seen in cyclopentadiene. The SH loss channel, which seems to occur from a linear diradical, is nearly isoenergetic with CH_3 loss from cyclopentadiene. Its visible yield in thiophene is due primarily to the fact that all of the lower energy pathways available in cyclopentadiene become much less favorable in thiophene. The dissociation energy for this channel identifies the C_4H_3 species as HCCHCCH. The barrier to H atom transfer to the sulfur atom does not appear to cause a peak in the translational energy distribution and is probably quite small.

Dissociation to HCS and C_3H_3 is a second possibility to explain the m/e 45 data. The proposed mechanism would be ring opening followed by 4,5 H atom migration and bond cleavage to yield HCS and propargyl radical. The dissociation energy required for this channel does not correspond to vibrationally cold propargyl radical or to the vibrational ground state of any other form of C_3H_3. In fact a minimum of 23 kcal/mol of energy must be in vibration of the fragments. This value is quite close to that previously observed for the minimum internal energy of C_3H_3 produced in allene photodissociation. If this assignment of the m/e 45 signal is correct, it would strengthen the idea that the C_3H_3 moiety undergoes a geometry change as it breaks away from a partner fragment.

It does not seem that a definitive answer to the origin of the m/e 45 signal can be made. Its existence is certainly not in question as it is one of the clearer time-of-flight signals. However, neither experimental nor theoretical evidence conclusively identifies it. In fact, thermochemical and kinetics arguments would suggest that both possibilities should occur, and that may well be the case. Through chemical coincidence, the two channels have different energetics but nearly identical experimental footprints.

The final channel, CS loss, is the second to show a substantial barrier, indicating a concerted reaction. The mechanism must transfer an H atom from C2, but the derived $P(E_T)$ does not indicate the geometry of the C_3H_4 species formed. The C_3H_4 species must be vibrationally excited allene, methyl acetylene, or cyclopropene: the diradical forms cannot be reached. A diradical partner would also be inconsistant

with the barrier to reaction. This does not help much in defining the transition state geometry.

Finally I will attempt an answer to the question of whether thiophene behaves as a cyclopentadiene molecule without a weak C-H bond. The two molecules share at least one mechanism involving dissociation from the bicyclic isomer. They may also share channels that go through the ring opened diradical. However, one of these, S/CH_2 loss, would produce vibrationally hot C_4H_4 in thiophene and cold C_4H_4 in cyclopentadiene. Two other channels in thiophene, SH + C_4H_3 and HCS + C_3H_3, also seems to involve the ring opened diradical, but their analogues in cyclopentadiene are higher in energy and should not compete well with the observed channels. The other thiophene channel, CS + C_3H_4, and the S loss channel, could be indicative of ring contracted or more exotic intermediates. Both produce hydrocarbon fragments that must be vibrationally hot and/or cyclic. Thus, overall, the differences in dissociation seem to be mainly a function of the changed thermodynamics of the product fragments rather than completely new mechanisms appearing in thiophene. However, there are indications, beyond the fact that thiophene has two more observed dissociation channels than cyclopentadiene, that its photodissociation chemistry, like its solution photoisomerization chemistry, is more complex than that of cyclopentadiene.

m/e	% of signal	m/e	% of signal
82	0.09%	44	6.03%
81	0.16%	40	0.89%
80	0.08%	39	9.34%
72	0.00%	38	5.78%
71	0.04%	37	3.21%
70	0.07%	36	1.47%
69	0.33%	36	0.00%
68	0.45%	35	0.20%
60	0.04%	34	0.65%
59	0.13%	33	3.32%
58	1.89%	32	8.83%
57	3.78%	28	0.00%
56	1.11%	27	0.73%
52	3.71%	26	10.65%
51	5.14%	25	6.15%
50	6.37%	24	1.67%
49	4.16%	16	0.00%
48	1.73%	15	0.62%
48	0.00%	14	0.93%
47	0.46%	13	1.39%
46	0.62%	12	2.12%
45	5.67%		

Table 1. Dissociative Flux as a Function of Mass-to-Charge Ratio.

Mass	Ion Branching Ratio	Neutral Product Ratio	Corrected Neutral Product Ratio
82	4.482%	2.593%	2.489%
58	9.210%	7.185%	7.473%
26	13.570%	19.725%	15.514%
52	17.364%	12.738%	10.019%
32	7.181%	11.835%	19.201%
51	5.505%	4.407%	4.623%
33	2.252%	3.124%	4.339%
45	7.320%	7.752%	9.114%
39	14.284%	13.928%	10.955%
44	4.679%	5.636%	7.110%
40	9.671%	8.486%	6.675%

Table 2. Product Branching Ratios. Column 1 - Branching Ratio of the raw ion flux. Column 2 - Neutral Branching Ratio obtained by dividing the Ion Branching Ratio by ionization cross sections derived by the method of Fitch and Sauter. Column 3 - Neutral Branching Ratio derived using the method of Fitch and Sauter with an alternative value of 1.8×10^{-16} cm^2 for the S atom contribution to the cross section. (In all columns, the H_2 ratio (not shown) is assumed to be equal to that of the mass 82 fragment.)

	Branching Ratio	Alternate Branching Ratio	Heat of Reaction (kcal/mol)	Barrier Height (kcal/mol)
H_2 Loss (82+2)	< .04	< .04	~64	?? >120
'fast' Acetylene Loss (58+26)	0.23	0.24	110	>129
Sulfur Atom Loss (52+32)	0.29	0.35	132	>135
SH Loss (51+33)	0.09	0.1	136	136
C_3H_3 Loss (45+39)	0.2		<133	<133
'slow' Acetylene Loss (58+26)		0.14	>124.5	>124.5
C_3H_4 Loss (44+40)	0.14	0.15	118	>127

Table 3. Relative Yields, Heats of Reaction, and Estimated Barrier Heights for the Thiophene Dissociation Channels

References

(1) Verkoczy, B.; Sherwood, A. G.; Safarik, I.; Strausz, O. P. *Can. J. Chem.* **1983**, *61,* 2268.

(2) Mason, S. F. in Physical Methods in Heterocyclic Chemistry; Katritzky; Academic Press, New York, **1963**.

(3) Sabljic, A.; McDiarmid, R.; Gedanken, A. *J. Phys. Chem.* **1992**, *96,* 2442-2448.

(4) Kobayashi, Y.; Kumadaki, I.; Ohsawa, A.; Sekine, Y. *Tetrahedron Let.* **1975**, *19,* 1639-1642.

(5) Braslavasky, S.; Heicklen, J. *Chemical Reviews* **1977**, *77,* 473-511.

(6) Padwa, A. in Rearrangements in Ground and Excited States; de Meyo, P.; Academic Press, New York, **1980**; pp 501-547.

(7) Skancke, P. N.; Yamashita, K.; Morokuma, K. *J. Am. Chem. Soc.* **1987**, *109,* 4157-4162.

(8) Kellogg, R. M. *Tetrahedron Let.* **1972**, *15,* 1429-1432.

(9) Krishnamachari, S. L. N. G.; Venkitachalam, T. V. *Chem. Phys. Let.* **1978**, *55,* 116-118.

(10) Johns, J. W. C.; Ramsay, D. A. *Can. J. Phys.* **1961**, *39,* 210.

(11) Wiebe, H. A.; Heicklen, J. *Can. J. Chem.* **1969**, *47,* 2965.

(12) Wiebe, H. A.; Braslavsky, S.; Heicklen, J. *Can. J. Chem.* **1972**, *50,* 2721.

(13) Nayak, A. K.; Sarkar, S. K.; Karve, R. S.; Parthasarathy, V.; Rama Rao, K. V. S.; Mittal, J. P.; Krishnamachari, S. L. N. G.; Venkitachalam, T. V. *Appl. Phys. B.* **1989**, *48,* 437-443.

(14) Sabljic, A.; McDiarmid, R. *J. Phys. Chem.* **1991**, *95,* 6455-62.

(15) Fitch, W. L.; Sauter, A. D. *Anal. Chem.* **1983**, *55,* 832.

(16) Stenhagen, E.; Abrahamsson, S.; McLafferty, F. W., Atlas of Mass Spectral Data; **1969**.

(17) Balko, B. A., Ph.D. Thesis, University of California at Berkeley, **1991**.

(18) Melius, C., Sandia National Laboratory, private communication.

(19) Pope, S. A.; Hillier, I. H.; Guest, M. F. *J. Am. Chem. Soc.* **1985**, *107,* 3789-3800.

(20) Collin, G. J.; Deslauriers, H.; De Mare, G. R.; Poirier, R. A. *J. Phys. Chem.* **1990**, *94,* 134-141.

(21) Jackson, W. M.; Anex, D. S.; Continetti, R. E.; Balko, B. A.; Lee, Y. T. *J. Chem. Phys.* **1991**, *95,* 7327-7336.

(22) Karni, M.; Oref, I.; Barzilai-Gilboa, S.; Lifshitz, A. *J. Phys. Chem.* **1988**, *92,* 6924-6929.

(23) Kawasaki, M.; Sato, H.; Kikuchi, T.; Fukuroda, A.; Kobayashi, S.; Arikawa, T. *J. Chem. Phys.* **1987**, *86,* 4425-4430.

(24) Yang, S. C.; Freedman, A.; Kawasaki, M.; Bersohn, R. *J. Chem. Phys.* **1980**, *72,* 4058-4062.

(25) Yokoyama, A.; Zhao, X.; Hintsa, E. J.; Continetti, R. E.; Lee, Y. T. *J. Chem. Phys.* **1990**, *92,* 4222-4233.

Figure Captions

Fig. 3-1.

m/e 51 Power Dependence. The integrated signal count from the time-of-flight spectrum at m/e 51 is plotted vs. the estimated laser fluence in mJ/cm^2 (squares). The dotted line represents a linear extension of the low fluence signals to high fluence. From comparison of the measured signals with this line, it is estimated that secondary processes become significant above 20 mJ/cm^2.

Fig. 3-2.

H_2 Loss/ Dimer Dissociation Time-of-Flight Spectra. In the top half of the figure, time-of-flight spectra at a laboratory angle of 13° are shown for m/e 83 and m/e 82. Assignment of most of the signal to H_2 loss comes from the lack of signal at m/e 83. If the signal at m/e 82 were solely from dimer dissociation, the expected signal at m/e 83 would be greater than 50 counts for the spectrum shown (see text for details). The lower two spectra show signal from the same H_2 loss channel appearing at m/e 68 at 10° and 20°. The signal at 20° implies that the $P(E_T)$ for H_2 elimination, shown in Fig. 3-3, must have a high energy tail.

Fig. 3-3..

$H_2 + C_4H_2S$ Translational Energy Distribution ($P(E_T)$). The curve represents the normalized product flux as a function of total center-of-mass translational energy for the $H_2 + C_4H_2S$ dissociation channel. This $P(E_T)$ could have some

contribution from misinterpretation of dimer dissociation signal (see text).

Fig. 3-4.

C_2H_2S + C_2H_2 Time-of-Flight Spectra. The m/e 58 (C_2H_2S) spectrum at 30° is shown in the top half of the figure. The spectrum for the conjugate C_2H_2 fragment is shown in the m/e 26, 50° in the lower half. The data is represented by circles. The heavy black line is the fit to the data using the $P(E_T)$ shown in Figure 3-5. The grey line in the lower spectrum represents signal from other channels. From power dependence measurements at smaller angles, a small fast secondary contribution is expected in the m/e 26 spectrum shown here.

Fig. 3-5.

C_2H_2S + C_2H_2 Translational Energy Distribution ($P(E_T)$). The curve represents the normalized product flux as a function of total center-of-mass translational energy for the C_2H_2S + C_2H_2 dissociation channel. 34 kcal/mol is the theoretically derived maximum thermodynamically possible translational energy for production of thiirene and acetylene. The $P(E_T)$ shown here extends to 41 kcal/mol and cannot be truncated to less than ~37 kcal/mol without producing a visibly worse fit to the data, suggesting that the theoretical value for the ΔH_f of thiirene is too high by at least 3 kcal/mol.

Fig. 3-6.

m/e 52 and m/e 32 Time-of-Flight Spectra. These spectra, at a laboratory angle of 20° show contributions from the C_4H_4 (mass 52) + S (mass 32) channel. In each graph, the data is represented as circles and the total signal

by the heavy black line. The calculated m/e 52 signal is composed of contributions from mass 52 (thin black line) and mass 51 (gray line) signals. The mass 52 (C_4H_4) fragment has the $P(E_T)$ shown in Fig. 3-7. The nominally mass 51 signal can appear at mass 52 because of isotopic effects and bleedthrough of the adjacent masses in the quadrupole mass spectrometer. The mass 32 (S) fragment conjugate to the mass 52 fragment is shown in the lower graph as the thin black line. Other channels apparent are mass 58 from the C_2H_2S + C_2H_2 channel (thick dark gray line), mass 33 from the C_4H_3 + SH channel (thin dark gray line), and mass 45 from the possible HCS + C_3H_3 channel (light gray line). The fast lump in the m/e 32 spectrum that is not fit is secondary signal.

Fig. 3-7.

C_4H_4 + S Translational Energy Distribution ($P(E_T)$). The curve represents the normalized product flux as a function of total center-of-mass translational energy for the C_4H_4 + S dissociation channel. 13.3 kcal/mol is the theoretically derived maximum thermodynamically possible translational energy for dissociation to S atom and the proposed 3-methylene cyclopropene form of C_4H_4. The derived $P(E_T)$ for this channel shows a peak at ~2.6 kcal/mol. Because this channel can be observed in isolation at m/e 52, the $P(E_T)$ is well determined down to ~0.65 kcal/mol (the first nonzero point).

Fig. 3-8.

m/e 51 Time-of-Flight Spectrum. The m/e 51 spectrum at 20° is shown twice

in this figure. It is fit once without assuming a mass 51 + 33 channel (upper graph), and once with the proposed mass 51 +33 channel (lower graph). As can be seen, the latter fit to the data is superior. The data is shown as circles in both graphs with the total fit shown as a heavy black line. The mass 52 contribution is shown as a gray line while a possible contribution from the H_2/dimer channel is shown as a thin black line (a dimer channel mass 84 product could crack to mass 51 while the nominal mass 82 fragment from an H_2 loss channel could only appear here due to isoope effects of leakage of m/e 50 signal to m/e 51). The $P(E_T)$ for the proposed 51 (C_4H_3) + 33 (SH) is shown in Figure 3-10.

Fig. 3-9.

m/e 33 Time-of-Flight Spectrum. The m/e 33 spectrum is shown for a 20° laboratory angle. The data (circles) and the total calculated signal (thick black line) are shown along with the mass 33 SH contribution (medium black line) nominal mass 32 S signal (thick gray line) and 'mass 45 HCS' signal (thin gray line). An almost nonexistant contribution fron the mass 44 CS fragment is also shown (thinnest black line). The fast signal that is not fit by the calculated curve is known to be from secondary channels from power dependence studies.

Fig. 3-10.

C_4H_3 + SH Translational Energy Distribution ($P(E_T)$). The curve represents the normalized product flux as a function of total center-of-mass translational energy for the C_4H_3 + SH dissociation channel. The maximum translational

energy of this $P(E_T)$ is 12 kcal/mol which is in excellent agreement with the maximum thermodynamically possible translational energy for dissociation to SH and the HCCHCCH forms (cis and trans are .3 kcal/mol apart) of C_4H_3.

Fig. 3-11.

m/e 45 Time-of-Flight Spectrum. The m/e 45 spectrum is shown for a 20° laboratory angle. The possible origins of this signal are discussed in the text. Here it is fit as the mass 45 (HCS) fragment from an HCS $+C_3H_3$ channel using the $P(E_T)$ shown in Figure 3-12. The data (circles) and the total calculated signal (thick black line) are shown along with the major mass 45 HCS contribution (medium black line) and minor mass 58 C_2H_2S (gray line) and mass 82 C_4H_2S (thin black line) contributions.

Fig. 3-12.

'HCS + C_3H_3' Translational Energy Distribution ($P(E_T)$). The curve represents the normalized product flux as a function of total center-of-mass translational energy for the possible HCS + C_3H_3 dissociation channel. The maximum translational energy of this $P(E_T)$ is $\geq$ ~14 kcal/mol would agree with an assignment to HCS and internally excited propargyl radical. Alternatively, this $P(E_T)$ could represent a 'slow' mass 58 (SCHCH diradical) + 26 (acetylene) which is observed mainly at m/e 45 due to dissociative ionization of the mass 58 species. For this interpretation, the energy scale should be multiplied by 1.93. The apparent maximum translational energy would then be ~27 kcal/mol which would be just over the the expected thermodynamic limit (~23 kcal/mol)

for this assignment. See the text for details.

Fig. 3-13.

m/e 39 Time-of-Flight Spectrum. The m/e 39 spectrum is shown for a 20° laboratory angle. The data (circles) and the total calculated signal (thick black line) are shown along with the fast mass 40 C_3H_4 signal that appears mainly at m/e 39 due to dissociative ionization (thin black line). The slower signal is fit as a combination of mass 39 (thick gray line) and mass 51 (thin gray line) products. See the text for an alternative explanation of the slow signal.

Fig. 3-14.

m/e 44 and m/e 40 Time-of-Flight Spectra. The m/e 44 spectrum is shown for a 30° laboratory angle in the upper graph. The data (circles) and the total calculated signal (thick black line) are shown with contributions from the mass 44 CS fragment from a CS + C_3H_4 channel (thin black line) and from the 'mass 45 HCS' fragment (gray line). The lower graph shows the m/e 40 spectrum at 20°. Contributions from the mass 40 C_3H_4 fragment (gray line) and possibly leakage of mass 39 C_3H_3 signal to m/e 40 (thin black line). The conjugate CS and C_3H_4 fragments are assumed to have the $P(E_T)$ shown in Figure 3-15.

Fig. 3-15.

CS + C_3H_4 Translational Energy Distribution ($P(E_T)$). The curve represents the normalized product flux as a function of total center-of-mass translational energy for the CS + C_3H_4 dissociation channel. The $P(E_T)$ shows a peak at 8.75 kcal/mol and has maximum translational energy of 30 kcal/mol. This

$P(E_T)$ would be in agreement with assignments of the C_3H_4 fragment as vibrationally excited allene, methylacetylene, or cyclopropene.

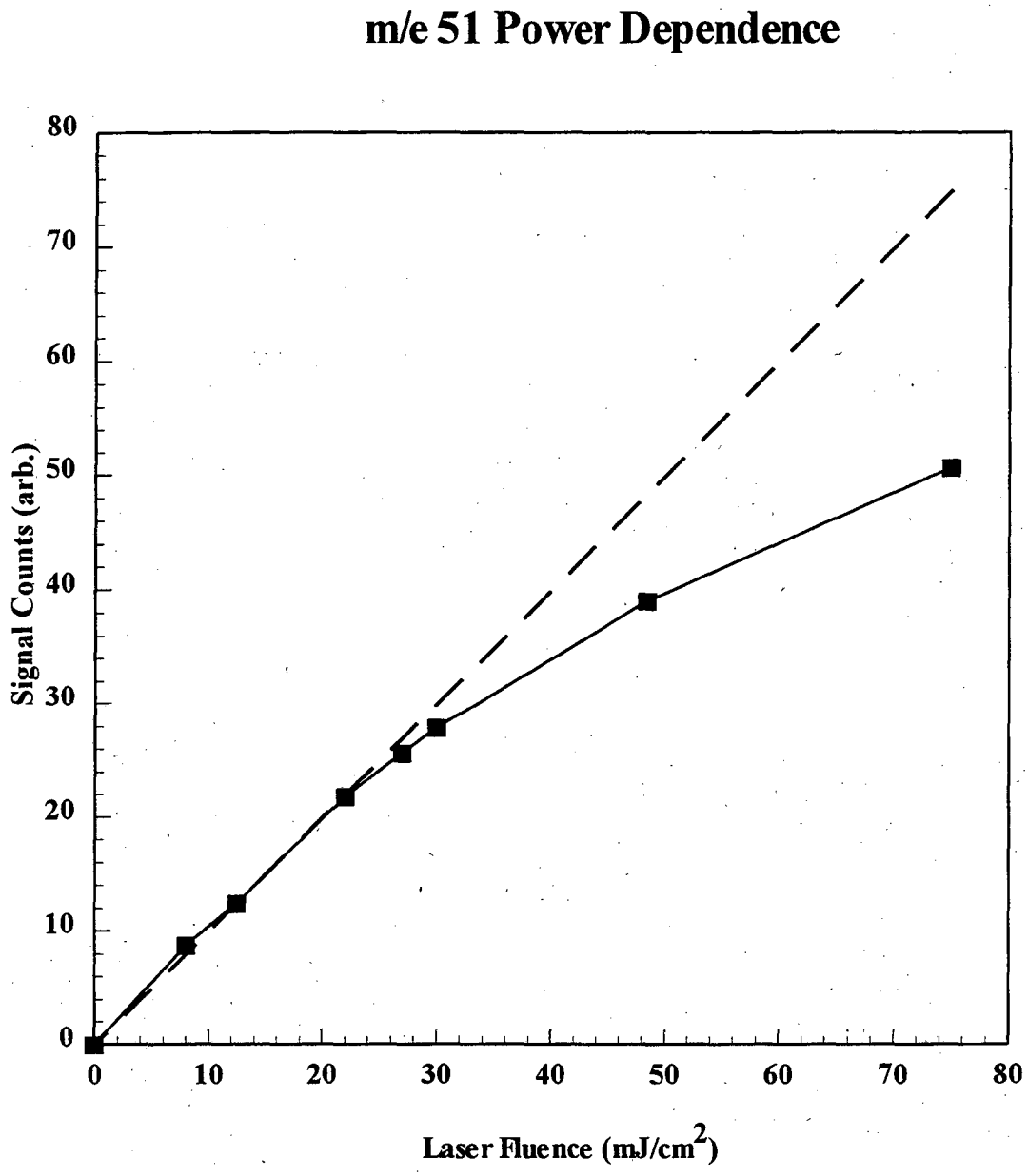
m/e 51 Power Dependence
Signal Counts (arb.)
0
10
20
30
40
50
60
70
80
Laser Fluence (mJ/cm2)

Figure 1.

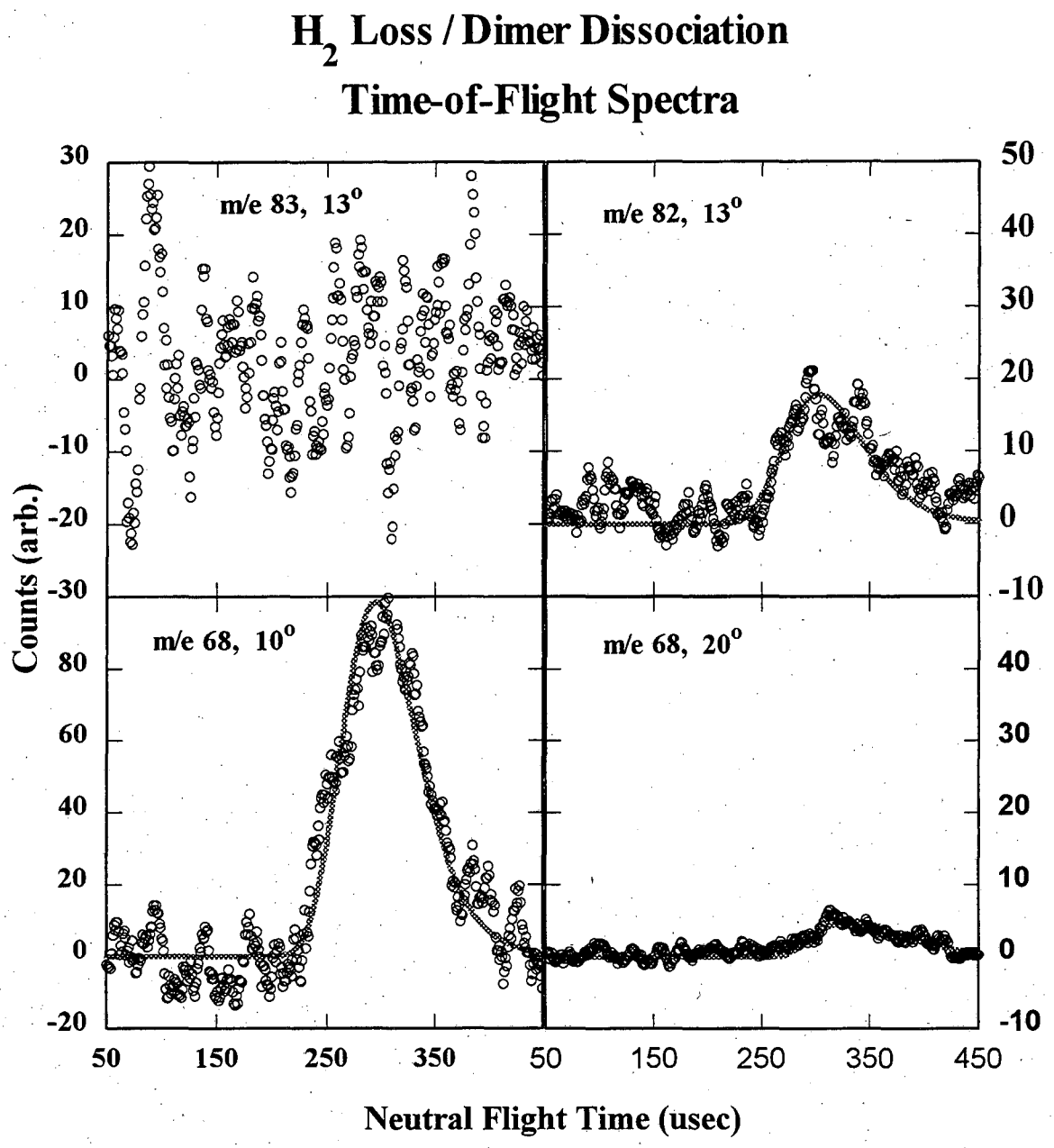
H2 Loss / Dimer Dissociation
Time-of-Flight Spectra
m/e 83, 13°
m/e 82, 13°
m/e 68, 10°
m/e 68, 20°
Counts (arb.)
Neutral Flight Time (usec)
30
20
10
0
-10
-20
-30
80
60
40
20
0
-20
50
40
30
20
10
0
-10
50
150
250
350
450

Figure 2.

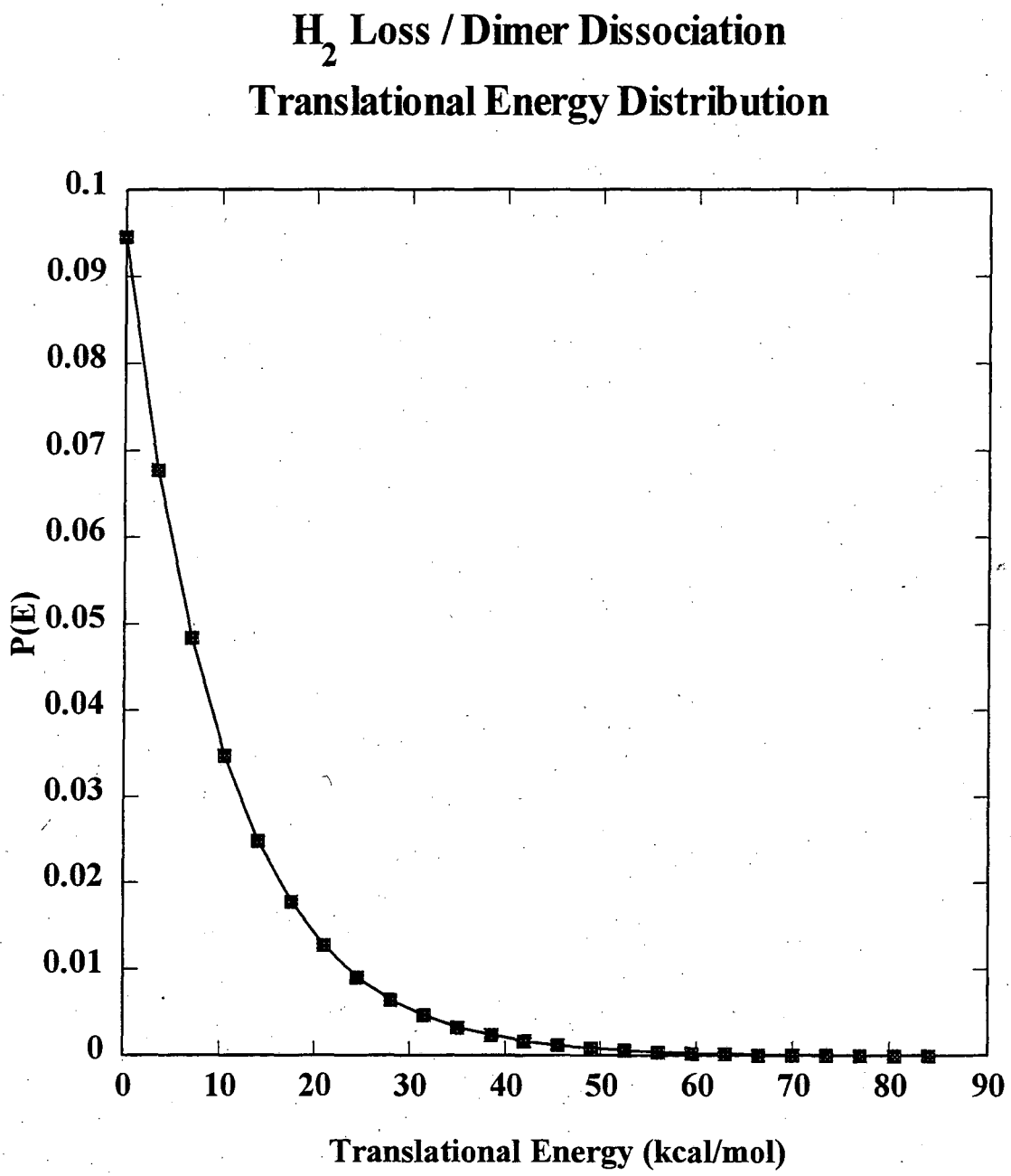
H_2 Loss / Dimer Dissociation
Translational Energy Distribution
P(E)
0.1
0.09
0.08
0.07
0.06
0.05
0.04
0.03
0.02
0.01
0
0
10
20
30
40
50
60
70
80
90
Translational Energy (kcal/mol)

Figure 3.

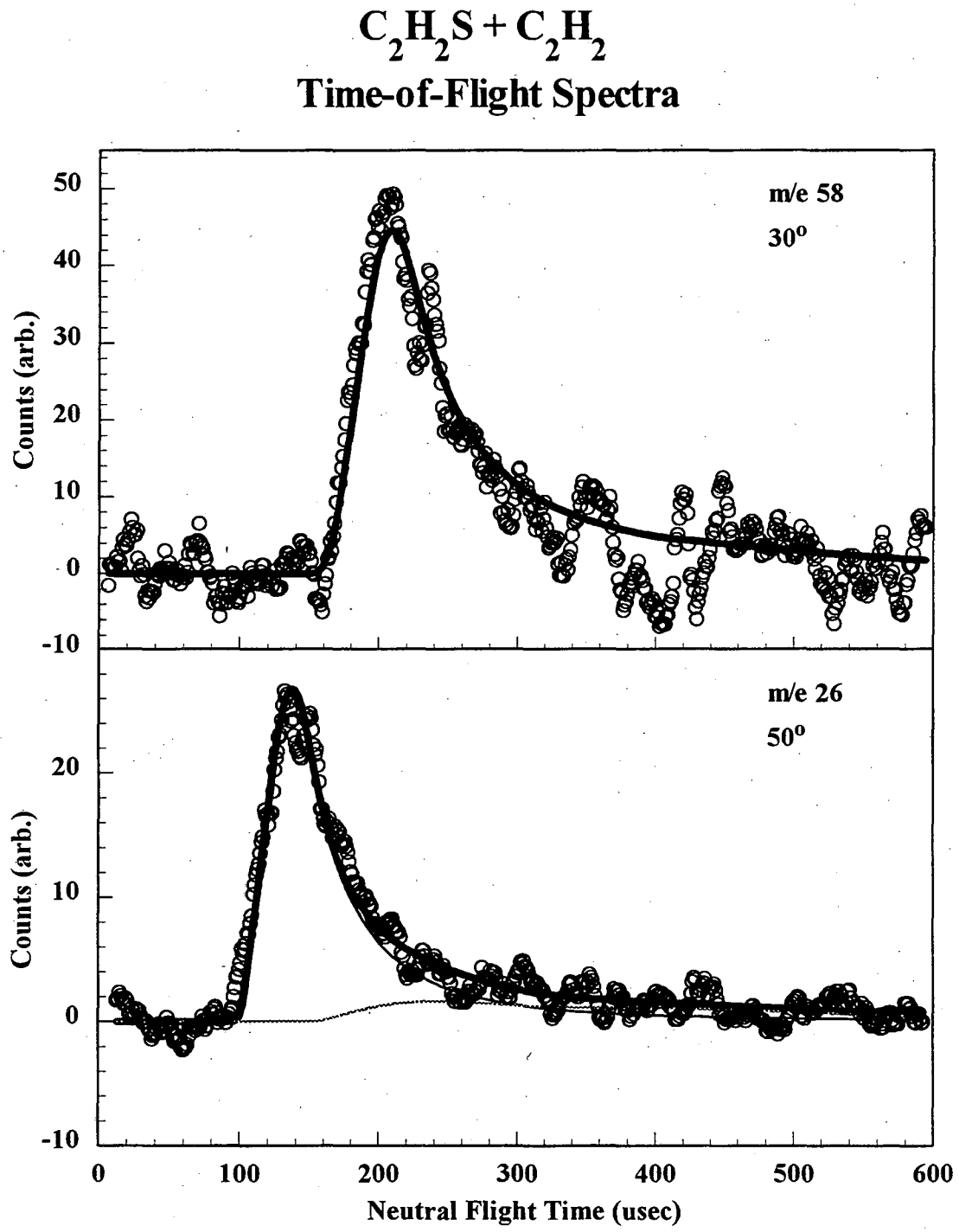
$C_2H_2S + C_2H_2$
Time-of-Flight Spectra
m/e 58
30°
m/e 26
50°
Counts (arb.)
Counts (arb.)
50
40
30
20
10
0
-10
20
10
0
-10
0
100
200
300
400
500
600
Neutral Flight Time (usec)

Figure 4.

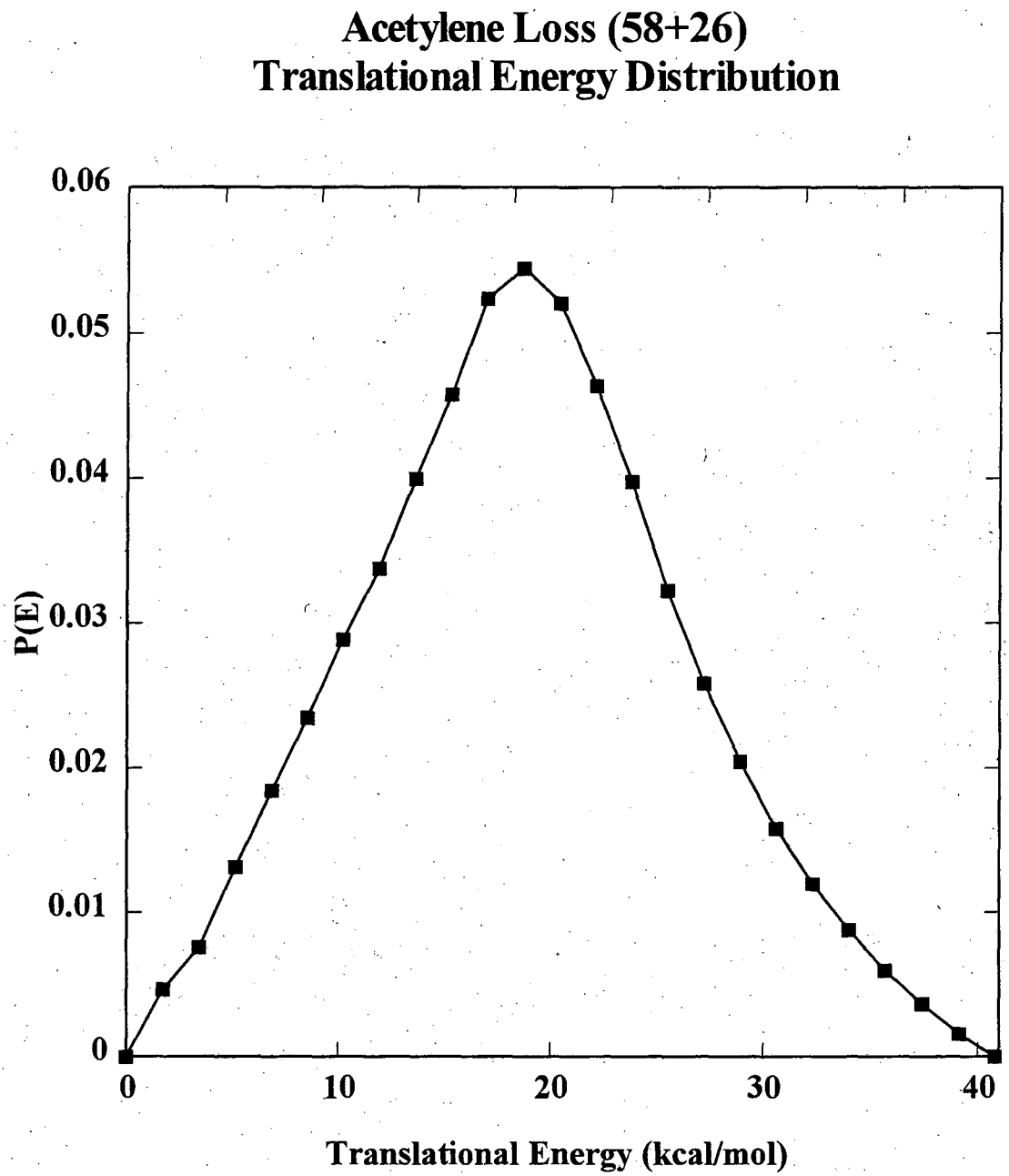
Acetylene Loss (58+26)
Translational Energy Distribution
0.06
0.05
0.04
0.03
0.02
0.01
0
P(E)
0
10
20
30
40
Translational Energy (kcal/mol)

Figure 5.

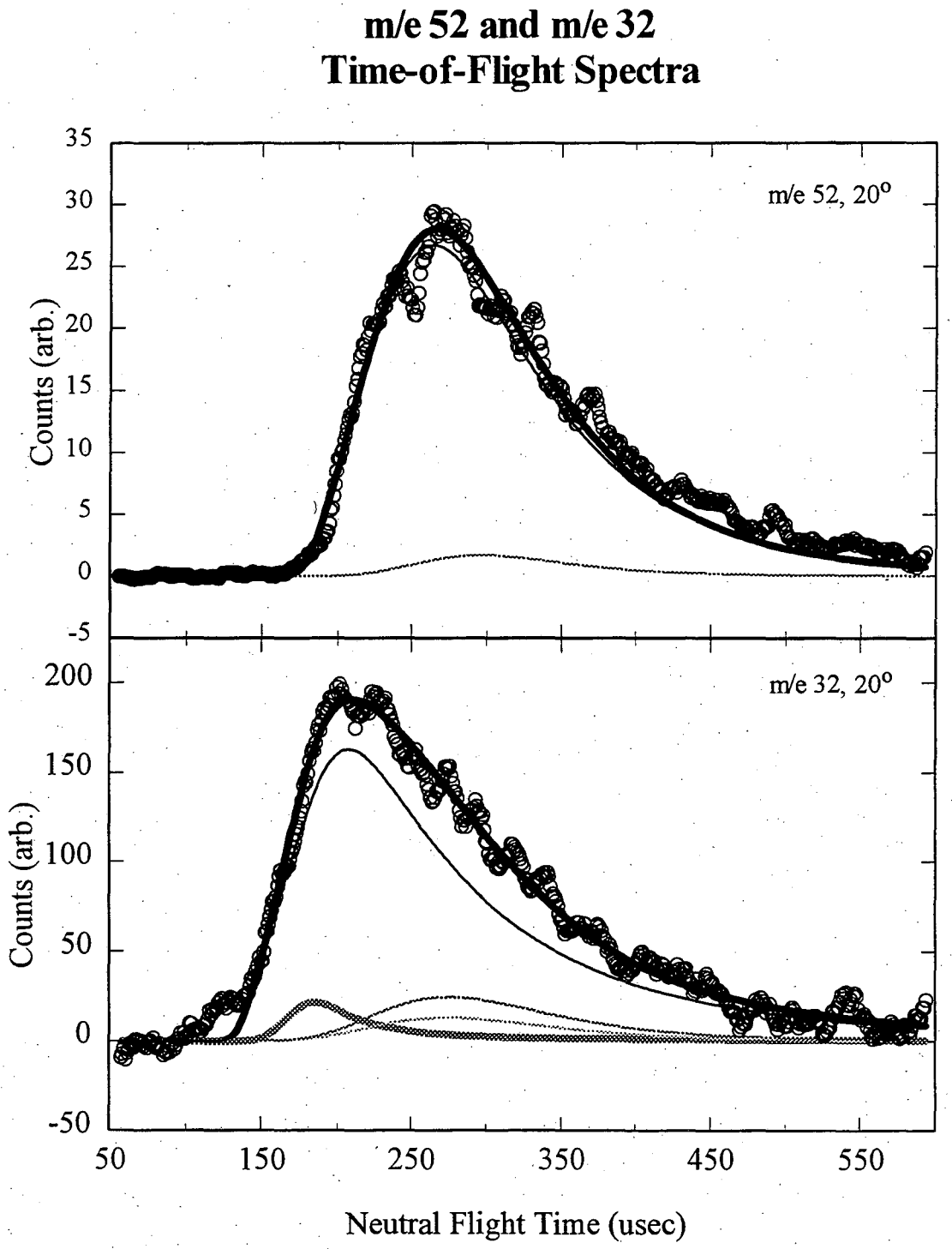
m/e 52 and m/e 32
Time-of-Flight Spectra
m/e 52, 20°
m/e 32, 20°
Counts (arb.)
Counts (arb.)
35
30
25
20
15
10
5
0
-5
200
150
100
50
0
-50
50
150
250
350
450
550
Neutral Flight Time (usec)

Figure 6.

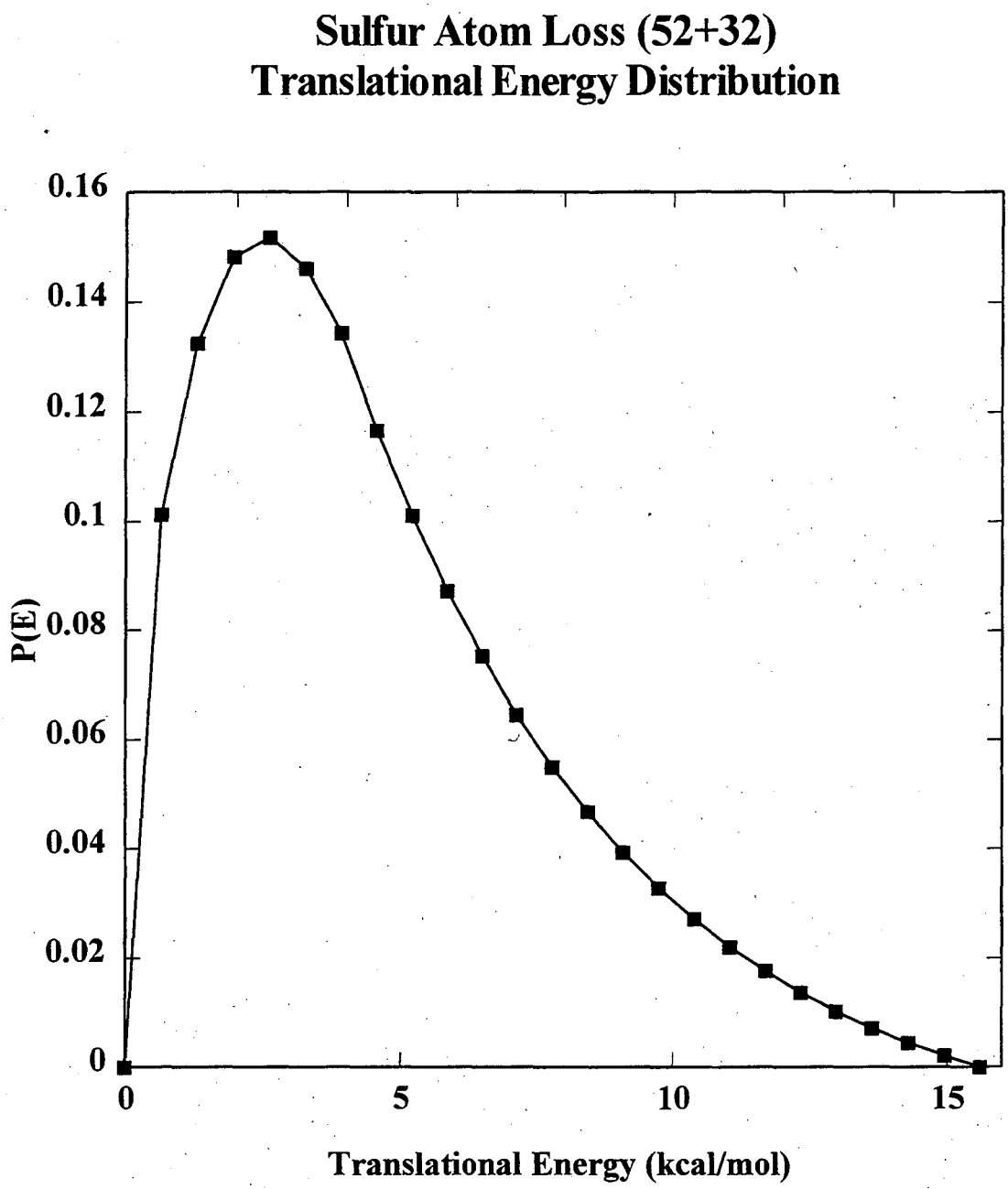
Sulfur Atom Loss (52+32)
Translational Energy Distribution
0.16
0.14
0.12
0.1
0.08
0.06
0.04
0.02
0
P(E)
0
5
10
15
Translational Energy (kcal/mol)

Figure 7.

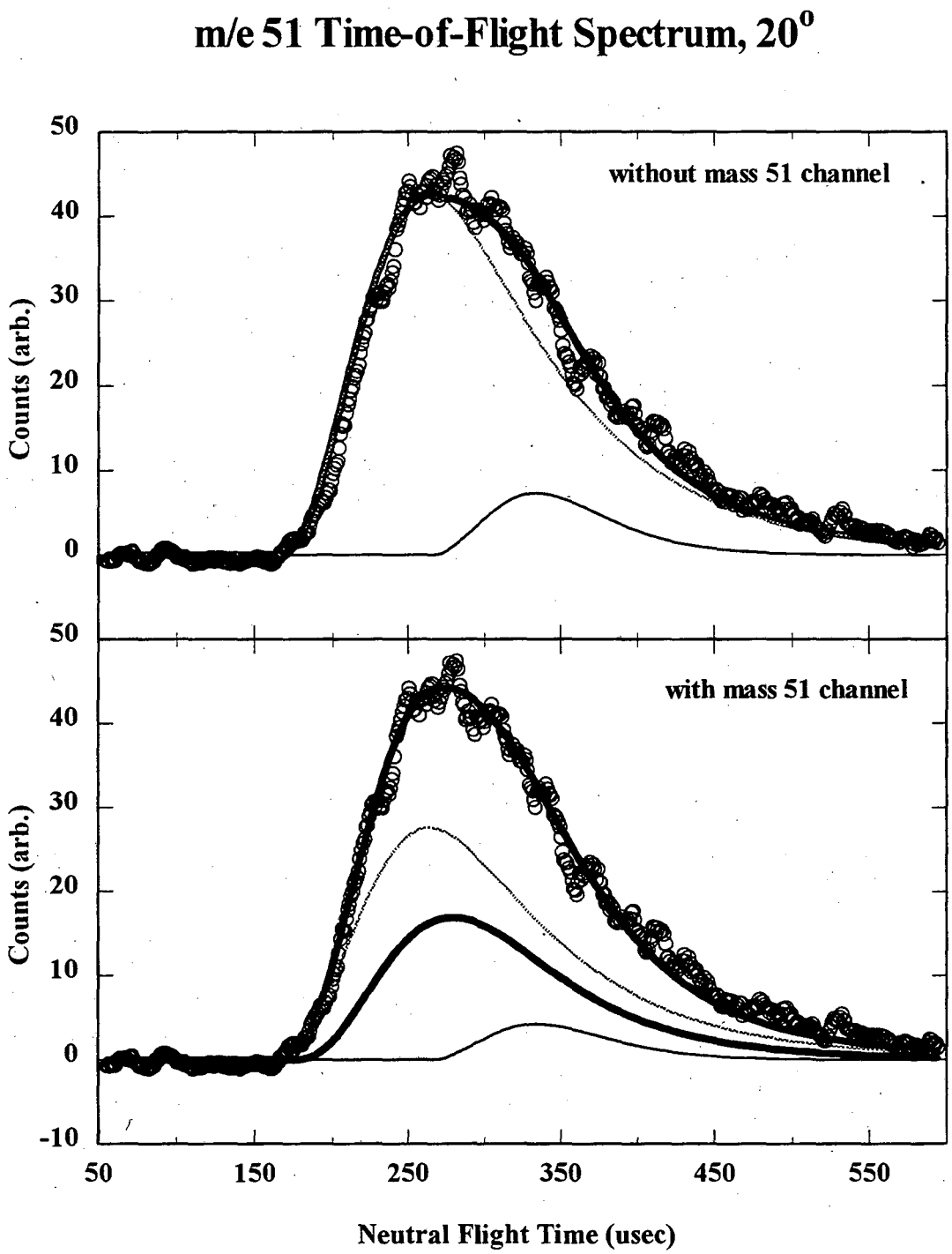
m/e 51 Time-of-Flight Spectrum, 20°
without mass 51 channel
with mass 51 channel
Counts (arb.)
Counts (arb.)
50
40
30
20
10
0
50
40
30
20
10
0
-10
50
150
250
350
450
550
Neutral Flight Time (usec)

Figure 8.

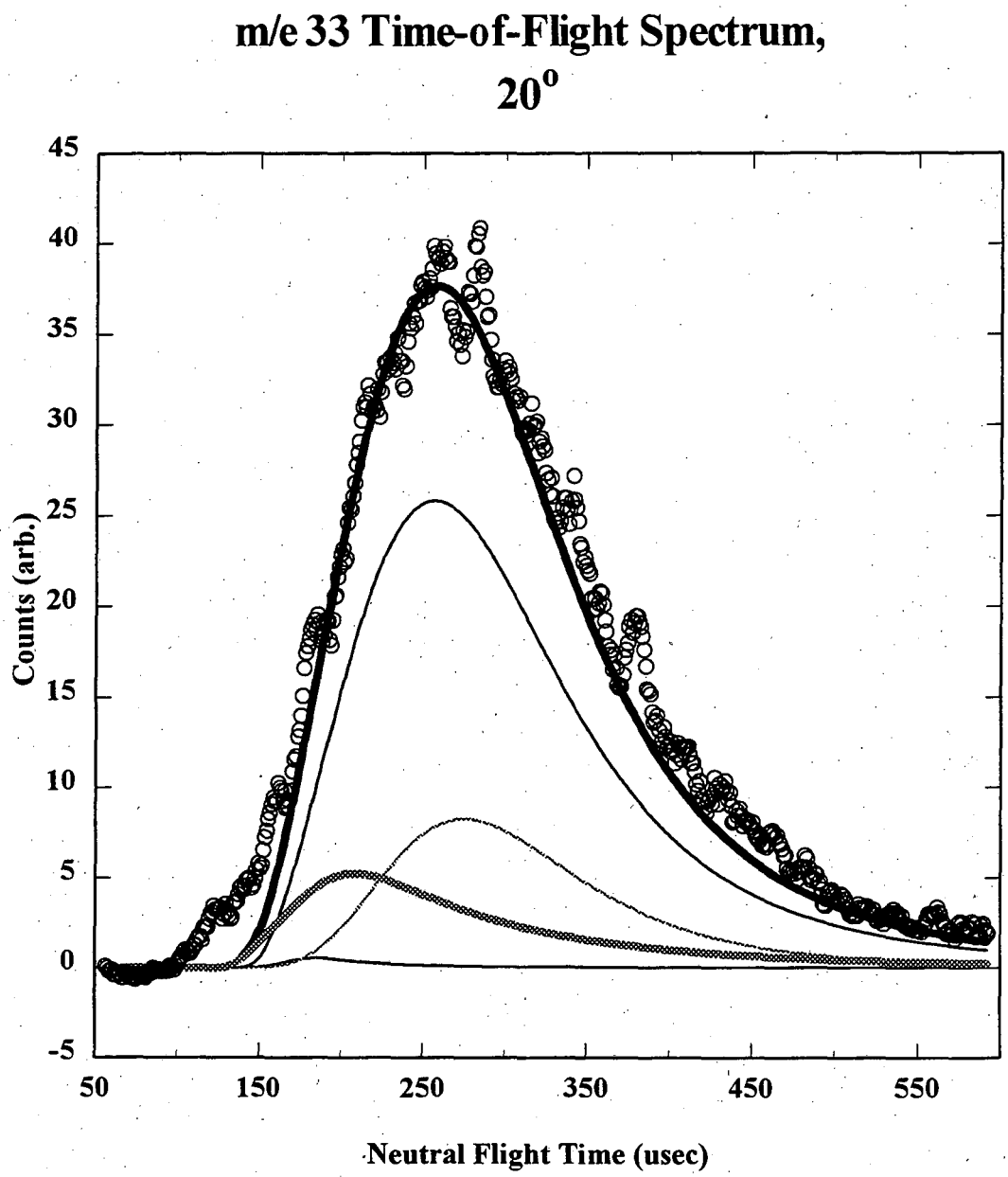
m/e 33 Time-of-Flight Spectrum,
20°
Counts (arb.)
45
40
35
30
25
20
15
10
5
0
-5
50
150
250
350
450
550
Neutral Flight Time (usec)

Figure 9.

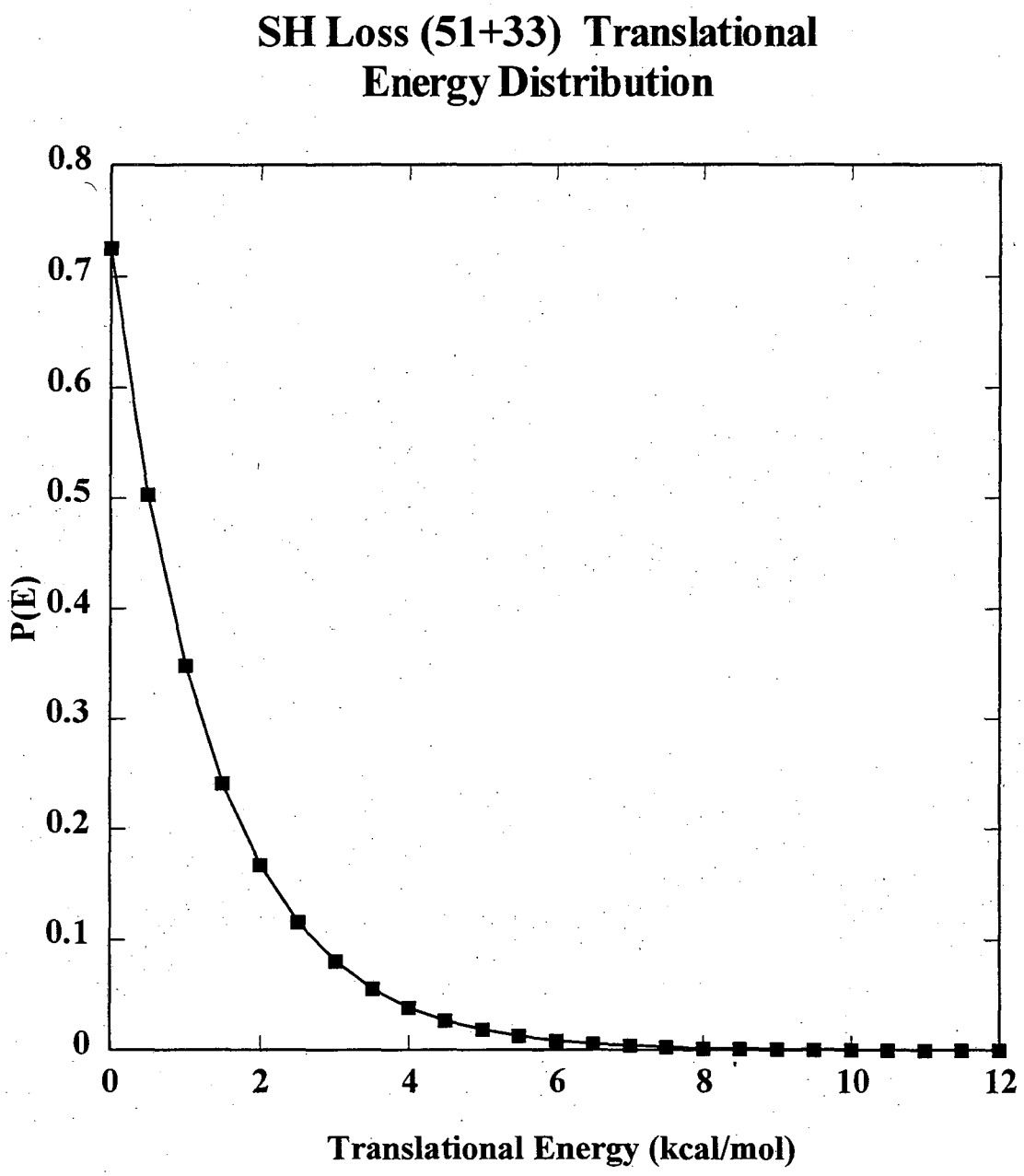
SH Loss (51+33) Translational
Energy Distribution
0.8
0.7
0.6
0.5
0.4
0.3
0.2
0.1
0
P(E)
0
2
4
6
8
10
12
Translational Energy (kcal/mol)

Figure 10.

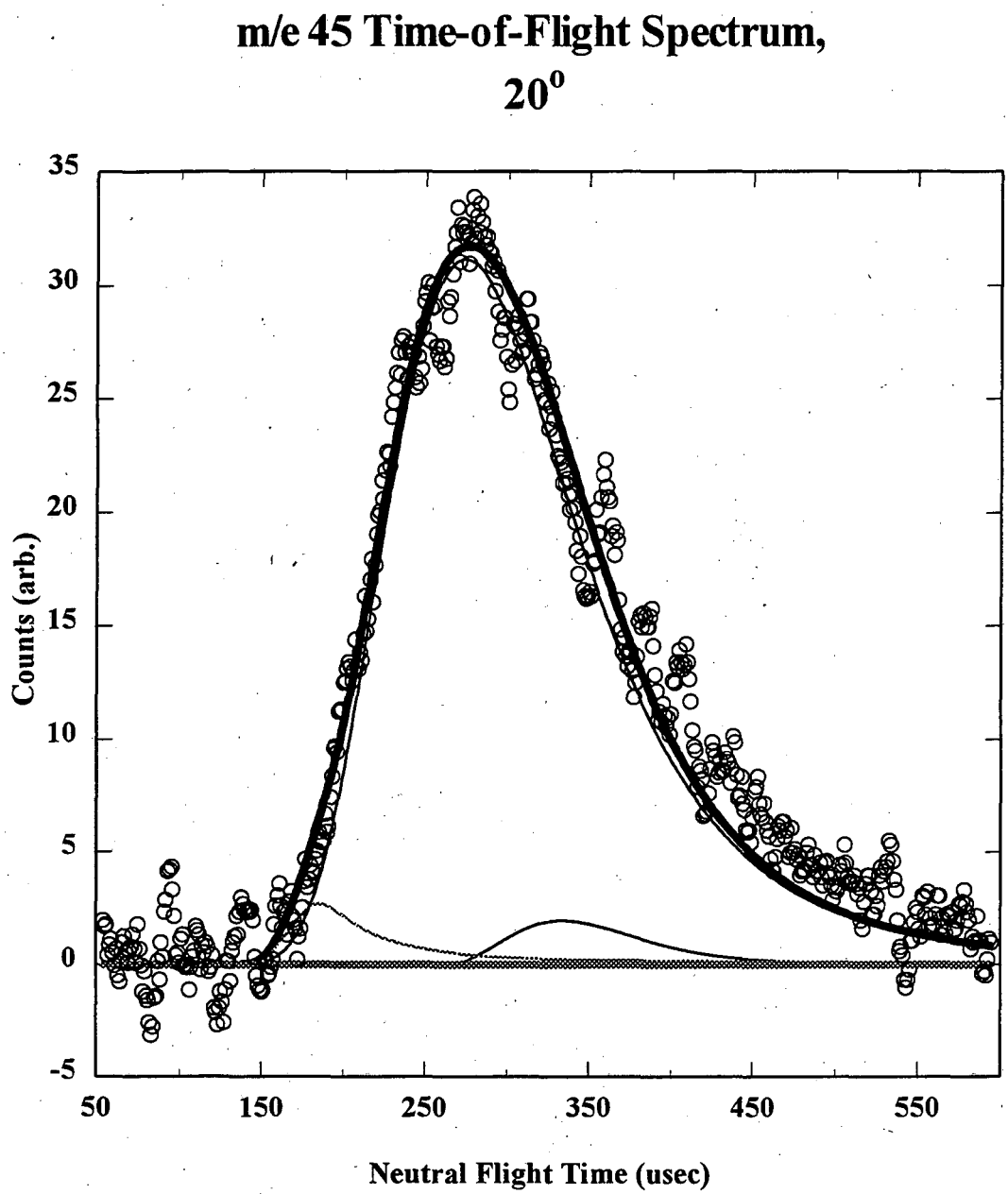
m/e 45 Time-of-Flight Spectrum,
20°
Counts (arb.)
35
30
25
20
15
10
5
0
-5
50
150
250
350
450
550
Neutral Flight Time (usec)

Figure 11.

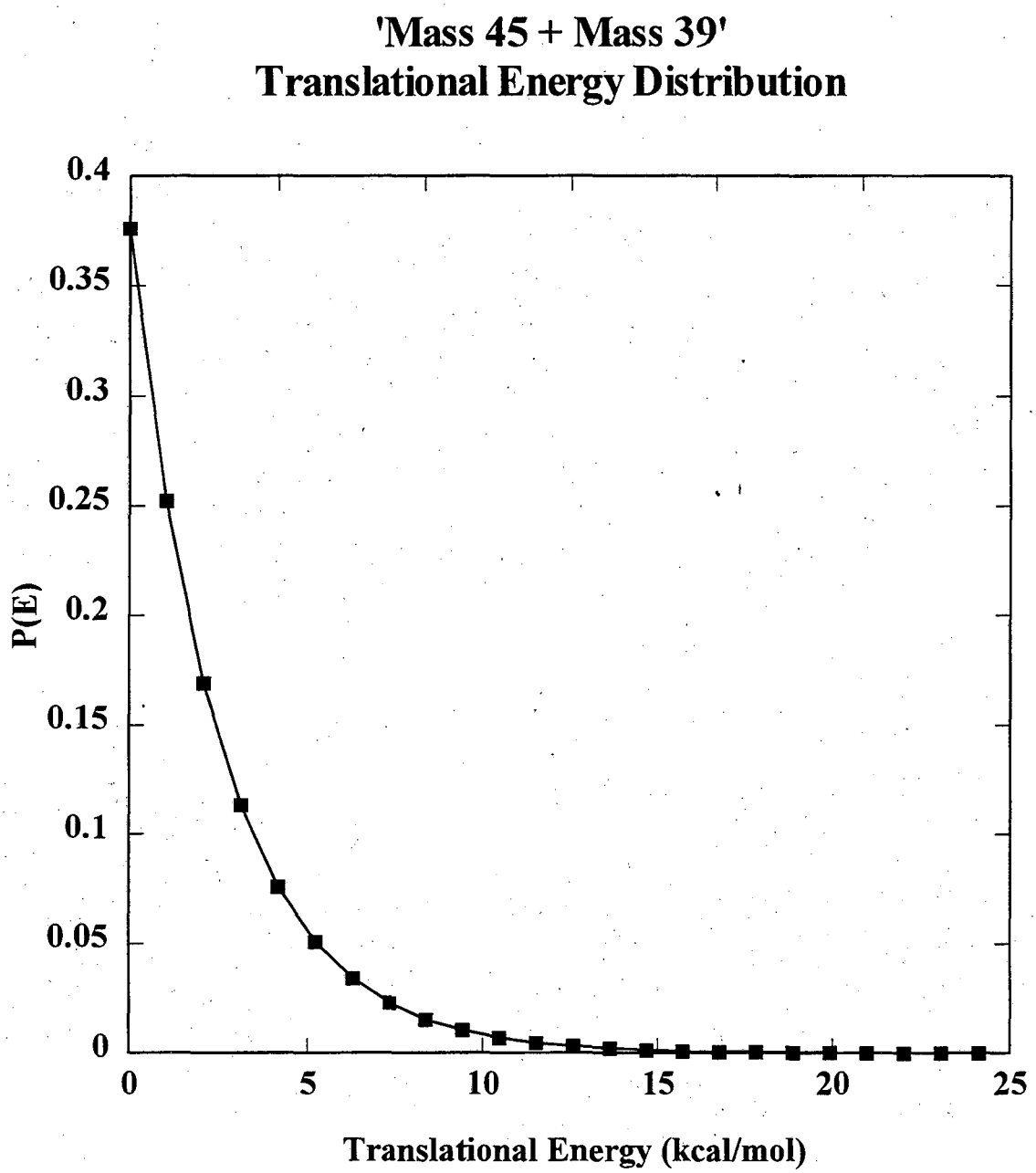
'Mass 45 + Mass 39'
Translational Energy Distribution
0.4
0.35
0.3
0.25
0.2
0.15
0.1
0.05
0
P(E)
0
5
10
15
20
25
Translational Energy (kcal/mol)

Figure 12.

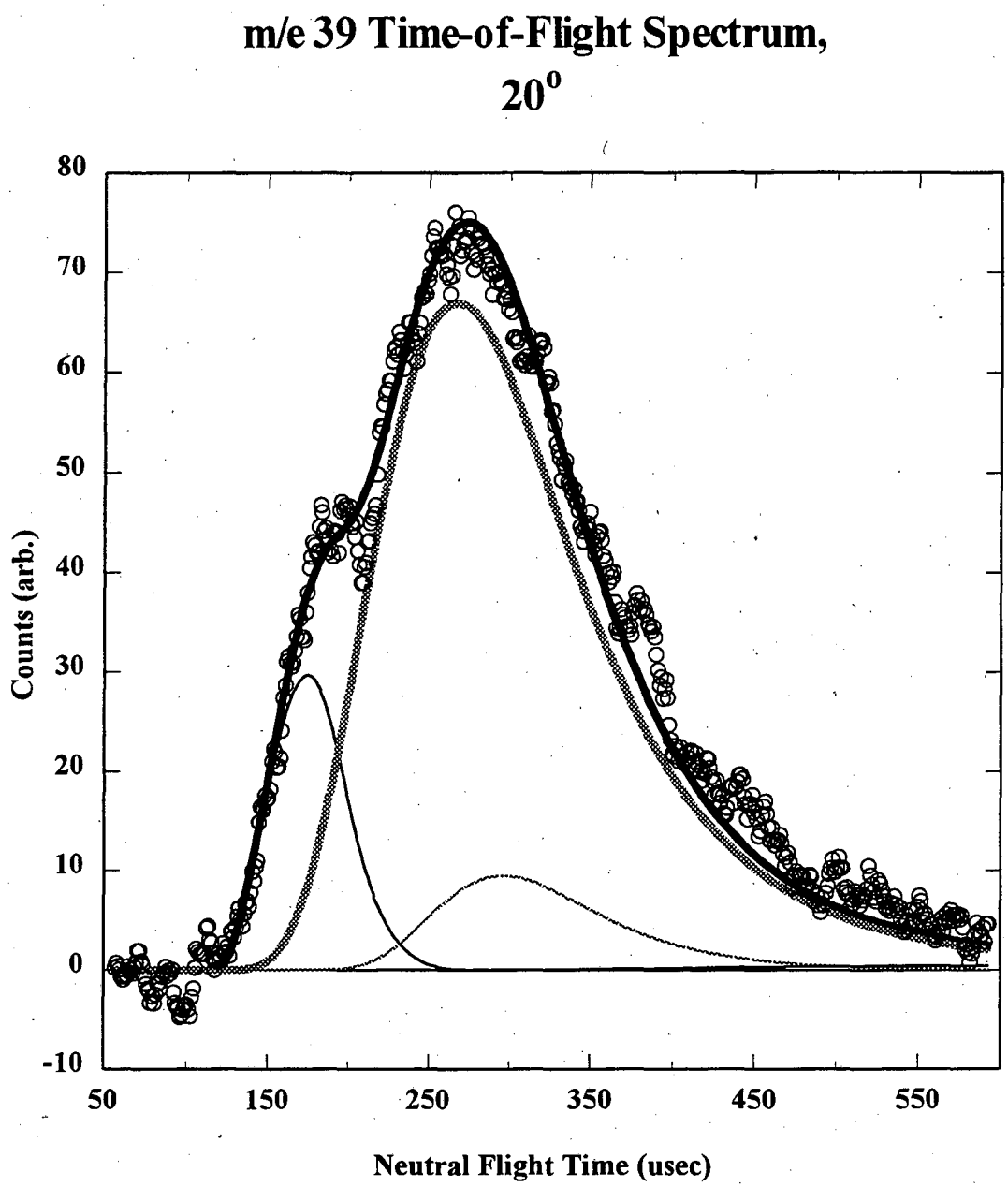
m/e 39 Time-of-Flight Spectrum,
20°
Counts (arb.)
80
70
60
50
40
30
20
10
0
-10
50
150
250
350
450
550
Neutral Flight Time (usec)

Figure 13.

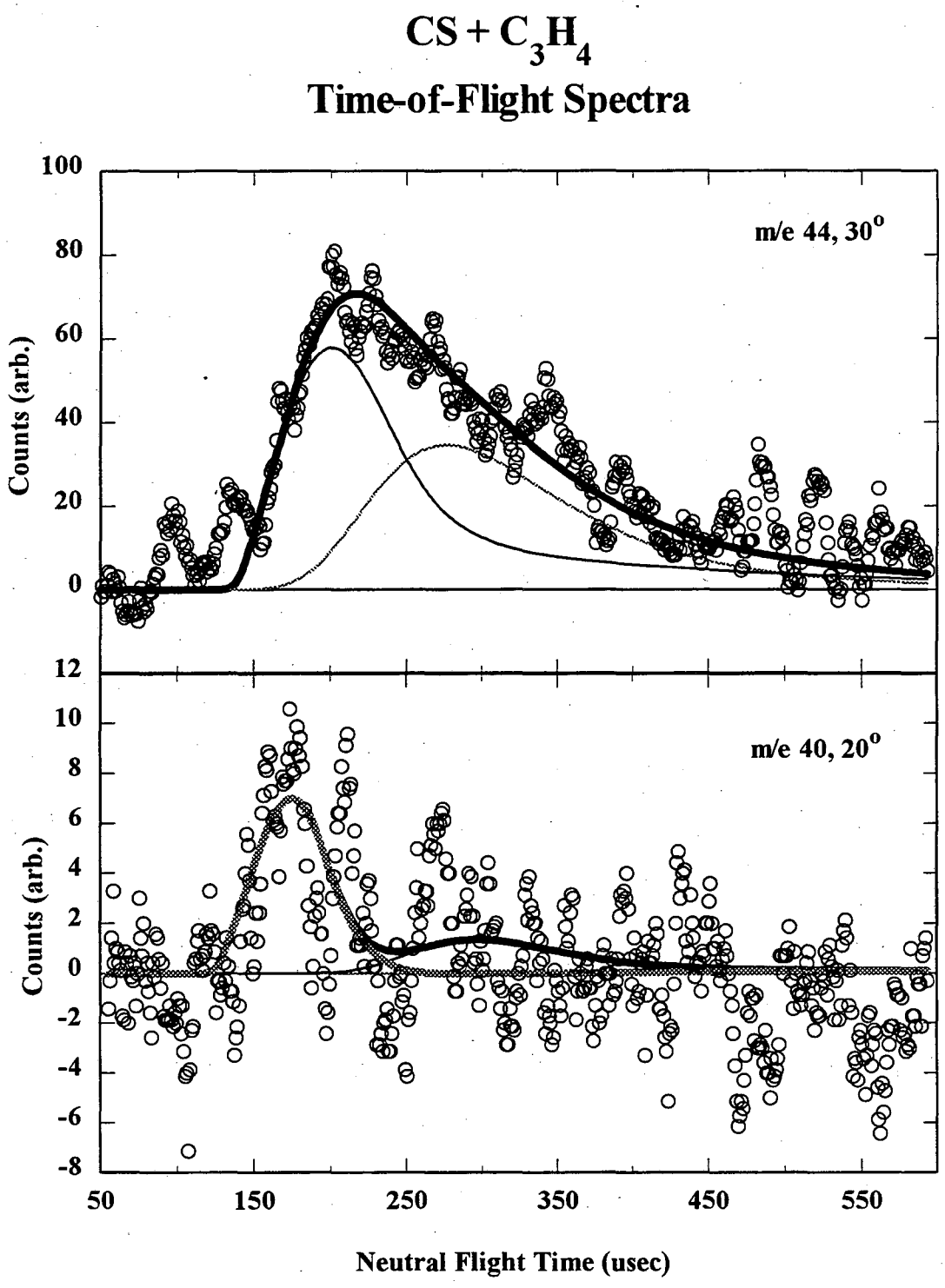
CS + C3H4
Time-of-Flight Spectra
m/e 44, 30°
m/e 40, 20°
Counts (arb.)
Counts (arb.)
100
80
60
40
20
0
12
10
8
6
4
2
0
-2
-4
-6
-8
50
150
250
350
450
550
Neutral Flight Time (usec)

Figure 14.

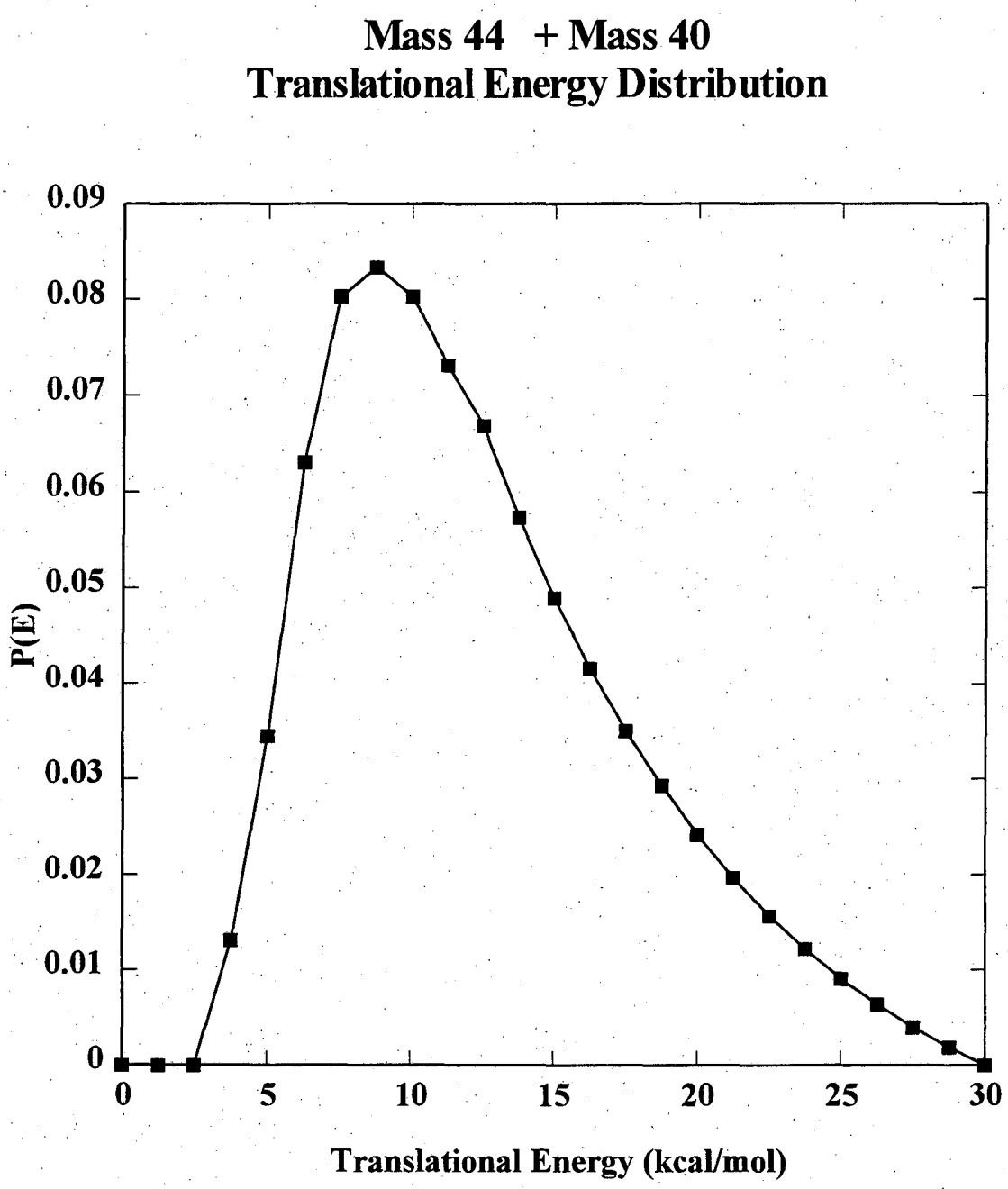
Mass 44 + Mass 40
Translational Energy Distribution
0.09
0.08
0.07
0.06
0.05
0.04
0.03
0.02
0.01
0
P(E)
0
5
10
15
20
25
30
Translational Energy (kcal/mol)

Figure 15.

LAWRENCE BERKELEY LABORATORY
UNIVERSITY OF CALIFORNIA
TECHNICAL INFORMATION DEPARTMENT
BERKELEY, CALIFORNIA 94720